# Studies Towards the Total Synthesis of Eleutherobin and Biologically Active Carbasugars

**by**

**Anthony Fers-Lidou**

M.Sc., Ecole Nationale Supérieure de Chimie de Montpellier, 2016

B.Sc., Ecole Nationale Supérieure de Chimie de Montpellier, 2014

Thesis Submitted in Partial Fulfillment of the

Requirements for the Degree of

Doctor of Philosophy

in the

Department of Chemistry

Faculty of Science

© Anthony Fers-Lidou 2022

SIMON FRASER UNIVERSITY

Spring 2022

Copyright in this work rests with the author. Please ensure that any reproduction or re-use is done in accordance with the relevant national copyright legislation.

## Declaration of Committee

| | |
|---|---|
| **Name:** | **Anthony Fers-Lidou** |
| **Degree:** | **Doctor of Philosophy** |
| **Title:** | ***Studies Towards the Total Synthesis of Eleutherobin and Biologically Active Carbasugars*** |
| **Committee:** | **Chair: Hua-Zhong "Hogan" Yu**<br>Professor, Chemistry |
| | **Robert Britton**<br>Supervisor<br>Professor, Chemistry |
| | **Roger Linington**<br>Committee Member<br>Professor, Chemistry |
| | **David Vocadlo**<br>Committee Member<br>Professor, Chemistry |
| | **Andrew Bennet**<br>Examiner<br>Professor, Chemistry |
| | **Fred West**<br>External Examiner<br>Professor<br>Department of Chemistry<br>University of Alberta |

# Abstract

Efforts have been directed towards the total synthesis of eleutherobin, a natural product with promising anticancerous properties. Indeed, Taxol-like activity of eleutherobin could provide an interesting alternative to Taxol-resistant cancers. The generation of the 10-membered ring has been performed via an exotic Knoevenagel condensation and paves the path for a concise, robust and efficient synthesis of the marine natural product.

An additional study describes the synthesis of several inhibitors for the production of afucosylated antibodies that will ultimately provide a considerable enhancement of their antibody dependent cell-mediated cytotoxicity. Alone or combined with toxic payloads (i.e., ADC), these antibodies will contribute to better and cheaper immunotherapies for cancer.



**Keywords:** total synthesis, natural product, chemotherapy, immunotherapy, cancer, eleutherobin

# Table of Contents

# List of Tables

# List of Figures

# List of Schemes

# List of Abbreviations

| | |
|---|---|
| **°C** | Celsius Degrees |
| **δ** | Chemical shift in ppm from tetramethylsilane |
| **$[\alpha]_D^{20}$** | Specific rotation at the sodium D line at 20 °C (589 nm) |
| **Ac** | Acetyl |
| **AIBN** | 2,2'-azobis(isobutyronitrile) |
| **aq** | Aqueous |
| **BAIB** | [Bis(acetoxy)iodo]benzene |
| **br.** | Broad |
| **Bu** | Butyl |
| **cat.** | Catalytic amount |
| **COSY** | Correlation Spectroscopy |
| **dba** | Dibenzylideneacetone |
| **D*t*BPF** | 1,1'-bis(di-*tert*-butylphosphino)-ferrocene |
| **DBU** | 1,8-Diazabicyclo[5.4.0]undec-7-ene |
| **DCE** | 1,2-Dichloroethane |
| **DCM** | Dichloromethane |
| **DIBALH** | Diisobutylaluminium hydride |
| **DIPEA** | Diisopropylethylamine |
| **DMAP** | 4-Dimethylaminopyridine |
| **DMDO** | Dimethyldioxirane |
| **DMF** | *N*,*N*'-Dimethylformamide |
| **DMPU** | 1,3-Dimethyl-3,4,5,6-tetrahydro-2(*1H*)-pyrimidinone |
| **DMSO** | Dimethylsulfoxide |
| **DNA** | Deoxyribonucleic acid |
| **d.r.** | Diastereomeric ratio |
| **E** | Entgegen (trans) |
| **EA** | Ethyl acetate |
| **ee** | Enantiomeric excess |
| **equiv.** | Equivalents |
| **Et** | Ethyl |
| **$Et_2O$** | Diethyl ether |

| | |
|---|---|
| **FDA** | Federal Drug Administration |
| **hex** | Hexyl |
| **HMBC** | Heteronuclear Multiple Bond Correlation |
| **HMDS** | Hexamethyldisilazane |
| **HMPA** | Hexamethylphosphoramide |
| **HPLC** | High-performance liquid chromatography |
| **HRMS** | High-resolution mass spectrometry |
| **HSQC** | Heteronuclear Single Quantum Coherence |
| **Hz** | Hertz |
| ***i*** | Iso- |
| **$IC_{50}$** | Half maximal inhibitory concentration |
| ***J*** | Coupling Constant |
| **$LD_{50}$** | Lethal Dose, 50% |
| **LDA** | Lithium diisopropylamide |
| **lit.** | Literature |
| **M** | Molar |
| ***m*-CPBA** | *Meta*-Chloroperoxybenzoic acid |
| **Me** | Methyl |
| **MeCN** | Acetonitrile |
| **MeOH** | Methanol |
| **mmol** | Millimole(s) |
| **mol** | Mole(s) |
| **MOM** | Methoxymethyl ether |
| **Ms** | Methanesulfonyl |
| **MS** | Molecular Sieves |
| **NBS** | *N*-bromosuccinimide |
| **NCS** | *N*-chlorosuccinimide |
| **NIS** | *N*-iodosuccinimide |
| **NMR** | Nuclear Magnetic Resonance |
| **nOe** | Nuclear Overhauser effect |
| **Nu** | Nucleophile |
| **p** | Para |
| **PCC** | Pyridinium chlorochromate |
| **pH** | $-\log_{10}[H^+]$ |

| | |
|---|---|
| **Ph** | Phenyl |
| **PMB** | *Para*-methoxybenzyl |
| **ppm** | Parts-per-million |
| **PIFA** | Phenyliodine bis(trifluoroacetate) |
| **Piv** | Pivaloyl |
| **pKa** | $-\log_{10}[Ka]$ |
| **PMP** | *Para*-methoxyphenyl |
| **Pr** | Propyl |
| **RCM** | Ring closing metathesis |
| **r.t.** | Room temperature |
| **SAR** | Structure-activity relationship |
| **sec** | Secondary |
| ***t*** | Tert |
| **t** | Time |
| **T** | Temperature |
| **TBDPS** | *Tert*-butyldiphenylsilyl |
| **TBS** | *Tert*-butyldimethylsilyl |
| **TES** | Triethylsilyl |
| **Tf** | Trifluoromethanesulfonyl |
| **THF** | Tetrahydrofuran |
| **TIPS** | Triisopropylsilyl |
| **TLC** | Thin layer chromatography |
| **TMEDA** | N,N,N′,N′-Tetramethylethylenediamine |
| **TMS** | Trimethylsilyl |
| **Ts** | Toluenesulfonate |
| **Z** | Zusammen (*cis*) |

# Chapter 1.

# Introduction

## 1.1. Cancer: The Disease of the 21st Century

### 1.1.1. Cancer: Facts and Numbers

Cancer is the second leading cause of death worldwide and incidence of cancer continues to increase on an annual basis.[1] The increase in cancer diagnosis is partly due to increasing life expectancies in the developed world, which accounts for two-thirds of all cancers.[2] Indeed, the median age for cancer diagnosis was 66 in the United States in 2018.[3] The remaining third of cancers can be directly attributed to lifestyle and causes that vary within different communities.[2] For example, the pronounced rise of bowel cancers has been attributed to increased consumption of red and processed meat in certain countries.[4] Similarly, the culture of sunbathing has resulted in increased risk of melanomas in the United Kingdom.[5] Among all cancers, lung cancer continues to claim the largest number of lives with almost two million deaths worldwide in 2017. Colon (900,000), stomach (860,000), liver (820,000) and breast cancer (610,000) are the next most common causes of cancer-related deaths.[6] However, the prevalence of cancer around the world shows important disparities, and higher-income countries tend to see a higher prevalence of disease.[7] For instance, 0.4% of the population had cancer in Angola in 2017, whereas Canada displays more alarming numbers (4.6%).[8] Not surprisingly, the Canadian Cancer Society estimates that nearly 1 in 2 Canadians will develop cancer in their lifetime and 1 in 4 will die from it.[9]

To assess whether progress has been made in battling this disease, three parameters must be dissected: the number of deaths, the death rate (the number of cancer deaths divided by world population), and the age-standardized death rate. From 1990 to 2017, the number of cancer deaths increased by 66% worldwide while the death rate from cancer increased by 17%. The death rate by age shows that for those who are 70 and older, 1% die from cancer every year while the death rate is 40 times lower for those younger than 50. To correct for the difference in age profiles over time, epidemiologists use the age-standardized death rate that accounts for the changes in

age structure of a population. Quite positively, this metric shows a 15% decline in cancer deaths worldwide since 1990.[8] Not surprisingly, the change in age-standardized death rate is more important in developed countries where the progress in cancer treatment is higher. For instance, France's age-standardized death rate decreased by 25% while Uganda's rates increased by 2.4%.[8] Thus, it is clear that slow but meaningful progress has been made toward the treatment of this disease. It is expected that this trend will further improve along with continued decreases in smoking rates, and better treatments and diagnostics are also expected to further improve survival rates.[10]

### 1.1.2. How to Treat Cancer?

Intending to eliminate or slow disease progression, research over the last several decades has led to the identification of a diverse portfolio of cancer therapies. Indeed, the most common treatments are surgery, chemotherapy, radiation therapy, hormone therapy, immunotherapy, targeted therapy, and in some specific cases stem-cell transplant.[11] Many diverse factors are taken into consideration in planning the treatment regime for each individual and include the type and stage of cancer, the patient's age, and personal preferences. While some cancers can be treated with a single therapy or intervention, the majority rely on a combination of approaches. Amongst those, neoadjuvant therapy comes before surgery and is critical in cases where the tumor is too large to be removed. Neoadjuvant therapies can take the form of chemotherapy, radiation therapy, or hormone therapy. Radiation therapy uses focused beams of intense energy (X-ray or protons) to kill cancer cells whereas hormone therapies either block the production of a specific hormone or interfere with how hormones behave in the body and are commonly used to treat prostate and breast cancers. Adjuvant therapies are given after surgery to destroy the remaining cancerous cells and reduce the risk of relapse. These various cancer treatments can be further divided into subclasses that include localized therapy, which aims to target a specific region of the body that includes the tumor (e.g., radiation therapy and surgery) and systemic therapy, which involves the distribution of small-molecules or monoclonal antibodies throughout the bloodstream. Efforts directed towards the identification of cancer-specific proteins and receptors, the targeting of which can impart selectivity to adjuvant therapies, have increased dramatically and are referred to as targeted therapy.[12]

## 1.2. Chemotherapy

### 1.2.1. History

The concept of “chemotherapy” was first introduced by the German scientist Paul Ehrlich who defined chemotherapy as the use of chemicals to treat disease.[13] His early studies focused on developing animal models to assess the utility of different chemicals in treating specific diseases and represent a breakthrough in drug discovery.[14] Interestingly, while he pursued the use of aniline dyes and alkylating agents for the treatment of cancers, his pessimism about the feasibility of discovering a chemotherapy for cancer is well documented and his lab’s door had a sign stating: “Give up all hope oh ye who enter”.[15]

Until the 1960s, cancer was mainly dealt with by surgery and radiation therapy, which resulted in poor overall success rates (~ 33%) mostly due to metastasis.[15] After World War II, research that had focused on the biological effects of war gases revealed that many of these agents cross-link DNA and lead to impaired cell division. As a result of these studies, nitrogen mustard became a common treatment for lymphomas in the United States in 1946.[16] Unfortunately, remissions were brief and incomplete, which led to negative sentiments surrounding the feasibility of fighting cancer with small molecules. However, the discovery of methotrexate in 1948 and its efficiency in treating children with leukemia removed any remaining doubts about the power of chemotherapy.[17] Following these findings, many new anticancer drugs were discovered in the 1950s, including the thiopurines (e.g., 6-thioguanine) in 1951 and 5-fluorouracil in 1958, the latter of which remains the cornerstone of today’s colorectal cancer treatment.[18,19]

In 1963, the discovery of the plant alkaloids vinblastine and vincristine from *Vinca rosea* provided a breakthrough for leukemia treatment.[20] Using these alkaloids, the rate of remission increased from 25% to 60% and natural product-based cancer therapeutics attracted considerable attention.[15] In 1971, the passage of the National Cancer Act in the United States launched a “war on cancer”[21] that led to the discovery and development of numerous chemotherapies over the following decades. Investment in cancer research in the United States increased from $9 million in 1972 to $119

million in 1980.[15] Among the many drugs discovered during this era, paclitaxel was reported in 1972 and approved by the FDA in 1993.[22]

## 1.2.2. An Arsenal of Weapons

Even though cancer therapies have improved tremendously over the past 70 years, many cancers still have low survival rates or do not respond well to current front-line therapies. Most notable among difficult-to-treat cancers are liver cancer, pancreatic cancer, and some forms of brain cancer.[23] Moreover, long-term treatment side-effects are a burden for patients and can cause the appearance of a second cancer. Drug resistance also represents an important concern in cancer therapy and a major barrier to improving survival for patients. Thus, access to a broad range of treatments is critical to coping with this delicate situation. Given that DNA replication, transcription, and protein synthesis are the major pillars of cellular growth and division, many chemotherapeutics target these processes. Similarly, RNA, enzymes, and other proteins represent compelling targets for anticancer drug development. Below, several classes of chemotherapeutics used for the treatment of cancers are described.

A key class of chemotherapeutics are the angiogenesis inhibitors.[24] As tumors grow and metastasize, they require a large supply of nutrients. Ultimately, tumor growth relies on the development of its own blood supply. Angiogenesis inhibitors reduce the production of pro-angiogenic factors that help with vascularization and therefore block vascularization of the tumor microenvironment. A commonly used angiogenesis inhibitor is axitinib (**1**), marketed as Inlyta® by Pfizer for kidney cancer (Figure 1.1).

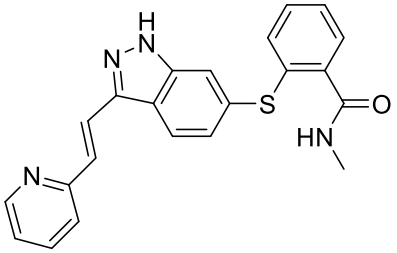


axitinib (**1**)

**Figure 1.1. Molecular structure of axitinib (1)**

A second important class of chemotherapeutics are DNA intercalators.[25] Here, insertion of the drug between DNA base pairs impacts the length and helical twist of a DNA strand. Interactions with DNA-associated proteins are then disturbed by the conformational changes to the DNA strand leading to inhibition of replication. For instance, doxorubicin (**2**), marketed as Adriamycin® by Pfizer is used to treat breast cancer, bladder cancer, lymphoma, leukemia, and Kaposi's sarcoma (Figure 1.2).

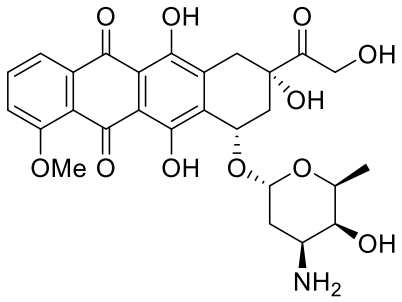


doxorubicin (**2**)

**Figure 1.2. Molecular structure of doxorubicin (2)**

DNA synthesis inhibitors aim to block DNA production by preventing folic acid use.[26] It is well-established that nucleobases and amino acids are crucial building blocks in the *de novo* synthesis of DNA. Similarly, folate polyglutamates are essential in the *de novo* synthesis of nucleobases and amino acids by acting as monocarbon donors. The inhibition of dihydrofolate reductase leads to thymidine biosynthesis blockage. Amethopterin (**3**), marketed as Methotrexate® by Pfizer acts as a folic acid antagonist for breast cancer, leukemia, lung cancer, lymphoma and osteosarcoma (Figure 1.3).

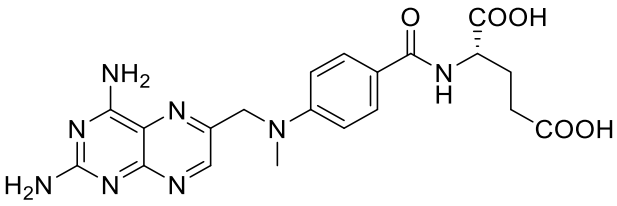


amethopterin (**3**)

**Figure 1.3. Molecular structure of amethopterin (3)**

Transcription regulators represent a powerful class of chemotherapeutics[27] as tumors often require an elevated level of transcription for survival and to maintain uncontrolled growth. By disrupting transcription factors (TF), cancer cells are more susceptible to apoptosis.[28] Palbociclib (**4**), marketed as Ibrance® by Pfizer for the

treatment of breast cancer is an inhibitor of the cyclin-dependent kinases CDK4 and CDK6 (Figure 1.4).

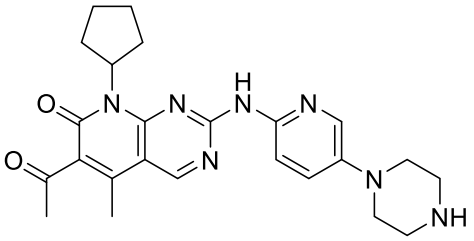

palbociclib (**4**)

**Figure 1.4. Molecular structure of palbociclib (4)**

Numerous additional enzymes are crucial for tumor growth and selective inhibitors of these enzymes provide important weapons in cancer chemotherapy.[29] For example, a high level of estrogen is beneficial to breast cancer proliferation by increasing mutations and/or affecting DNA repair pathway. It has been shown that the inhibition of estrogen synthetase results in a dose-dependent decrease in the level of estrogen. In breast cancer, where estrogen synthetase is abundant, inhibitors of this enzyme have proven to be effective treatments. For example, the estrogen synthetase inhibitor formestane (**5**), marketed as Lentaron® is commonly used to treat breast cancer (Figure 1.5).

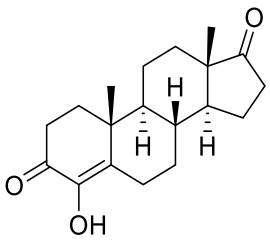

formestane (**5**)

**Figure 1.5. Molecular structure of formestane (5)**

Targeting cancer-specific gene regulation has also led to an important class of chemotherapeutics.[30] For example, histone deacetylases (HDACs) are overexpressed in many cancers and inhibit the expression of tumor suppressor genes. Inhibitors of these HDACs have now become front-line anticancer agents. Vorinostat (**6**) has been commercialized under the name of Zolinza® by Merck for the inhibition of HDACs in lymphomas (Figure 1.6).

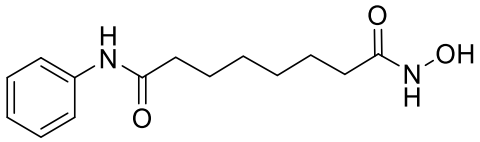

vorinostat (**6**)

**Figure 1.6. Molecular structure of vorinostat (6)**

Finally, microtubule targeting agents (MTAs) also represent an important class of cancer drugs.[31] By binding to microtubules, these agents interfere with mitotic spindle formation thus leading to the inhibition of mitosis and early apoptosis. Paclitaxel (**7**) belongs to this class of cancer drugs and is sold under the brand name Taxol® by Bristol-Myers Squibb and used for the treatment of several cancers including lung, breast and ovarian (Figure 1.7).

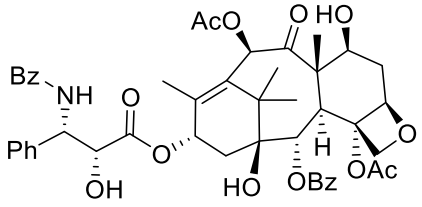

paclitaxel (**7**)

**Figure 1.7. Molecular structure of the MTA paclitaxel (7)**

## 1.3. Immunotherapy

The immune system is composed of white cells, organs and lymph tissues whose purpose is to “detect and destroy” foreign bodies that can include bacteria and viruses. Although the immune system is also effective at detecting and destroying abnormal cells, some tumors develop complex strategies to evade detection. For example, cancer cells can undergo genetic changes or display specific proteins on their surface that turn the immune system off or alter the behavior of healthy cells in their vicinity to confuse the immune system.

### 1.3.1. History

The concept of immunotherapy can be traced back to China’s Qin dynasty around the 3rd century. Here, the use of *variola* inoculation was explored to prevent smallpox.[32] Many centuries later, the Father of Immunotherapy, William B. Coley,

clarified the concept and became the first surgeon to harness the immune system for treating cancer in 1891. Remarkably, Coley noticed that several patients with cancer had a spontaneous remission after developing an *erysipelas* bacterial infection. From there, he performed several inoculations of live and inactivated mixtures of *Streptococcus pyogenes* and *Serratia marcescens* into the patient's tumors. Quite remarkably, a durable remission was observed in patients suffering from sarcomas, lymphomas and testicular carcinomas.[33] Unfortunately, the prospect of infecting a patient to treat cancer was not well received by the scientific community. Consequently, surgery and radiation therapy remained the standard course of treatment for several decades.[34] Similar strategies did not resurface until 1976 when BCG (*Bacillus Calmette-Guerin*) was used to treat bladder cancer.[35]

In 1957, the theory of cancer immunosurveillance provided a path for the use of immunotherapy in oncology.[36] Indeed, Thomas and Burnet proposed that lymphocytes played a crucial role in the identification and elimination of mutated cells.[37] A further key advance occurred in 1976 when the T-cell growth factor interleukin 2 (IL-2) was discovered, and *in vitro* culture of T-cells became accessible. Injection of a high dosage of IL-2 to cancer patients appeared to be very effective.[38] In 1991, the FDA approved the first immunotherapeutic treatment for metastatic kidney cancer. In the 1970s, the production of monoclonal antibodies by Milstein and Kohler also led to the development of rituximab that was approved in 1997 for the treatment of non-Hodgkin's lymphomas.[39] The development of vaccines for cancer offers many advantages over chemotherapeutics and in 2010 sipuleucel-T became the first FDA-approved vaccine for castration-resistant prostate cancer.[40]

### 1.3.2. Classes of Immunotherapeutics

Immunotherapies are divided into five distinct categories. The first involves the injection of immune checkpoint inhibitors with an aim to eliminate the normal barriers established by a patient's immune system and allow an above-normal immune response.[41] Natural immune cells are then able to overload cancerous cells with effector cells. Pembrolizumab, also known as Keytruda and marketed by Merck, is used to treat several indications such as lung and neck cancer via this mechanism.

Another important class of immunotherapy relies on T-cell transfer.[42] Here, a tumor biopsy allows for a thorough analysis of the most effective immune cells. Then, a patient's T-cells are genetically engineered with a chimeric antigen receptor (CAR) to recognize and target a specific protein on the cancer cells. These CAR T-cells are grown and multiplied before being injected into the patient's bloodstream. Depending on the half-life of the engineered T-cells, regular injections are necessary. In 2017, tisagenlecleucel sold under the brand name Kymriah became the first FDA-approved treatment that included a gene therapy step in the United States. Similarly, vaccine technology is gaining recognition as a method to boost patients' immune systems. Here, cancer-specific antigens are selected and encoded into cassettes to create a personalized vaccine that triggers the formation of cancer-specific B-cells, T-cells and antibodies.[43]

Immune system modulators also represent a valuable class of cancer treatments and function by enhancing the body's immune system response through specific cytokine release.[44] For instance, interleukins (IL) and interferons (IF) boost and trigger the activation of white cells and slow abnormal cell growth.[45] Likewise, hematopoietic growth factors reduce chemotherapy side effects by promoting the growth of damaged blood cells. [46] For example, erythropoietin increases the production of red blood cells,[47] IL-11 the production of platelets[48] and GM-CSF (Granulocyte-macrophage colony-stimulating factor) the count of white blood cells.[49] Interleukin 2, also known as Aldesleukin, was the first FDA approved cytokine for the treatment of metastatic renal cancers and melanomas.[50]

Finally, monoclonal antibodies (mAbs) constitute the last class of immunotherapy and will be thoroughly discussed in *Chapter 3*. Although all checkpoint inhibitors are also monoclonal antibodies and have been discussed above, this last category gathers all mAbs as a whole. Indeed, antibodies possess several functions such as blocking vital molecules to reach cancer cells, flagging cancer cells for natural killers and delivering harmful substances to cancer cells (e.g., antibody-drug-conjugates (ADCs). Antibodies are proteins that can be designed to identify and bind to specific cellular targets. Their binding triggers a cascade of events that leads to the destruction of the targeted cells. The effectiveness of this approach relies on several factors, one of which involves the interaction between the antibody fragment crystallizable (Fc) region and its corresponding receptors on the effector cells. This interaction can be modulated

by alterations to the *N*-glycan present on the antibody Fc region and thus lead to more effective therapies. For instance, trastuzumab known as Herceptin® and commercialized by Roche is a very effective treatment in patients suffering from breast cancer.

## 1.4. At the Border of Immunotherapy/Chemotherapy

### 1.4.1. Natural Products as Drug Leads

With advances discussed above, medical intervention for the treatment of cancer is at its zenith. However, not long ago, the probability of surviving cancer or indeed many other common illnesses was low. Adaptation to disease relied on individuals taking advantage of their surroundings. The first record of a sophisticated medicine system dates from 2600 BCE at which time roughly 1000 plants were commonly used as medicine in Mesopotamia.[51] Similarly, Egyptians, Chinese, Greeks, Romans, Arabs, and many other civilizations have long used plants for medicinal purposes.[52] Not surprisingly, those plant-based systems still play a significant role in society. Indeed, according to the WHO, about 65% of the world population relied on plant-based medicine in the 2000s for their primary healthcare.[53]

With the advent of the self-contained underwater breathing apparatus (SCUBA), the world's oceans have become a second major source of natural medicines. Indeed, more than 250,000 species have been described from our oceans, many of which produce secondary metabolites that have proven to be a rich source of drug leads.[54] Among these are several cytotoxins that have found a prominent role in cancer treatment such as bryostatin-1 (**8**) and salinosporamide A (**9**) (Figure 1.8).[55] Similarly, the serendipitous discovery of penicillin from a microorganism in 1928 prompted intensive investigation of various sources such as fungi and bacteria as a source of structurally-innovant bioactive agents.[56] These later efforts have led to the discovery of numerous antibacterial agents including the cephalosporins, as well as immunosuppressive agents, cholesterol-lowering agents, and antiparasitic drugs such as ivermectin.[57]

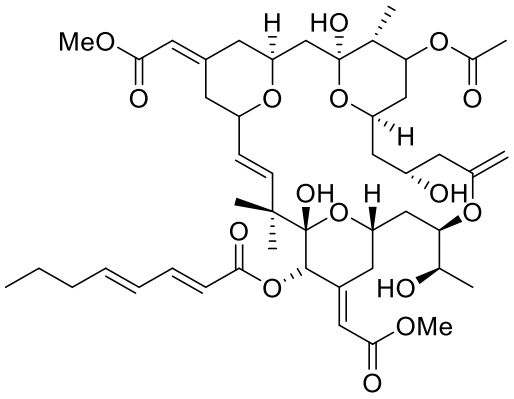


bryostatin-1 (**8**)

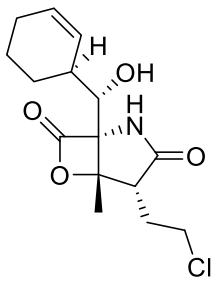


salinosporamide A (**9**)

**Figure 1.8. Example of natural products displaying anticancer activity**

A recent summary of new chemical entities (NCEs) introduced into clinical use from 1981 to 2010 reveals that 54 % of the 1355 NCEs introduced during that time frame were derived from natural products or designed based on a natural product pharmacophore.[58] However, natural product-based discovery was largely deemphasized in the 1990s by the pharmaceutical industry due to the development of new laboratory techniques. Indeed, the widespread use of high-throughput screening (HTS) against defined molecular targets prompted many companies to move from natural product libraries to more “screen-friendly” synthetic libraries.[59] The advent of combinatorial chemistry offered the prospect of rapidly synthesizing simple and more drug-like libraries of wide chemical diversities.[60] Additionally, slow and steady abandonment of infectious disease programs, a traditional area of strength for natural products, further emphasized this phenomenon.[61]

The number of newly discovered natural products has continued to increase from relatively few compounds per year in the 1940s to an average of ~1600 per year over the last two decades. More specifically, the rate of increase of newly reported compounds was the greatest from the 1970s through the mid-1990s (i.e., almost doubling every decade) and is believed to be triggered by a general enthusiasm fueled by the success of antibiotics discovery programs combined with the advent of improved instrumentation techniques such as NMR spectroscopy, mass spectroscopy and HPLC that contributed to rapid isolation and characterization. Although major pharmaceutical companies have largely exited the field of natural product discovery, the number of newly reported natural products remains steady and can be explained by the increasing globalization of natural product research in emergent countries (e.g., China, Brazil,

India).[62] However, the raw number of newly discovered natural products does not provide any information regarding the structural novelty of these compounds. The Linington group recently published an article in which they calculated and compared the Tanimoto similarity scores (i.e., algorithm that gives a number comprised between 0 and 1 that represents the percentage of chemical structure similarities in a given pair of molecules) between all molecule pairs of a dataset comprising all microbial and marine-derived natural products reported between 1941 and 2015.[62] Their work showed that the median Tanimoto scores rapidly increased from the 1950s (~0.3) to the 1980s (~0.6) where it finally reached a plateau (~0.65). These results might suggest that the natural products space has been largely described and that newly discovered natural products are likely to be derivatives of known molecules. However, numerous molecules in this dataset are unique with unprecedented structural and/or functional attributes which led the Linington group to also evaluate the distribution of molecules with low Tanimoto scores ($T < 0.4$). This analysis showed that the number of discovered molecules with low similarities remained high (i.e., ~300 in 1990) and has been consistent since the origins of this field. However, the number of structurally unique compounds represents a decreasing percentage of the total number of compounds isolated from natural sources, suggesting that a high percentage of newly discovered entities constitute derivative structures (Figure 1.9). While rediscovery has tempered enthusiasm in natural products, it is also well appreciated that subtle structural changes can have dramatic effects on compound potency. Thus, the discovery of new active natural products within a known structural subclass can still be profitable as long as they possess unique attributes from a biological standpoint. Additionally, many diseases such as HIV, cancers, and other infectious diseases are yet to be cured despite generating numerous libraries of synthetic compounds. As Danishefsky stated in 2002, *"a small collection of smart compounds may be more valuable than a much larger hodgepodge collection mindlessly assembled"*.[63] The complexity and molecular diversity of natural products coupled with their highly selective and specific biological activities continue to make them essential to drug discovery.

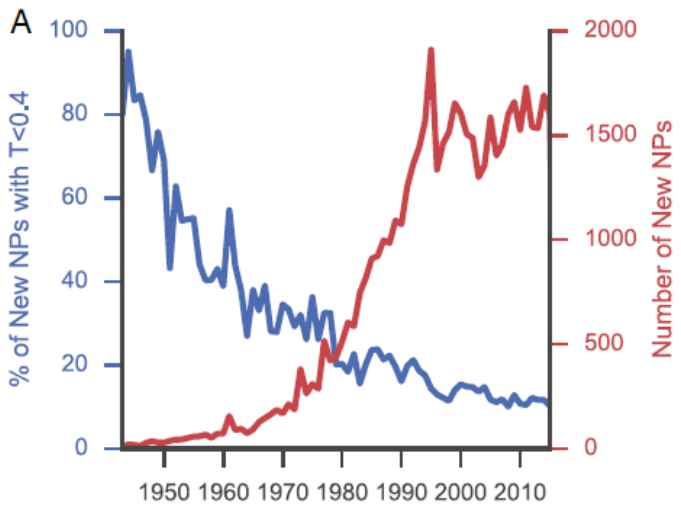


**Figure 1.9. Examining structural diversity[62]**
Note: Examining structural diversity. Number of compounds published per year and rate of novel compound isolation as a percentage of total natural product isolation. This graph was adapted from ref. 62 with permission.

## 1.4.2. Antibody-Drug Conjugates

Antibody-drug conjugates (ADCs) are an emerging class of anticancer treatment agents that combine the selectivity of targeted therapy with the potency of chemotherapy.[64] While the chemotherapy era that started in the 1940s offered new approaches to treat cancer, the use of chemotherapeutics is often complicated by factors such as high toxicity, narrow therapeutic window, and drug resistance. The emergence of monoclonal antibodies (mAbs) in the 1970s, provided a new avenue for cancer therapy. To date, around 30 mAbs have been approved by the FDA for this purpose.[65]

ADCs are made from three defined parts: an antibody, a linker, and a cytotoxin (Figure 1.10).[66] Once a protein target (antigen) is selected, it is then necessary to design the corresponding monoclonal antibody that will bind to the antigen. This target should be specific to non-healthy cells or at minima, be largely overexpressed by tumor cells. Furthermore, the target must have an extracellular epitope capable of internalizing the cytotoxin through a specific binding with the antibody.[66] The second essential piece is the active ingredient attached to the linker. Those toxins usually have a very low $IC_{50}$ (sub-nanomolar range in cell culture) and target tubulin or DNA. The high potency of these compounds is essential as only a small portion of the drug will be internalized.

Among other key determinant factors, the molecular structure of the drug must allow for conjugation with the third piece of the ADC: the linker. The main role of the linker is to connect the cytotoxic payload to the monoclonal antibody and maintain this conjugate in a stable state. Usually, linkers are labile in the intracellular environment and undergo enzymatic cleavage and release of the cytotoxic payload once the ADC is internalized.

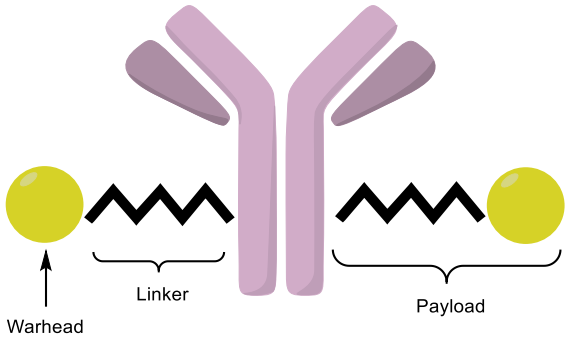


**Figure 1.10. Antibody-drug conjugate (ADC)**

Even though ADCs have been under investigation for decades, the first treatment to be approved by the FDA and the European Medicines Agencies (EMA) was brentuximab vedotin in 2011 (MTA: monomethyl auristatin E (MMAE) (**10**)). This was made possible thanks to significant advances in the development of linker technologies. After the first approval in 2011, a second ADC called ado-trastuzumab emtansine (ATE) was approved by the FDA and the EMA in 2013. ATE binds to HER2 receptors that are overexpressed in metastatic breast cancer and consequently release a microtubule targeting agent (MTA) known as mertansine (**11**) (Figure 1.11). After that, three more ADCs approvals occurred in 2017 and 2019. Currently, more than 100 ADCs are in various stages of clinical development for treating solid tumors or hematological malignant diseases.[67] With the clinical benefits that ADCs bring to patients (e.g., better therapeutic window, reduction of non-specific toxicities and overcoming drug resistance), these numbers are expected to grow over time.

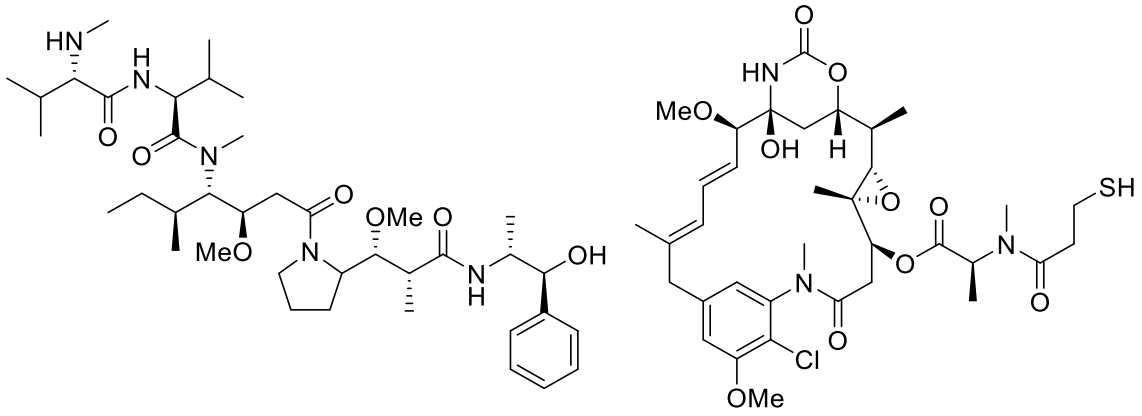


**Figure 1.11. Structure of MMAE (10) and mertansine (11)**

## 1.5. Thesis Overview

The primary focus of the research described in this thesis is the synthesis of biologically active compounds that directly or indirectly target cancerous cells. Specifically, this thesis describes efforts to i) synthesize a natural product with anticancer properties (direct) to enable further testing in animals and ii) synthesize small molecules that improve the production of antibodies designed for treating cancer (indirect).

*Chapter 2* describes the total synthesis of eleutherobin (**12**), a natural product with potentially useful anticancer activity (Figure 1.12). Eleutherobin (**12**) was originally extracted from an Australian soft coral (*Eleutherobia sp.*) in 1997[68] and reported as a microtubule targeting agent (MTA). Preliminary biological testing identified eleutherobin to be a potent microtubule-stabilizing cytotoxin ($IC_{50}$ = 10 nM).[69] Unfortunately, the lack of natural material hampered further development. To support the evaluation of eleutherobin (**12**) as a cancer therapy, a reliable and scalable method of production is required, which will ultimately rely on the development of a short and efficient synthesis. While two total syntheses[70,71] and one formal synthesis[72] of eleutherobin have been reported, their overall length and low yield have complicated their use for eleutherobin production. A concise synthesis of eleutherobin (**12**) would also engender access to structural analogs that may further improve its biological properties.

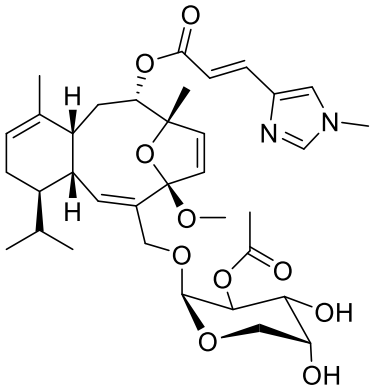

eleutherobin (**12**)

**Figure 1.12. Molecular structure of eleutherobin (12)**

Several strategies for the synthesis of the main core of eleutherobin (**12**) have been investigated and are described. Previous work in the Britton group successfully constructed valuable tetralone intermediates on a multi-gram scale via an unprecedented palladium-catalyzed α-arylation reaction/Friedel-Crafts cyclization strategy.[73] The first approach described in *Chapter 2* represents a continuation of previous efforts directed towards the formation of the large (10-membered) ring by a fragmentation approach. The second part of *Chapter 2* presents a new strategy in which the 10-membered ring is constructed through the addition of a vinyl anion onto an unsaturated lactone. The final part of *Chapter 2* describes our ultimately successful efforts directed towards ring formation by an exotic Knoevenagel condensation reaction.

*Chapter 3* describes the synthesis of inhibitors of fucosyltransferase that may be useful for the production of afucosylated antibodies, which have proven to be more effective as cancer therapeutics. Here, the endocyclic oxygen of the carbohydrate fucose is replaced with a methylene group, forming carbafucose **13** (Figure 1.13). When added to feedstock used in antibody production, carbafucose **13** caused a 70% decrease in fucosylated antibodies. In addition, several analogs of carbafucose were prepared to assess their effect on antibody fucosylation.

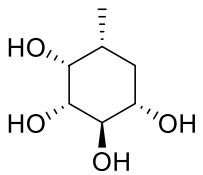

(**13**)

**Figure 1.13. Molecular structure of carbafucose (13)**

# Chapter 2.

# Eleutherobin

## 2.1. Introduction

### 2.1.1. Microtubules: Important Target for Cancer Therapy

Microtubules (MTs) ─ key components of the cytoskeleton ─ are protein polymers that play an essential role in various cellular processes of eukaryote cells including cell signaling, intracellular transport (e.g., mitochondria and other components), and maintenance of cell shape and cell division (i.e., meiosis, mitosis).[74] Microtubules are comprised of polymerized α- and β-tubulin heterodimers that are rigorously arranged into protofilaments (several μm long). The minus-end of microtubules is characterized by a layer of α-tubulin whereas the opposite end includes a terminal layer of β-tubulin subunits and is called the plus-end. MTs are highly dynamic polymers that are synthesized via a mechanism similar to crystal growth involving a nucleation phase that involves the spontaneous formation of a stable aggregate of tubulins monomers known as the nucleus. Next, an elongation phase is promoted through the reversible addition of heterodimers onto the preformed nucleus.[75] To display a broad range of functional diversity, differentiation of microtubules is also required. For instance, tubulin isotypes (i.e., 6 α-tubulin and 7 β-tubulin in humans) and post-translational modifications (e.g., phosphorylation, glycosylation) can have profound effects on stability and rate of formation, thus modulating their intrinsic functions within the cell.[76] Similarly, microtubule-associated proteins (MAPs) play a significant role in defining the role of microtubules. Indeed, MAPs can foster specific interactions between the protofilaments and intracellular proteins that ultimately confer specific activities in various biological processes.[77]

The biological function of MTs is determined and regulated in large part by their polymerization dynamics.[78] The most common dynamic behavior is known as “dynamic instability” and describes the process in which individual microtubules switch randomly between slow-growing and rapid-shrinking cycles via transition phases.[79] The presence- or absence- of a GTP cap (i.e., tubulin-GTP) on tubulin at the plus-end stabilizes- or

destabilizes- the microtubule, thus promoting growth or shrinkage accordingly.[80] The association/dissociation rate can be altered by the presence of specific regulatory proteins or drugs that impact polymerization dynamics and consequently, microtubule function.[81] When the dynamics of tubulin polymerization switch from growth to shrinkage the situation is referred to as a "catastrophe", while the reverse is termed a "rescue". The second major dynamic behavior is referred to as treadmilling and describes the process in which one end of the microtubule is lengthening while the other is shrinking.[82] This behavior is caused by a difference in tubulin subunit concentration (α- and β- tubulins) between the microtubule extremities thus triggering the migration of tubulins from one end to the other preserving the overall polymer mass balance. Notably, both dynamic instability and treadmilling behaviors do not conflict but take place simultaneously.

The visualization of mitotic-spindle microtubules has emphasized the importance of rapid microtubule dynamics for successful mitosis by allowing for a broad reorganization of the entire microtubule network.[83–85] For instance, microtubules are responsible for chromosome attachment at the kinetochore during prometaphase (Figure 2.1a), their alignment during metaphase (i.e., congression) (Figure 2.1b), as well as their separation in anaphase and telophase (Figure 2.1c/d). The non-attachment of a single chromosome to the spindle is sufficient to prevent cell division. This feature is of particular interest for the treatment of cancer, where disruption of cell-regulatory mechanisms leads to uncontrolled growth. By carefully monitoring their density, healthy cells can regulate their own growth rate. Indeed, once the maximum density threshold is reached (determined by growth factors), normal cells automatically become quiescent and unable to further proliferate by entering their resting state (i.e., $G_0$). In contrast, mutated cells rarely respond to this regulated mechanism, and thus grow frenetically and attain high-cell densities.[86] Considering these disparities in cell growth (i.e., normal vs cancer cells), mitosis inhibition is considered one of the most efficient strategies to slow or stop the spread of cancer. For instance, when human osteosarcoma cells are incubated with 10 nM paclitaxel (Figure 2.1e) and 50 nM of vinflunine (Figure 2.1f), two compounds that disrupt microtubule dynamics, the mitotic process is impacted.[87] Indeed, in both cases the chromosomes remain at the spindle pole consequently triggering programmed cell death (i.e., apoptosis). These cells were imaged by confocal

microscopy and published in *Nature Reviews* by Mary Ann Jordan and Leslie Wilson in 2004.

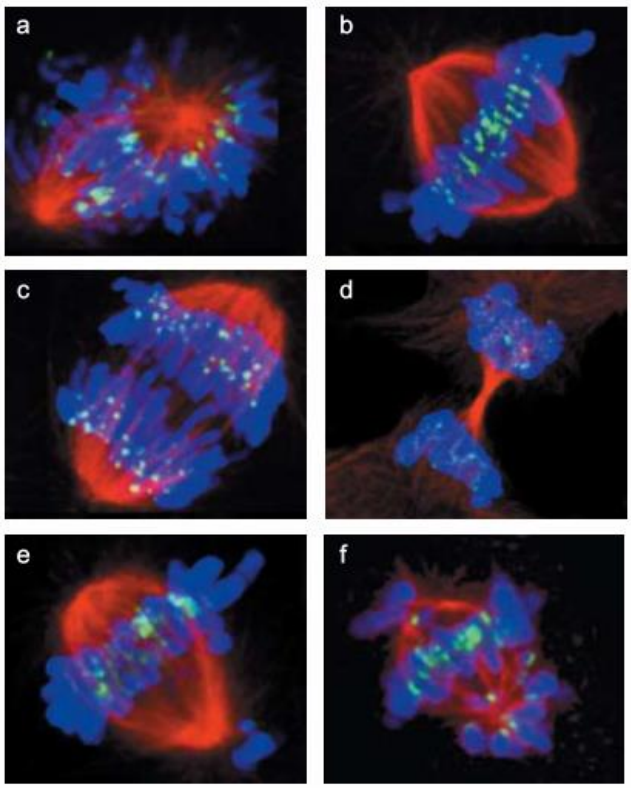


**Figure 2.1. Human osteosarcoma cells in different stages of the mitosis**[87]
Note: Microtubules are shown in red, chromosomes in blue, and kinetochores in green. a) At prometaphase, the nuclear envelope has broken down, chromosomes are condensed. b) In early metaphase, chromosomes have congressed to the equator to form the metaphase plate. c) In anaphase, the duplicated chormosomes have separated and are moving towards the spindle poles. d) In telophase, the separated chromosomes have reached the spindle poles. e) In the presence of 10 nM paclitaxel, some chromosomes remain at the spindle poles and have not congressed to the metaphase plate. f) Similarly, in the presence of 50 nM vinflunine some chromosomes remain at the spindle poles. This graph was adapted from ref. 87 with permission.

MTAs are separated into two different subclasses: microtubule-stabilizing agents (MTSAs) and microtubule-destabilizing agents (MTDAs). Microtubule-destabilizing agents inhibit the polymerization of tubulin and consequently disturb the dynamic behavior of the microtubules.[88] Among them, vinblastine (**14**), vinflunine (**15**) belonging to the *Vinca* alkaloids family but also, eribulin (**16**), colchicine (**17**), combretastatin (**18**), and some other members have been discovered (Figure 2.2a). Microtubule-stabilizing agents such as paclitaxel (**7**), epothilones (A-(**19**), B(**20**)) discodermolide (**21**), and some others promote microtubule polymerization (Figure 2.2b).[88] Notably, the differentiation between stabilizing and destabilizing agents does

not impact their mechanism of action. Indeed, it has been shown that, at lower concentrations, microtubule dynamics are suppressed without affecting the polymer mass, meaning that the sole disruption of microtubule spindle dynamic blocks the mitosis.[87]

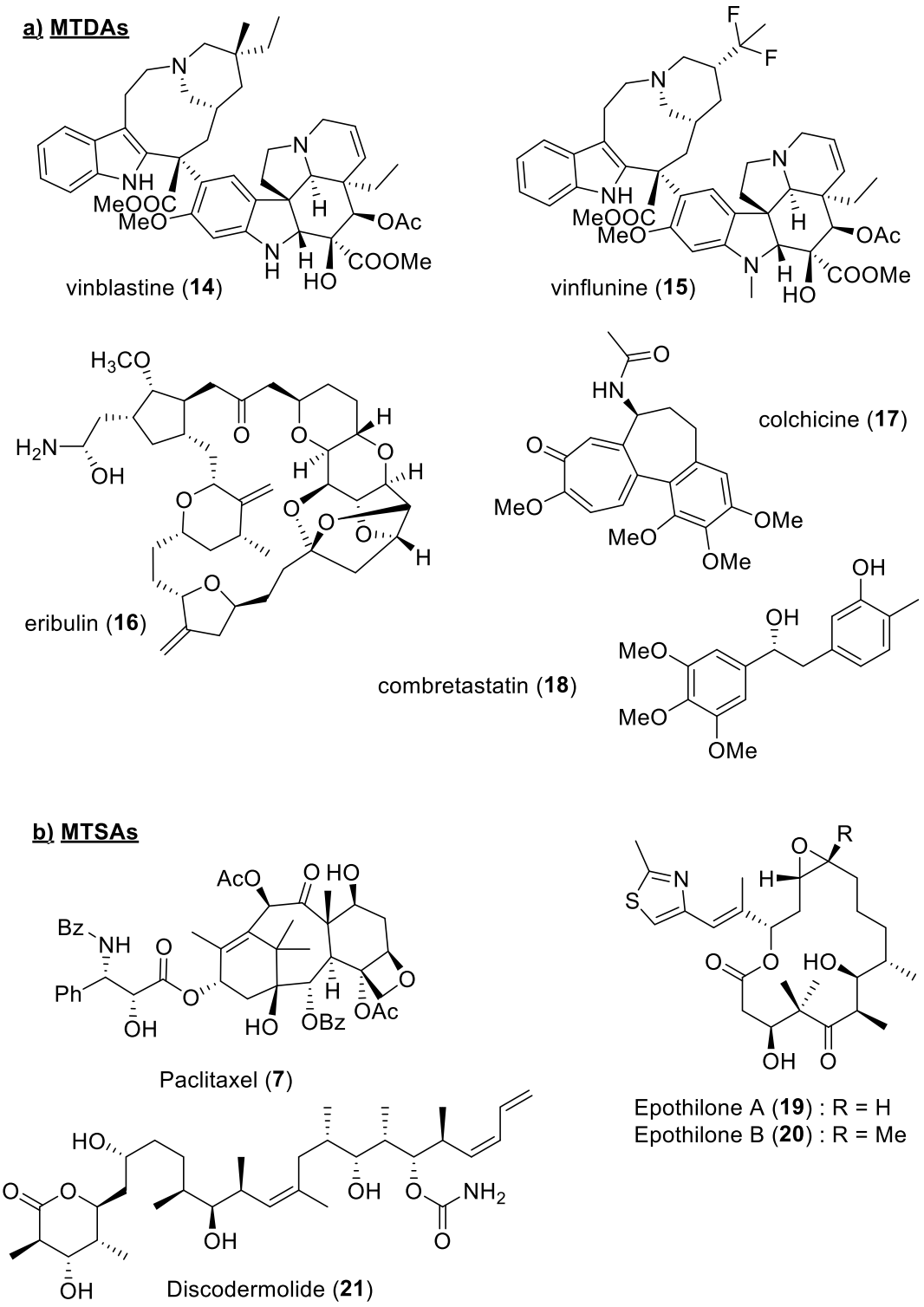


**Figure 2.2. Examples of MTDAs and MTSAs**

Presently, three MTA binding sites have been discovered and are all located on β-tubulin subunits as depicted in Figure 2.3 published in *Nature Reviews* by Mary Ann Jordan and Leslie Wilson in 2004. The drugs falling in the "*Vinca* binding-domain"[89] bind

to both soluble tubulin and microtubules rapidly and reversibly. Only one or two molecules per microtubules are sufficient to reduce the MT's dynamic behavior (treadmilling and dynamic instability) by 50%.[87] The "paclitaxel" binding site is located on the inside surface of the microtubule. This site has accurately been determined with an electron crystal structure of a tubulin/paclitaxel complex. It is also believed that passive diffusion through the microtubule lattice enables paclitaxel-like drugs to reach the internal surface of the polymer.[90] Finally, the "colchicine domain" is found on soluble tubulin.[91] Binding to this domain induces conformation change that inhibits the dynamics of tubulin polymerization, thus ultimately leading to apoptosis.

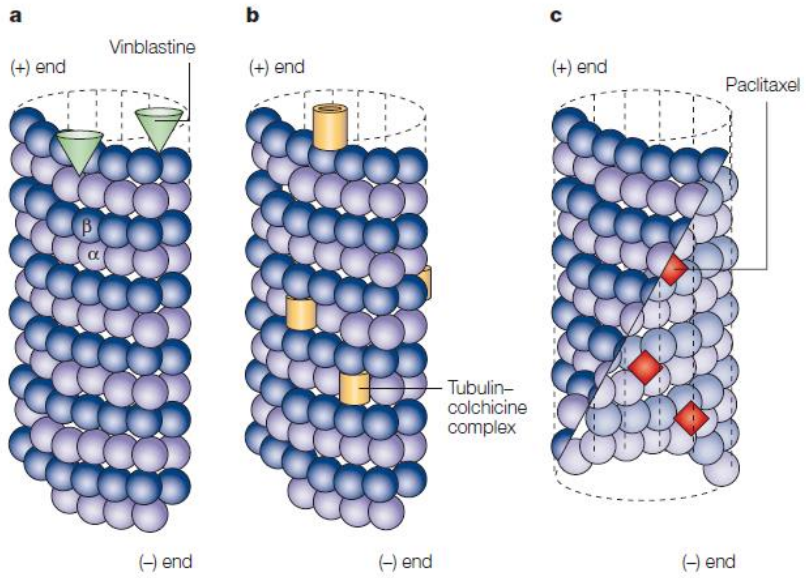


**Figure 2.3. Antimitotic drugs binding sites on microtubules[87]**
Note: a) Vinblastine molecules are bound to high-affinity sites at the microtubules plus end suffice. b) Colchicine forms complexes with tubulin dimers and copolymerizes into the microtubules lattice. c) Paclitaxel binds along the interior surface of the microtubule. These different binding-types lead to a similar outcome: suppression of microtubule dynamics. This graph was adapted from ref. 87 with permission.

Although cancer therapies involving MTAs have proven effective for decades, numerous questions regarding their mechanism of action, cancer sensitivity and susceptibility to resistance mechanisms remain unanswered. For instance, epothilone A (**19**) is highly effective against breast cancer and non-Hodgkin's lymphoma but ineffective against numerous tumors such as colorectal, melanoma and ovarian cancer.[92] Similarly, V*inca* alkaloids are a very potent class of therapeutics used in the treatment of hematological cancers but are mostly ineffective against solid tumors.[87] These limitations emphasize the need to gain additional insights into the characteristics

of individual tubulin-targeting antimitotic drugs to ultimately inform the development of better cancer therapies. For instance, it is now well understood that a class of membrane transporter proteins (MTPs) called ABC-transporters is associated with the failure to respond to MTAs. Amongst these MTPs, P-glycoprotein (P-gp)[93] serves to decrease intracellular drug concentrations through constant excretion into the extracellular matrix thus leading to cross-resistance (multidrug resistance (MDR)).[87,94] Unfortunately, there are currently no FDA-approved P-gp inhibitors though this approach is under intense investigation.[95–97] Several other pathways can also lead to multi-drug resistance, including cancer's ability to manipulate microtubules' behavior. For example, the activity of the MTAs paclitaxel and vincristine can be diminished based on the predominant tubulin's isotype in specific cancer tissues.[98,99]

Despite the clear potential for MDR, microtubule-targeting agents have proven to be highly effective for the treatment of different types of cancers.[100] However, by virtue of their mechanism of action, these drugs also have toxic effects on healthy cells with the most common side-effects being neurological and hematological.[94] For example, peripheral neuropathy is a common side-effect and is characterized by weakness, numbness and pain most commonly in hands and feet. This is thought to come from the damage to the nerves outside of the brain or the spinal cord. When using *Vinca* alkaloids and taxanes, cranial neuropathy may also be observed in patients, which in turn causes different symptoms such as vocal cord dysfunction or jaw pain.[101] From a hematological standpoint, myelosuppression is a very serious side-effect of MTAs leading to decreases in the production of essential cells such as leukocytes, erythrocytes, and thrombocytes, which respectively results in immunosuppression, hypoxia and hemophilia. It is not a coincidence that hematopoietic and brain cells are more susceptible to being targeted by MTAs given that they are rapidly dividing.[94]

## 2.1.2. Eleutherobin

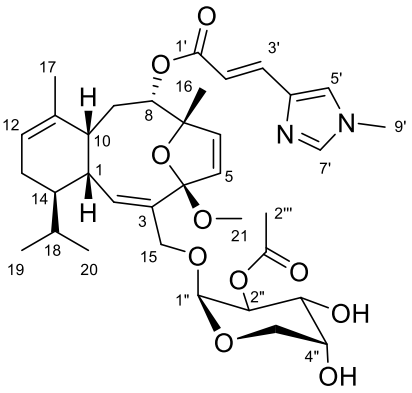


eleutherobin (**12**)

**Figure 2.4. Structure of eleutherobin (12)**

In 1997, Fenical and coworkers isolated a new diterpene glycoside from the soft coral *Eleutherobia sp.* collected off the coast of Western Australia and named it eleutherobin **(12)** (Figure 2.4).[68] Eleutherobin's structure and relative stereochemistry were elucidated through intense investigations involving 1D and 2D NMR spectroscopic experiments whereas its absolute chemistry was proven a couple of years later with the achievement of the first total synthesis.[68,70] Eleutherobin (**12**) belongs to a class of oxygenated cembranoid natural products named sarcodictyins (**23**), that arise from a C2-C11 cyclization and C5-C8 oxidation of cembranes (**22**) (Scheme 2.1).[102,103] This sarcodictyin family is comprised of the valvidones[104], sarcodictyins[105] and eleuthosides,[106] that of which possess a bicyclo[8.4.0]tetradecane carbocyclic skeleton as a common structural characteristic. Eleutherobin differs by the presence of a 2-acetylarabinose glycoside side chain at C15. Although a few members of the sarcodictyin family have been discovered, their promising biological profiles have attracted significant enthusiasm from the scientific community.

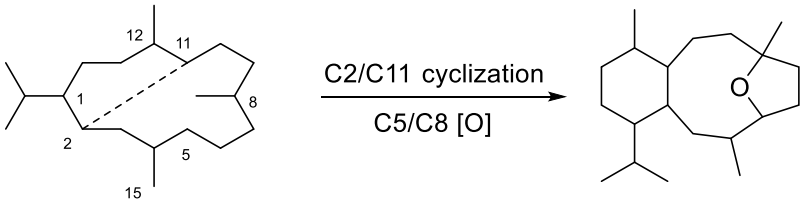


Cembranes (**22**) Sarcodictyins (**23**)

**Scheme 2.1. Proposed biological structure formation of sarcodictyins**

When eleutherobin was assayed for biological activities, significant cytotoxic effects were observed including the inhibition of the proliferation of different cancer cells such as breast, ovarian, renal and lung cancer cells ($IC_{50}$ ~ 10 nM).[107] Lindel *et al*. compared eleutherobin and paclitaxel activities in colon carcinoma (i.e., HCT116) and ovarian (i.e., A2780) cell lines. Additionally, both compounds were evaluated in MDR cell lines overexpressing P-glycoprotein (i.e., HCT116(VM46)) and cell lines containing mutated tubulins (i.e., A2780/Tax22).[107] Although eleutherobin was slightly less potent in HCT116 and A2780 cell lines, the cross-resistance effect of HCT116(VM46) and A2780/Tax22 were lower for eleutherobin compared to paclitaxel (e.g., 52 vs 117 and 4.3 vs 13.4). These findings indicate that eleutherobin could be a promising alternative for patients who developed resistance to paclitaxel (Table 2.1). Further evaluation of the inhibition mechanism revealed that eleutherobin binds and stabilizes microtubules. Interestingly, a competitive assay with labeled [$^3$H]paclitaxel demonstrated that eleutherobin and paclitaxel shared a common binding domain on microtubules, thus disrupting microtubule dynamic behaviors further leading to cell death.

**Table 2.1.** ***In vitro*** **cytotoxicity ($IC_{50}$) of eleutherobin and paclitaxel[107]**

| | Cytotoxic $IC_{50}$ (nM)[a] | | | |
|---|---|---|---|---|
| **compound** | **HCT116** | **HCT116(VM46)** | **A2780** | **A2780/Tax22** |
| **eleutherobin** | 10.7 | 554 (52)[b] | 13.7 | 59 (4.3)[b] |
| **paclitaxel** | 4.6 | 537 (117)[b] | 6.7 | 90 (13.4)[b] |

Note: [a] Cytotoxicity was determined after 72-h exposure. [b] value in parentheses is fold resistance relative to corresponding parental cell line.

Unfortunately, only small quantities of eleutherobin are available from natural sources and 5.3 kg of freshly collected specimens of *E. caribaeroum* (wet) were required to provide only 2 mg of eleutherobin (i.e., 0.000038% extraction yield).[108] Attempts in large-scale aquaculture of this coral failed to provide eleutherobin demonstrated that the natural living habitat of this coral has a tremendous impact on the biosynthesis of eleutherobin. Although intensive efforts have been directed towards eleutherobin structural modifications (e.g., hydrogenation, epoxidation, oxidation and protection), the amount of material provided by natural sources was not sufficient to support a thorough SAR study (e.g., glycoside and ester modifications) and *in vivo* testing.[109] To further assess the potential of eleutherobin as a chemotherapeutic agent and to develop a thorough screening of different substituent at the carbohydrate

domain, the development of a robust, concise and scalable total synthesis was deemed essential.

### 2.1.3. Previous Published Syntheses

#### *Nicolaou's Total Synthesis of Eleutherobin*

The first total synthesis of eleutherobin was reported in 1997 by Nicolaou and used (+)-carvone (**24**) as a cheap and commercially available starting material.[70,110] This terpenoid possesses one stereocenter bearing an isopropyl group allowing for enantioselective synthesis of eleutherobin (**12**). A series of well-established reactions generated intermediate **25** in 9 steps, which allowed for installation of the different functionalities required for the macrocyclization. Aldehyde **25** was converted to terminal alkyne **26** via 1,2 addition of ethyl vinyl ether followed by Grignard addition of the terminal alkyne. After a series of deprotection/oxidation steps, secondary aldehyde **27** was generated, providing a useful precursor for the functionalization of the second sidechain. With an aim to synthesize a 3-carbon chain aldehyde, a Knoevenagel condensation was performed in presence of ethyl cyanoacetate to provide **28**. Further reduction with DiBAlH provided allylic alcohol **29** that was in turn glycosylated with the arabinose moiety **30** to yield the advanced intermediate **31**. To perform the macrocyclization, alkyne **31** spontaneously reacted with α,β-unsaturated aldehyde under basic conditions. A subsequent sequence of oxidation/deprotection steps afforded macrocycle **32**. Selective hydrogenation of alkyne **32** in presence of Lindlar catalyst offered its corresponding alkene that spontaneously cyclized to form the cyclic hemiketal **33** that was further protected into methyl ketal **34**. Finally, esterification of the secondary alcohol with *N*-methylurocanic anhydride **35** followed by TBS deprotection with TBAF provided eleutherobin (**12**) (Scheme 2.2).

Nicolaou's synthesis not only provided a synthetic route to eleutherobin (**12**) but also confirmed the absolute stereochemistry and relative stereochemistry between the carbohydrate and the terpenoid domain. Overall, the synthesis required 28 steps with a yield of less than 1%, which renders the production of sufficient amounts of eleutherobin (**12**) to support further biological testing challenging.

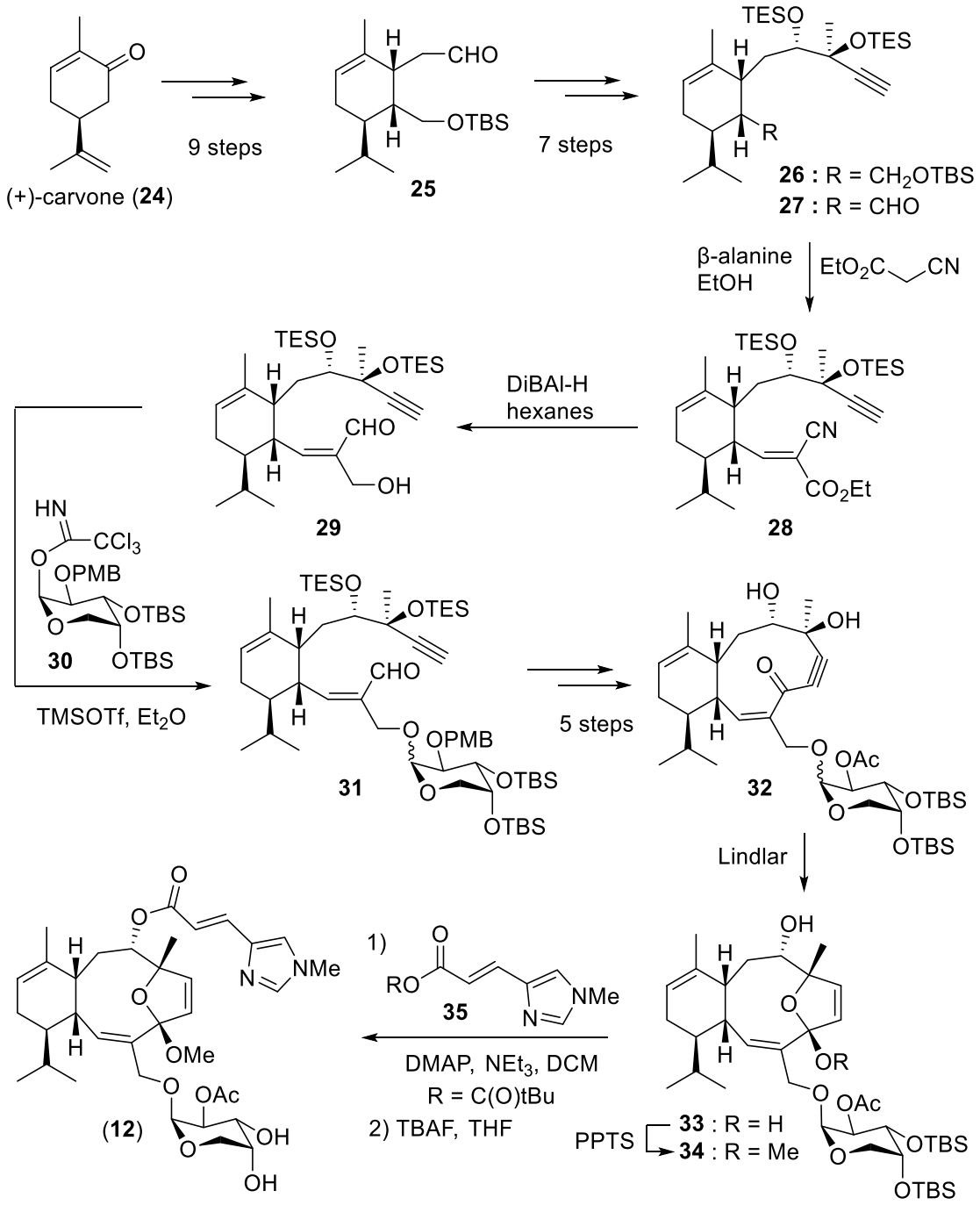


**Scheme 2.2. Nicolaou's total synthesis of eleutherobin (12)**

### *Danishefsky's Total Synthesis of Eleutherobin*

In 1999, Danishefsky reported a second total synthesis of eleutherobin[71,111,112] that started with (α)-phellandrene (**36**). Similar to (+)-carvone, this monoterpene has one defined stereocenter bearing an isopropyl group and is accessible as a single enantiomer. To build aldehyde **37**, a sequence of 4 reactions was performed including

an [2+2] addition of an *in situ* generated ketene, followed by cyclobutanone functionalization and fragmentation. Next, 2,5-dibromofuran was lithiated **38** and reacted with aldehyde **37** to yield the corresponding alcohol that was further protected with a TBDPS group to deliver **39**. At this stage, a one-carbon homologation was performed via a 4-step sequence involving a nitrile addition (i.e., nucleophilic substitution) followed by a subsequent reduction that provided aldehyde **40**, a precursor for the macrocyclization. The Nozaki-Hiyama-Kishi (HNK) coupling between the 2-bromofuran moiety and the aldehyde offered the corresponding alcohol which was further protected with pivalate while the TBDPS group was removed to generate **41**. The presence of the free hydroxyl group was crucial to achieving clean oxidation of the furan using DMDO in acetone. These conditions yielded hydroxypyranone **42** in a very good yield (94%). Subsequent protection of the acetal function before methyl addition on the carbonyl was essential to deliver **43** with a good yield (i.e., 86% vs 42%). Next, methyl acetal **44** was synthesized in a *one-pot* process. After a series of protecting group manipulations and oxidation steps, ketone **45** was reached. This ketone was anticipated to provide the required unsaturation via the formation of enol triflate **46**, which was further coupled with the corresponding tin-arabinose derivative **47** via a Stille coupling to yield **48**. Finally, TBS deprotection, esterification with methylurocanic acid (**49**) and ultimate arabinose deprotection led to eleutherobin (**12**). This synthesis provided 60 mg of eleutherobin in 25 linear steps with an overall yield of less than 1%. Outstandingly, this work relies on several key steps such as the use of a ketene [2+2] reaction to install C1-C10 stereochemistry, an NHK coupling for the macrocyclization, and a modified Stille coupling to install the arabinose moiety (Scheme 2.3).

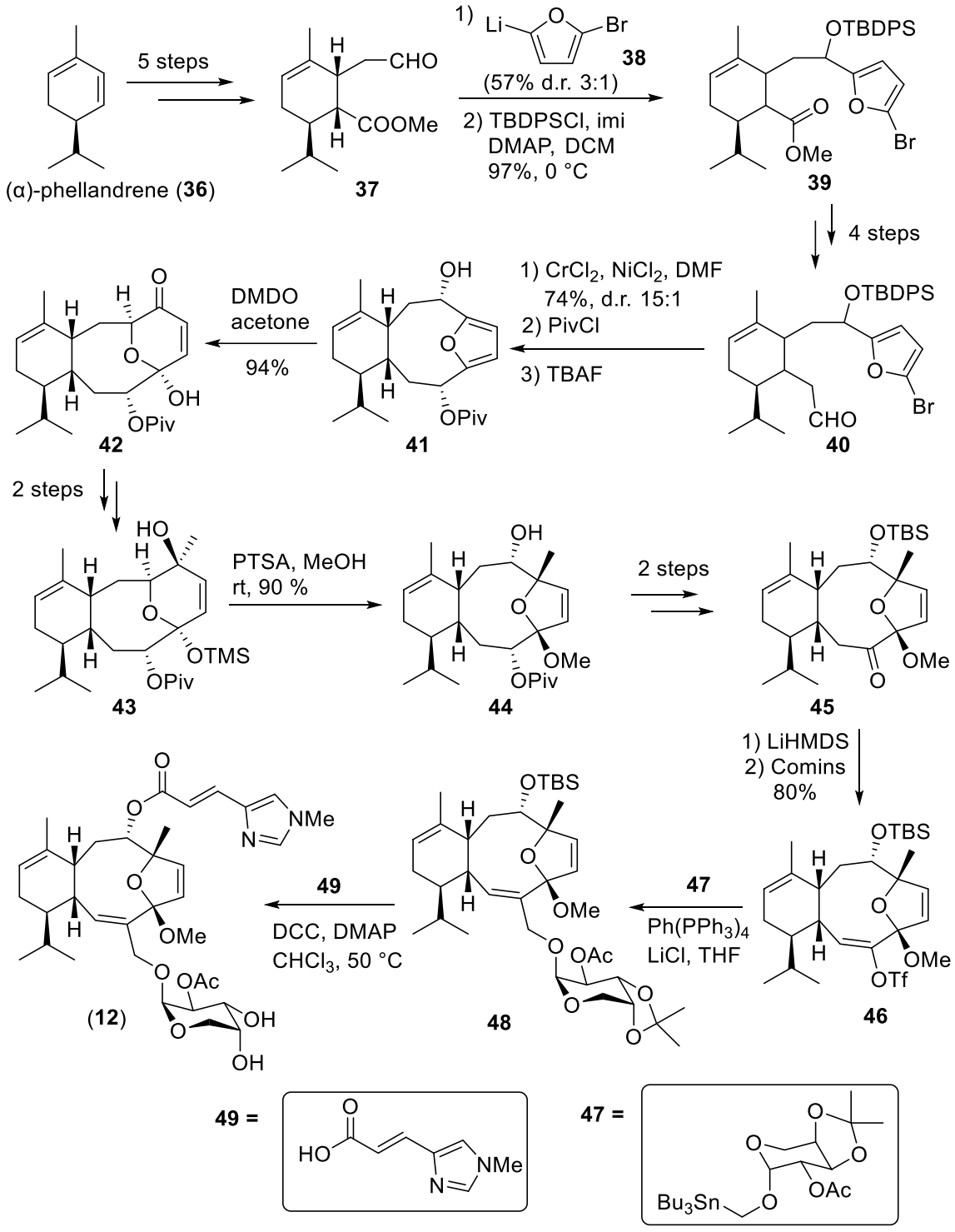


**Scheme 2.3. Danishefsky's total synthesis of eleutherobin (12)**

### *Gennari's Formal Synthesis of Eleutherobin*

In 2005, Gennari and coworkers developed a third approach for the synthesis of eleutherobin.[72] Their strategy relied on a ring-closing-metathesis reaction (RCM) to lead to Danishefsky intermediate **42**. To commence their synthesis, (+)-carvone (**24**) was transformed via a 6-step sequence into aldehyde **50**. To provide diene **56**, two sequential Hafner-Duthaler oxyallylation reactions were performed.[113] The first reaction was performed in the presence of titanium complex (*S*,*S*)-**51** and provided **52** as a single diastereoisomer in 73% yield. After a series of well-established reactions (i.e., deprotection, oxidation, $S_N2$ reaction, reduction), homologated aldehyde **54** underwent a second Hafner-Duthaler oxyallylation with titanium complex (*R*,*R*)-**55** to generate **56** as a single diastereoisomer. To evaluate the key step of the synthesis, the Piv-protected version of **56** was subjected to RCM conditions. More specifically, treatment with Grubb's second-generation catalyst **57** led to the kinetically favored (*E*)-**58** macrocycle. Subsequent PMP removal and allylic oxidation provided (*E*)-dione **59** that was further isomerized into the thermodynamically more stable isomer (*Z*)-**60** in presence of iodine. The presence of water after column chromatography led to the formation of bis-hemiacetal **61**. Finally, MOM deprotection delivered enone **42** that displayed a set of data that was in full agreement with that previously reported by Danishefsky.[71] This intermediate could be transformed to eleutherobin (**12**) in 10 additional steps. Overall, Gennari's synthesis of intermediate **42** was achieved in 20 steps with an overall yield of 4% (Scheme 2.4).

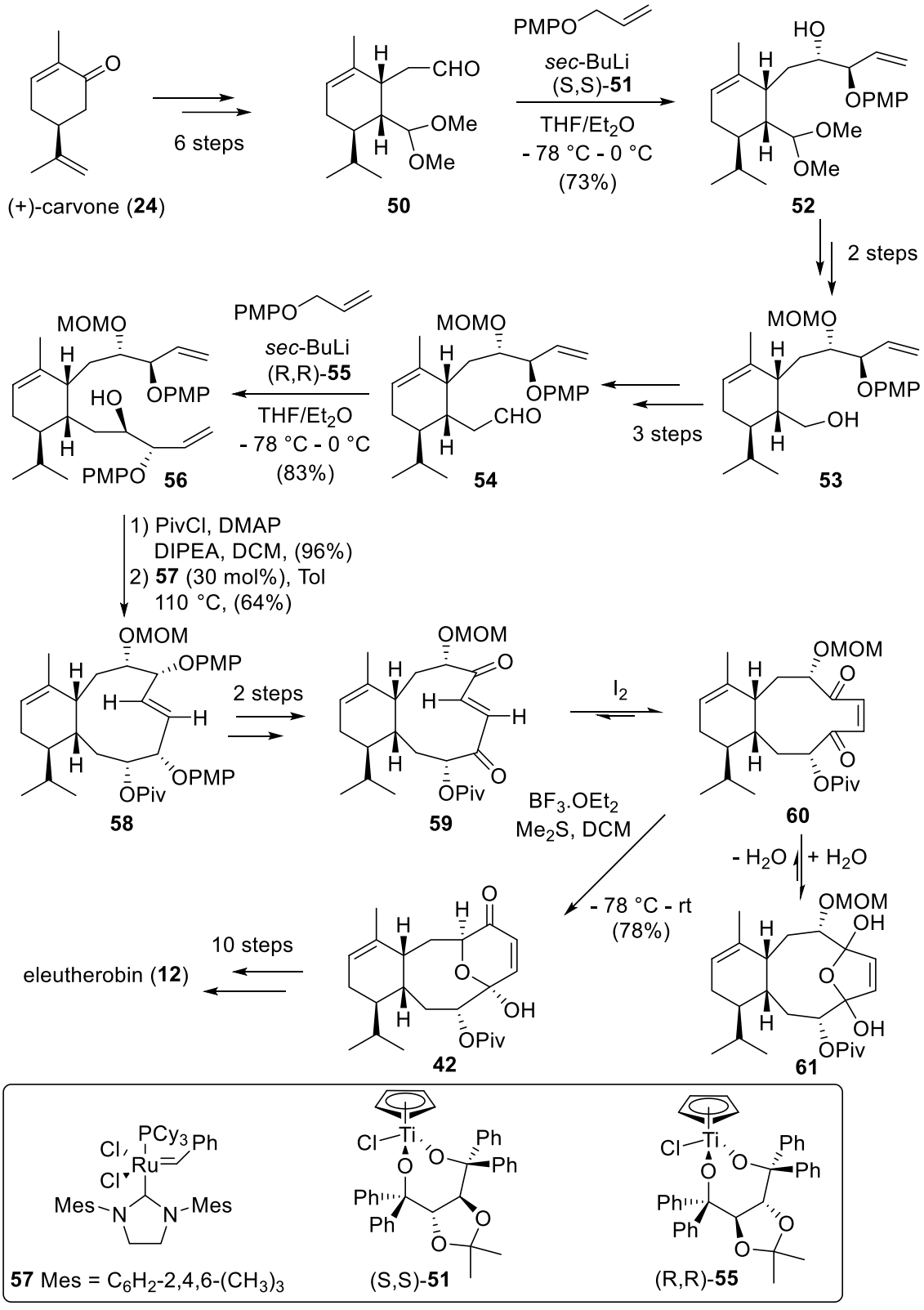


**Scheme 2.4. Gennari's formal synthesis of eleutherobin (12)**

## 2.1.4. Structure-Activity-Relationship (SAR)

Despite intensive efforts applied to the total synthesis of eleutherobin (**12**), the number of steps required and overall low yields have hampered additional biological testing. Nonetheless, preliminary investigations have provided access to several synthetic analogs, which combined with the modifications performed on eleutherobin extracted from natural sources, have provided impressive insights regarding the relationship between structure and antimitotic properties.[109] From these studies, four key regions of the molecule can be discerned where structural modifications have proven particularly insightful (Figure 2.5). First, modifications to the A-ring indicated that reactions occurring on the α-face that force the C11 methyl to the top face are more tolerated than those on the β-face (e.g., epoxidation: $IC_{50}$ 30 vs $IC_{50}$ 300). The addition of a hydroxyl group on the β-face ($IC_{50}$ >2000) emphasizes this phenomenon by displaying a >100-fold decrease in activity compared to eleutherobin.[109] Unfortunately, too few compounds with A-ring modifications have been studied to draw any additional conclusions about the importance of this region to eleutherobin's antimitotic activity. In contrast, peripheral modifications have been investigated more closely (i.e., *N*-urocanic ester, carbohydrate, and ketal domains).[108,109,114–117] Interestingly, ketal substitutions showed little to no effects on eleutherobin's activity.[108,109,115] Here, regardless of the "R" group, a similar potency was displayed. Regarding C8 modifications (i.e., urocanic ester), modifications have a much more significant impact. While isomerization of C2'-C3' alkene results in a compound with similar biological activity, reduction of the double bond leads to an inactive compound (i.e., $IC_{50}$ ~ 20,000 nM).[108,109] Similarly, the presence of the two nitrogen in the imidazole ring is essential. Indeed, the replacement of one with oxygen or sulfur led to a decrease (i.e., $IC_{50}$ ~ 300 nM) or complete loss (i.e., $IC_{50}$ > 2000 nM) of activity.[115] With respect to the carbohydrate domain, several interesting observations were made. First and foremost, both methyl and hydroxyl substitution of C15 led to a near loss of activity.[117] On the contrary, using the β-L-arabinopyranose or methyl ester only resulted in a 5 to 10-fold decrease in activity, demonstrating that this domain can be modified without observing a deleterious loss of activity.[114] Additionally, while aglycons (e.g., esters) retain microtubule-stabilizing properties, the sugar group is crucial for activity in paclitaxel-sensitive- and paclitaxel-resistant cell-lines.[114] These limited examples emphasize the importance of further SAR studies to better understand the eleutherobin pharmacophore required to support the

development of improved analogs. For instance, the first eleutherobin's X-ray structure generated by Andersen largely contributed to refinements of the microtubule-stabilizing pharmacophore models.[118]

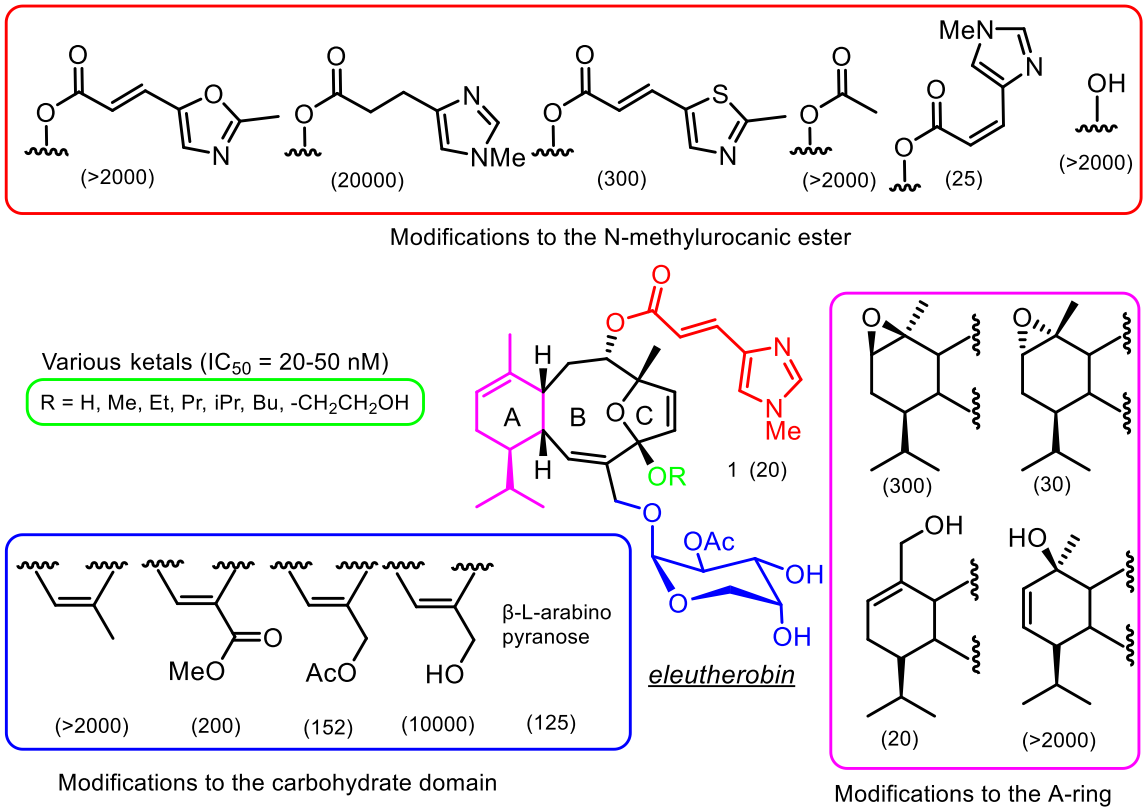


**Figure 2.5. Structural modifications and biological effect of eleutherobin analogues ($IC_{50}$ value)**

## 2.1.5. Objectives

Despite possessing potentially useful biological activity, eleutherobin's development has stalled due to the lack of material. While several groups have tried to address this problem, none of the published total syntheses have provided a sustainable synthesis of the natural product or an improved analog. To assess the potential of eleutherobin as cancer chemotherapy, several questions regarding its toxicity, metabolic stability, mechanism of resistance, as well as its role on the conformation of microtubules, remain unanswered. Therefore, our primary objective was to develop a concise, efficient and scalable synthesis that would allow us to

synthesize grams of this antimitotic agent. It was expected that this would also support the production of analogs designed to better understand eleutherobin SAR.

## 2.2. Previous Approaches in the Britton Group

Dr. Jeffrey Mowat, who joined the Britton group in 2006, was the first to take on the eleutherobin challenge. At the time, the 10-membered macrocycle was envisaged to be made from the fragmentation of a tricyclic intermediate. Following this key step, D-arabinose and urocanic ester could easily be installed to generate eleutherobin (**12**). The fragmentation would involve a retro-aldol or retro-Mannich reaction that would result in the formation of the 10-membered ring **62** after subsequent deprotection of the ketone and spontaneous ketal formation. Notably, the precursor to the fragmentation would require two characteristics: a heteroatom at the C8 position and a functional methylene at the C3 position as shown in **63**. It was imagined that this could be achieved via epoxidation of the tetrasubstituted alkene in **64** followed by opening with a heteroatom. The tertiary alcohol **64** would be obtained from the corresponding ketone **65** via a diastereoselective methyl addition, and the ketone itself would be accessed through an oxidative dearomatization reaction using hypervalent iodine and tetralone **66** (Scheme 2.5)

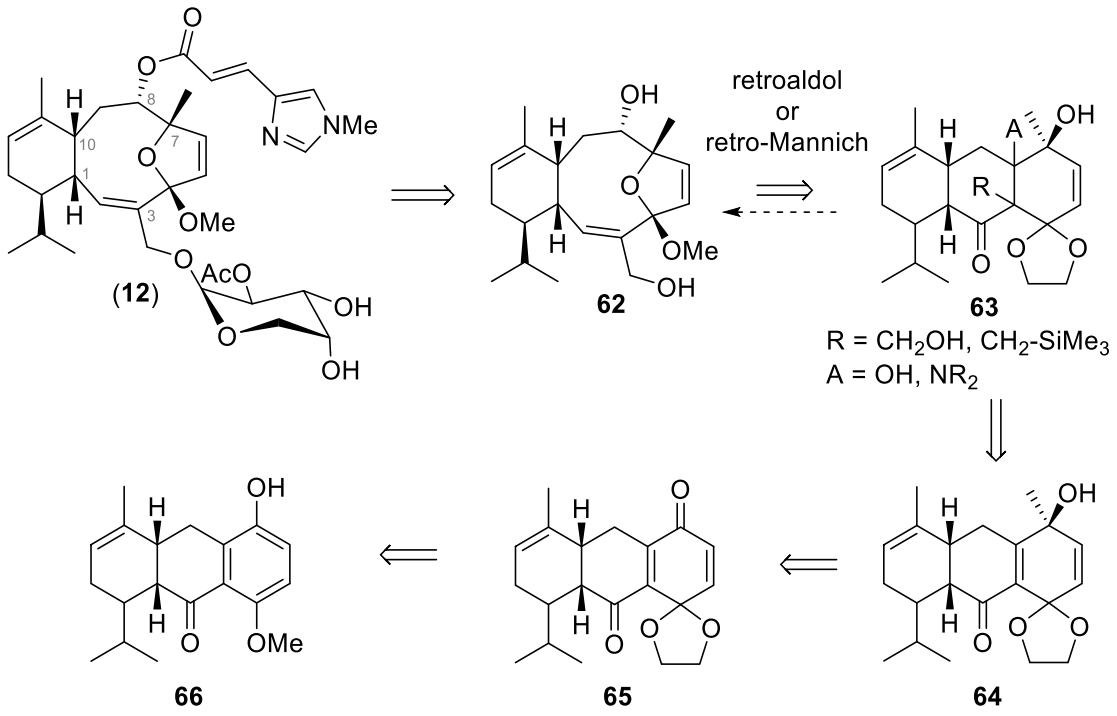


**Scheme 2.5. Dr. Mowat's retrosynthetic approach for eleuterobin (12)**

Impressively, Dr. Mowat developed an efficient new process for the synthesis of α-tetralones. Through the investigation of several strategies including electrocyclization, Pd-catalyzed ring expansion of cyclobutanols, and ketene [2+2] additions, he was successful in accessing a wide range of α-tetralones. As depicted in Scheme 2.6, [2+2] addition of the ketene generated *in situ* from trichloroacetylchloride in the presence of zinc led to the formation of dichlorocyclobutanone **67** in very good yield. Then, dechlorination offered the required cyclobutanone **68**, a necessary precursor for the tetralone synthesis. Palladium-catalyzed coupling of aryl bromide **69** and cyclobutanone **68** in the presence of lithium *tert*-butoxide was investigated. Unfortunately, the first attempt using the conditions developed by Colacot and coworkers ((DtBPF)$PdCl_2$, KOtBu, Toluene, 110 °C) only led to a poor 15% yield of the α-aryl cyclobutanone **70**.[119] While a change in temperature and solvent did not improve the outcome of this reaction, replacing KOtBu with LiOtBu provided the desired product **70** in high yield. The subsequent Haller-Bauer fragmentation offered carboxylic acid **71** in very good yield.[120] Finally, intramolecular Friedel-Crafts reaction on the corresponding acyl chloride followed by the TBS deprotection provided phenol **66** in a short (6 steps) and efficient sequence (40%) (Scheme 2.6).

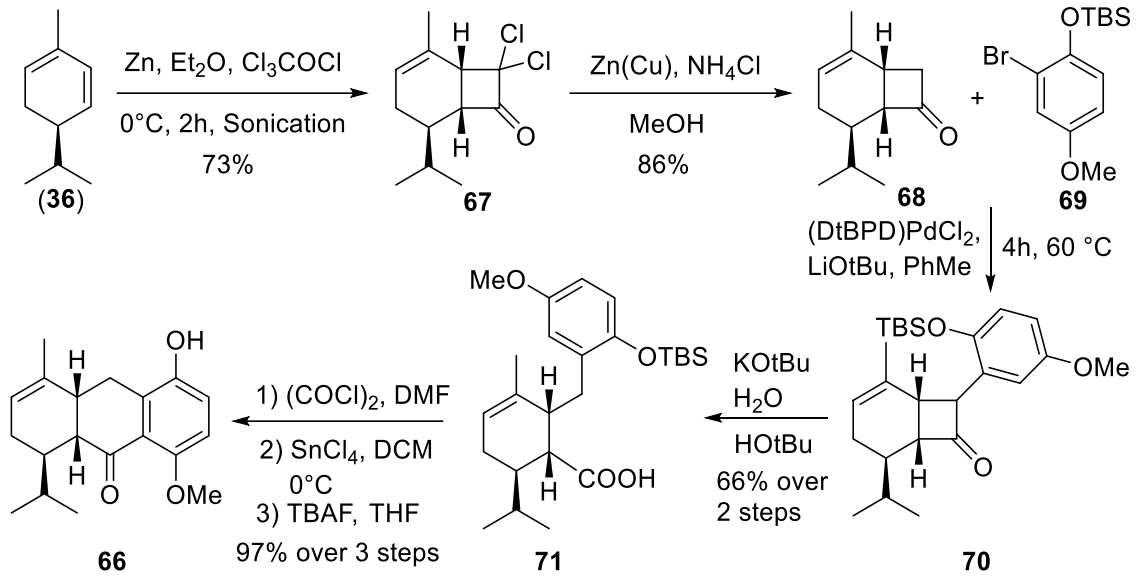


**Scheme 2.6. Synthesis of tetralone 66 via α-arylation/ring expansion sequence**

Building on these results, Dr. Stanley Chang (2009) focused on making the desired intermediate for the retro-aldol/Mannich reaction. A brief summary of his efforts is depicted in Scheme 2.7. Thus, oxidative dearomatization of phenol **66** in presence of [bis(trifluoroacetoxy)iodo]benzene (PIFA) and ethane-1,2-diol offered diene dione **65** in good yield. Subsequent methyl addition proved challenging. Optimally, using methyl lithium, a diastereoisomeric ratio of 2:3 (**64**:**72**) disfavoring the desired tertiary alcohol **64** was formed. With tertiary alcohol **64** in hand, carbamate **73** formation was performed using trichloroacetyl isocyanate that subsequently underwent an aza-Michael addition under basic conditions to afford cyclic carbamate **74**. Unfortunately, the inability to functionalize C3 prevented further evaluation of the feasibility of the fragmentation strategy for the ring expansion.

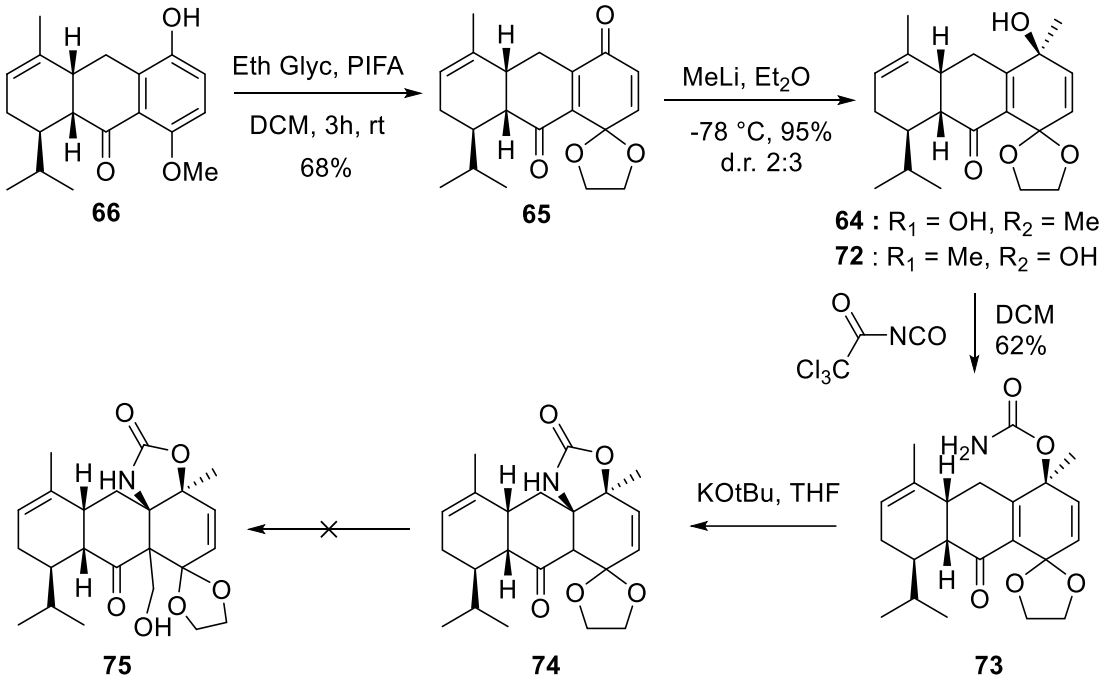


**Scheme 2.7. Most advanced Dr. Chang' s synthetic approach**

Dr. Michael Holmes (2011) planned for functionalization of C3 through a late-stage Tamao-Kumada-Fleming oxidation of the C-Si bond **76** prior to performing the fragmentation. Concerning the C8 position, it was believed that a hydroxyl group could be easily added via oxidation of the α-carbonyl position (e.g., Davis oxaziridine). It was anticipated that dione **77** could be synthesized via radical cyclization of quinone **78** after cleavage of the C-Br bond. As used in the previous strategies, dearomatization of the phenol **66** followed by a series of reduction, protection and oxidation steps was thought to provide quinone **78** (Scheme 2.8).

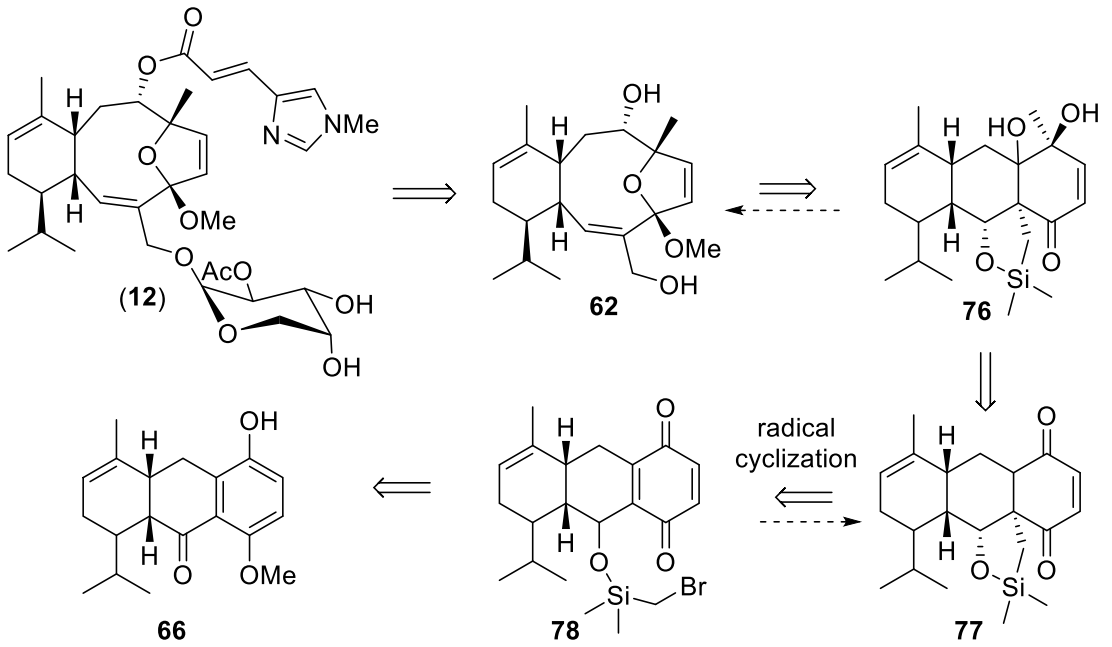


**Scheme 2.8. Dr. Michael Holmes' retrosynthetic approach**

Unfortunately, while access to the silane **79** was realized, functionalization of the C8 position proved challenging (Scheme 2.9). Notably, under no conditions investigated was oxidation or deprotonation α- to the ketone function possible. However, while efforts to functionalize the silafuran **79** proved fruitless, the installation of the C3-C15 bond was viewed as a significant advance.

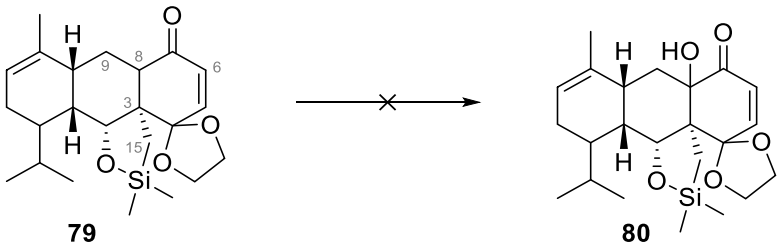


**Scheme 2.9. α-hydroxylation of enone 79**

Dr. Ren (2017) first repeated Dr. Holmes' work to generate a sufficient amount of **79**. Dr. Ren commenced the synthesis with the preparation of alcohol **82**, accessible through reduction of the corresponding tetralone **81**. Further protection of **82** using bromomethyl dimethylsilyl chloride yielded intermediate **83**. Phenol deprotection followed by oxidative dearomatization delivered dienone **85** in decent yield. With AIBN, *in situ* formation of methide radical spontaneously delivered pentacyclic product **79** in good yield (Scheme 2.10).

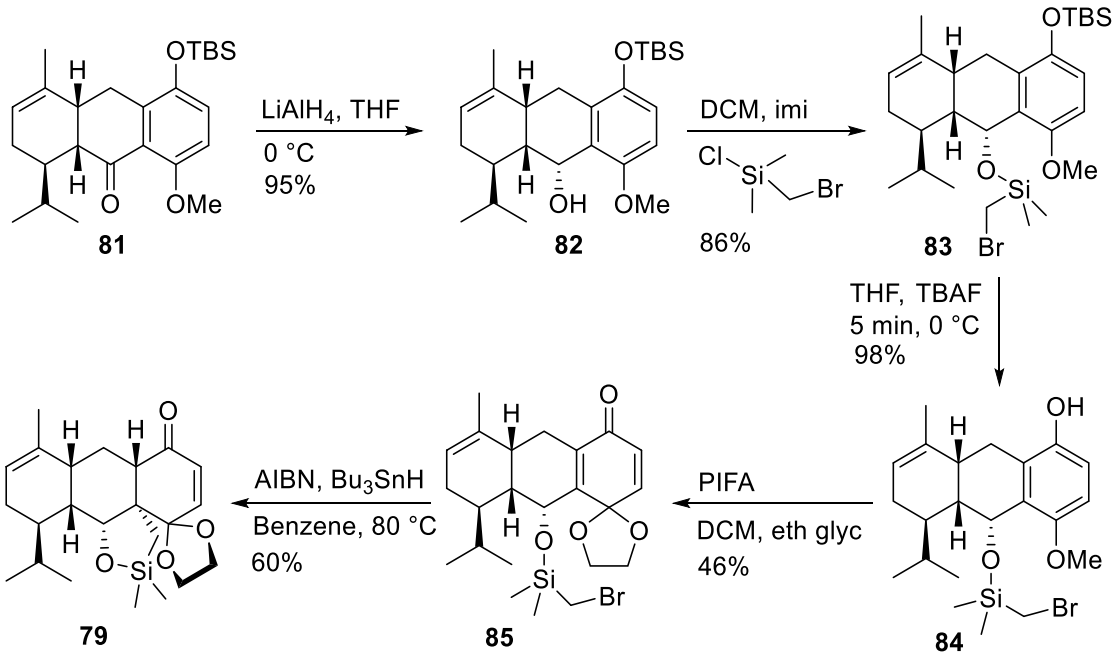


**Scheme 2.10. Synthetic route towards precursor 79**

With compound **79** in hand, Dr. Ren attempted the C8-functionalization via deprotonation with several bases. For instance, submitting enone **79** to cesium carbonate in the presence of oxygen left starting material completely unreacted.[121] The use of NaHMDS followed by the addition of Davis oxaziridine led to immediate decomposition of enone **79**. Unfortunately, employing milder bases promoted a similar outcome or did not deprotonate C8 at all (e.g., $Cs_2CO_3$, KO*t*Bu). Finally, a Rubottom oxidation was attempted but failed to provide the corresponding vinyl silyl ether. Dr. Ren speculated that removal of the C8 proton was particularly difficult given that the tetrasubstituted enol formation was unfavorable due to the molecule conformation (i.e., too hindered). To assess deprotonation itself, Dr. Ren attempted to replace the proton at C8 with a deuterium atom (Scheme 2.11). Enone **79** was treated separately with several bases in THF but none of them were able to deprotonate the C8 proton (e.g., NaHMDS, LiHMDS, LDA) forcing Dr. Ren to abandon this strategy.

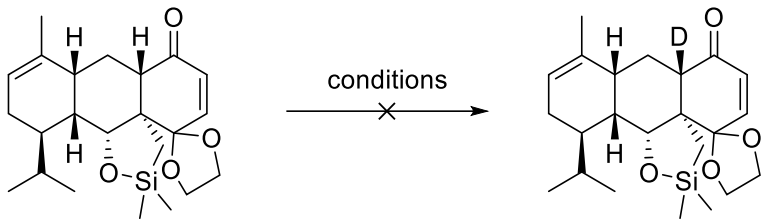


**79** **86**

**Scheme 2.11. Installation of deuterium at C8**

## 2.3. Initial Proposal: Ring Expansion

### 2.3.1. Tetralone Oxidative Dearomatisation

Our retrosynthetic analysis was based on the results of Dr. Holmes. Thus, esterification and glycosylation were envisioned to represent late-stage functional steps and efforts were directed towards the formation of the sarcodictyin core. To access the large ring in eleutherobin (**12**), the fragmentation of smaller rings (e.g., fused cyclohexanes) through retro-aldol, retro-Mannich, or Grob fragmentation processes was planned. Diketone **87** would provide a useful intermediate accessible via oxidative dearomatization and subsequent modifications of tetralone **81**. Further disconnection would lead to cyclobutanone **68**, which could be subjected to the established α-arylation process for the formation of tetralone.[73] As previously reported,[71] cyclobutanone can be traced back to R-(-)-phellandrene (**36**), cheap and commercially available monoterpene (Scheme 2.12).

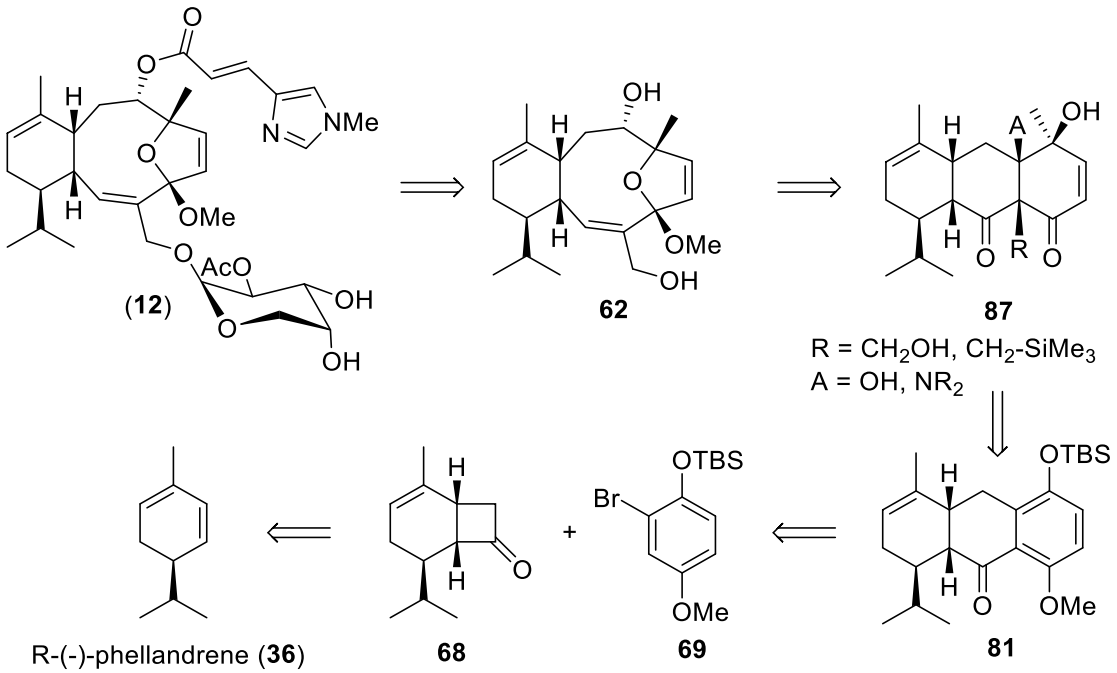


**Scheme 2.12. Initial retrosynthetic strategy**

As noted above, three distinct methods were considered for the ring expansion: a retro-aldol, a retro-Mannich and a Grob fragmentation. A retro-aldol reaction involves the reaction of a β-hydroxyl ketone **89** to yield two carbonyl moieties **87** and **88** (e.g., ketones or aldehydes). Reaction conditions (e.g., acid, basic, temperature, solvent) dramatically affect the equilibrium leading to a mixture of aldol or retro-aldol adducts (Scheme 2.13a). In contrast, a retro-Mannich reaction only differs by the nature of the reagents involve (i.e., iminium vs ketone). Indeed, a β-amino ketone **92** is consumed to yield an amine **90** and two carbonyls **87** and **91** (Scheme 2.13b). Finally, developed by the British scientist Cyril A. Grob, the Grob reaction is described as a "fragmentation of a 1,3-diheterofunctionalised compound featuring a nucleophilic atom and a leaving group situated in a 1,3-relationship".[122] The nucleofugal fragment takes the form of a good leaving group such as OMs, OTs, halogen or trialkyl amine (Scheme 2.13c).

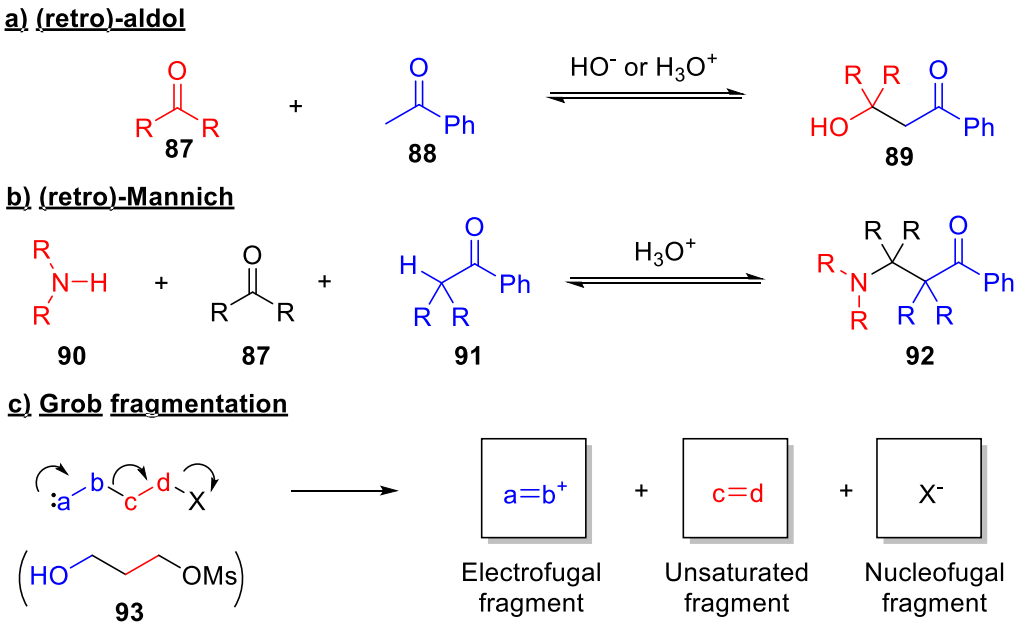


**Scheme 2.13. (retro)-aldol, (retro)-Mannich and Grob reactions**

The first objective consisted in repeating the synthesis of tetralone **65** developed by the previous Ph.D. students: Dr. Mowat, Dr. Chang and Dr. Holmes. Cyclobutanone **68** was previously synthesized by Danishefsky *et al*. in 2 steps with an overall yield of 56%.[71] A yield improvement (i.e., 76%) was observed when dichloroketone **67** was directly submitted to dehalogenation without purification. As previously reported, α-arylation of cyclobutanone **68** was performed via palladium catalysis in the presence of lithium *tert*-butoxide. The lithium counterion is crucial in this sequence to promote a reversible self-aldol reaction that slowly releases the required enolate without suffering a high percentage of side-products.[73] Since product **70** is silica-sensitive, the crude was immediately taken in a mixture of *tert*-butanol and water in the presence of potassium *tert*-butoxide to promote the Haller-Bauer fragmentation which generated carboxylic acid **71** in good yield. Subsequent acylation of **71** followed by an intramolecular Friedel-Crafts cyclization yielded tetralone **81**. Finally, a sequence of TBS deprotection followed by subsequent oxidative dearomatization allowed for the formation of dienone **65**. This was made possible through the electrophilic enhancement of the carbon bearing the methoxy group by coordination of the hydroxyl moiety to PIFA (i.e., hypervalent iodine) that implicitly facilitated the attack of ethylene glycol (i.e., nucleophile) (Scheme 2.14).

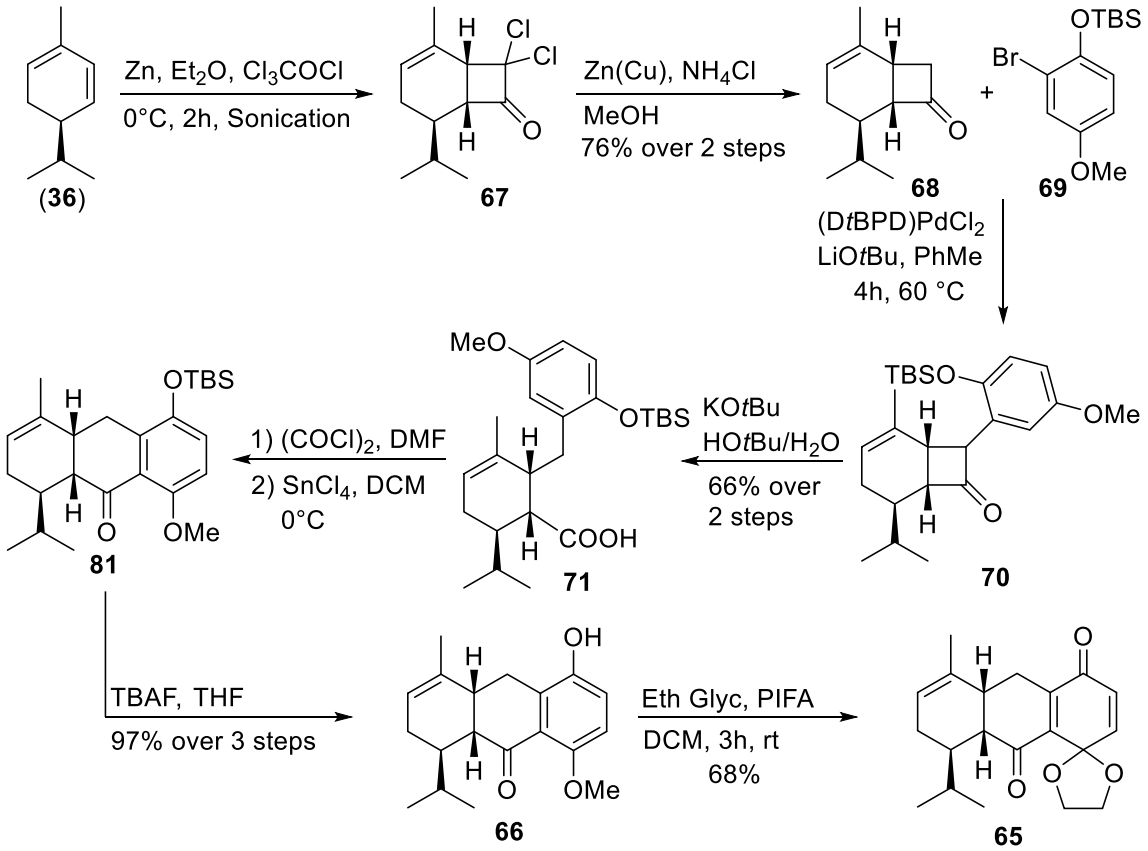


**Scheme 2.14. Synthesis of dienedione 65**

With dienone **65** in hand, improvement of the methyl addition was deemed necessary. Indeed, preliminary work offered a 2:1 diastereoisomeric ratio (d.r.) in favor of the undesired isomer **88** and did not provide an adequate amount of material for further assessment of the key step (i.e., fragmentation). Changes in the nature of nucleophiles, temperature, additives, and solvents were thought to have a significant impact on diastereoselectivity. Table 2.2 highlights the impact of changing these parameters on the outcome of the reaction. First, Dr. Chang's conditions were repeated using methyl lithium in THF to reaffirm the observed poor diastereoisomeric ratio (entry 1). Keeping methyl lithium as the methyl source, switching from THF to toluene slightly improved the ratio (entry 2). In contrast, the use of hexane favored the wrong diastereoisomer **88** (entry 3). Independent of solvent nature, an increase in reaction temperature to 0 °C resulted in a 1:1 d.r. (entries 4, 5). Unfortunately, none of the employed Lewis acids led to a considerable improvement of d.r. (entries 6, 7). Switching from methyl lithium to methyl magnesium chloride had an unfavorable impact on the d.r. (entries 8). Increasing the size of the halogen counter ion (e.g.,

methylmagnesium iodide) had a tremendous impact on the outcome of the reaction varying on the solvent of choice. Indeed, although the d.r. ratio in THF (entry 9) was similar to Dr. Chang's, the use of toluene and DCM dramatically impacted the ratio to offer desired product **60** as the major isomer (i.e., d.r. 3:2) (entries 10, 11). Unfortunately, further screening of Lewis acids did not further improve the d.r. (entries 12, 13).

**Table 2.2. Methyl addition on tetralone 65**

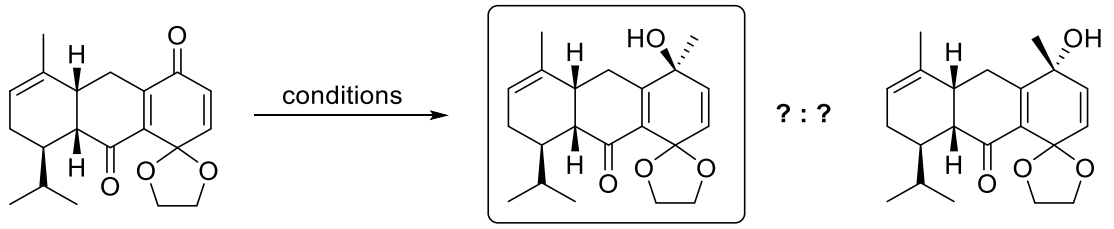


**65** | **64** desired | **94** undesired

| entry | nucleophile | T (°C) | additives | solvent | ratio (64:94)[a] |
|---|---|---|---|---|---|
| **1** | MeLi ($Et_2O$) | -78 °C | - | THF | 2:3 |
| **2** | MeLi ($Et_2O$) | -78 °C | - | Toluene | 2.4:3 |
| **3** | MeLi ($Et_2O$) | -78 °C | - | hexane | 1.5:3 |
| **4** | MeLi ($Et_2O$) | 0 °C | - | THF | 2.7:3 |
| **5** | MeLi ($Et_2O$) | 0 °C | - | Toluene | 2.8:3 |
| **6** | MeLi ($Et_2O$) | -78 °C | $ZnCl_2$ | Toluene | 2.6:3 |
| **7** | MeLi ($Et_2O$) | -78 °C | $CeCl_3$ | Toluene | 2.4:3 |
| **8** | MeMgCl ($Et_2O$) | -78 °C | - | THF | 1.5:3 |
| **9** | MeMgI ($Et_2O$) | -78 °C | - | THF | 1.5:3 |
| **10** | MeMgI ($Et_2O$) | -78 °C | - | Toluene | 3:1.9 |
| **11** | MeMgI ($Et_2O$) | -78 °C | - | DCM | 3:1.9 |
| **12** | MeMgI ($Et_2O$) | -78 °C | $CeCl_3$ | Toluene | 3:2.3 |
| **13** | MeMgI ($Et_2O$) | -78 °C | $MgBr_2$ | Toluene | 3:2.1 |

Note: [a] d.r. determined by $^1H$ NMR (integration of signals)

Although the ratio of diastereoisomers was significantly improved, the combined 72% yield of the mixture of isomers (i.e., **64** + **94**) did not fulfill our expectations in providing a sufficient amount of material to advance. As an alternative strategy, tertiary alcohol **95** was envisioned to be selectively delivered via dearomatization of tetralone **96** using water as nucleophile (Scheme 2.15). Indeed, previous screening led us to believe that the top face of the anthracene core was less hindered which had resulted in the unfavorable ratio of products. By slightly modifying the substrate, we anticipated that the sequence should deliver **95** in a selective, short, and efficient manner.

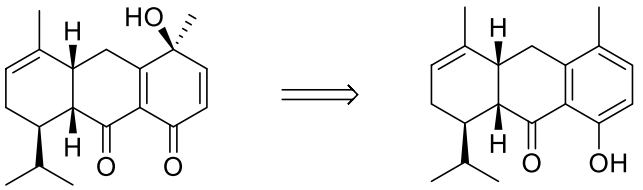


**95** **96**

**Scheme 2.15. Retrosynthetic modification**

With a view to adopting this strategy, aryl bromide **99** was synthesized in two steps from methyl bromoaniline **97** via **98** in a very efficient manner (i.e., 67% over 2 steps). Using the same strategy as depicted before (i.e., Scheme 2.14), tetralone **96** was synthesized from cyclobutanone **68** in good yield (31% over 4 steps). Notably, phenol deprotection spontaneously takes place *in situ* during the Friedel-Crafts cyclization process, which offered tetralone **96** in a shorter number of steps. Subsequent oxidative dearomatization with PIFA led to rapid decomposition presumably due to the acidic nature of the iodine reagent. To overcome this challenge, a milder alternative (i.e., (diacetoxyiodo)benzene (BAIB)) was used that smoothly delivered isomer **95** in good yield (Scheme 2.16).

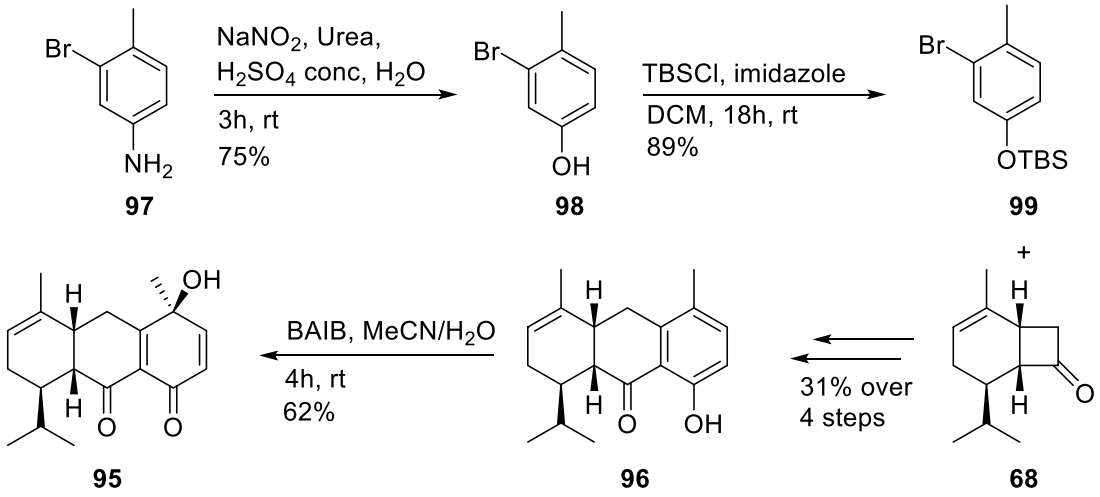


**95** **96** **68**

**Scheme 2.16. Oxidative dearomatization alternative**

In contemplating a concise synthesis of the bicyclo[8.4.0]tetradecane core of eleutherobin (**12**) from alcohol **95**, we first envisaged the addition of a nucleophilic heteroatom (i.e., alcohol or amine) to the C8 position via Michael addition to either synthesize retro-aldol **100** or retro-Mannich **101** precursors (Scheme 2.17).

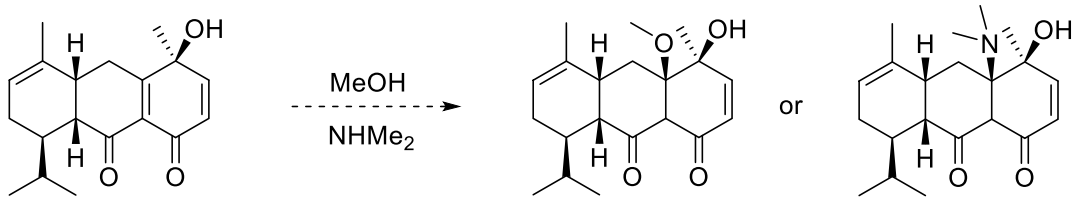


**95** **100** **101**

**Scheme 2.17. Potential precursors for the ring expansion**

Unfortunately, none of these precursors were successfully prepared, mainly leaving starting material unreacted. Here, we speculated that the disubstituted enone was not sufficiently reactive whereas the more reactive tetrasubstituted dienone was too hindered to be engaged in Michael addition processes. To tackle this problem, we believed that tethering the tertiary alcohol via a linker (e.g., acetal **102**, boronic ester **103**, or carbamate **104**) would enable intramolecular delivery of an *O*/*N*-nucleophile (Figure 2.6). As a matter of fact, a similar carbamate was reported by Dr. Chang but subsequent failure to functionalize C3 hampered its use as a retro-Mannich precursor for the key fragmentation.

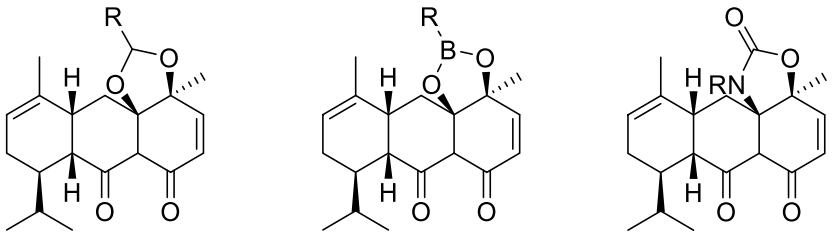


**102** **103** **104**

**Figure 2.6. Possible intramolecular oxo/aza-Michael addition**

The use of a model was believed to be insightful in determining the optimal conditions for the intramolecular Michael addition. First, methyl addition was performed on benzoquinone **105** thus providing dienone **106** in excellent yield (95%). Delightedly, the three selected strategies (i.e., cyclic carbamate, acetal, and boronic ester synthesis) were successful and delivered the corresponding adducts **107**, **108** and **109** (Scheme 2.18).

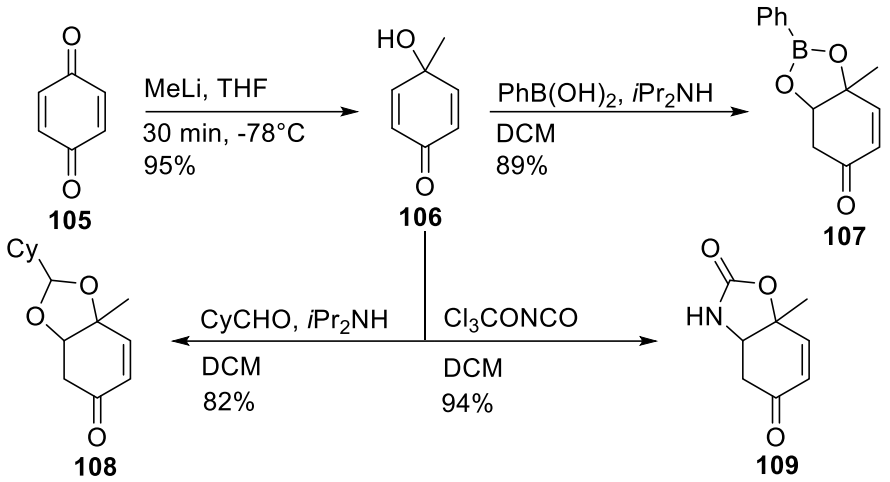


**Scheme 2.18. Intramolecular Michael additions on model 106**

Delighted with the success of the model studies, these conditions were translated to substrate **95**. Unfortunately, efforts directed towards the intramolecular oxo-Michael addition using several aldehydes (i.e., **110**, **111**, **112**, **113**) proved to be fruitless. Indeed, diketone **95** did not appear stable under basic conditions and quickly decomposed. In contrast, protected ketone **64** was stable under basic conditions but did not lead to any of the desired products (i.e., **114**, **115**, **116**, **117**). Although the reactions were heated for extended periods of time, starting material remained unreacted. Similar results were observed while attempting boronic ester formation (i.e., **118**, **119**) (Figure 2.7).

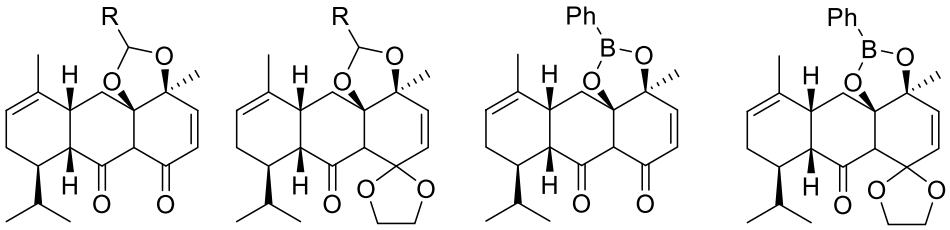

**110** : R = Cy
**111** : R = Ph
**112** : R = Et
**113** : R = H

**114** : R = Cy
**115** : R = Ph
**116** : R = Et
**117** : R = H

**118**

**119**

**Figure 2.7. Attempts in intramolecular Michael additions**

With attempts to form of oxo-Michael adducts leading to an impasse, we decided to repeat Dr. Chang's work to further assess the retro-Mannich strategy. The nucleophilic addition of tertiary alcohol **64** on trichloroacetyl isocyanate provided the corresponding carbamate that spontaneously reacted on the tetrasubstituted enone

while being purified to provide cyclic carbamate **74**. Further benzyl protection followed by ketal deprotection delivered γ-hydroxyl-α,β unsaturated ketone **120** in good yield (Scheme 2.19). Pursuing Dr. Chang's efforts, electrophilic additions at C3 were investigated. Dr. Chang previously demonstrated that the use of formaldehyde as electrophile led to the formation of numerous side-products via rearrangements. We believed that using iodomethyl pivaloate would address this issue and provide a stable product **121** lacking a free alcohol that would undergo such rearrangements. Submission to inorganic bases (e.g., potassium and cesium carbonate) in several solvents (e.g., THF and MeCN) left starting material unreacted. Similarly, no reactions occur when using stronger bases (e.g., NaH, LiHMDS and KHMDS).

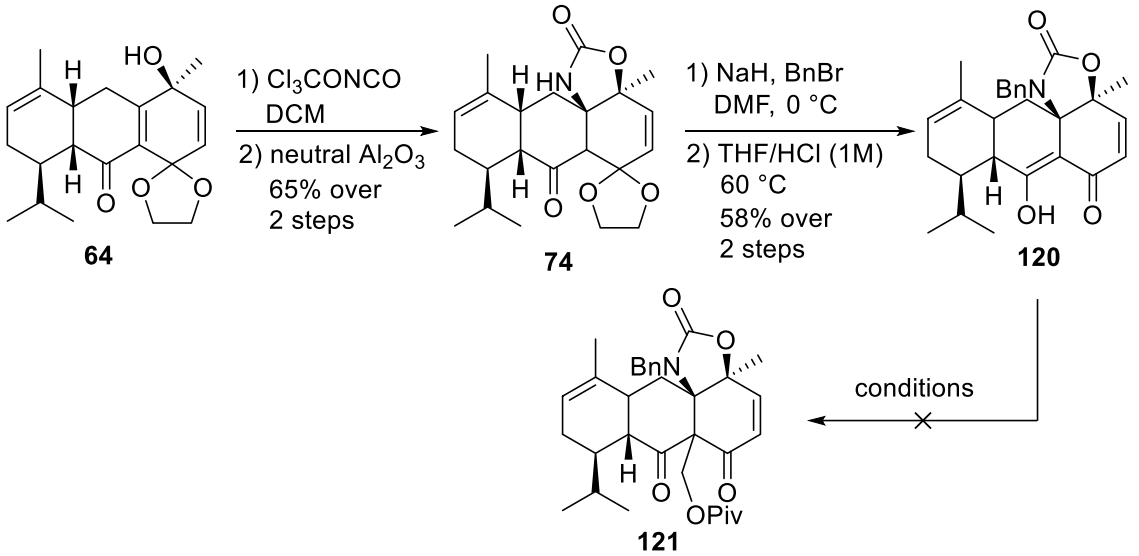


**Scheme 2.19. C3-functionnalization of 120**

As a result of this failure and in addition to the lack of reactivity observed amongst all the intramolecular substrates tested, we were forced to abandon the oxidative dearomatization strategy.

## 2.3.2. Birch Alkylation of Tetralone

The Birch alkylation was anticipated to not only provide an efficient alternative to the dearomatization of the tetralone but also provide a highly functionalized product at the C3 position. The use of ammonia, high pressured apparatus and metal makes the Birch alkylation a very challenging reaction. The first two retrosynthetic disconnections remained the same (i.e., glycosylation and esterification). However, Birch alkylation of

tetralone **124** was anticipated to deliver cyclohexa-1,4-diene **123** while incorporating an electrophile at C3. After a series of epoxidation/elimination steps, precursor **122** would be generated and would provide an excellent intermediate for the assessment of the retro-aldol ring expansion (Scheme 2.20).

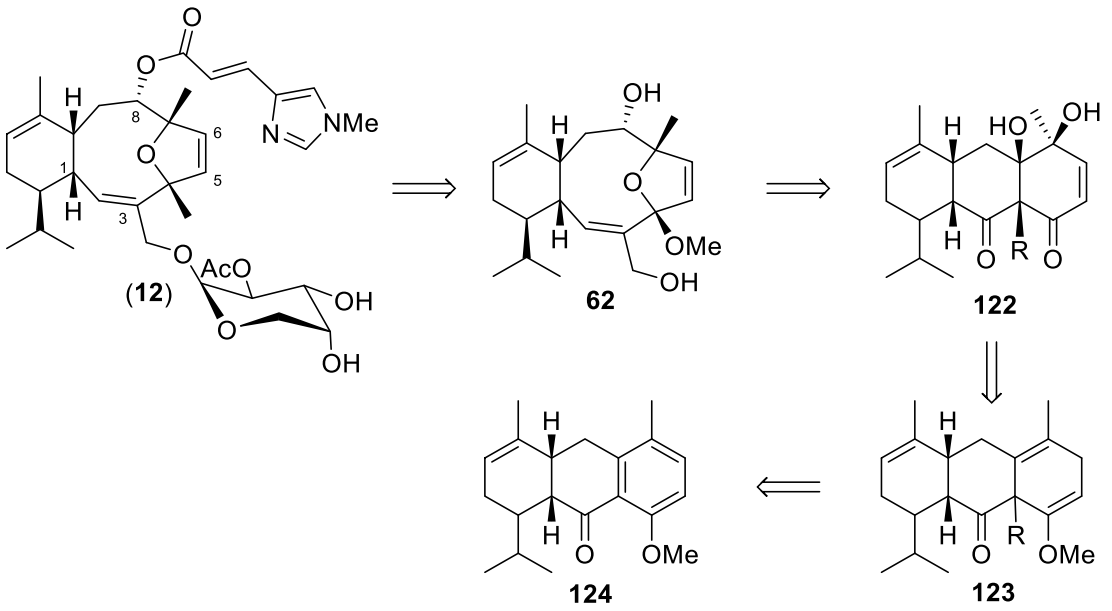


**Scheme 2.20. New retrosynthesic approach involving a Birch reaction**

To generate the required precursor, methylation of previously synthesized phenol **96** was performed and yielded the corresponding anisole **124** in good yield. Surprisingly, Birch reduction of 8-methoxy-1-tetralone has not been reported. Toward this goal, we employed the most common Birch reaction conditions (i.e., Li (s), *t*-BuOH, $NH_{3\,(g)}$, THF). After 10 minutes, monitoring of the reaction (by TLC analysis) showed the appearance of a new product as well as the complete disappearance of starting material **124**. Further $^{1}H$ NMR spectroscopic analysis of the crude reaction mixture indicated two new protons as well as a general shielding effect on numerous protons of the molecule. In-depth spectroscopic analysis confirmed the formation of **126** leaving the aromatic moiety intact. This preliminary result cast some doubt on the use of Birch conditions onto 8-methoxy-1-tetralone (Scheme 2.21).

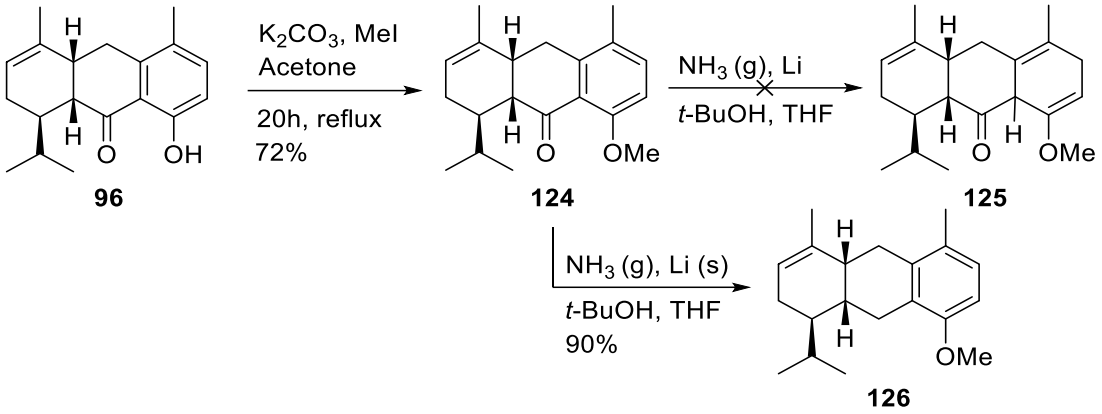


**Scheme 2.21. Birch reaction on 124 with lithium**

A recent review of developments in the Birch reduction of aromatic compounds by Mander *et al.*[123] showed that potassium was the metal of choice for the Birch reduction of tetralones.[123] Application of these conditions on 2-methoxyacetophenone **127** provided the desired diene **128** in excellent yield (Scheme 2.22).

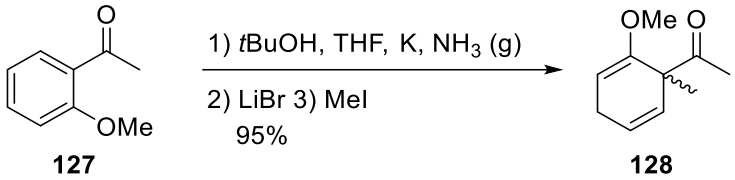


**Scheme 2.22. Attempt on reported phenylketone 127**

Delighted with the outcome of the reaction on the model, we translated the same set of conditions to tetralone **124** with the aim of generating diene **155**. Disappointedly, the total reduction of ketone **126** was the only product of the reaction (Scheme 2.23).

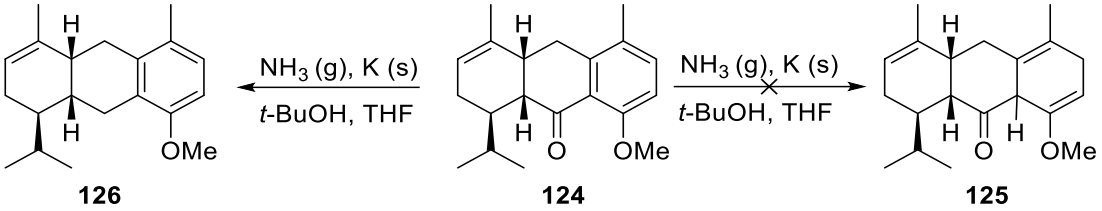


**Scheme 2.23. Birch reaction on 124 with potassium**

Convinced that the position of the methoxy group was the reason for failure, we envisaged tackling this problem by synthesizing a regioisomer analog **129**. Moreover, we believed that commercially available 5-methoxy-1-tetralone **130** would constitute a reliable model system to evaluate our new strategy (Figure 2.8).

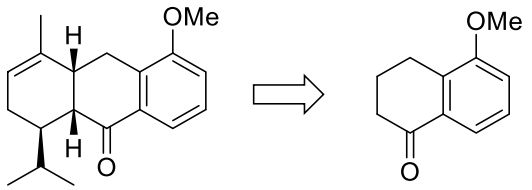


**129** **130**

**Figure 2.8. Tetralone 129 and the corresponding model 130**

The investigation commenced with the Birch alkylation of **130** in presence of potassium metal, ammonia and lithium bromide in THF (Table 2.3). Further treatment of the reaction mixture with methyl iodide delivered **131** in good yield (entry 1). Based on this result, we elected to screen different electrophiles to examine the scope of potential products. Although the yields were significantly lower, several useful products were isolated without further optimization such as the primary alcohol **137** (entry 7), its corresponding Piv-protected analog **138** (entry 8), benzyl **136** (entry 6), and silyl **132** (entry 2).

**Table 2.3. Birch alkylation on model 130**

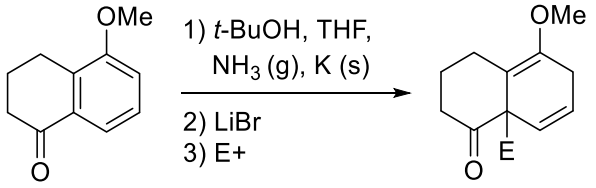


**130**

**131** : E = Me
**132** : E = $CH_2Si(Me)_2Ph$
**133** : E = BOM
**134** : E = MOM
**135** : E = $CH(OH)CH_3$
**136** : E = Bn
**137** : E = $CH_2OH$
**138** : E = $CH_2OPiv$

| entry | electrophile | -E | conversion[a] | yield[b] |
|---|---|---|---|---|
| **1** | MeI | -Me | 100% | 62% |
| **2** | $ICH_2Si(Me)_2Ph$ | $-CH_2Si(Me)_2Ph$ | 12% | 10% |
| **3** | BOMCl | -BOM | 5% | 2% |
| **4** | MOMCl | -MOM | 8% | 5% |
| **5** | $CH_3CHO$ | $-CH(OH)CH_3$ | 100% | 0% |
| **6** | BnBr | -Bn | 20% | 15% |
| **7** | $(CH_2O)_n$ | $-CH_2OH$ | 25% | 20% |
| **8** | $ICH_2OPiv$ | $-CH_2OPiv$ | 61% | 47% |

Note: [a] conversion after 30 minutes [b] yield determined by $^1H$ NMR (internal standard)

A summary of the synthesized alkylated products is depicted below (Figure 2.9). Notably, primary alcohol **137**, Piv-protected alcohol **138** and silane **132** are potential precursors for further glycosylation at C15.

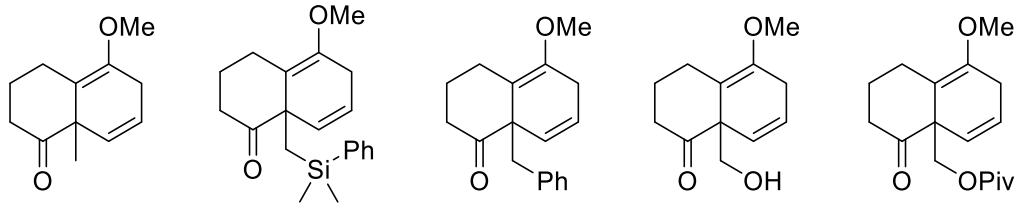


**131** **132** **136** **137** **138**

**Figure 2.9. Birch alkylated products (131, 132, 136, 137, and 138)**

From this study, the methyl adduct **131** proved to be the most stable and was selected to carry out the next steps of the synthesis. Compound **139** was designed as the target to assess the ring expansion via retro-aldol reaction (Figure 2.10).

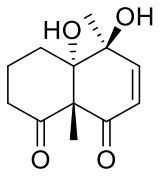


**139**

**Figure 2.10. Targeted precursor 139 for ring expansion assessment**

Regioselective epoxidation of vinyl ether **131** led to tetrasubstituted epoxide **140**, which required careful handling to prevent decomposition. During the isolation, the use of sodium sulfite followed by slow evaporation of methanol and extraction delivered methoxy epoxide **140,** which was directly opened under acidic conditions to provide diketone **141**. Here again, the choice of work-up was essential, and we found that the use of a pH 7 buffer was necessary to generate diketone **141** in decent yield. Product **141** possesses the required functionalities at C9 and C10 for the key step. A second epoxidation was performed to install the requisite oxygen at C8. Spontaneous elimination of the epoxide **142** during the purification process on silica gel provided enone **143** in good yield. To complete the synthesis of **139**, methyl addition to the enone carbonyl provided triol **144** as a single diastereoisomer. From there, oxidation of the secondary alcohol was necessary to generate the first target **139**. Unfortunately, selective oxidation with manganese dioxide did not provide the desired product. Dess-Martin oxidation led to rapid decomposition of alcohol **144** most likely due to the slight acidity of the reagent. We were pleased to find then that the Ley oxidation with tetrapropylammonium perruthenate (TPAP) and *N*-methyl morpholine *N*-oxide (NMO) offered diol **139** in good yield (Scheme 2.24).

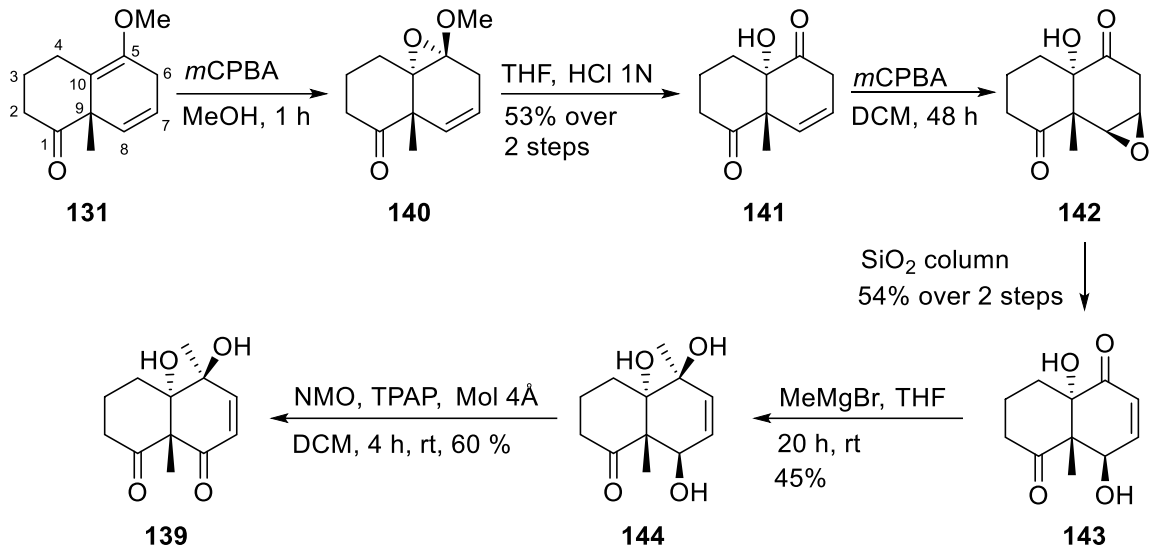


**Scheme 2.24. Synthesis of retro-aldol precursor 139**

With the retro-aldol precursor **139** in hand, we commenced our investigation on the ring expansion. We envisioned that deprotonation of tertiary alcohol (at C9) would trigger the C9-C10 bond fragmentation to generate **145** pushing the equilibrium towards the formation of the locked hemiketal **146** (Scheme 2.25). Amongst all attempted conditions (i.e., KO*t*Bu, NaOH, $K_2CO_3$, LiO*t*Bu, $CeCl_3$), only sodium hydride was able to convert diketone **139** into new products.

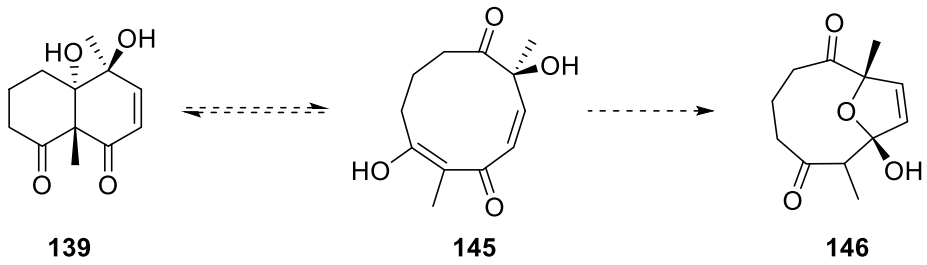


**Scheme 2.25. Ring expansion expected mechanism**

Within 5 minutes of reaction with NaH, TLC analysis of the reaction mixture indicated that diketone **139** was consumed and two new products had been formed. When the reaction mixture was stirred for an additional hour, the “major” product disappeared and the “minor” product became more prominent. Unfortunately, analysis of various NMR spectra (i.e., $^{13}C$, HMBC, HSQC) showed that diketone **139** underwent an unexpected C8-C9 bond cleavage. Here, allylic alcohol adds to the carbonyl group in generating unsaturated lactone **148** (Scheme 2.26).

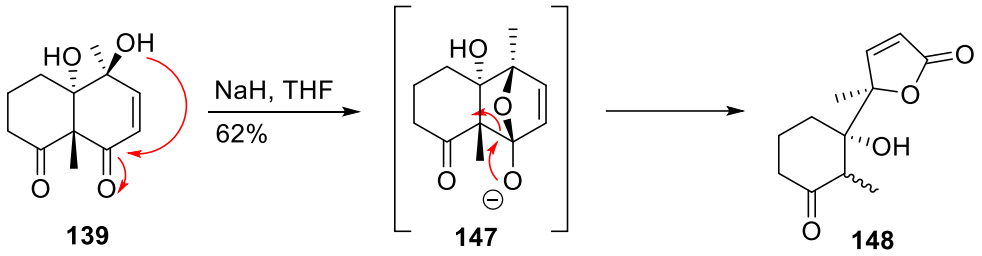


**139** **147** **148**

**Scheme 2.26. Potential mechanism for the formation of 148**

Interestingly, from this reaction, the recovered starting material **139** was not observed as a single compound but was rather in equilibrium with another form. Indeed, even after standing in $CDCl_3$ for 1 hour, a $^{1}H$ NMR spectrum of **139** showed the presence of two products. The ratio of compounds also varied depending on the nature of the solvent. In the $^{13}C$ NMR spectrum, a signal at 105 ppm was observed that corresponds to hemiketal **149** (Scheme 2.27). The formation of the hemiketal may explain the reluctance of this substrate to undergo retro-aldol fragmentation.

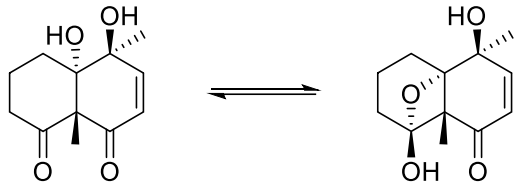


**139** **149**

**Scheme 2.27. Equilibrium of enone 139 with hemiketal 149**

Here, we speculated that this equilibrium would not take place on eleutherobin's precursor due to the presence of the extra cis-fused ring ultimately preventing the free alcohol from intramolecularly reaction. Therefore, we decided to apply the developed conditions to tetralone **124** and further assess the synthesis of eleutherobin (**12**). With a view to generating the precursor for the Birch reaction, we commenced the synthesis of tetralone **124** with the coupling of cyclobutanone **68** and modified aryl bromide **150**. Haller-Bauer fragmentation followed by acylation delivered acyl chloride **151** in good yield. Unfortunately, intramolecular Friedel-Crafts with tin chloride (IV) did not provide tetralone **124** but only the isomer **152** through *in situ* migration of the double bond (Scheme 2.28).

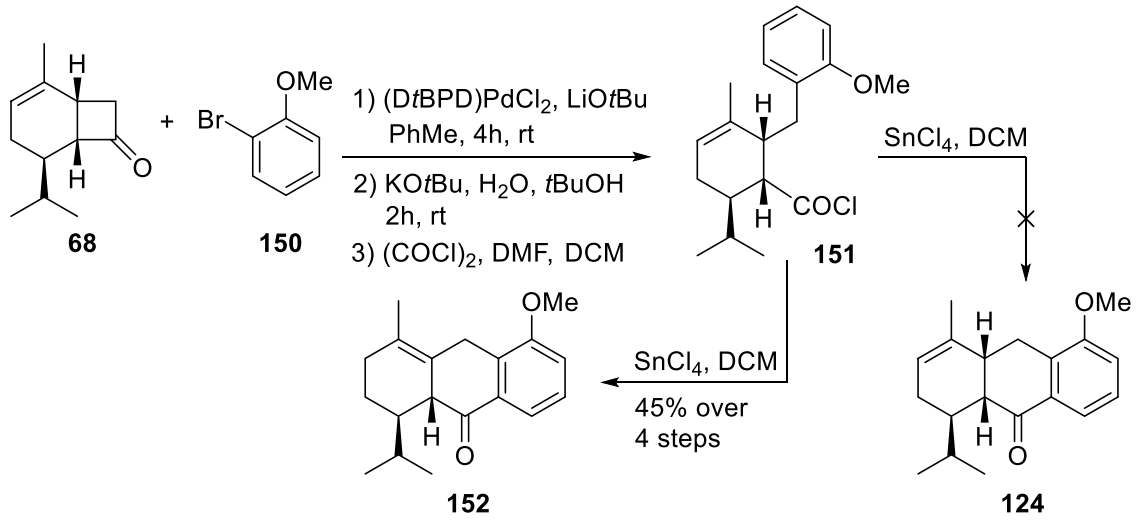


**Scheme 2.28. Failure to synthesize tetralone 124**

A thorough screening of Lewis acids was performed to determine a set of conditions that would prevent the migration of the double bond (Table 2.4). The majority of Lewis acids (e.g., $SnCl_4$, $TiCl_4$, $FeCl_3$, $BF_3.Et_2O$) solely generated isomer **141**. Amongst the dozens of conditions attempted, aluminum trichloride seemed to offer the best results. Indeed, the reaction reached full conversion in less than 3 hours at 0 °C and delivered a ratio of 4:1 in favor of the desired tetralone **119** (entry 1). Lowering the temperature led to the same ratio but displayed a lower conversion over the same period of time (entries 2 and 3).

**Table 2.4. Friedel-Crafts reaction screening**

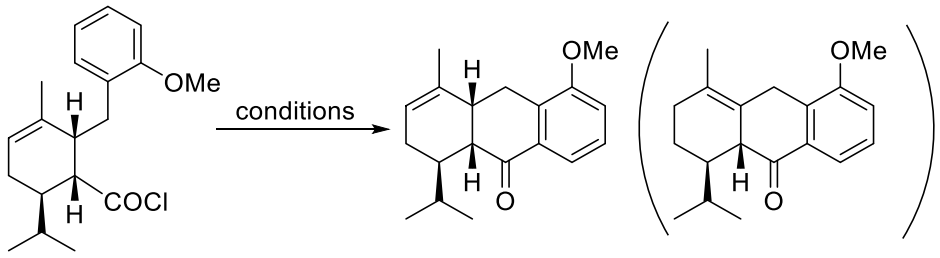


| entry | T (°C) | solvent | Lewis acid | conversion[a] | ratio (124:152)[b] |
|---|---|---|---|---|---|
| **1** | 0 °C | DCM | $AlCl_3$ | 100% | 4:1:0 |
| **2** | -20 °C | DCM | $AlCl_3$ | 70% | 4:1:0 |
| **3** | -40 °C | DCM | $AlCl_3$ | 30% | 4:1:0 |

Note: [a] Conversion after 3 hours [b] Ratio determined by $^1H$ NMR (signals integration)

Delighted with these results, we immediately scaled up this process to generate half a gram of tetralone **124** from carboxylic acid **153** in 67% yield over two steps. With

a sufficient amount of tetralone **154** in hand, efforts were directed towards the application of the Birch alkylation by applying the same conditions that were developed for the model. A careful flush of methyl iodide through a plug of basic alumina, dehydration of the lithium bromide, as well as pre-distillation of the ammonia were all crucial steps to perform a safe and efficient Birch reaction. To our delight, vinyl ether **154** was delivered rapidly in good yield (Scheme 2.29).

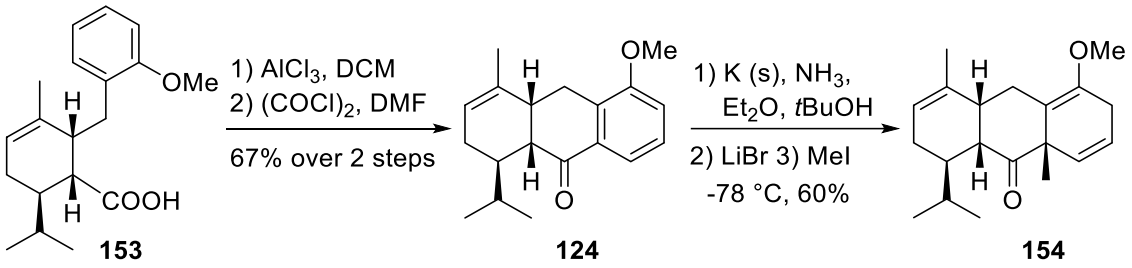


**Scheme 2.29. Tetralone synthesis and subsequent Birch reaction**

The key difference between model **131** and eleutherobin's substrate **154** that should be highlighted was the presence of the extra tertiary olefin in **154**. It was anticipated that this double bond may interfere with late-stage selective epoxidation. As depicted in Figure 2.11, the blue circled olefins are the most reactive alkenes due to the presence of the methoxy group, which greatly increases the nucleophilicity of the double bond. However, we were concerned that the trisubstituted olefin, circled in red, would be more accessible to react.

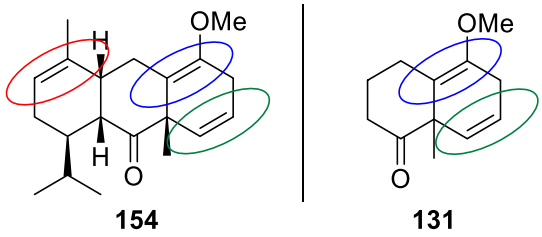


**Figure 2.11. Model 131 and substrate 154 similarities and differences**

Unfortunately, when the triene **154** was treated with *m*CPBA, the allylic hydroxyl ketone **157** was the only product observed. We hypothesized that due to the acidity of *m*-chlorobenzoic acid (pKa = 3.8) contained in the commercial bottle of *m*CPBA, the vinyl ether isomerized into the conjugated diene in **155**. Subsequent epoxidation generated **156** en route to the undesired α-hydroxy ketone **157** (Scheme 2.30).

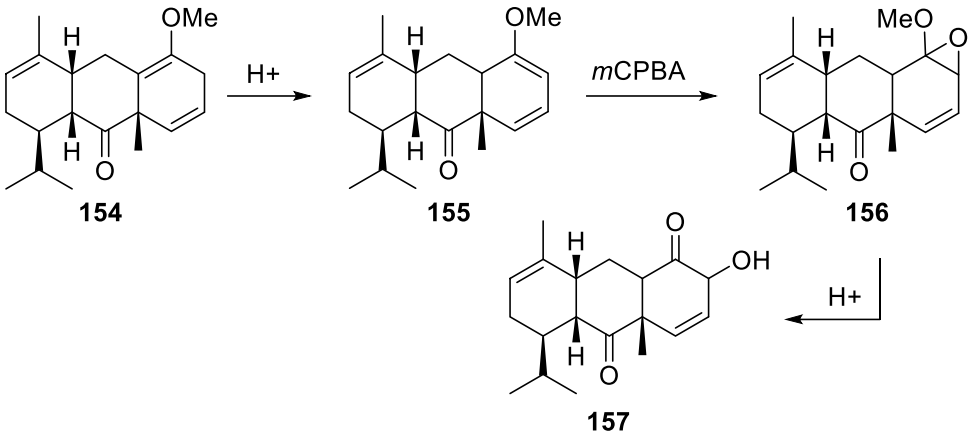


**154** **155** **156** **157**

**Scheme 2.30. Synthesis of side-product 157**

Surprised by this turn of events, we elected to evaluate different solvents, temperatures, and additives (Table 2.5). While holding to methanol as the solvent, neither lowering the temperature to 0 °C (entry 1) nor adding a pH 10 buffer (entry 2) impacted the outcome of the reaction. Similarly, the use of additives to decrease acidity (e.g., $NaHCO_3$, $K_2CO_3$) did not affect the reaction outcome independently of the nature of the solvent (entry 3-5). Finally, the combination of methanol and water in presence of sodium bicarbonate solely provided desired epoxide **158** (entry 6). Relieved by this result, a large-scale reaction was performed using these conditions. Unfortunately, the selective epoxidation was not reproducible on a large scale. From there, we decided to screen different peroxy acids with less intrinsic acidity. To our delight, magnesium monoperoxyphtalate (MMPP), a milder and water-soluble peroxy acid that is typically used to convert ketones to esters, alkenes to epoxides, sulfides to sulfoxides, and sulfones or amines to amine oxides,[124] cleanly converted **154** into the desired epoxide **158** (entry 7).

**Table 2.5. Epoxidation of vinylether 154**

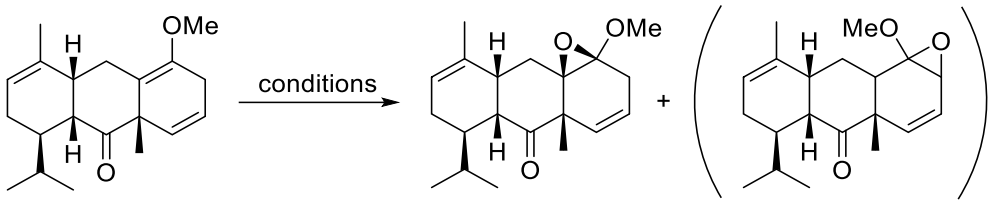


**154** **158** **156**

| entry | peroxy acid | solvent | base | T (°C) | ratio (158:156)[a] |
|---|---|---|---|---|---|
| **1** | *m*CPBA | MeOH | / | 0 | 0:1 |
| **2** | *m*CPBA | MeOH/pH 10 buffer (2/1) | / | rt | 0:1 |
| **3** | *m*CPBA | MeOH | $NaHCO_3$ | rt | 0:1 |
| **4** | *m*CPBA | DCM | $K_2CO_3$ | 0 | 0:1 |
| **5** | *m*CPBA | THF | $NaHCO_3$ | rt | 0:1 |
| **6** | *m*CPBA | MeOH/$H_2O$ (2/1) | $NaHCO_3$ | rt | 1:0 |
| **7** | MMPP | MeOH/pH 7 buffer (1/1) | / | rt | 1:0 |

Note: [a] ratio determined by $^1H$ NMR (signals integration)

After extraction, the crude material in THF was exposed to hydrochloric acid (1M) thus generating α-hydroxyl ketone **159** in 60% yield over 2 steps (Scheme 2.31).

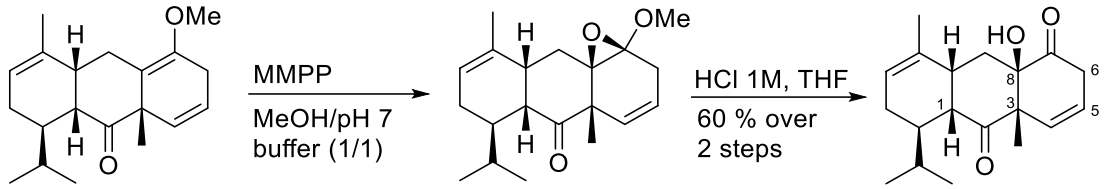


**154** **158** **159**

**Scheme 2.31. Sequence of epoxidation/opening on 154**

With the fully functionalized C3/C8 precursor in hand, installation of an oxygen atom at C4 was the last challenge before assessing the ring expansion (Scheme 2.32). To overcome potential selectivity issues, we anticipated that vanadyl acetylacetonate in the presence of tertiary homoallylic alcohol **159** would selectively direct the epoxidation event.[125] Unfortunately, submitting **159** to these conditions resulted in no reaction, even when exposed to higher temperatures for an extended period of time (i.e., 100 °C). We speculated that the bridged position of the tertiary alcohol was very hindered, preventing the formation of the vanadyl complex. Failing to selectively direct the epoxidation led us to screen more standard peroxy acids. As expected, *m*CPBA only provided trisubstituted epoxide **161**. A similar outcome was observed with MMPP. Use of the Jacobsen catalyst rapidly decomposed diketone **159**. Unfortunately, Mukaiyama epoxidation conditions also epoxidized the trisubstituted olefin yielding **161**.[126] Mizuno

*et al.* have reported a highly efficient and selective epoxidation of disubstituted alkenes over trisubstituted alkenes using a silicotungstate catalyst ($[(C_4H_9)_4N]_4[\gamma\text{-}1,2\text{-}H_2SiV_2W_{10}O_{40}].H_2O$) in the presence of hydrogen peroxide.[127] This catalyst was necessarily prepared and tested on limonene to confirm its reactivity. Unfortunately, when applied to diketone **159**, starting material **159** was recovered. Similarly, a Shi epoxidation failed to provide the desired epoxide **160**.

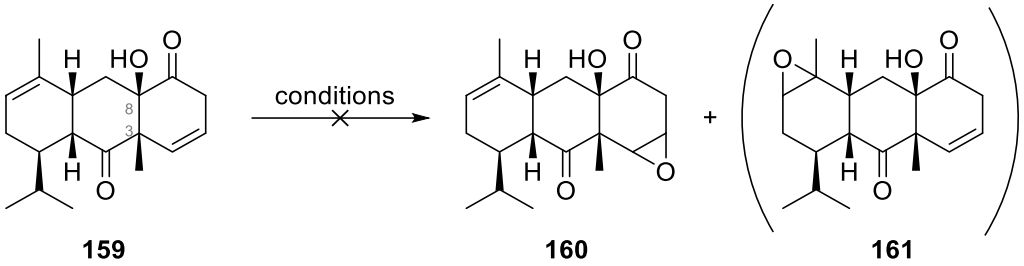


**Scheme 2.32. Failure to regioselectively epoxidized 159**

Disappointed with these results, we attempted to install the oxygen atom at C4 through several alternative strategies (Scheme 2.33). Naturally, dihydroxylation was envisioned to achieve the desired result although similar selectively issues were anticipated. Surprisingly, standard conditions for dihydroxylation using osmium tetroxide in presence of NMO generated enedione **162**. Unfortunately, a further selective methyl addition failed to deliver diol **163** in part due to the instability of triketone **162**. Disappointingly, Woodward and Prevost reactions were also unsuccessful in providing triol **164**.

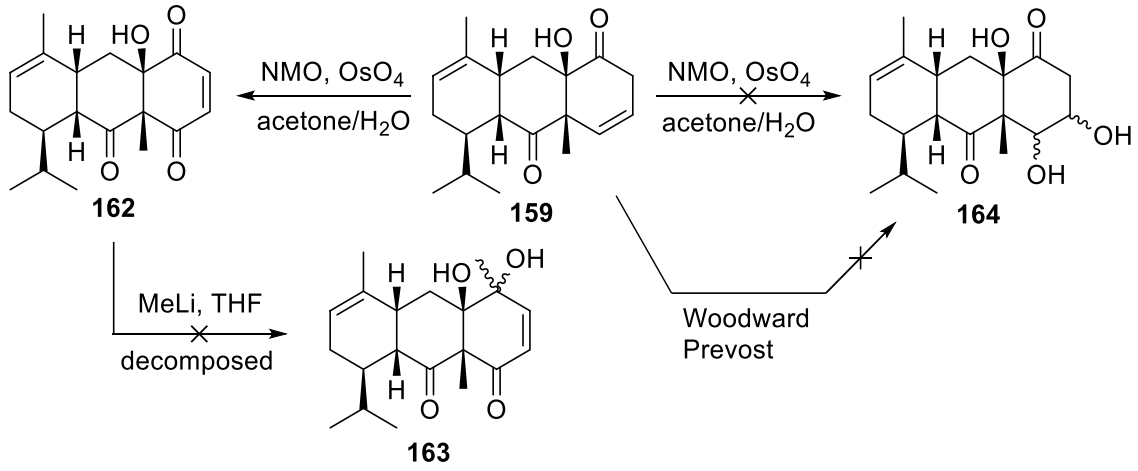


**Scheme 2.33. Dihydroxylation attempts on 159**

We moved on to another strategy that relies on the synthesis of an α-azide-β,γ-enone. Davies *et al*. used a diazonium displacement to provide γ-methoxy-α,β-enone in a steroidal derivative in good yield.[128] The use of diazotransfer agent **165** quantitively yielded diazo compound **166**. Unfortunately, no diazonium displacement was observed in our system, preventing the formation of products **167**, **168** and **169**. At this stage, substrate modifications were thought necessary to differentiate the reactivity of the disubstituted alkene. Specifically, we believed that isomerization of the disubstituted olefin would provide the corresponding enone, hence differentiating the nucleophilic/electrophilic nature of the two double bonds. Submitting diketone **159** to 1,8-diazabicyclo(5.4.0)undec-7-ene (DBU) instantaneously generated enone **170** in very good yield (Scheme 2.34).

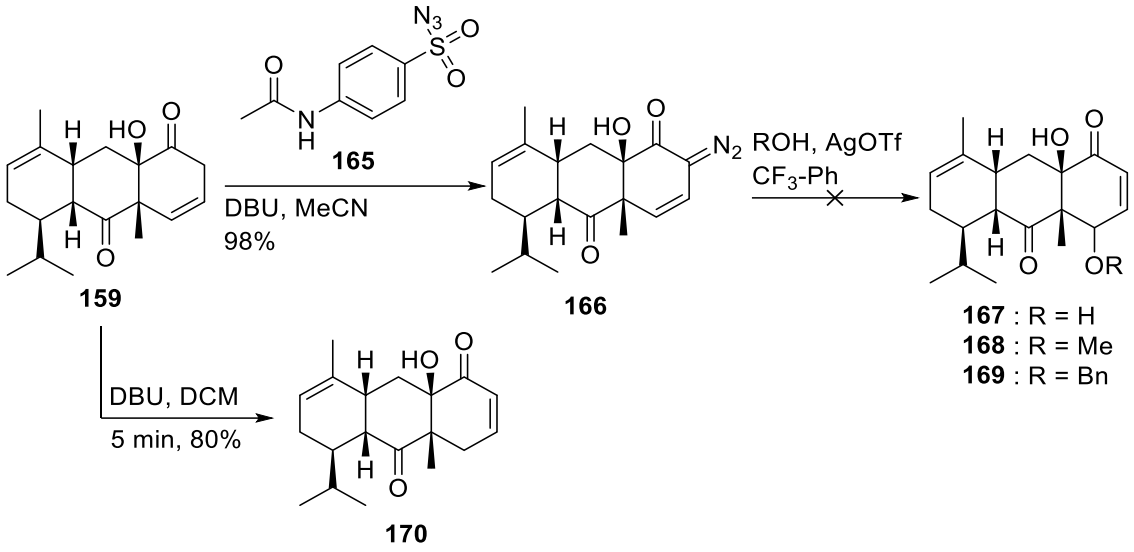


**Scheme 2.34. Diazonium displacement strategy and isomerizaion of 159**

With enone **170** in hand, several strategies were envisaged. Guerra and coworkers have developed a method to effect γ-hydroxylation of α,β-unsaturated ketones in the presence of a copper oxide catalyst (CuAlOx), potassium *tert*-butoxide, and oxygen.[129] Unfortunately, this catalyst system quickly and aggressively decomposed enone **170**. To confirm that the catalyst was properly prepared, we submitted (+)-carvone (**24**) to a freshly prepared Cu-Al-Ox catalyst and the reaction ran smoothly, delivering the corresponding γ-hydroxyl-α,β-enone in very good yield. Finally, allylic bromination to generate **172** was attempted in the presence of *N*-bromosuccinimide (NBS) but only delivered the regioisomeric allylic bromide **173** (Scheme 2.35).

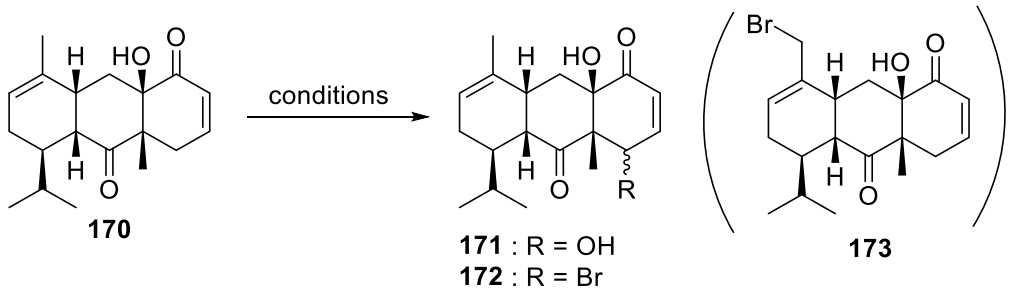


**Scheme 2.35. Allylic oxidation/bromination attempts on enone 170**

In the last effort to functionalize C4, we relied on the synthesis of silyl dienolether **174** that could further react with an electrophilic oxygen source (e.g., Davis oxaziridine, $VO(acac)_2$). This strategy was predicted to selectively provide γ-hydroxyl-α,β-enone **175**. Submission of diketone **159** to triethylsilyl chloride and lithium diisopropylamide (LDA) generated silyl dienol ether **174** in quantitative yield (Scheme 2.36). With compound **163** in hand, several conditions were investigated by varying the electrophile. Disappointingly, treatment with DMDO left the starting material **174** unreacted. The use of *m*CPBA in toluene and DCM with and without $NaHCO_3$ preferably led to the epoxidation of the trisubstituted alkene yielding **178**. A similar outcome was observed when using MMPP. In contrast, vanadyl acetylacetonate in DCM surprisingly offered triketone **177** in low yield that slowly decreased as reaction times were increased. The mechanism for the synthesis of triketone **177** could not be rationalized. Finally, Davis oxaziridine and iodine failed to provide **175** and **176** respectively.

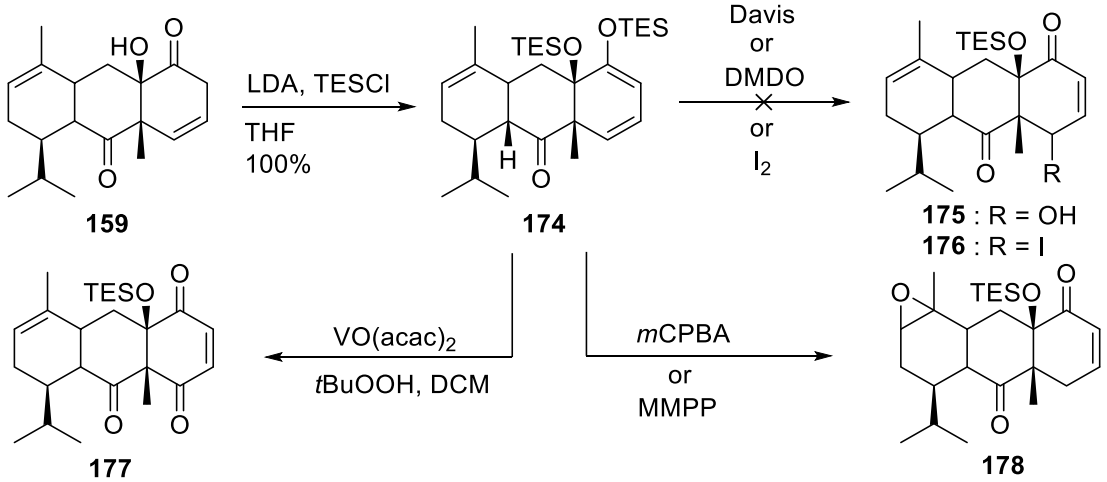


**Scheme 2.36. C5-functionnalization attempts on 174**

As a result of these fruitless efforts, we were forced to abandon the ring expansion strategy. We realized that even if this strategy had come to fruition, the number of steps would have not fulfilled our expectations in designing a concise, scalable, and efficient total synthesis of eleutherobin (**12**).

## 2.4. Revised Proposal: Macrocyclization

### 2.4.1. Macrocyclization Via Vinyl Addition to a Lactone

Our revised strategy rested upon the formation of eleutherobin's cyclodecane core through the coupling of two distinct carbon chains to the phellandrene scaffold. It was envisioned that the intramolecular addition of a vinyl bromide **180** onto a lactone group via *in situ* lithium halogen exchange could provide macrocycle **179**. To assess this cyclization, precursor **180** would be generated through the ethyl propiolate addition on ketone **181** followed by hydrogenation of the alkyne into the corresponding alkene thus triggering the spontaneous cyclization into lactone **180**. Vinyl bromide **181** was anticipated to be made via a Horner-Wadsworth-Emmons (HWE) olefination after a series of reduction, oxidation, and oxidative cleavage steps on ester **182**. The latter could be synthesized via fragmentation of diketone **183** in the presence of sodium methoxide. Further disconnection of **183** would trace back to cyclobutanone **68** which is easily accessible from R-(-)-phellandrene (**36**) (Scheme 2.37).

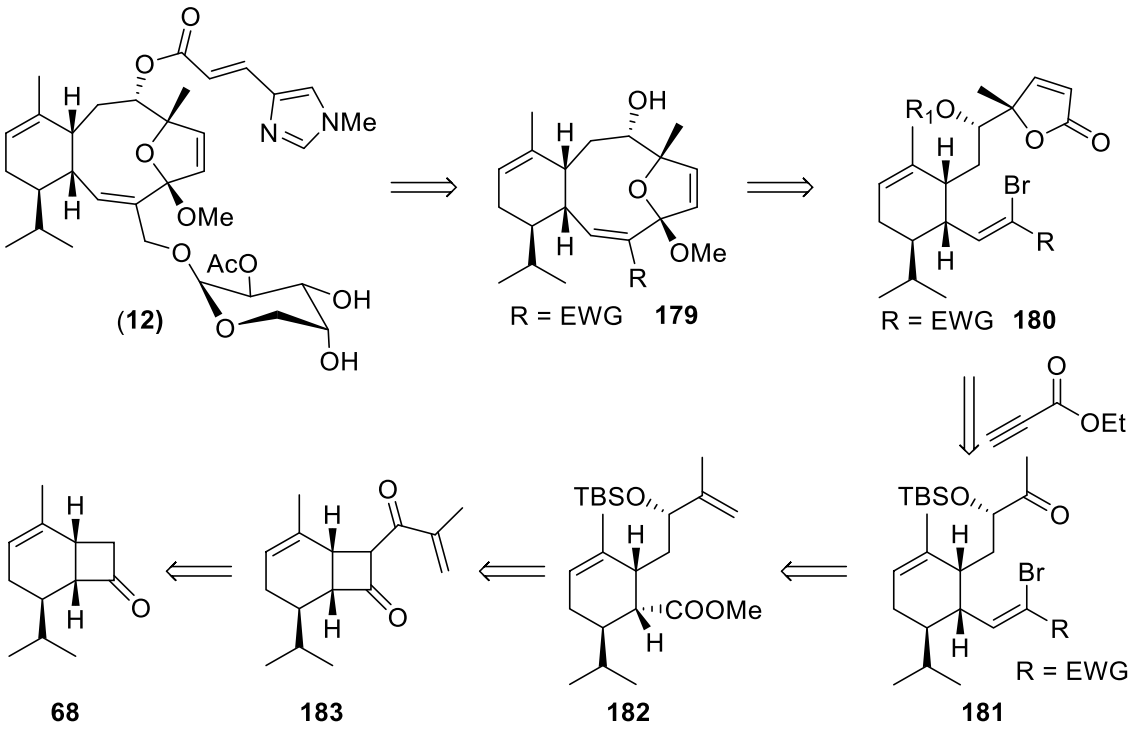


**Scheme 2.37. New retrosynthesic disconnections**

Submitting cyclobutanone **68** to LiHMDS and methacrolein (**184**) offered aldol product **185** in 64% yield and as a mixture of two diastereoisomers (Scheme 2.38). Subsequent oxidation allowed for the formation of the stable 1,3-diketone **183** as a single isomer. The reaction of methoxide with the most reactive ketone quickly led to methyl ester **186** via a ring-opening mechanism in a quantitative manner. Finally, a sequence of reduction and protection delivered ester **187** in excellent yield that was subsequently reduced into the corresponding alcohol **188** which in turn was oxidized with DMP to provide aldehyde **189** in 69% yield over two steps.

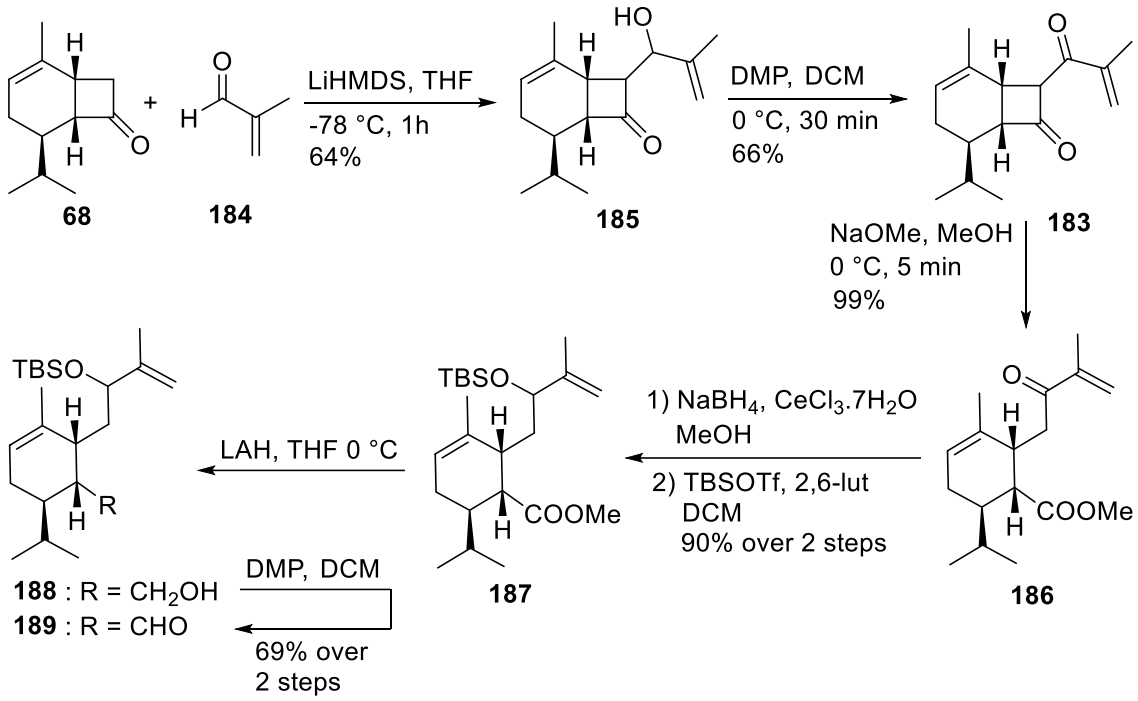


**Scheme 2.38. Synthesis of aldehyde 189**

To install the Michael acceptor, the HWE reaction was thought to be ideal. Commercially available triethyl phosphonoacetate **190** was used to determine the right set of conditions. Deprotonation of phosphonate **190** with sodium hydride followed by the addition of aldehyde **189** offered α,β-unsaturated esters **192** and **193** as a mixture of diastereoisomers (d.r = 1:1). A similar outcome was observed when performing the reaction with the Wittig reagent **191** (Scheme 2.39).

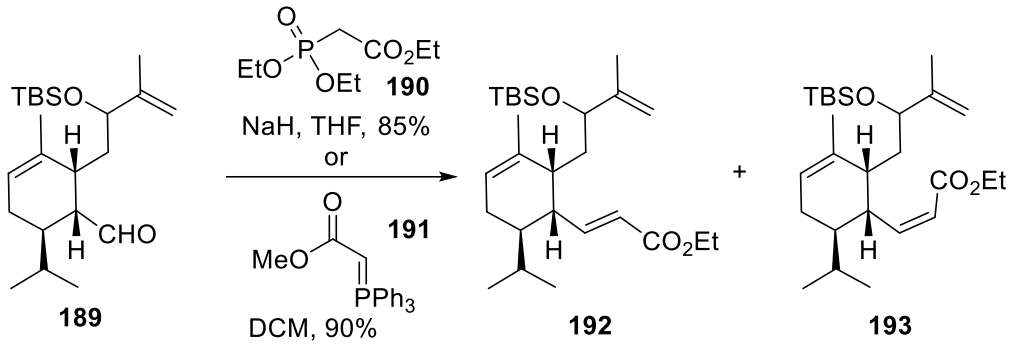


**Scheme 2.39. Olefination of 189**

To synthesize the trisubstituted vinyl bromide analog **196**, phosphonate **184** was rapidly synthesized. Initial deprotonation of **190** followed by NBS addition delivered triethyl bromophosphonoacetate **194** in good yield. With **194** in hand, efforts were

directed towards the HWE reaction. Additionally, applying the previous conditions (NaH) did not lead to any product **196**, leaving starting material **189** unreacted. Unfortunately, the screening of different bases (KO*t*Bu, LiHMDS) did not impact the outcome of the reaction. We speculated that the presence of an additional large atom (i.e., bromine, A-value = 0.38) influenced reactivity by increasing the steric interactions. Unfortunately, carrying out the Wittig reaction demonstrated a similar pattern in the reactivity of **189**. Indeed, although commercially available phosphonium ylide **191** smoothly reacted with aldehyde **189** to provide α,β-unsaturated esters **192** and **193**, the use of the bromine counterpart **195** provided none of the desired product **196** (Scheme 2.40).

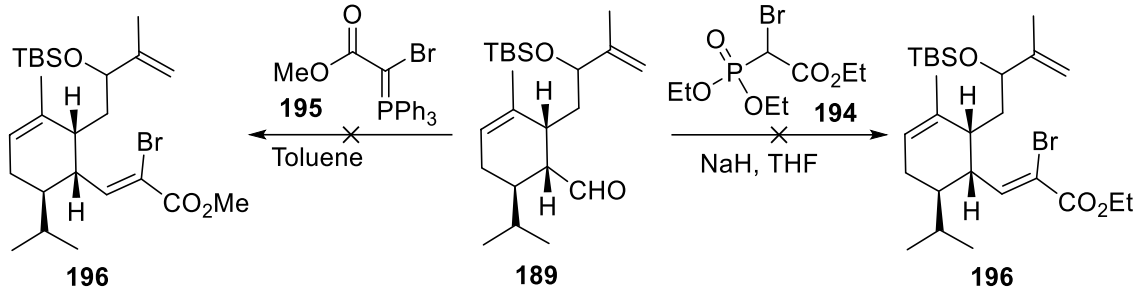


**Scheme 2.40. Failure to synthesize vinyl bromide 196**

Based on these results, we expected that replacing the ester with a smaller group would address this problem. A-values give a general representation of the steric bulk of a particular substituent (Table 2.6).[130] A higher A-value indicates a larger steric effect for that substituent. A-values come from energy measurements of the different cyclohexane conformations of a monosubstituted cyclohexane. In this system, substituents prefer conformations in which they are equatorially positioned and the difference between the high-energy conformation (axial) and the low-energy conformation (equatorial) is known as the A-value for this substituent (difference in Gibbs free energy ΔG). According to Table 2.6, bromine has the smallest A-value amongst easily exchangeable halogens (i.e., Br, Cl, I). The methyl ester's A-value is relatively large (i.e., 1.27) while the A-value of a nitrile group is similar to fluorine (0.17 vs 0.15) and would dramatically decrease the steric bulk of the corresponding phosphonate.

**Table 2.6. A-value of different substituents[130]**

| substituent | a-value | substituent | a-value | substituent | a-value |
|---|---|---|---|---|---|
| F | 0.15 | CN | 0.17 | $COCH_3$ | 1.17 |
| Cl | 0.43 | NC | 0.21 | COCl | 1.25 |
| Br | 0.38 | $CH=CH_2$ | 1.35 | $CO_2CH_3$ | 1.27 |
| I | 0.43 | $CH_3$ | 1.7 | | |

To assess our hypothesis, phosphonate **198** was synthesized via bromination of commercially available **197** in the presence of LiHMDS in THF. Aldehyde **189** and phosphonate **198** were used in acetonitrile and submitted to Masamune and Roush conditions (LiCl, DBU).[131] As soon as DBU was added, the reaction mixture immediately turned brown and subsequent TLC monitoring showed full conversion of the starting material into two new products. A mixture of diastereoisomers (d.r = 2:1) was observed by $^1$H NMR. To determine the nature of each isomer, both nitriles **199** and **200** were reduced to their corresponding primary alcohols **201** and **202**, respectively. Further analysis of $^1$H NOESY spectroscopic experiments confirmed the major diastereoisomer corresponds to the undesired olefin **200** (Scheme 2.41).

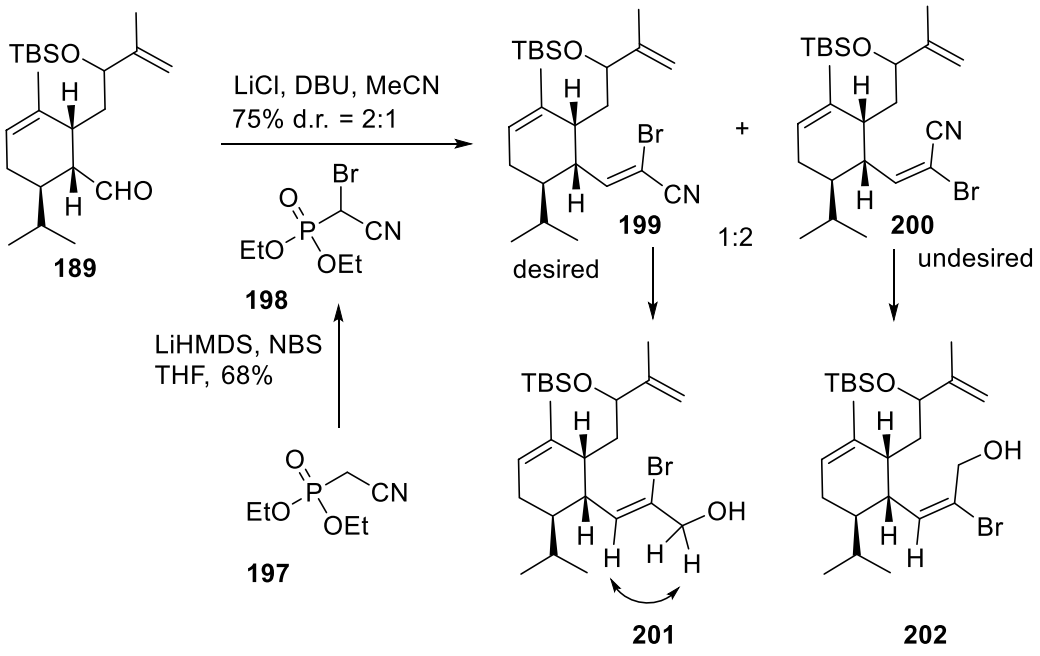


**Scheme 2.41. HWE reaction and ratio determination**

In an attempt to reverse the ratio of diastereoisomers, phosphonates **203**, **204**, **205** and **206** were tested in the HWE reaction (Figure 2.12). Unfortunately, these efforts were fruitless and only led to similar or worse ratios of products.

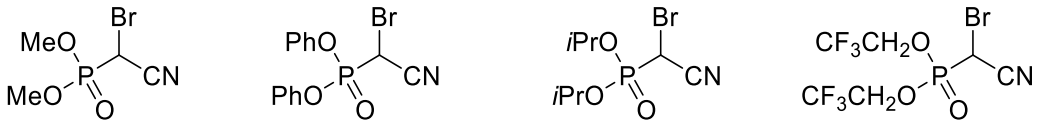

**203** **204** **205** **206**

**Figure 2.12. Screening of phosphonate for HWE reaction**

Although we could not improve the *E/Z* ratio, we speculated that further lithium halogen exchange during the macrocyclization step could potentially isomerize the undesired isomer **207** (Scheme 2.42) via an 'aza-allene' like intermediate **210**.

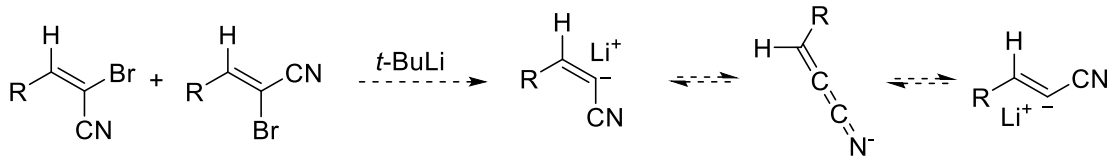

**207** **208** **209** **210** **211**

**Scheme 2.42. Possible interconversion between 209 and 2011**

To determine if this strategy was feasible, the diastereoisomer **200** was reacted with isopropyl magnesium bromide and quantitatively delivered the cis-alkene **213** (entry 1) indicating that no isomerization had occurred during this process. Fortunately, repeating this experiment with *tert*-butyllithium (entry 2) gave a 1:1 mixture of *E* and *Z* alkenes **212** and **213** (Table 2.7).

**Table 2.7. Isomerization attempts of diastereoisomer 200**

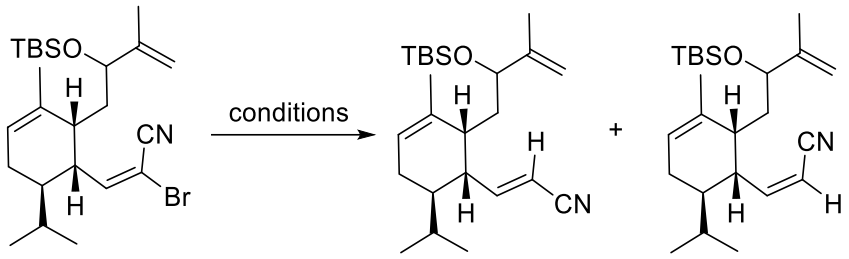

**200** **212** **213**

| entry | reagent | solvent | T (°C) | conversion[a] | yield[b] | ratio (212:213)[c] |
|---|---|---|---|---|---|---|
| **1** | *i*-PrMgBr | THF | -40 °C | 100% | 100% | 0:1 |
| **2** | *t*-BuLi | THF | -78 °C | 100% | 80% | 1:1 |

Note: [a] conversion after 30 minutes [b] yield determined by $^1$H NMR (internal standard) [c] determined by $^1$H NMR (signal integration)

These results were crucial for several reasons. First, it meant that the d.r. of the HWE reaction was not important. Given that only the *Z*-alkene **199** is capable of

reacting intramolecularly with the lactone (due to conformational considerations), the equilibrium would ultimately lead to the formation of the desired vinyl anion **211** during the macrocyclization. Furthermore, treating the equilibrating mixture of vinyl anions with a bromine source (e.g., NBS or $Br_2$) could also lead to the formation of the desired isomer **199** through a recycling process (Scheme 2.43).

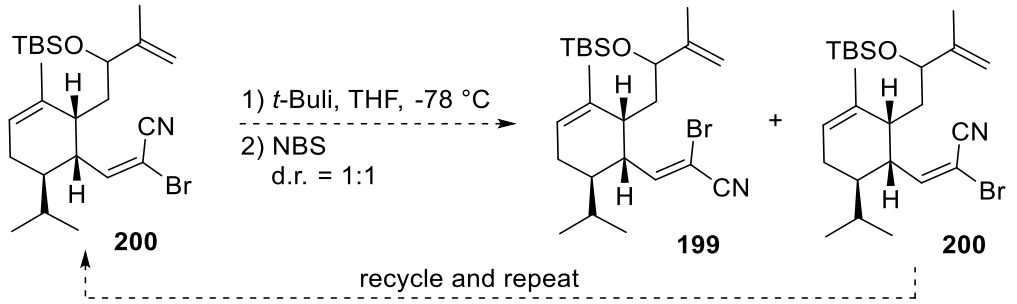


**Scheme 2.43. Recycling process for 200 synthesis**

At this stage of the synthesis, we believed we could install the requisite lactone in a one-step process via an aldol reaction involving cyclobutanone **68** (Scheme 2.44). Further fragmentation in the presence of a hydride source (e.g., sodium borohydride) would provide the desired aldehyde **216**, the precursor for the HWE reaction. This revised strategy would support a more concise synthesis of eleutherobin (**12**).

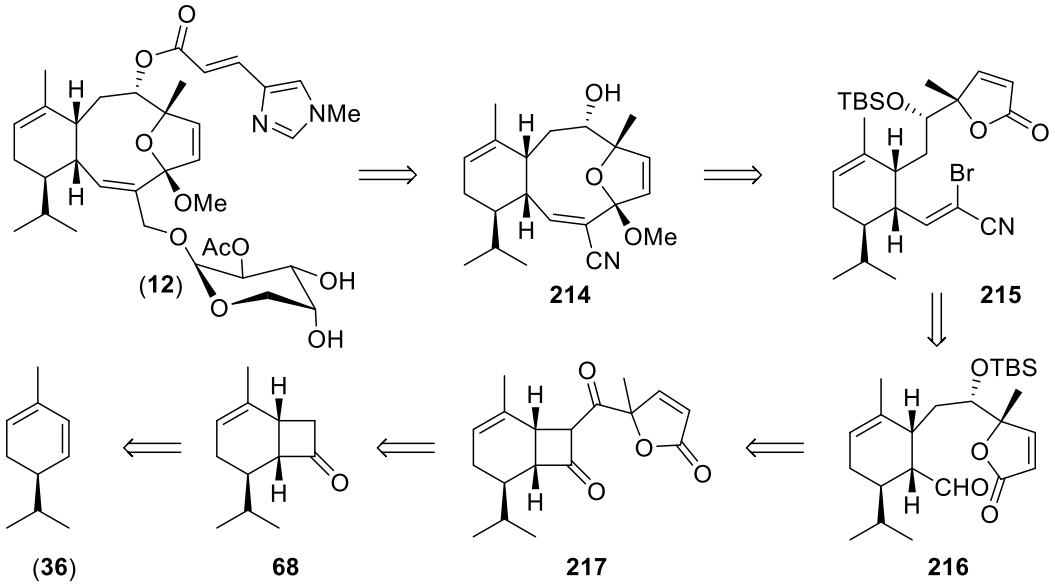


**Scheme 2.44. Remodeled retrosynthetic approach via 217**

For this approach, we envisaged aldehyde **218** and acyl chloride **219** as potential coupling partners for the reaction with cyclobutanone **68** (Figure 2.13). The

aldehyde **218** was designed as a priority target since the reaction of cyclobutanone **68** with aldehydes was established.

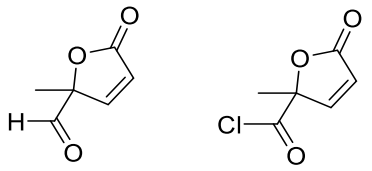

**218** **219**

**Figure 2.13. Potential precursors to react with cyclobutanone 68**

Deprotonation of ethyl propiolate **220** with *n*-butyllithium followed by subsequent addition on methylvinyl ketone **221** provided alcohol **222**. Then, selective hydrogenation of alkyne with the Lindlar catalyst provided the corresponding diene which spontaneously cyclized to generate α,β-unsaturated lactone **223**. While the oxidative cleavage of terminal alkene **223** was anticipated to provide the desired aldehyde, this target molecule has only been reported once and was described as highly unstable.[132] Unfortunately, classical oxidative cleavage conditions using $OsO_4$ and $NaIO_4$ did not provide any of the desired aldehyde due to rapid decomposition. Similarly, an ozonolysis attempt was fruitless (Scheme 2.45).

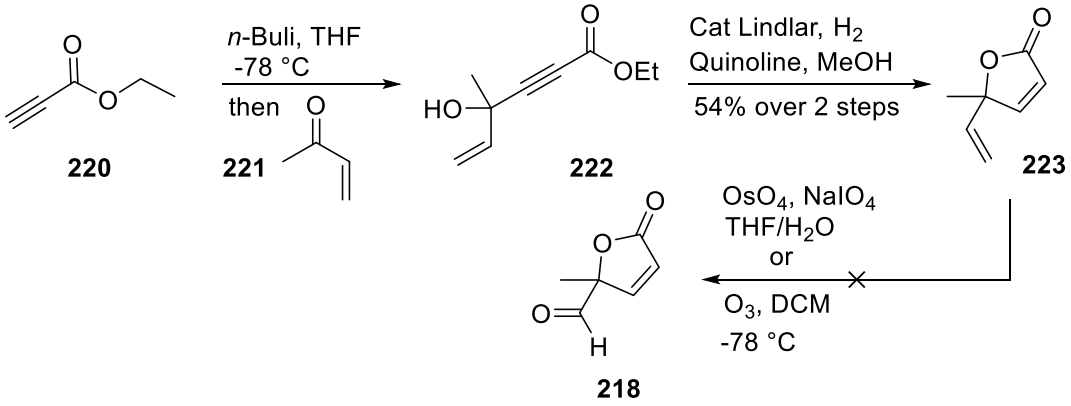


**220** **221** **222** **223** **218**

**Scheme 2.45. Synthesis of α,β-unsaturated lactone 223**

To overcome this problem, we anticipated that a protected alcohol could be used as a precursor to the desired aldehyde. Thus, a similar sequence of reactions was performed using a TBS-protected α-hydroxyl ketone **224** to deliver lactone **226**. Finally, acidic deprotection provided primary alcohol **227** (Scheme 2.46).

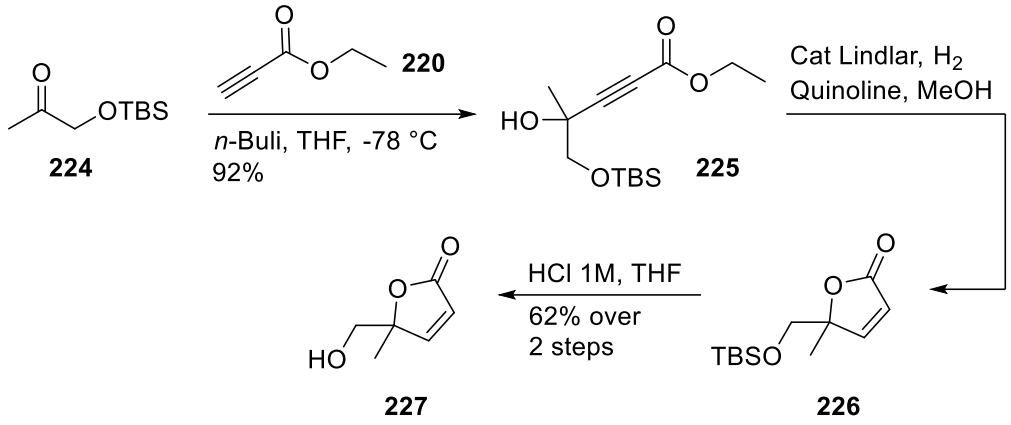


**Scheme 2.46. Synthesis of primary alcohol 227**

Several conditions were attempted for the formation of aldehyde **218** (Table 2.8). First, alcohol **227** was submitted to purified Dess-Martin periodinane in DCM (entry 1). Although an immediate consumption of starting material was apparent by TLC analysis, numerous new spots were visible. After $^{1}$H NMR spectroscopic analysis of the crude reaction mixture, less than 1% of aldehyde **218** was detected (internal standard). This first result corroborated the instability of this compound. Similarly, Swern and PCC oxidations led to complete decomposition of alcohol **227** (entry 2, 3). On the contrary, TEMPO and Ley oxidations left starting material unreacted (entry 4, 5).

**Table 2.8. Alcohol oxidation into aldehyde 218**

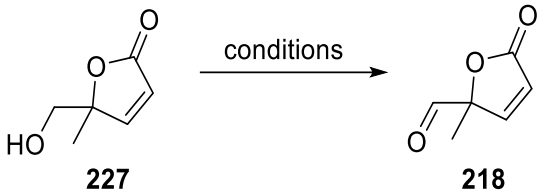


| entry | reagent | solvent | T (°C) | conversion[a] | yield[b] | outcome |
|---|---|---|---|---|---|---|
| **1** | DMP | DCM | 0 | 80% | < 1% | traces of **218** +decomposition |
| **2** | $(COCl)_2$, $Et_3N$ | DMSO | 0 | 75% | 0% | decomposition |
| **3** | PCC | DCM | 0 | 95% | 0% | decomposition |
| **4** | TEMPO, BAIB | DCM | 50 | 0% | 0% | only SM |
| **5** | TPAP, NMO | DCM | 50 | 0% | 0% | only SM |

Note: [a] conversion after 20 minutes [b] yield determined by $^{1}$H NMR (internal standard)

Based on these results, we explored the synthesis of the corresponding acyl chloride. Thus, we applied the same strategy to generate *tert*-butyl ester **228** in good yield and the corresponding carboxylic acid **229** was accessed quantitively under acidic conditions without observing any lactone-opening side-products. To finish the

sequence, carboxylic acid **229** was reacted in the presence of oxalyl chloride and DMF to provide acyl chloride **219**. Notably, the reaction mixture was concentrated on the Schlenk line to avoid any contact with oxygen or moisture (Scheme 2.47).

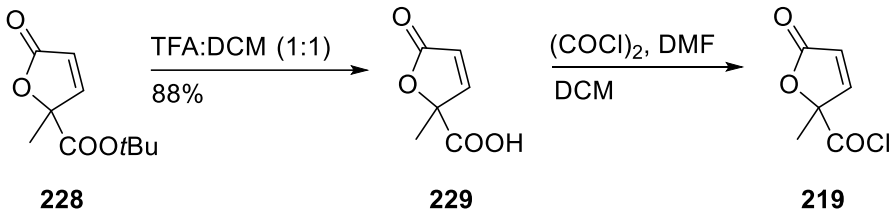


**Scheme 2.47. Synthesis of acyl chloride 219**

Delighted to be in possession of several milligrams of **219**, deprotonation of cyclobutanone **68** was followed by the addition of freshly prepared acyl chloride **219** as a solution in toluene (Scheme 2.48). After the complete disappearance of starting material by TLC, the reaction mixture was analyzed by NMR spectroscopy. Interestingly, two doublet of doublets (dd) were observed at ~4.5 ppm and could account for a mixture of diastereoisomers of **217**. A long-range coupling between the opposite proton on the cyclobutanone explained multiplicity. Unfortunately, attempts to isolate these products were fruitless and repetition of this experiment led to reproducibility issues. We believed that the instability of acyl chloride **219** was the source of problems and indeed NMR spectroscopic analysis of acyl chloride **219** (internal standard) immediately after preparation showed that the yield was less than 10%.

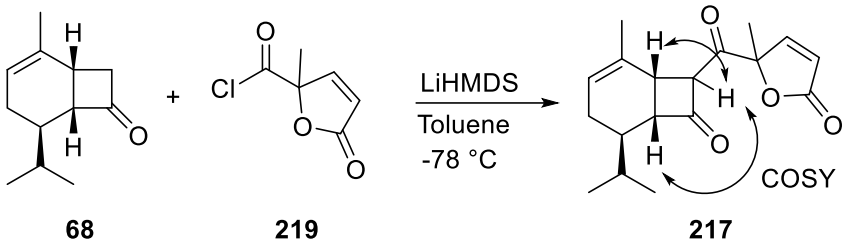


**Scheme 2.48. Coupling of 68 with acyl chloride 219**

To assess the feasibility of the coupling of cyclobutanone **68** with acyl chlorides in general, we envisioned the use of a simple trisubstituted acyl chloride that would deliver a stable 1,3 diketone while assessing the presence of a bulky partner. After some considerations, pivaloyl chloride **230** was chosen and submitted to the cyclobutanone enolate in toluene (Scheme 2.49). All starting material was rapidly

consumed to generate a new spot by TLC. Subsequent NMR spectroscopy of the crude mixture highlighted the presence of a doublet of doublets (dd) at 4.41 ppm. The reaction mixture was clean and included a single diastereoisomer. From this observation, it was clear that a more stable acyl chloride **231** was required.

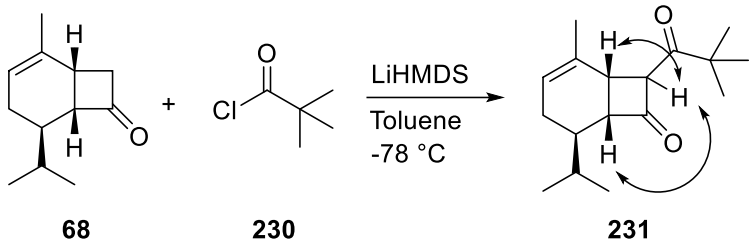


**68** **230** **231**

**Scheme 2.49. Coupling attempt with pivaloyl chloride 230**

Towards this goal, we believed that coupling cyclobutanone **68** with 5-methoxy furan-2-carbaldehyde would address the instability issues. The remainder of the synthetic plan remained the same with the exception of an extra step for the dearomatization of the furan (**215** from **233)** (Scheme 2.50).

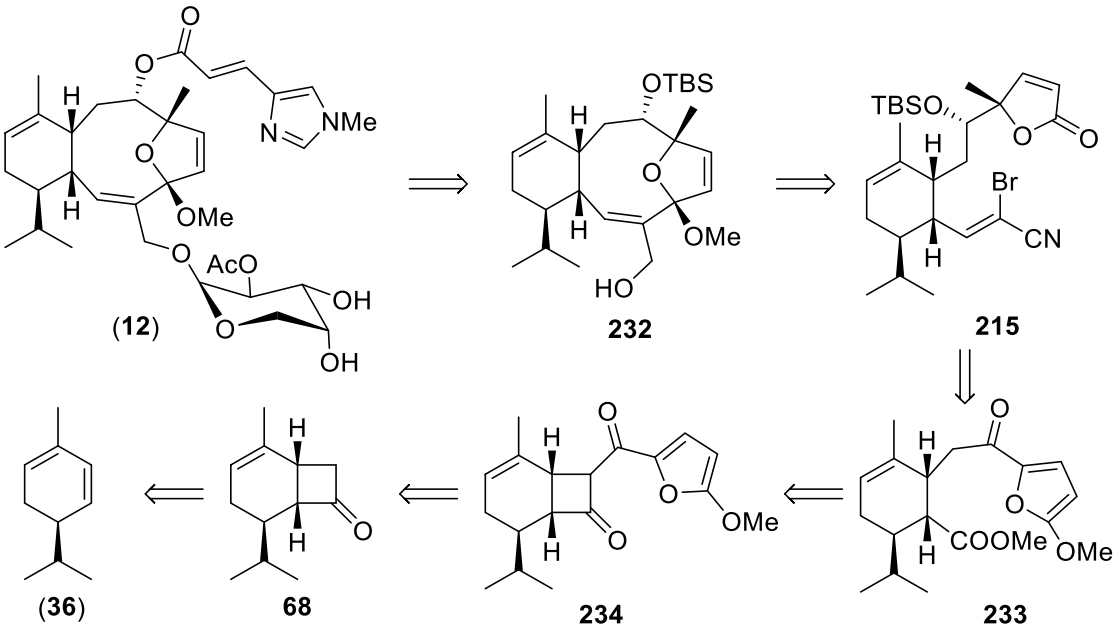

(**12**) **232** **215**

(**36**) **68** **234** **233**

**Scheme 2.50. Retrosynthetic approach using furan intermediate 234**

Following this new strategy, aldehyde **236** was synthesized from commercially available 2-methoxyfuran **235**. Deprotonation of C5 with *n*-butyllithium and subsequent addition of DMF provided the desired aldehyde **236** in good yield (53 %). With aldehyde

**236** in hand, the aldol reaction was performed and rapidly delivered the desired product **237** in 67% as a mixture of diastereoisomers (Scheme 2.51).

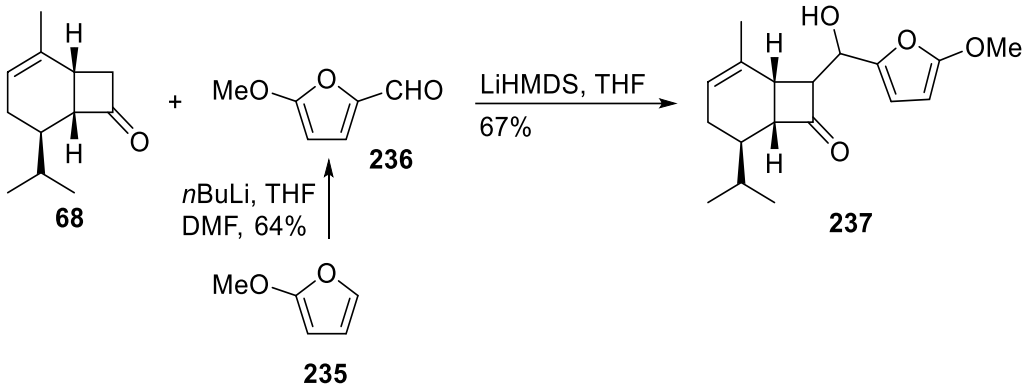


**Scheme 2.51. Aldol reaction of cyclobutanone 68 with aldehyde 236**

To trigger the cyclobutanone fragmentation, it was required to oxidize the alcohol function. Surprisingly, this step proved to be more challenging than expected as the methoxyfuran group was prone to competitive oxidation (Table 2.9). Indeed, DMP oxidation mainly led to decomposition with minor formation of side-product **238** (entry 1). Oxidations using PCC, Parikh-Doering, $MnO_2$, tempo/BAIB and DDQ all provided **238** as the main product (entry 2-6) Finally, a Ley oxidation provided the desired product in 25% yield (internal standard) (entry 7). Notably, the lactone **238** derives from the decomposition pathway of furfuryl alcohol under oxidative conditions is depicted below. First, oxidation of the furane **239** leads to the formation of an enedione intermediate **240** that further cyclizes to hemiketal **241**. When the furan bears a methoxy group, a ketone is generated as seen with side-product **238**.

**Table 2.9. Oxidation of secondary alcohol 237**

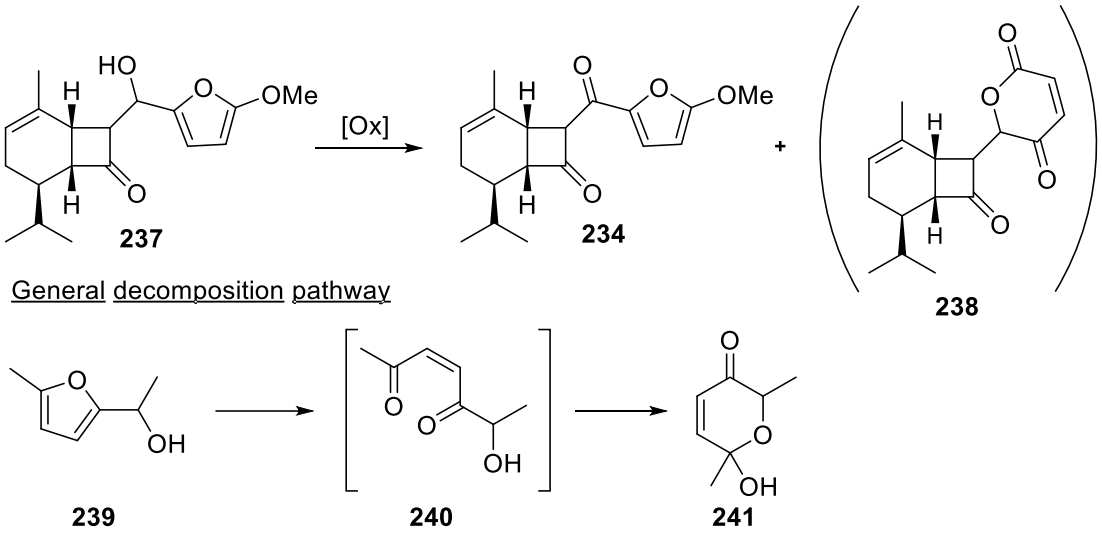


| entry | reagent | solvent | conversion[a] | yield[b] | outcome |
|---|---|---|---|---|---|
| **1** | DMP, $NaHCO_3$ | DCM | 100% | 0% | **238** + decomposition |
| **2** | PCC | DCM | 100% | 0% | **238** |
| **3** | $NEt_3$, $SO_3$.pyr, DMSO | DCM | 80% | 0% | decomposition |
| **4** | $MnO_2$ | DCM | 20% | 0% | **238** |
| **5** | TEMPO, BAIB | DCM | 50% | 0% | **238** |
| **6** | DDQ | benzene | 70% | 0% | **238** |
| **7** | TPAP, NMO, 4A MS | DCM | 100% | 25% | **234** |

Note: [a] conversion after 30 minutes [b] yield determined by $^1H$ NMR (internal standard)

Due to its instability, diketone **234** was immediately subjected to ring-opening conditions of the cyclobutanone using methoxide in methanol. To our delight, methyl ester **233** was purified and isolated in 22% yield over these two steps. Although the yield was low, this reaction was thought to provide sufficient material to reach and assess the key step. Moving forward, we first reduced both the ester and ketone function to afford the corresponding diol **242**. Unfortunately, classic work-up conditions led to the conversion of **242** into **243** during the solvent evaporation process (probably due to basicity). To overcome this problem, the reaction mixture was extracted with dichloroethane (DCE) which ultimately allowed us to evaporate the THF without having the mixture go to dryness. A subsequent Ley oxidation in DCE generated ketoaldehyde **244** in a poor 14% yield over two steps. Finally, the HWE reaction provided a mixture of both vinyl bromide **245** and **246** in 64% yield with a 2:3 mixture of diastereoisomers in favor of the 'undesired' product **246** (Scheme 2.52).

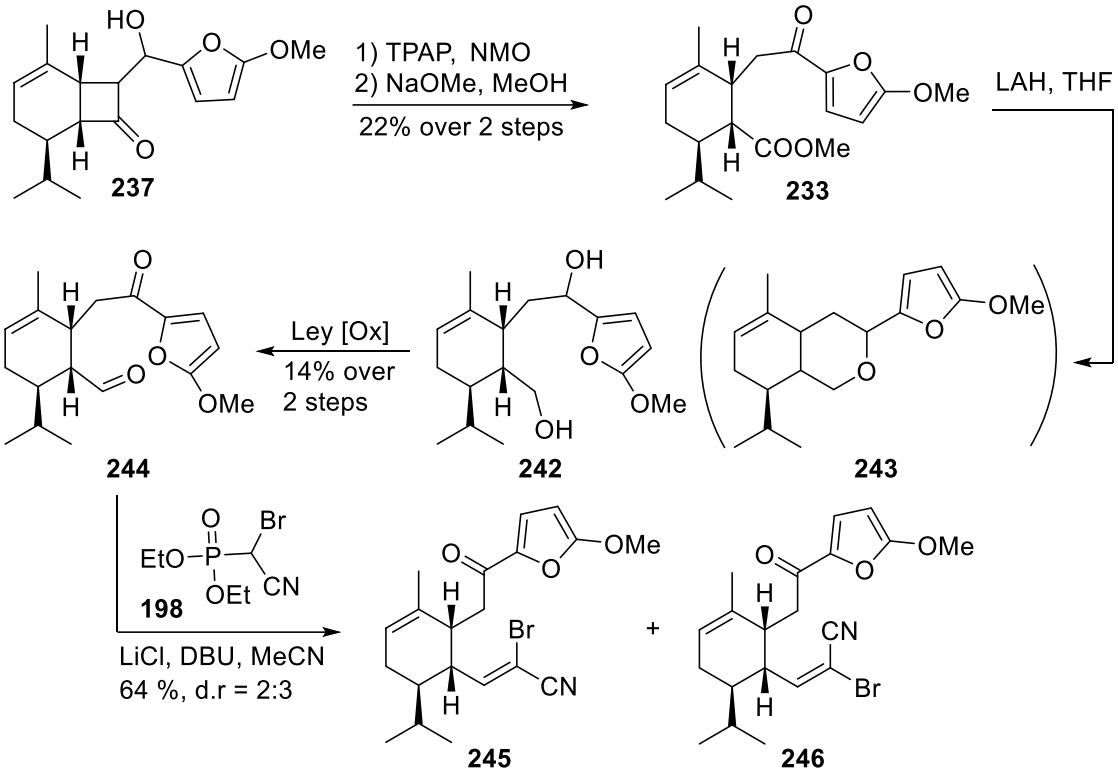


**Scheme 2.52. Synthesis of bromo cyano alkene 245**

Although this synthetic sequence led to the formation of vinyl bromide **245**, the overall yield was poor due to numerous steps of oxidation and reduction. To tackle this issue, we designed an alternative synthesis using acyl chloride **247** to remove the low-yielding oxidation step (Scheme 2.53). This new strategy proceeded with a 12% yield over 5 steps compared to 1.1% over 8 steps for the previous route.

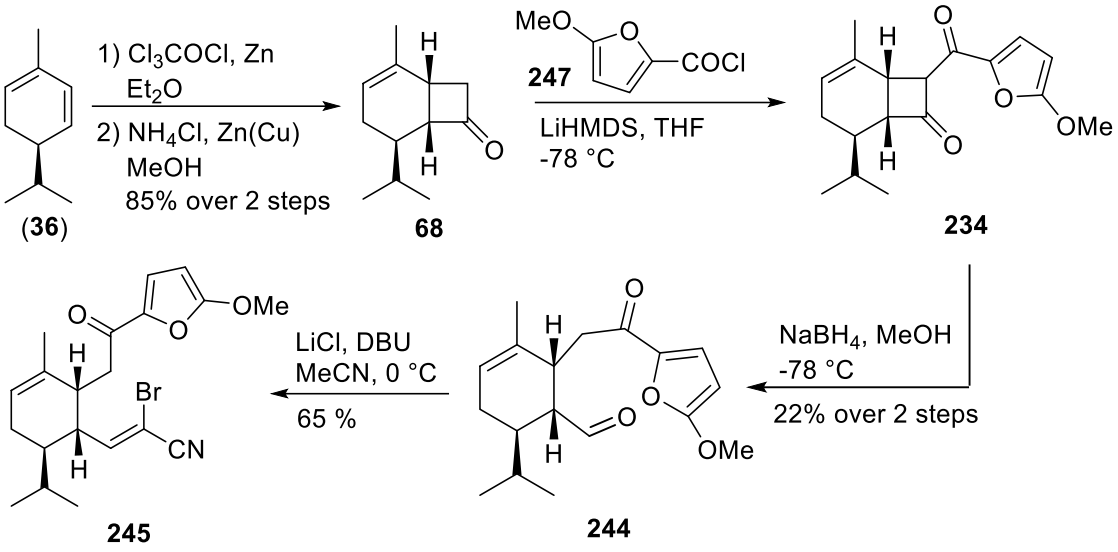


**Scheme 2.53. Alternative strategy toward bromo cyano alkene 245**

Before investigating the methoxy furan cleavage of **245**, a model system was first investigated to determine the optimal reaction conditions. Thus, 2-methoxyfuran **235** was treated with *n*-butyllithium followed by hydrocinnamaldehyde **248**. A subsequent Ley oxidation provided the ketone **249** (Scheme 2.54).

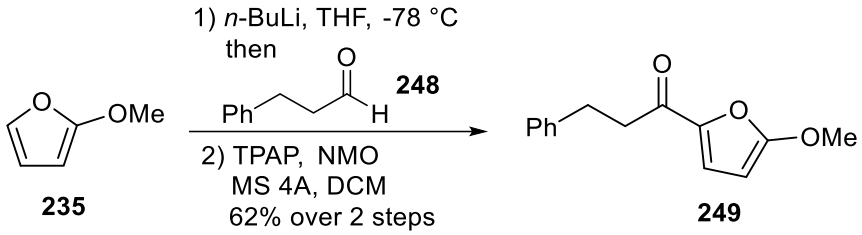


**Scheme 2.54. Synthesis of 249 to assess "OMe" cleavage**

Shengming Ma *et al.* have reported the use of sodium iodide for the formation of α,β-unsaturated lactones from alkoxy furans.[133] Unfortunately, repeating these conditions on furan **249** failed to provide lactone **250**. Screening of a range of solvents (e.g., THF, acetone, acetonitrile, EA) at temperatures up to their boiling points gave only unreacted starting material. In contrast, acidic conditions (i.e., PTSA) consumed methoxyfuran **249** but generated side-product **251** in the presence of water (Scheme 2.55).

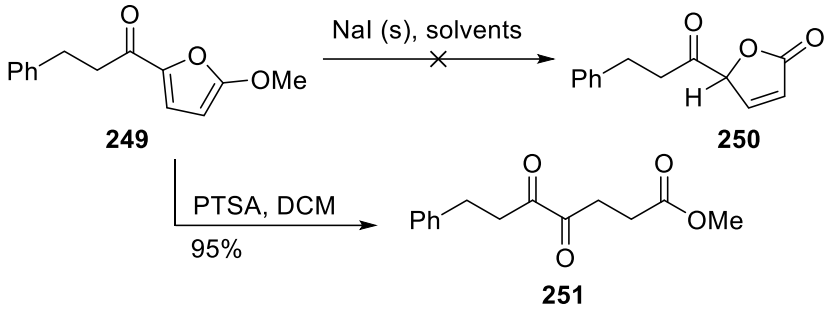


**Scheme 2.55. "OMe" cleavage attemp under acidic conditions**

Disappointed with these preliminary results, we turned to the use of TMSI and $BBr_3$, both known as useful reagents for the removal of aromatic methoxy groups. In both cases, the desired product **252** and regioisomer **253** were produced. Further submission to base (i.e., $K_2CO_3$) and methyl iodide led to a mixture of different products that included SM (**252**, **253**) ~ 10%, **250** ~ 15%, **254** ~ 8%, **255** ~ 11%, **256** ~ 56% (Scheme 2.56).

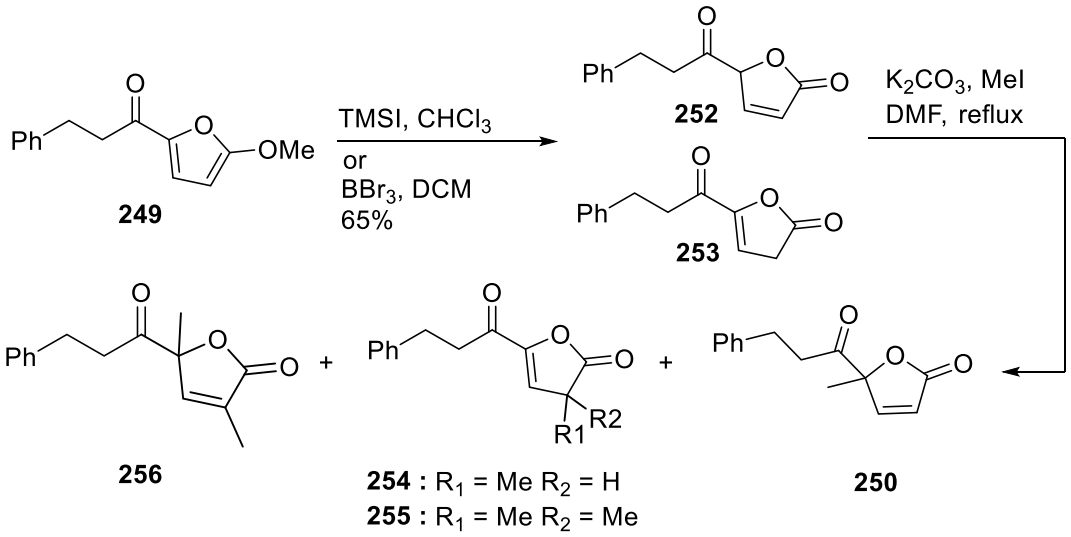


**Scheme 2.56. Dearomatization and subsequent methylation**

When these conditions were applied to the more elaborate methoxy furan **245** and the reaction was monitored by mass spectroscopy, the expected mass (392 and 394) was found after 15 min. After work-up, analysis of the reaction mixture by $^1H$ NMR spectroscopy showed less than 1% of the expected product and purification on silica gel provided us with a mixture of 4 non-separable diastereoisomers. NMR spectroscopic analysis combined with mass spectroscopy experiments indicated the formation of the pyran **259**. Mechanistically, deprotection of the methoxy group is likely

followed by the formation of a stabilized enolate anion **258** that engages in a 1,4 addition to yield compound **259** as a mixture of 4 diastereoisomers (i.e., (*E*)-(*E*), (*Z*)-(*Z*), (*E*)-(*Z*), (*Z*)-(*E*)).

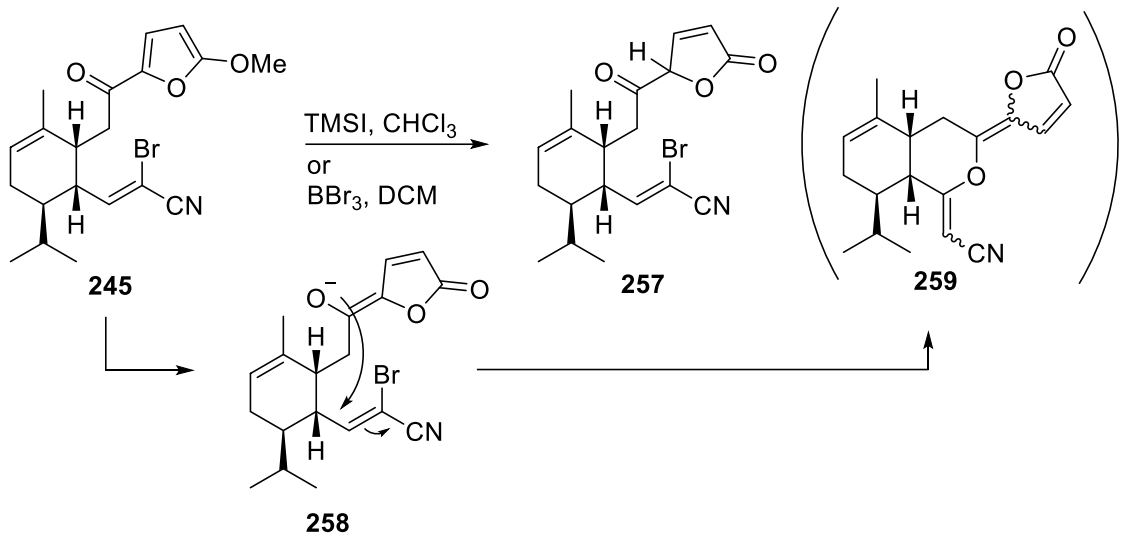


**Scheme 2.57. Dearomatization attempt bromo cyano alkene 245**

To further assess the propensity of the extended enolate to engage in intramolecular reactions, we applied the same conditions to the corresponding aldehyde **244** (Scheme 2.58). The presence of a doublet at 5.1 ppm in the $^{1}$H NMR spectrum and a signal at 120 ppm in the $^{13}$C NMR spectrum were consistent with the acetal **260**. These results suggested that having an electrophilic group (e.g., aldehyde or α,β-unsaturated nitrile) at this position would present problems.

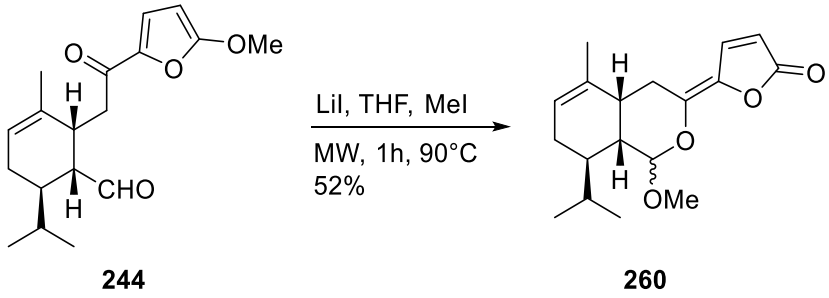


**Scheme 2.58. Dearomatization attempt on aldehyde 244**

Moving forward, we envisioned that nitrile could be reduced to the corresponding protected allylic alcohol to reduce the reactivity of the alkene function. For the sake of convenience, we took advantage of Danishefsky's intermediate **264** to evaluate our new strategy. To commence the synthesis, cyclobutanone **68** was

submitted to Bredereck's reagent (i.e., *t*-BuOCH($NMe_2$)$_2$) to provide enone **263** that was opened under acidic conditions to generate Danishefsky's intermediate **262**. A sequence of reduction/oxidation furnished the aldehyde **263** that underwent an HWE olefination to provide vinyl bromide **264** and **265** in good yield and as a mixture of diastereoisomers. As planned, the nitrile group was reduced to the corresponding alcohol following a 2-step sequence involving diisobutylaluminum hydride and sodium borohydride. Subsequent TBDPS-protection delivered the protected allylic alcohol **266** in 90% yield over 3 steps. To install the methoxyfuran, ketal **266** was deprotected to provide the corresponding aldehyde, which underwent reaction with lithiated 2-methoxyfuran to deliver alcohol **267** as a mixture of diastereoisomers. Finally, oxidation of furfuryl alcohol **267** generated the advanced intermediate **268**. With great excitement, vinyl bromide **268** was submitted to lithium iodide in THF and was heated at 80 °C for 1 hour in the microwave reactor (Scheme 2.59). Unfortunately, the starting material was recovered intact. Increasing the temperature and the time of the reaction only led to decomposition.

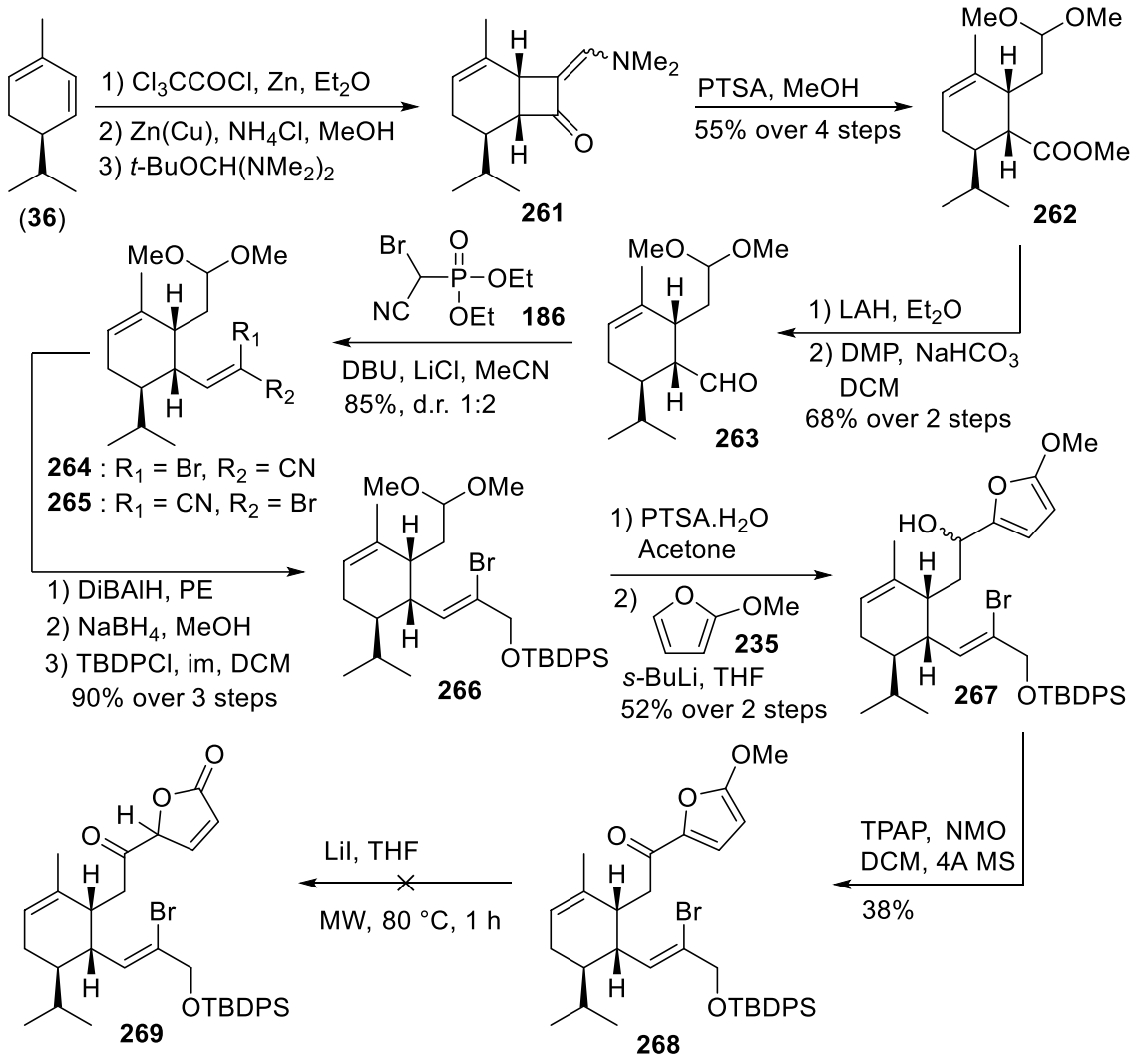


**Scheme 2.59. Synthesis of 268 and "OMe" cleavage attempt**

At this stage, the challenges associated with the conversion of methoxyfuran **268** into the requisite lactone **269** as well as the lack of diastereocontrol in this sequence forced us to pursue an alternative synthesis. We anticipated that addition of commercially available α-angelicalactone **271** to aldehyde **270** would avoid the challenging deprotection (Table 2.10). Our initial attempts to effect this transformation using sodium *tert*-butoxide in THF provided **272** as a minor product accompanied by several products of decomposition (entry 1). Unfortunately, in toluene, decomposition was the exclusive pathway (entry 2). The use of potassium *tert*-butoxide led to a similar outcome (entries 3 and 4). Surprisingly, the use of lithium *tert*-butoxide only led to a mixture of isomer **273** and diene **274** in both THF and toluene (entry 5, 6). The use of amine bases such as DBU (entry 7) provided product **275** from homocoupling.

**Table 2.10. Screening of α-angelicalactone addition on 270**

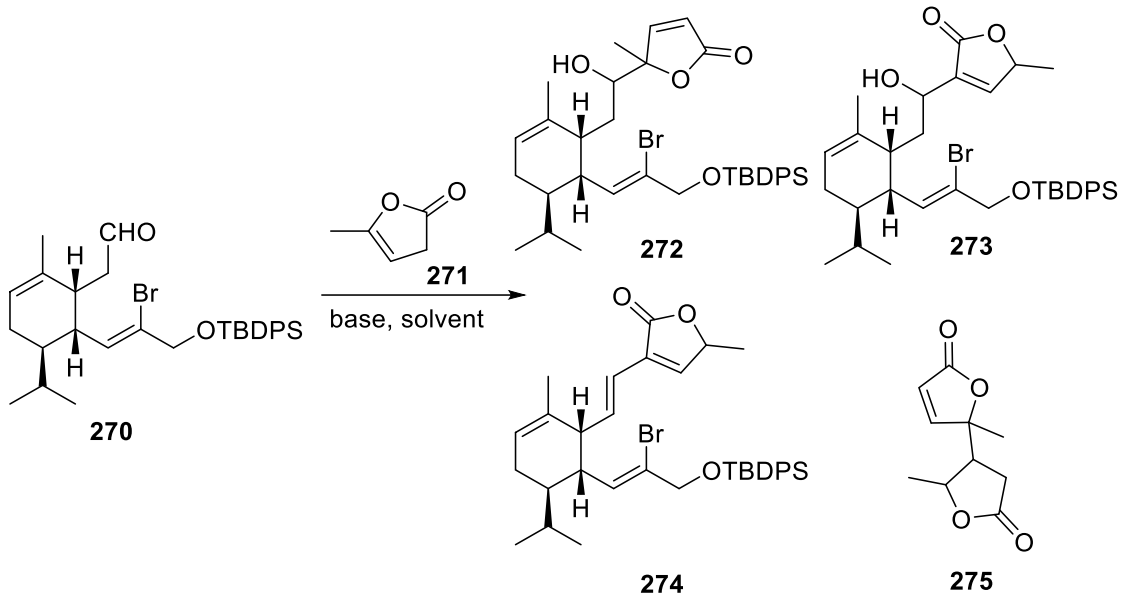


| entry | base | solvent | base (eq) | lactone (eq) | conversion[a] | yield[b] | outcome |
|---|---|---|---|---|---|---|---|
| **1** | NaOtBu | THF | 2 | 2 | 100% | 8% | **272** |
| **2** | NaOtBu | Toluene | 2 | 2 | 90% | 3% | **272** |
| **3** | KOtBu | THF | 2 | 2 | 100% | 12% | **272** |
| **4** | KOtBu | Toluene | 2 | 2 | 90% | 5% | **272** |
| **5** | LiOtBu | THF | 2 | 2 | 65% | 0% | **273** + **274** |
| **6** | LiOtBu | Toluene | 2 | 2 | 85% | 0% | **273** + **274** |
| **7** | DBU | DCM | 4 | 5 | 15% | 0% | **275** |

Note: [a] conversion after 30 minutes [b] yield of **272** determined by $^1$H NMR (internal standard) Purification (KO*t*Bu): Potassium *tert*-butoxide (10 g) was stirred in THF (100 mL) for 10 min. Subsequent filtration and evaporation provided a clean powder of KO*t*Bu (1 g) that was stored under inert atmosphere.

From these results, potassium *tert*-butoxide proved to be the most promising base and we next explored equivalents of reagents. Specifically, we examined the use of excess lactone **271** (5 eq) while varying the equivalents of KO*t*Bu (Table 2.11). Notably, purification of KO*t*Bu was essential for reaction reproducibility. As indicated in entries 1 and 2, catalytic amounts of base led to a low yield (<15%). Increasing the equivalents improved the yield of the reaction, with 51% using 2.5 equivalents of base (entries 3 and 4). A large excess of base was detrimental to the reaction (entries 5 and 6).

**Table 2.11. Impact of the base equivalents**

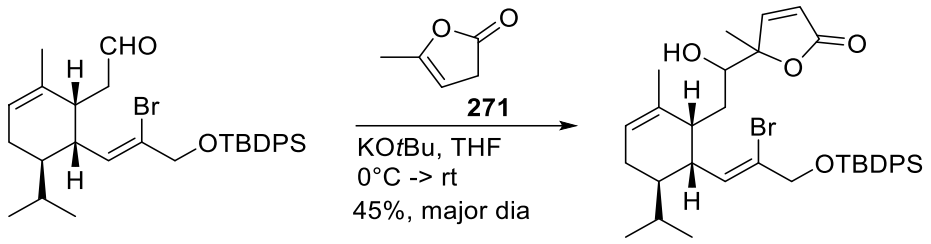


**270** **272**

| entry | lactone (eq) | base (eq) | conversion[a] | yield[b] |
|---|---|---|---|---|
| **1** | 5 | 0.05 | 100% | <15% |
| **2** | 5 | 0.25 | 100% | <15% |
| **3** | 5 | 0.50 | 100% | 28% |
| **4** | 5 | 2.5 | 100% | 51% (45% major dia) |
| **5** | 5 | 5 | 100% | <15% |
| **6** | 5 | 10 | 100% | <15% |

Note: [a] conversion after 1 hour [b] yield determined by $^1$H NMR (internal standard)

Finally, TBS protection of alcohol **272** led to precursor **276** in modest yield for this type of reaction. With compound **276** in hand, we were finally able to assess the macrocyclization. Surprisingly, when vinyl bromide **276** was treated with *tert*-butyllithium, no lithium-halogen exchange was observed, even at elevated temperatures. At room temperature, *tert*-butyllithium addition to the lactone only generated **278**. This result confirmed that the lactone was sufficiently electrophilic to engage in reactions with organometallic reagents and that perhaps the TBDPS group creates a steric barrier to lithium-halogen exchange. Thus, the TBDPS group was removed with HF/pyridine to afford alcohol **279**. Unfortunately, using substrate **279** with an excess of *tert*-butyllithium, no lithium-halogen exchange occurred and only *tert*-butyl addition was observed in the generation of **281**. As a final attempt, we submitted substrate **279** to Nozaki-Hiyama-Kishi conditions. Even though there are no reports of this reaction using an ester, the goal was to assess the feasibility of a chromium insertion between the $Csp^2$-Br bond thus gaining insights into the reactivity of vinyl bromide **279**. Here again, starting material **279** was recovered unreacted (Scheme 2.60). Overall, these results suggested that the vinyl nitrile was essential for facile lithium halogen exchange (vide supra).

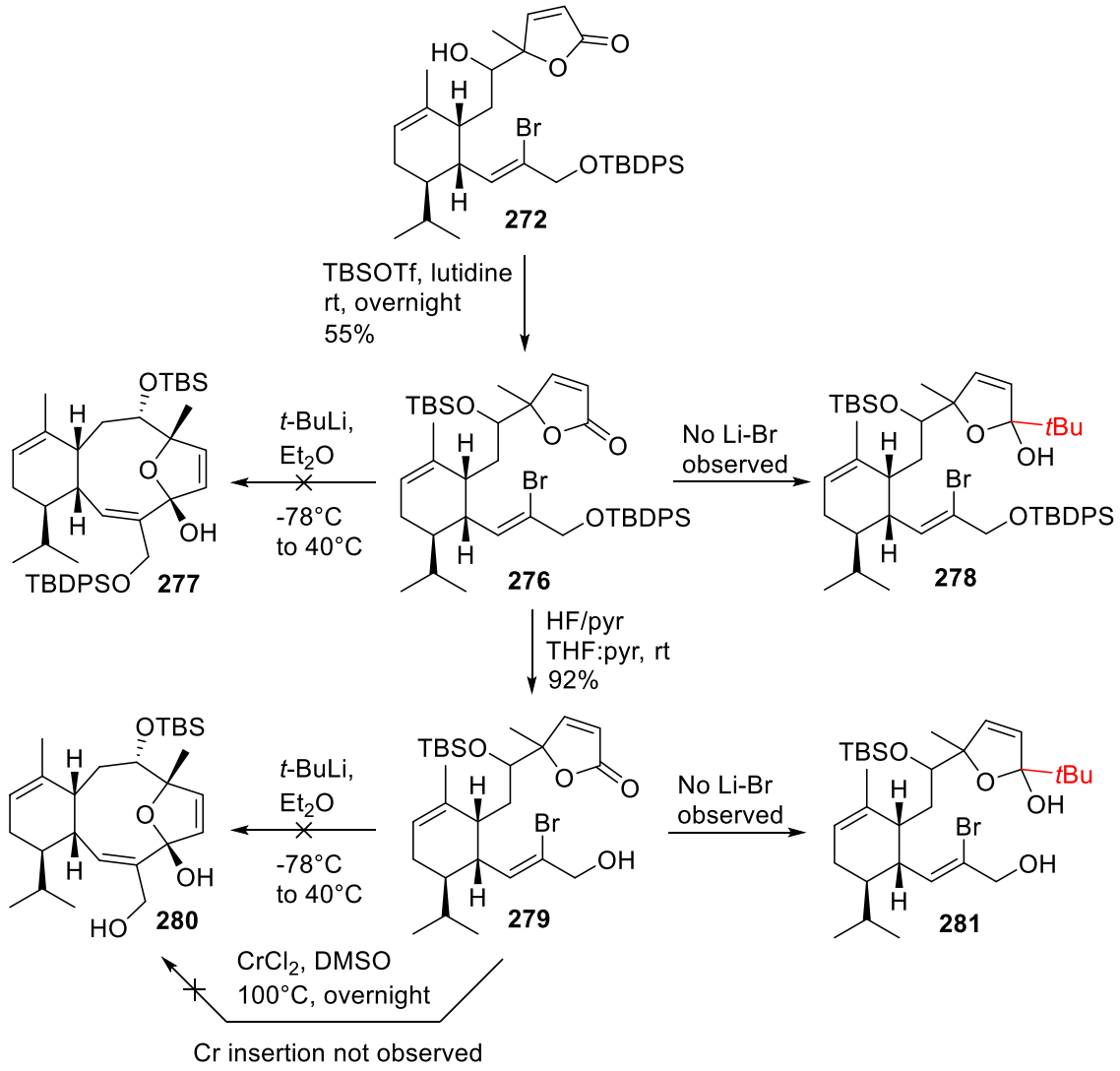


**Scheme 2.60. No halogen-lithium exchange observed**

To test this theory, a cyclization precursor that contained both lactone and cyano bromo alkene function was required (Scheme 2.61). Towards this goal, reduction of ester **262** with $LiAlH_4$ provided alcohol **282**. A subsequent sequence of protection/deprotection steps generated aldehyde **283** in good yield.

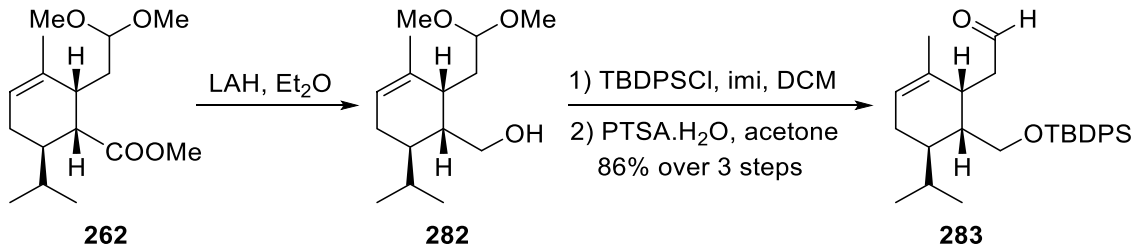


**Scheme 2.61. Synthesis of aldehyde 283**

Interestingly, Mateo and coworkers reported that in reaction with aldehydes, an electron-donating group, such as an alkylamine at the C4 position of 5H-furan-2-one favored the formation of C5 substituted derivatives **285**.[134] Similarly, Royer and coworkers used lactone **284** to selectively react at C5 with aldehydes and acyl chlorides (Scheme 2.62).[135] To test this reagent, lactone **284** was prepared in 2 steps from commercially available tetronic acid in 89% yield following a literature procedure.

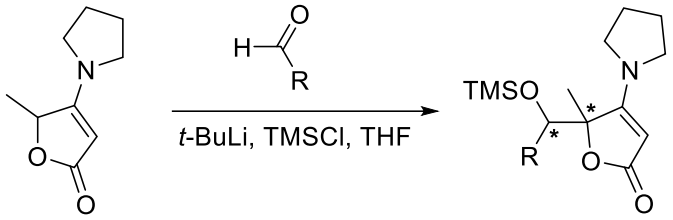


**284** **285**

**Scheme 2.62. Reported examples from the Royer group**

Further coupling of aldehyde **283** with lactone **284** afforded a mixture of free and TMS-protected alcohol that was directly treated with PPTS to generate free alcohol **286** as a main diastereoisomer (not characterized). While attempts to protect the alcohol function with a TBS group failed, using the smaller SEM protecting group delivered **287** in good yield. Deprotection of the pyrrolidine was performed through a two-step sequence. The first step consisted of reducing the double bond with sodium cyanoborohydride. Then, formation of *N*-oxide triggered a Cope-like elimination that reinstalled the unsaturation in **288** via elimination of the pyrrolidine group. Deprotection of TBDPS followed by oxidation of the alcohol led to aldehyde **289**, which was immediately submitted to HWE conditions to generate the cyano bromo alkene (**290**:**291**) as a 2:1 mixture of diastereoisomers favoring the undesired *E* isomer **291** (Scheme 2.63).

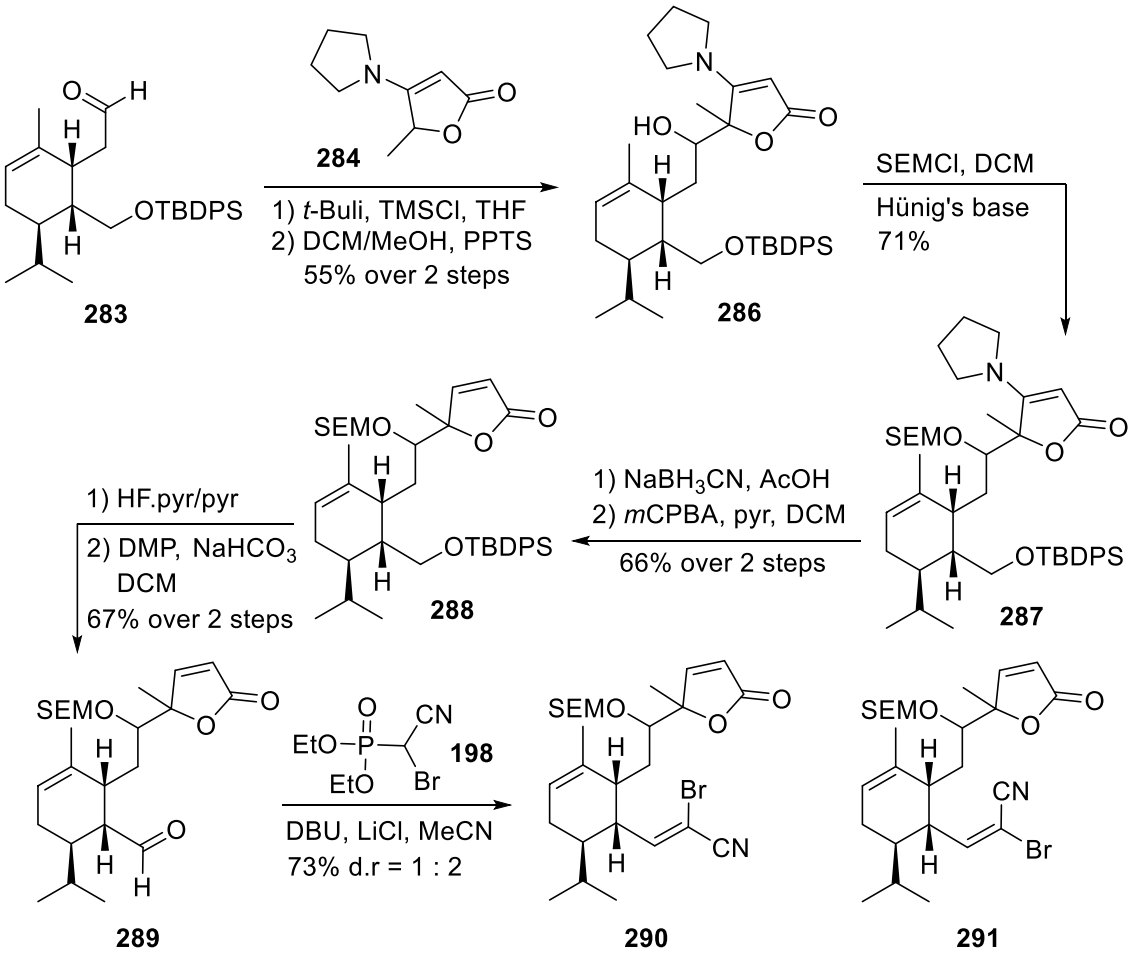


**Scheme 2.63. Synthesis of bromo cyano alkene 290**

To our delight, submission of precursor **290** to *tert*-butyllithium immediately generated vinyl anion **292**, confirming that electron-withdrawing cyano group was essential for bromine-lithium exchange (Scheme 2.64). Unfortunately, the vinyl anion did not react with the lactone function at low or elevated temperatures. Similarly, isopropyl magnesium bromide also promoted a magnesium-bromide exchange but did not provide any desired product, instead affording after work up the olefin **294** as the exclusive product. Repetition of this reaction in several solvents (e.g., petroleum ether, $Et_2O$, THF, and THF/TMEDA) failed to provide **293**. The failure of the vinyl anion to react with the lactone carbonyl may well be due to one of several issues that include steric (i.e., incapability of properly aligning with π* carbonyl due to C7 or C8 hindrance), diminished reactivity (i.e., weak lactone electrophilicity or vinyl anion nucleophilicity), entropic factors (i.e., energy of the product increases). Interestingly, both macrocyclizations performed by Nicolaou and Danishefsky involve aldehydes and

planar/linear nucleophiles, which we are lacking in **290**. As a result of this failure, we were forced to readjust the strategy for the formation of the large ring in eleutherobin's core.

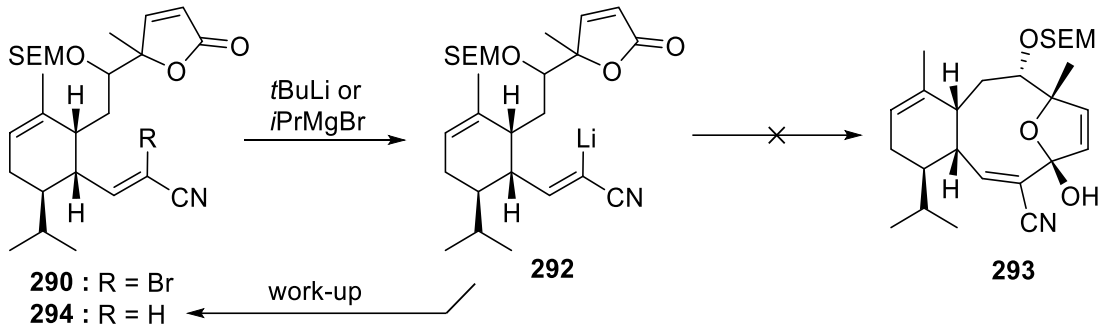


**Scheme 2.64. Cyclization attempts**

## 2.4.2. Macrocyclization Via Knoevenagel Condensation

At this stage, we aimed to design a unique cyclization strategy. It is known that aldehydes are amongst the best electrophiles and therefore have been used in many types of macrocyclizations (e.g., NHK, HWE, aldols) including the two prior syntheses of eleutherobin (Scheme 2.2 & 2.3). We anticipated that an intramolecular Knoevenagel condensation could provide bicyclo[8.4.0]tetradecane **295** from **296** which in turn would be functionalized to generate ketal **179** (Scheme 2.65).

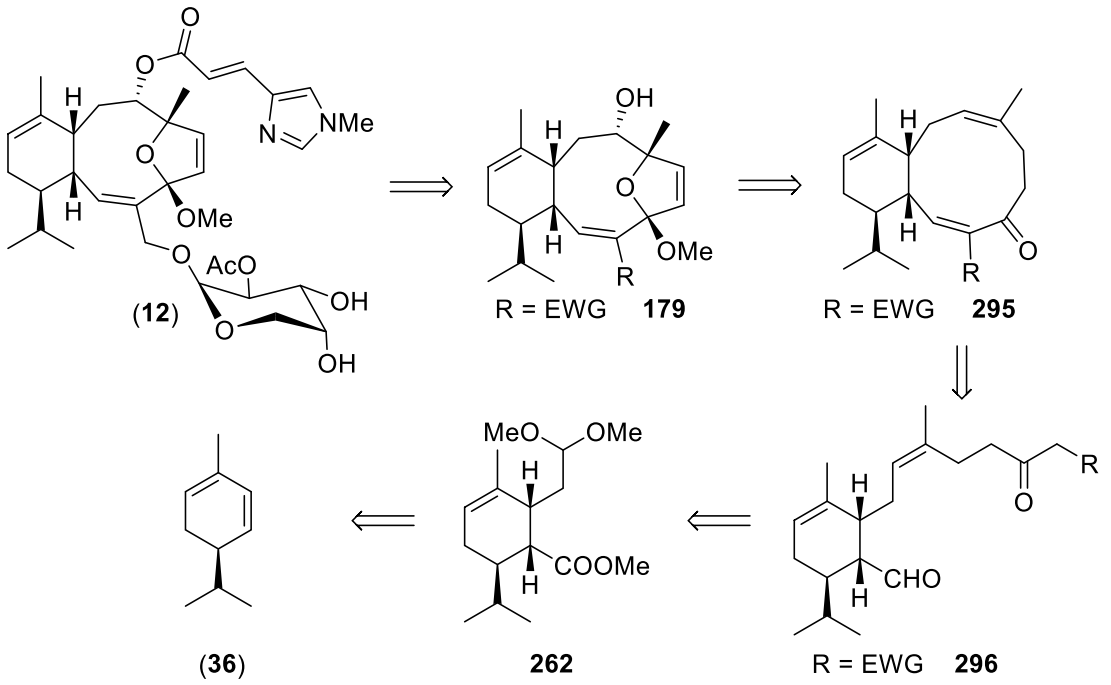


**Scheme 2.65. Ultimate retrosynthetic strategy**

To generate the precursor to the Knoevenagel reaction, we believed that either a Wittig or Corey-Chaykovsky reaction, using phosphorus ylide **297** and sulfur ylide **298**, respectively, would provide the corresponding alkene **299** or epoxide **300** in a short number of steps (Scheme 2.66).

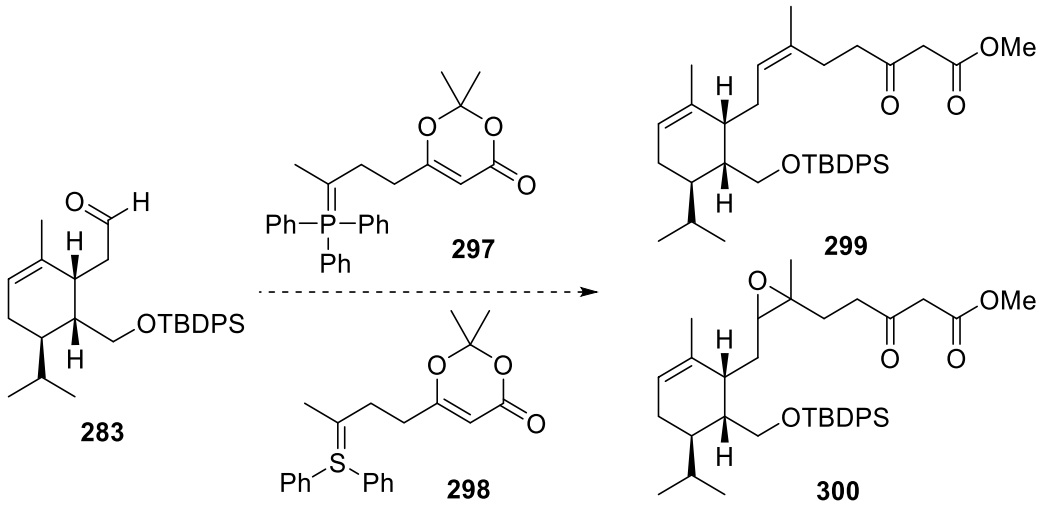


**Scheme 2.66. Synthetic route to potential precursors 299 and 300**

The corresponding alkyl bromide **306** was envisioned as a common building block for the synthesis of phosphorus ylide **297** and sulfur ylide **298**. Thus,

commercially available dioxinone **301** was brominated to generate allyl bromide **302** in good yield. The next step consisted of a displacement using benzyl acetoacetate. Conditions reported by Sato and coworkers using sodium hydride in DMF led to a poor 15% yield.[136] Screening different inorganic bases ultimately identified cesium carbonate as an improved alternative for the nucleophilic substitution, which delivered ketoester **303** in excellent yield. Hydrogenation effected the benzyl deprotection and spontaneous decarboxylation providing ketone **304**. Finally, reduction of ketone **305** followed by an Appel reaction in presence of $CBr_4$ provided the desired alkyl bromide **306** in excellent overall yield (Scheme 2.67).

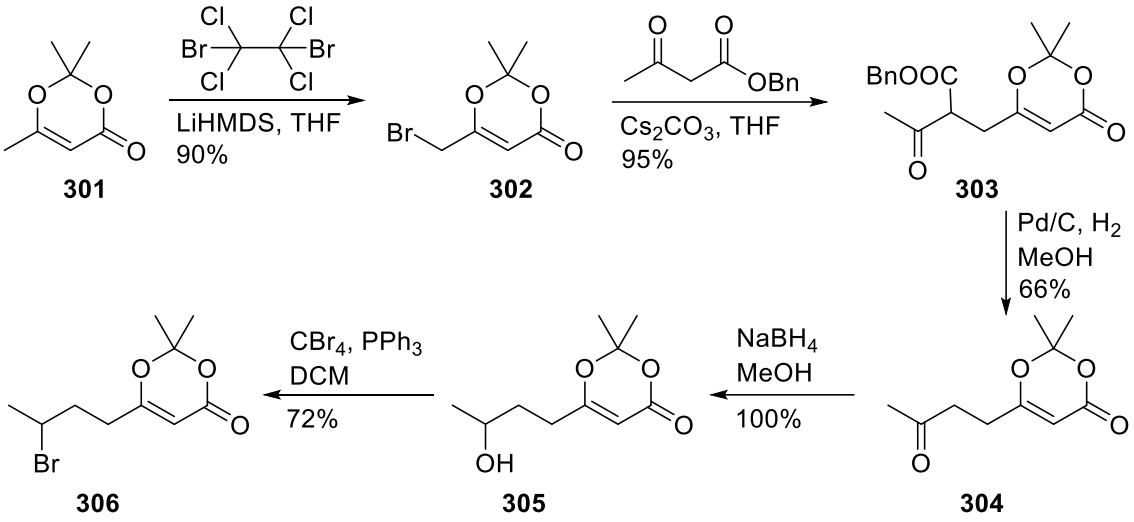


**Scheme 2.67. Synthesis of common building block 306**

With alkyl halide **306** in hand, we focused our primary efforts toward the synthesis of phosphonium salt **307**. To generate phosphonium salt **307**, alkyl bromide **306** was reacted with triphenylphosphine in toluene (Scheme 2.68). Unfortunately, heating the reaction mixture to 60 °C left starting material unreacted while any further increases in temperature only led to decomposition.

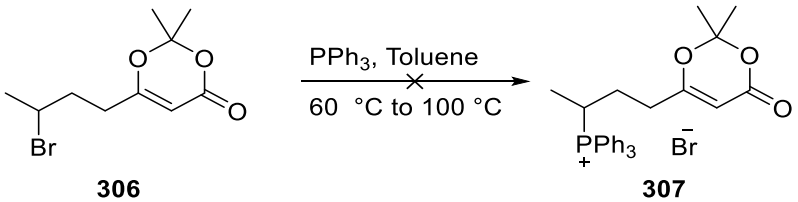


**Scheme 2.68. Attempt to synthesize Wittig reagent 307**

In parallel, the synthesis of sulfonium **309** was investigated. Nucleophilic substitution of alkyl bromide **306** with thiophenol quantitively provided phenyl sulfide **308**. Unfortunately, several failures to access the Corey-Chaykovsky reagent **309** forced us to abandon this route (Scheme 2.69).

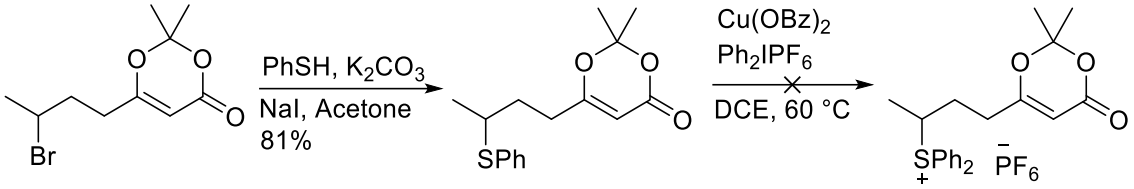


**306** **308** **309**

**Scheme 2.69. Attempt to synthesize Corey-Chaykovsky reagent 309**

With the aim to quickly assess the feasibility of this new strategy, we next followed a more robust but longer strategy that targeted the ketoester **315**. Toward this goal, aldehyde **283** was submitted to a Still-modified HWE olefination[137] providing the (*Z*)-alkene **211** with excellent selectivity (d.r = 15:1). Formation of allylic bromide **312** was achieved through a sequence of reduction/Appel reactions in very good yield. Then, use of the Weiler dianion[138] provided ketoester **313** that was ultimately deprotected and oxidized to generate the Knoevenagel precursor **315** (Scheme 2.70).

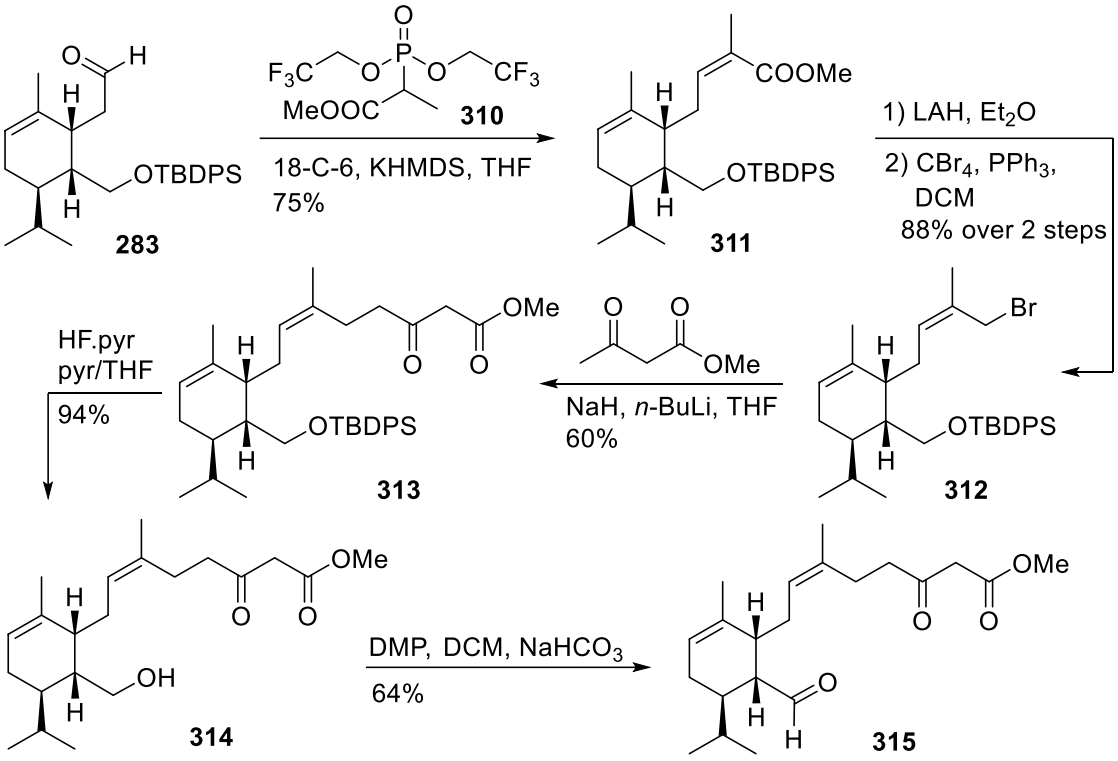


**Scheme 2.70. Step-by-step approach to ketoester 315**

With excitement, we commenced our investigation into the formation of the 10-membered ring (Table 2.12). Treating the keto ester with a mixture of acetic acid and pyridine in toluene left starting material **315** unreacted (entry 1). The use of $TiCl_4$ quickly led to the formation of a new product **319** generated from the attack of the trisubstituted alkene on the aldehyde (entry 2). The screening of several bases did not improve these results (entry 3-6). Likewise, the use of boron trifluoride led to the cyclized product **319** (entry 7). Interestingly, submitting ketoester **315** to β-alanine[70] in polar solvents (e.g., DMSO, EtOH) generated the desired product **316** in a low yield and as a mixture of diastereoisomers (entry 8, 9). It was speculated that the low yield resulted from the competing formation of dimers **317** and **318**.

**Table 2.12. Knoevenagel condensation screening**

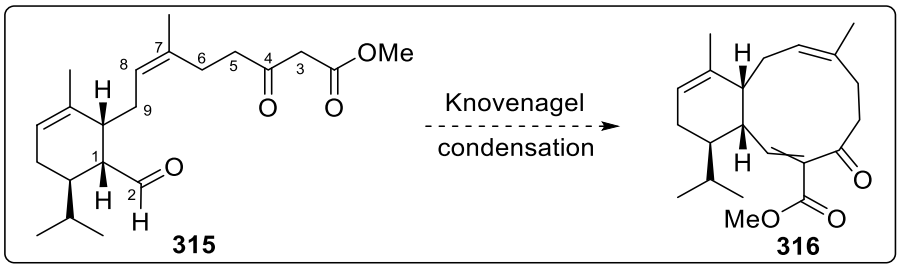


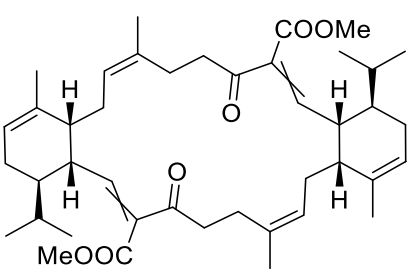


317

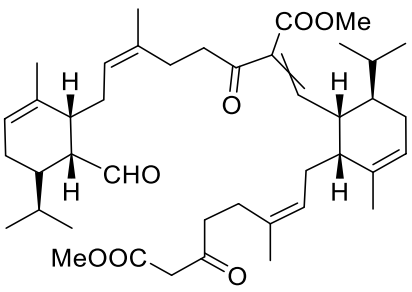


318

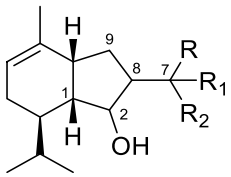


319

| entry | reagent | solvent | T (°C) | conversion[a] | yield[b] | outcome |
|---|---|---|---|---|---|---|
| **1** | AcOH/pyr/MS 4Å | Toluene | 120 | 0% | 0% | **315** only |
| **2** | $TiCl_4$/pyr | THF | rt | 100% | 0% | **319** |
| **3** | $K_2CO_3$ | MeOH | 70 | 0% | 0% | **315** only |
| **4** | KF | MeOH | 80 | 0% | 0% | **315** only |
| **5** | Na (s) | MeOH | 80 | 0% | 0% | **315** only |
| **6** | KHMDS, 18C6 | THF | 80 | 0% | 0% | **315** only |
| **7** | $BF_3.Et_2O$ | DCM | rt | 90% | 0% | **319** |
| **8** | β-alanine | EtOH | rt | 80% | 8% | **316** + **317** + **318** |
| **9** | β-alanine | DMSO | rt | 80% | 13% | **316** + **317** + **318** |

Note: [a] conversion after 24 hours [b] determined after purification on column chromatography

Delighted by the generation of trace amounts of product, we thought to improve the conversion by heating at 70 °C overnight. Unfortunately, the conversion remained approximately the same (~ 15%). After purification, an aldehyde that displayed spectral data similar to **315** was recovered along with dimers **317** and **318**. We speculated that the new aldehyde derived from epimerization at C1 (during the reaction) as a result of the formation of an enamine intermediate (Scheme 2.71). Here, racemization is more rapid than cyclization leading to the unreactive epimer **320**.

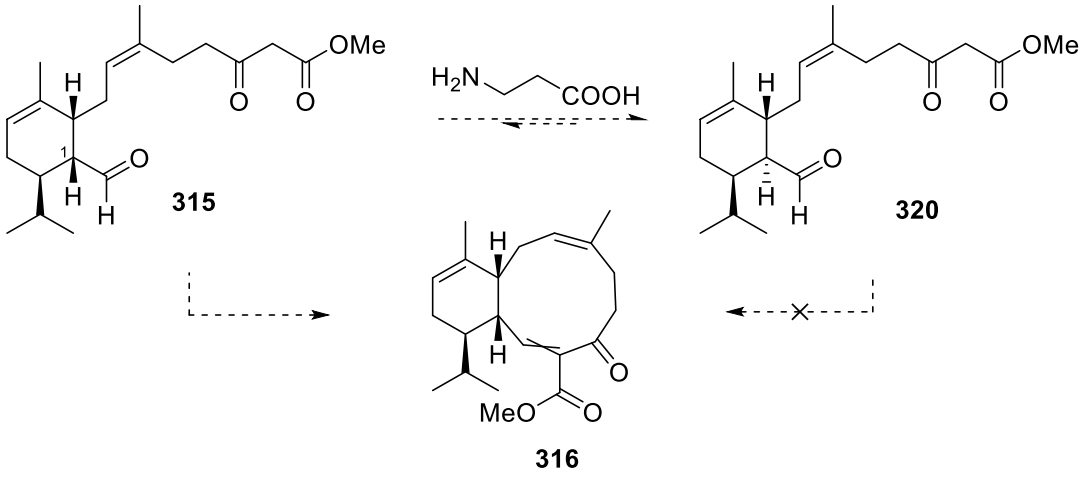


**Scheme 2.71. Potential explanation for the low conversion**

Previous studies showed that replacing a methyl ester (A-value = 1.27) with a nitrile group (A-value = 0.21) had resulted in considerable improvements in HWE reactions of a related aldehyde (see section 2.4.1). Based on this insight, we next targeted the corresponding ketonitrile **321** (Figure 2.14).

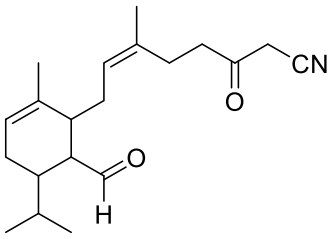


**321**

**Figure 2.14. Alternative ketonitrile 321**

Unfortunately, a displacement reaction of allyl bromide **312** with 3-oxobutanenitrile failed to provide the desired product **322**. To tackle this problem, *tert*-butyl acetate was added to allyl bromide **312** and provided the corresponding γ,δ-unsaturated ester **323** in excellent yield. Thereafter, careful addition of the anion derived from acetonitrile delivered ketonitrile **322** that was in turn deprotected and oxidized to yield aldehyde **321** (Scheme 2.72).

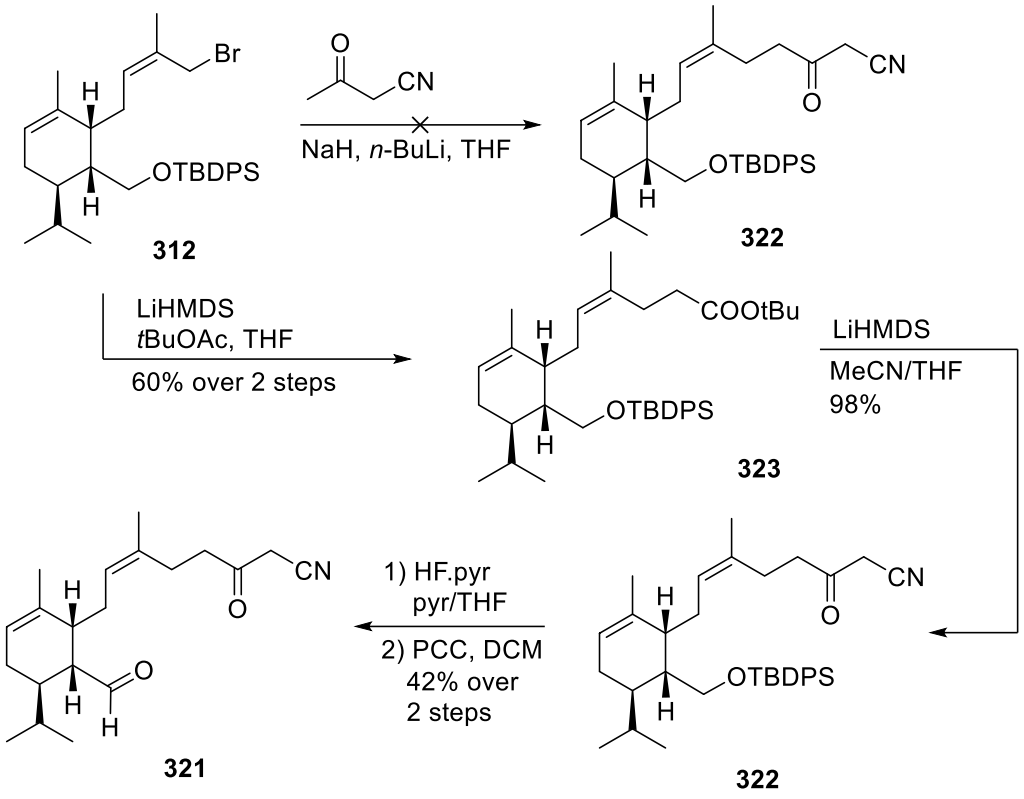


**Scheme 2.72. Synthesis of ketonitrile 321**

With aldehyde **321** in hand, we applied the same conditions that were previously used for ketoester **315** (Scheme 2.73). Surprisingly, after stirring for one hour at 70 °C in DMSO, no starting material remained. Thus, the steric bulk engendered by the methyl ester in **315** was likely the primary reason for the low conversion. By TLC analysis, two main products were visible. Subsequent spectroscopic analysis of these products indicated that the less polar product was the dimer **325** that arose from a bis-Knoevenagel condensation. The more polar product was the desired macrocycle **324**. Although cyclodecadienone **324** seemed to be the major product by TLC analysis, the isolated yield was poor (< 20%).

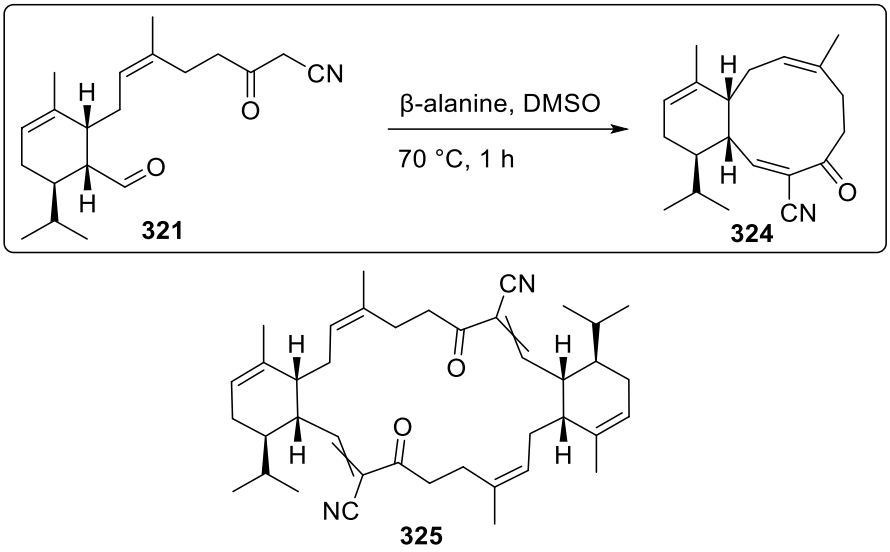


**Scheme 2.73. Macrocyclization of 324 in presence of β-alanine**

Interestingly, the $^{1}$H NMR spectra of cyclodecane **324** in various solvents indicated the presence of several slowly interconverting conformations. Only in benzene $d_6$ was a modestly resolved $^{1}$H NMR spectrum obtained (Figure 2.15). Unfortunately, the lower range of the spectrum was still poorly resolved. In order to gather improved spectral data, a series of variable-temperature NMR experiments were required. Indeed, increasing the temperature to 40 °C (red) led to a slight improvement in the shape of the resonances (Figure 2.16). For instance, the resonance assigned to one of the methyl groups of the isopropyl function is very characteristic at 0.6 pm and appears as a broad signal at lower temperatures. However, at 60 °C (green), this resonance became a clear doublet. This equilibrium of conformations had not been observed with methyl ester **315** and we speculated that the larger methyl ester (large) locked the molecule in a single conformation whereas, with the nitrile (small and linear), the macrocycle was free to alternate between several conformations.

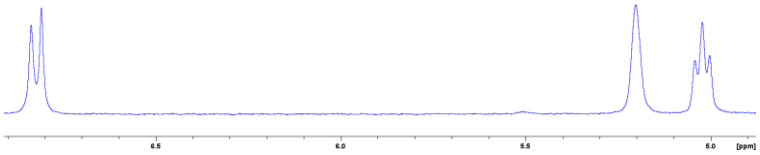

**Figure 2.15. $^{1}$H NMR spectrum of 324 from 5 ppm to 7 ppm at 20 °C**

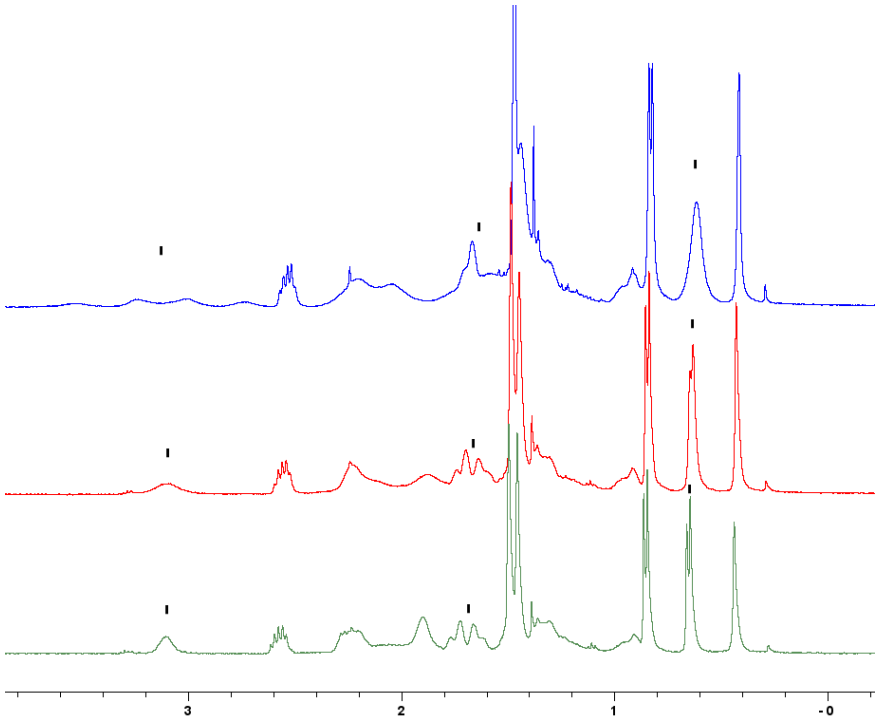


**Figure 2.16.** **$^{1}$H NMR spectrum of 324 from 0.5 ppm to 4 ppm**
Note: In blue, $^{1}$H NMR spectroscopy at 20 °C. In red, $^{1}$H NMR spectroscopy at 40 °C. In green, $^{1}$H NMR spectroscopy at 60 °C.

In an effort to improve the yield and the **324**:**325** ratio, several conditions were explored (Table 2.13). The standard conditions offer a 1:0.23 ratio in favor of product **324** (entry 1). Interestingly, performing the same reaction at room temperature for 24 hours provided the same product-to-dimer ratio (entry 2). When switching from DMSO to EtOH, product **324** is also generated but slowly decomposed over time (entry 3) which was confirmed when product **324** was separately left in EtOH overnight (entry 4). To diminish the amount of dimer, various concentrations of reactants were screened (entry 5-9). Logically, reducing the concentration improved the **324**:**325** ratio until at 0.0025M no more benefits were observed (entry 8). Increasing the time of the reaction did not provide a better ratio nor a better yield as new side-products were formed over time (entries 10 and 11). Switching from DMSO to DCM, MeCN or THF prevented any reaction from occurring, leaving starting material **321** intact (entry 12-14). However, the reaction did take place in DMF, but at a slower rate compared to DMSO (5% conversion vs 80% (DMSO) after 24 hours) (entry 15). Unfortunately, the use of acetone led to direct solvent condensation on ketonitrile **321** (entry 16) while the use of benzene led to the formation of dimer **325** as the sole product of the reaction (entry 17). Interestingly, decreasing the equivalents of β-alanine to 1 and 0.5 improved the ratio **324**:**325** but the

reaction stalled and had overall low conversion (entries 18 and 19). Finally, attempts at using L-asparagine as an amino acid alternative to β-alanine offered product **324** but again the conversion was low. Very interestingly, all conditions that did not involve amino acids (e.g., $K_2CO_3$, NaOMe) did not yield any product. We believed that the presence of the carboxylic acid function on the base plays an essential role in allowing the two chains to meet one another through coordination. The overall yield in these experiments was poor with an average of 25%. However, aldehyde **321** was also found to be unstable, which could obfuscate the actual yield of the Knoevenagel condensation.

**Table 2.13. Knoevenagel condensation on aldehyde 321**

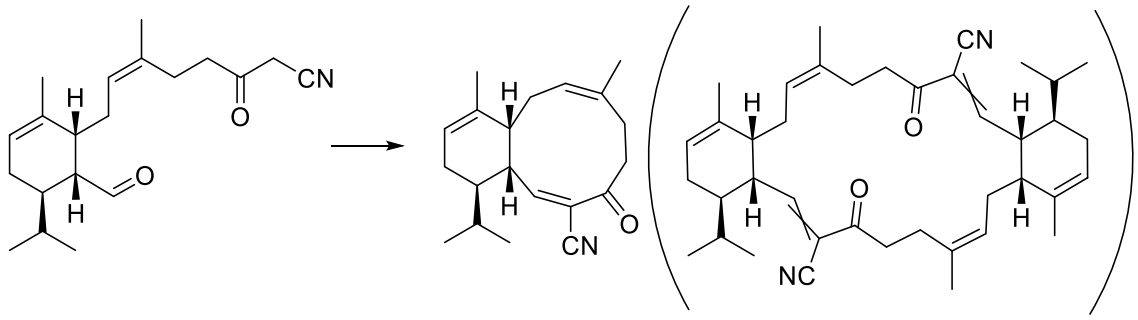


**321** **324** **325**

| entry | base (eq) | solvent | [C] | temp (°C) | time (h) | ratio (324:325)[a] |
|---|---|---|---|---|---|---|
| **1** | β-alanine (4) | DMSO | 0.04 | 70 | 1 | 1/0.23 |
| **2** | β-alanine (4) | DMSO | 0.04 | rt | 24 | 1/0.23 |
| **3** | β-alanine (4) | EtOH | 0.04 | rt | 1 | 1/1 |
| **4** | β-alanine (4) | EtOH | 0.04 | 60 | 1 | 0.3/1 |
| **5** | β-alanine (4) | DMSO | 0.02 | rt | 24 | 1/0.21 |
| **6** | β-alanine (4) | DMSO | 0.01 | rt | 24 | 1/0.19 |
| **7** | β-alanine (4) | DMSO | 0.005 | rt | 24 | 1/0.17 |
| **8** | β-alanine (4) | DMSO | 0.0025 | rt | 24 | 1/0.15 |
| **9** | β-alanine (4) | DMSO | 0.0010 | rt | 24 | 1/0.15 |
| **10** | β-alanine (4) | DMSO | 0.0025 | rt | 72 | 1/0.18 |
| **11** | β-alanine (4) | DMSO | 0.0025 | rt | 168 | 1/0.21 |
| **12** | β-alanine (4) | MeCN | 0.0025 | rt | 24 | N.D. |
| **13** | β-alanine (4) | THF | 0.0025 | rt | 24 | N.D. |
| **14** | β-alanine (4) | DCM | 0.0025 | rt | 24 | N.D. |
| **15** | β-alanine (4) | DMF | 0.0025 | rt | 24 | 1/0.22 |
| **16** | β-alanine (4) | acetone | 0.0025 | rt | 24 | N.D. |
| **17** | β-alanine (4) | benzene | 0.0025 | rt | 24 | 0/1 |
| **18** | β-alanine (1) | DMSO | 0.0025 | rt | 24 | 1/0.05 |
| **19** | β-alanine (0.5) | DMSO | 0.0025 | rt | 24 | 1/0.1 |
| **20** | L-asparagine (4) | DMSO | 0.0025 | rt | 24 | 1/0.1 |

Note: [a] determined by $^1$H NMR (signals integration)

As a result of this large screening, we selected entry 2 as the conditions of reference for the macrocyclization. Using these conditions, ~ 0.5 g of cyclodecadienone **324** was synthesized. The presence of rotamers made the characterization very challenging. To overcome this issue, we reduced nitrile moiety into the corresponding alcohol as we had speculated that the small size of the nitrile was the reason for the presence of rotamers. Moreover, the alcohol function is ultimately necessary to install the arabinose moiety later in the synthesis. Both ketone and nitrile were reduced into alcohol and aldehyde, respectively. Further reduction of **326** with sodium borohydride delivered diol **327** in an overall modest yield. Selective TBS-protection of primary alcohol **327** in DMF delivered allylic alcohol **328** that was in turn oxidized to generate enone **329** (Scheme 2.74). As expected, $^{1}$H NMR spectroscopic analysis of purified **329** did not show the presence of rotamers, which confirmed our hypothesis regarding the conformational flexibility of nitrile **324**.

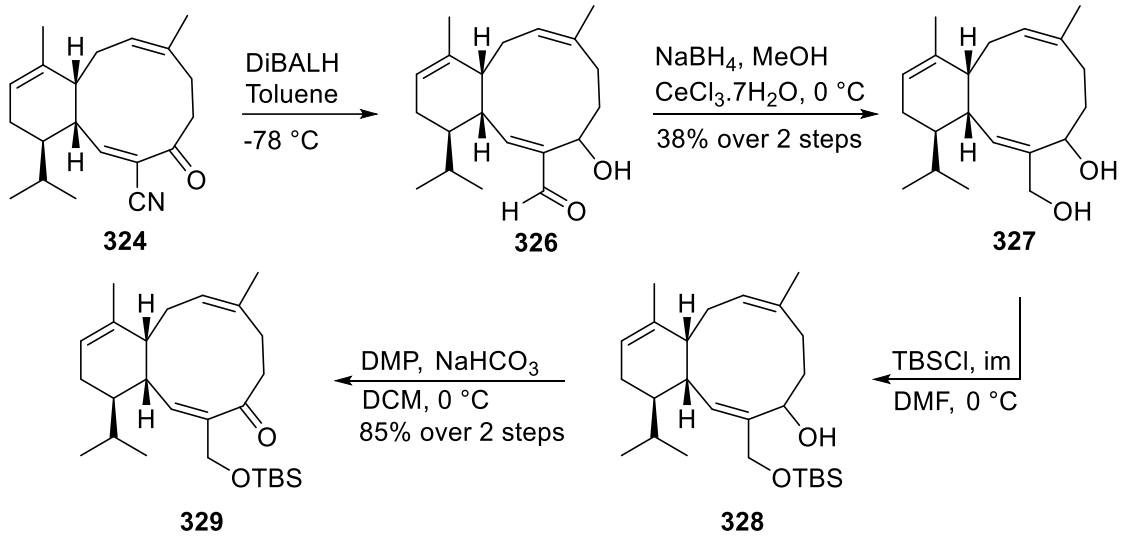


**Scheme 2.74. Synthesis of advanced intermediate 329**

With enone **329** in hand, we commenced the investigation of the C7-C8 functionalization. We believed that selective dihydroxylation of C7-C8 alkene would generate diol **330** which should spontaneously cyclize to form hemiketal **331** (Scheme 2.75). Enone **329** was submitted to a catalytic amount of osmium tetroxide, but no reaction was observed. The addition of a stoichiometric amount of $OsO_4$ led to immediate consumption of the starting material **329** and the production of a mixture of side-products. Modifying several parameters (e.g., cat loading, solvent, temperature) was fruitless in providing a reasonable quantity of diol **330**. Interestingly, switching to

$RuCl_3$ greatly improved the outcome of the reaction providing diol **330** in 52% yield as a single diastereoisomer. After purification, complete NMR spectroscopic analysis confirmed the regioselectivity of the reaction. Unfortunately, a series of NOESY spectroscopic experiments performed on **330** combined with the use of a hand model and a chemistry software confirmed the production of the wrong diastereoisomer **333** due to a highly hindered α-face of the cyclodecadienone **329**. The most stable conformation of **329** precludes di-hydroxylation on the top face, thus preventing the formation of diol **332**. Unfortunately, the C7 stereochemistry cannot be modified later in the synthesis unlike that of C8 (e.g., Mitsunobu esterification) forcing us to revise the strategy.

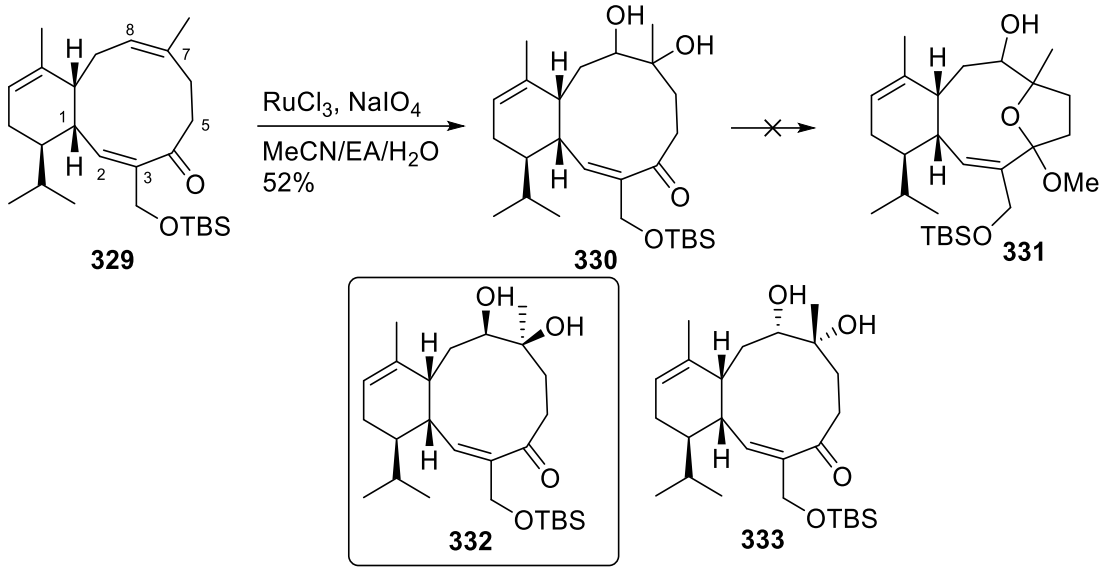


**Scheme 2.75. Dihydroxylation of enone 329**

As an alternative approach, we envisioned the synthesis of the corresponding epoxide **334** (Scheme 2.76). Indeed, epoxide formation on the bottom (alpha) face would allow us to further open the epoxide under acidic conditions to selectively provide the corresponding diol with the desired stereochemistry in both positions. Similar to the dihydroxylation, reaction of triene **329** with *m*CPBA was regio- and diastereoselective generating epoxide **334** as a single product. The stereochemistry of **334** was confirmed by NOESY spectroscopy experiments. Correlation from the proton at C10 to the one at C1 confirmed the *cis* ring juncture as expected. Moreover, a correlation from the proton at C1 and the protons at C20 further demonstrated that no isomerization was observed all along the sequence from cyclobutanone **68**.

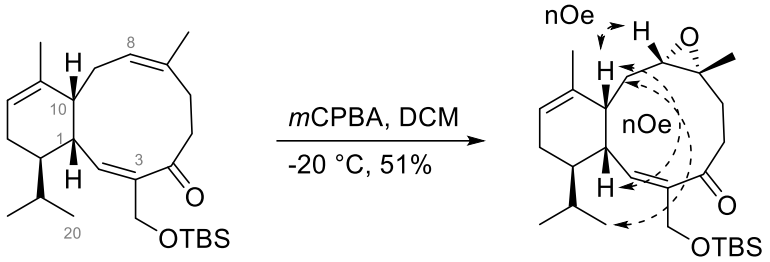


**329** **334**

**Scheme 2.76. Regio- and diastereoselective epoxidation of triene 329**

To properly control the C7/C8 stereocenters, three processes of epoxide opening were envisaged. The first process involves nucleophilic attack of water on epoxide **334** under acidic conditions (Scheme 2.77a). The second involves the intramolecular attack of the ketone onto the epoxide under acidic conditions providing ketal **337** (Scheme 2.77b). Finally, the addition of hydroxide anion to the ketone **334** could provide ketal **337** via intramolecular epoxide opening (via **338**) (Scheme 2.77c).

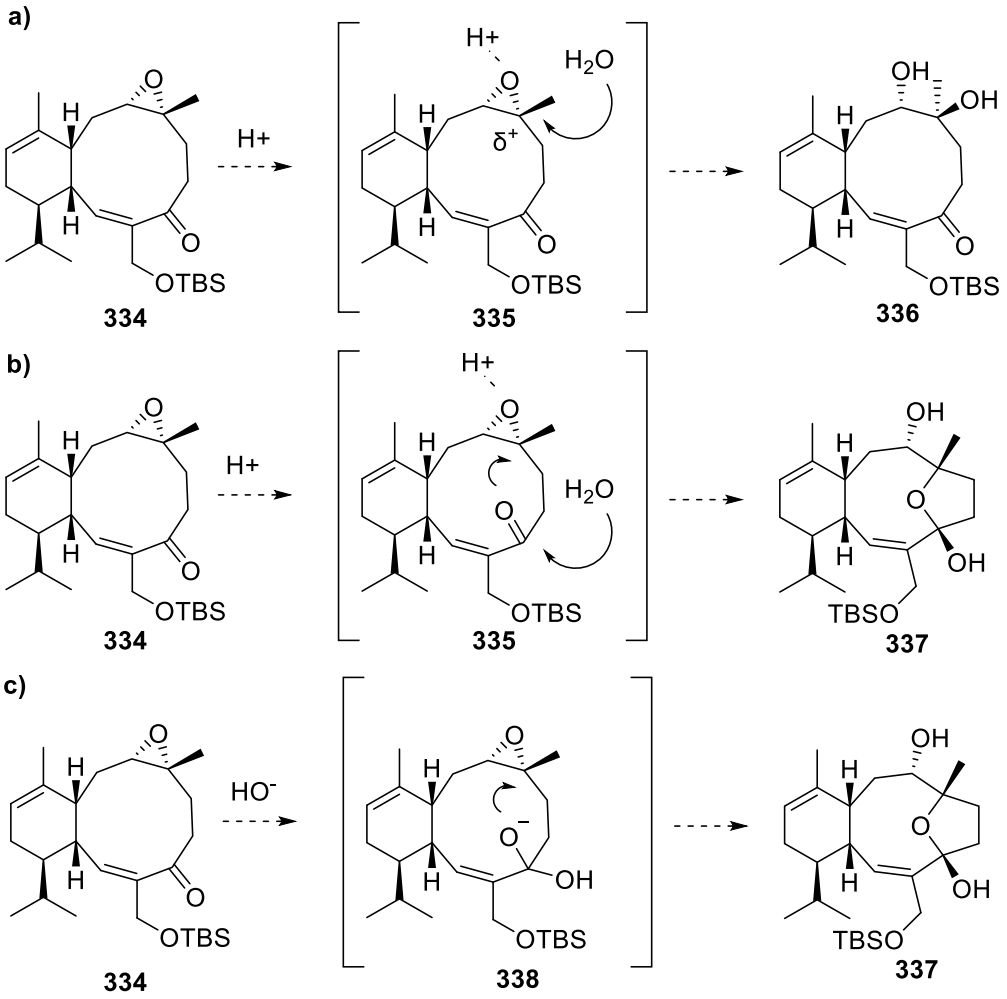


**Scheme 2.77. Possible mechanisms for epoxide opening**

The first attempt using lithium hydroxide only led to triol **339** via TBS deprotection. Scandium triflate is often reported for epoxide opening in the scientific literature.[139] Unfortunately, scandium triflate also led to **339** that further decomposed. Similarly, all aqueous acidic conditions ($H_2SO_4$, AcOH, citric acid, PTSA, CSA, TFA) triggered TBS deprotection with subsequent decomposition of triol **339** (Scheme 2.78).

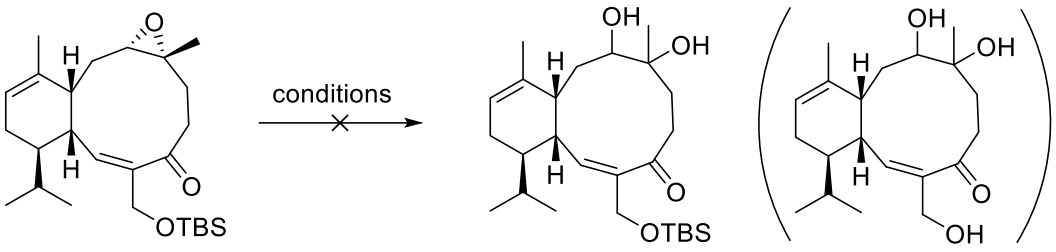


**334** **330** **339**

**Scheme 2.78. Attempts in opening epoxide 334**

To further facilitate the opening of the epoxide at the more substituted C7 position, we anticipated that initial installation of the C5-C6 olefin could help in stabilizing the carbocation intermediate. To install the double bond, α-selanylation of ketone **334** was performed in the presence of LiHMDS and PhSeCl in THF and generated α-phenylseleno ketone **340** as a single diastereoisomer. Subsequent oxidation and spontaneous elimination of the selenoxide generated dienone **341** in good yield (Scheme 2.79).

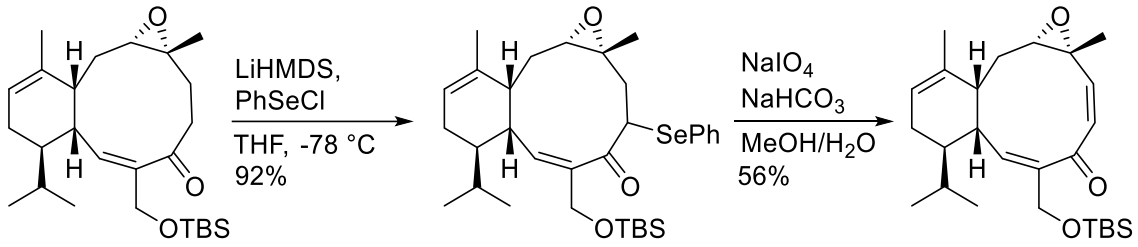


**334** **340** **341**

**Scheme 2.79. Installation of the C5-C6 olefin**

One step away from eleutherobin's macrocyclic core, we commenced the investigation of the epoxide opening starting with lithium hydroxide in THF at 80 °C (Scheme 2.80). These conditions only led to triol **343**. PTSA failed to promote epoxide opening, returning starting material unreacted. Attempts to reflux epoxide **341** in water were fruitless and the presence of a tertiary amine did not provide any benefits. The use of scandium triflate led to rapid decomposition, while iron chloride (III) promoted removal of the TBS protecting group. Several acidic reaction conditions were explored (i.e., PPTS, CSA) also without success. Although the use of $BF_3$ rapidly led to decomposition in DCM, switching to a mixture of water/THF gave a product with signals in the $^1H$ NMR spectra consistent with those in eleutherobin. In particular, two doublets at ~6.1 ppm with a coupling constant of 5.8 Hz were observed. Unfortunately, attempts

to purify this compound on small scale led to loss of material. At this point, due to lack of material and time, the project was stopped.

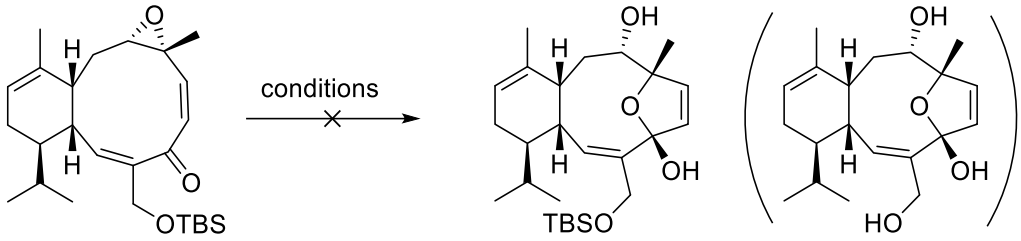


**341** **342** **343**

**Scheme 2.80. Final attempts in opening epoxide 341**

In parallel with the synthesis of the cyclodecane core of eleutherobin, both the urocanic ester **344** and arabinose **345** units were prepared in anticipation of completion of the synthesis (Scheme 2.81).

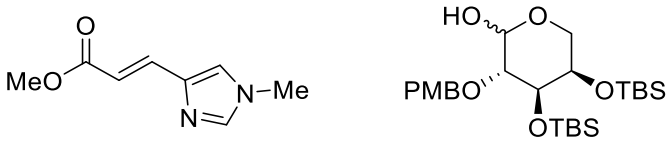


**344** **345**

**Scheme 2.81. Urocanic ester 344 and arabinose 345 units**

The synthesis of the arabinose **345** commenced with cheap and commercially available D-arabinose **346**. A series of protection, deprotection, and functionalization of the anomeric position quickly led us to the desired sugar in 8 steps (Scheme 2.82).[70,140]

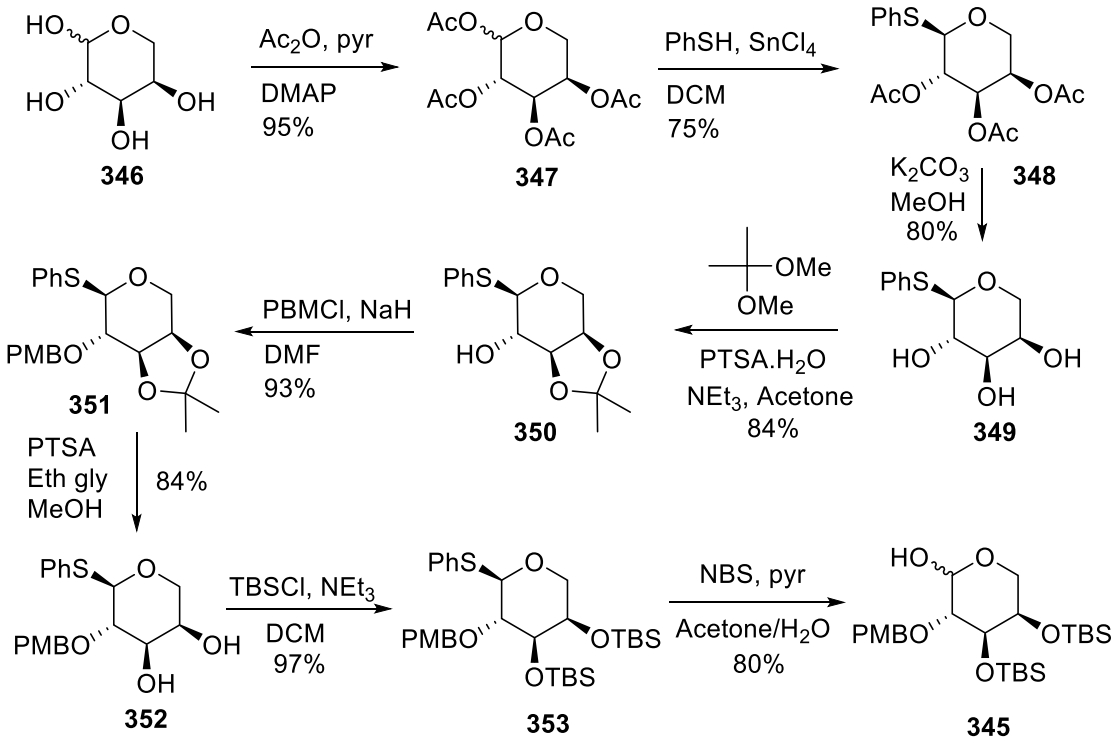


**Scheme 2.82. Synthesis of sugar precursor 345**

To synthesize **344**, commercially available urocanic acid was esterified followed by selective methylation of $N_1$. This 2-step sequence provided *N*-methyl urocanic ester **344** in 2 steps and good overall yield (Scheme 2.83).

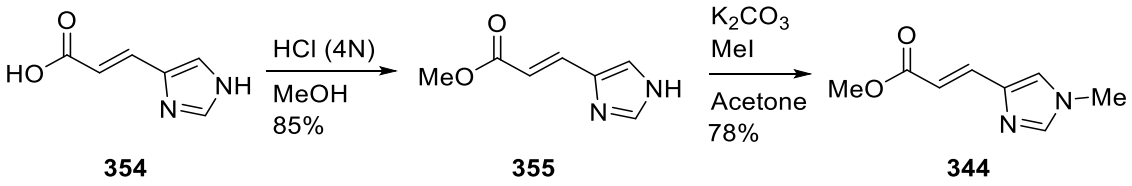


**Scheme 2.83. Synthesis of ester 344**

## 2.5. Future Directions

While our efforts towards the total synthesis of eleutherobin did not ultimately provide the natural product, the formation of the 10-membered ring represents a significant achievement. The Knoevenagel cyclization strategy is expected to ultimately deliver eleutherobin. However, several hurdles have yet to be overcome. First and foremost, opening of the epoxide represents a crucial and exciting challenge that needs to be further investigated to ultimately generate ketal **342** with the correctly configured

stereocenters. Moreover, the current synthetic pathway suffers several low-yielding steps that hamper a potential multigram-scale synthesis of eleutherobin. For instance, the macrocyclization, the aldehyde formation and the nitrile reduction all have yields of less than 50%. More importantly, the initial objective of producing eleutherobin in a short number of steps has not been fulfilled. Indeed, the current strategy would provide eleutherobin in a ~ 25-step sequence, similar to that in the Nicolaou and Danishefsky syntheses. To improve our synthesis, several strategies could be implemented. For instance, adjustment of Britton's methodology for the α-arylation of cyclobutanone could lead to an impressive synthesis of ketonitrile **321** in only 4 steps from phellandrene.[73] Indeed, we believe that a thorough screen of catalysts, ligands and bases would allow us to enlarge the scope of the potential coupling partners for cyclobutanone **68** including different vinyl bromides such as **356**. Subsequent submission of compound **357** to a hydride source (e.g., sodium borohydride) should fragment the 4-membered ring yielding aldehyde **321** while simultaneously skipping a low-yielding step (aldehyde oxidation) (Scheme 2.84).[73] Finally, intramolecular Knoevenagel condensation will deliver cyclodecane **324** in 5 steps, which would represent an outstanding improvement.

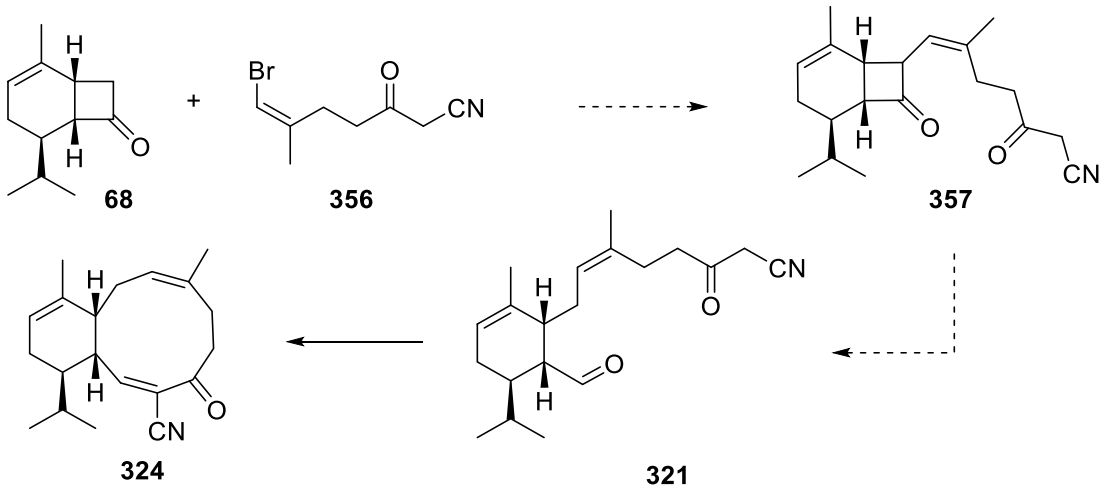


**Scheme 2.84. Potential strategy to generate 324 in 5 steps**

Another important study to complete pertains to the mechanism of the cyclization involving β-alanine. We showed that only amino acids were able to promote this cyclization. A better understanding of the mechanism could ultimately lead to an overall improvement in the yield of this process. A screen of a large number of natural

and unnatural amino acids possessing different functionalities and various carbon chain lengths should be undertaken to determine a general reactivity pattern.

Finally, once the synthesis of eleutherobin (**12**) is efficiently achieved – one that can ultimately lead to a sufficient amount of macrocycle – a structure-activity-relationship study should be executed. Indeed, previous investigations showed that the modifications of the glycan can impact eleutherobin's anticancer properties, especially in Taxol-resistant cell lines. As soon as a lead candidate is found, animal studies will give more insight into the potential use of eleutherobin (**12**) as future cancer therapeutic.

## 2.6. Conclusion

In conclusion, *Chapter 2* has presented a thorough overview of our synthetic advances directed towards the total synthesis of eleutherobin (**12**). We have investigated numerous synthetic approaches that ultimately rewarded us with the delivery of eleutherobin's macrocycle. Although most efforts were fruitless, each strategy paved the path to the final breakthrough. Hopefully, this significant progress will lay the groundwork for a near-term synthesis of this potentially important marine natural product (**12**).

## 2.7. Experimental

**General:**

All reactions described were performed under an atmosphere of dry argon using oven dried glassware. Tetrahydrofuran was distilled over Na/benzophenone and dichloromethane was dried by distillation over $CaH_2$. All other solvents were used directly from EMD drysolv septum sealed bottles unless otherwise specified. Cold temperatures were maintained by the use of following reaction baths: -115 °C, EtOH-$N_2$(l); -78 °C, acetone-dry ice; temperatures between -40 °C to -20 °C were maintained with a Polyscience VLT-60A immersion chiller.

All reagents and starting materials were purchased from Sigma Aldrich, Alfa Aesar, TCI America, Arcos or Carbosynth and were used without further purification. All solvents were purchased from Sigma Aldrich, EMD, Anachemia, Caledon, Fisher or ACP and used without further purification unless otherwise specified.

Flash chromatography was carried out with 230-400 mesh silica gel (E. Merck, Silica Gel 60) following the technique described by Still. Thin layer chromatography was carried out on commercial aluminum backed silica gel 60 plates (E. Merck, type 5554, thickness 0.2 mm). Visualization of chromatograms was accomplished using ultraviolet light (254 nm) followed by heating the plate after staining with one of the following solutions: (a) *p*-anisaldehyde in sulphuric acid-ethanol mixture (5% anisaldehyde v/v and 5% sulphuric acid v/v in ethanol); (b) 1% potassium permanganate w/v, 6.6% potassium carbonate w/v, and 1% v/v 10% sodium hydroxide in water. Concentration and removal of trace solvents was done via a Büchi rotary evaporator using acetone-dry-ice condenser and a Welch vacuum pump.

Nuclear magnetic resonance (NMR) spectra were recorded using $CDCl_3$ or $CD_3OD$. Signal positions (δ) are given in parts per million from tetramethylsilane (δ 0) and were measured relative to the signal of the solvent ($^1$H NMR: $CDCl_3$: *δ* 7.26, $CD_3OD$: *δ* 3.31, $D_2O$: *δ* 4.79; $^{13}$C NMR: $CDCl_3$: *δ* 77.16, $CD_3OD$: *δ* 49.00). Coupling constants (*J* values) are given in Hertz (Hz) and are reported to the nearest 0.1 Hz. $^1$H NMR spectral data are tabulated in the order: multiplicity (s, singlet; d, doublet; t, triplet; q, quartet; m, multiplet; br, broad), coupling constants, number of protons. Proton nuclear magnetic resonance ($^1$H NMR) spectra were recorded on a Bruker Avance II 600 equipped with a

QNP or TCI cryoprobe (600 MHz), Varian Inova 500 (500 MHz), Bruker Avance III 500 (500 MHz), or Bruker Avance III 400 (400 MHz). Carbon nuclear magnetic resonance ($^{13}$C NMR) spectra were recorded on a Bruker Avance 600 equipped with a QNP or TCI cryoprobe (150 MHz), Bruker Avance III 500 (125 MHz), or Bruker Avance III 400 (100 MHz). Assignments of $^{1}$H and $^{13}$C NMR spectra are based on analysis of $^{1}$H -$^{1}$H COSY, HSQC, HMBC and nOe spectra.

Infrared (IR) spectra were recorded on a MB-series Bomem/Hartman & Braun Fourier transform spectrophotometer with internal calibration as films between sodium chloride plates. Only selected, characteristic absorption data are provided for each compound.

High resolution mass spectra were performed on an Agilent 6210 TOF LC/MS using ESI-MS technique.

Optical rotation was measured on a Perkin Elmer 341 Polarimeter at 589 nm.

**Preparation of carboxylic acid 71**

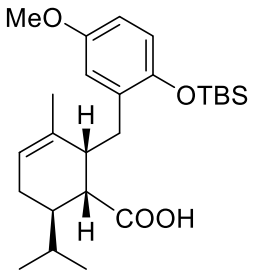


**71**

A stirred solution of (DtBPD)$PdCl_2$ (417 mg, 0.64 mmol), LiOtBu (36 mL, 36 mmol, 1M in THF) in toluene (21 mL) was purged 15 min with $N_2$ prior to addition of aryl halide **69** (3.92g, 12.4 mmol). The resulting reaction mixture was heated to 60 °C. After that, cyclobutanone **68** (2.87 g, 16.12 mmol) was added and the reaction mixture was heated for 4 hours at 60 °C. Then, at 0°C, the reaction mixture was diluted with EA and was quenched with a solution of 1M HCl until pH reached 2. The crude was directly used for the next step.

The previous crude was taken up in *t*-BuOH (66 mL) and $H_2O$ (0.23 mL, 12.4 mmol). To this solution was added *t*-BuOK (2.78 g, 24.8 mmol). The resulting reaction mixture was stirred 2 h at rt. The reaction mixture was quenched with a solution of 1M HCl and further extracted with EA. The combined organic phases were washed with brine, dried

over anhydrous $MgSO_4$, filtered, concentrated and the resulting crude product was purified by column chromatography (5% MeOH in DCM) to afford carboxylic acid **71** (4.75 g, 68% over 2 steps) as a colorless liquid.

$^1H$ NMR (400 MHz, $CDCl_3$) $\delta$ 6.67–6.57 (m, 3H), 5.33 (br s, 1H), 3.72 (s, 3H), 2.88–2.76 (m, 3H), 2.58 (dd, $J$ = 3.6, 8.6 Hz, 1H), 2.14–1.85 (m, 5H), 1.42 (s, 3H), 0.99 (s, 9H), 0.86 (d, $J$ = 6.8 Hz, 3H), 0.81 (d, $J$ = 6.7 Hz, 3H), 0.20 (s, 3H), 0.19 (s, 3H).

$^{13}C$ NMR (125 MHz, $CDCl_3$): $\delta$ 180.1, 153.7, 147.9, 136.4, 132.0, 121.0, 118.7, 116.6, 112.0, 55.7, 46.6, 39.1, 36.7, 32.0, 28.2, 26.0, 25.8, 24.0, 22.9, 20.8, 18.4, 17.3, 3.9, -4.1.

HRMS (ESI-TOF) *m/z*: $[M + NH_4]^+$ Calcd for $C_{25}H_{44}NO_4Si$ 450.3034; Found 450.3035.

IR (neat): v 2967, 2843, 1688, 1664, 1505, 1237, 831 $cm^{-1}$

**Preparation of tetralone 81**

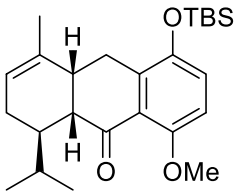


**81**

To a stirred solution of carboxylic acid **71** (4.70 g, 10.9 mmol) in DCM (110 mL) under $N_2$, was added DMF (75.8 µL, 0.98 mmol) followed by oxalyl chloride (2.81 mL, 32.7 mmol). After bubbling subsided, the reaction was stirred 1 h at rt before the solvent was removed in vacuo. The acyl chloride was directly used in the next step.

To an ice-cold solution (0 °C) of the previous crude in DCM (100 mL) was dropwise added $SnCl_4$ (1.53 mL, 13.1 mmol). The resulting reaction mixture was stirred 90 min at 0 °C. The reaction mixture was quenched with a solution of $NaHCO_{3(aq)}$, and further extracted with EA. The combined organic phases were washed with brine, dried over anhydrous $MgSO_4$, filtered, concentrated and the resulting crude product was purified by column chromatography (15% $Et_2O$ in pentane) to afford tetralone **81** (3.56 g, 68% over 2 steps) as a colorless liquid.

$^1$H NMR (400 MHz, $CDCl_3$) $\delta$ 6.89 (d, $J$ = 8.9 Hz, 1H), 6.70 (d, $J$ = 8.9 Hz, 1H), 5.36 (br s, 1H), 3.83 (s, 3H), 2.98 (dd, $J$ = 5.6, 17.5 Hz, 1H), 2.87 (dd, $J$ = 8.0, 17.5 Hz, 1H), 2.70–2.60 (m, 2H), 2.04–1.88 (m, 3H), 1.66 (s, 3H), 1.60 (m, 1H), 1.02 (s, 9H), 0.91 (d, $J$ = 6.7 Hz, 3H), 0.88 (d, $J$ = 6.9 Hz, 3H), 0.22 (s, 3H), 0.19 (s, 3H).

HRMS (ESI-TOF) *m/z*: $[M + NH_4]^+$ Calcd for $C_{25}H_{42}NO_3Si$ 432.2928; Found 432.2932.

**Preparation of diketone 65**

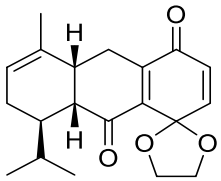


**65**

A solution of PIFA (460 mg, 1.07 mmol) in DCM (3 mL) was dropwise added to a stirred solution of the previous crude in THF (8.2 mL) and ethylene glycol (68.2 µL, 1.23 mmol) at 0 °C and was stirred at rt for 3 h. The reaction mixture was quenched with a solution of $H_2O$ and further extracted with $Et_2O$. The combined organic phases were washed with brine, dried over anhydrous $MgSO_4$, filtered, concentrated and the resulting crude product was purified by column chromatography (10% EA in pentane) to afford diketone **65** (146 mg, 54% over 2 steps) as a colorless liquid.

$^1$H NMR (400 MHz, $CDCl_3$) $\delta$ 6.59 (d, $J$ = 10.1 Hz, 1H), 6.20 (d, $J$ = 10.1 Hz, 1H), 5.42 (br s, 1H), 4.56–4.48 (m, 1H), 4.43–4.35 (m, 1H), 4.19–4.10 (m, 2H), 2.88 (dd, $J$ = 5.5, 19.5 Hz, 1H), 2.67–2.59 (m, 1H), 2.55–2.46 (m, 2H), 2.07–1.84 (m, 2H), 1.67 (s, 3H), 1.63–1.56 (m, 1H), 1.55 (s, 1H), 0.90 (d, $J$ = 2.3 Hz, 3H), 0.88 (d, $J$ = 2.4 Hz, 3H).

$^{13}$C NMR (125 MHz, $CDCl_3$): $\delta$ 201.4, 186.8, 145.5, 145.0, 139.2, 134.4, 126.4, 122.5, 99.5, 67.3, 66.6, 50.8, 36.2, 36.1, 28.2, 25.9, 24.5, 21.5, 21.2, 16.7.

HRMS (ESI-TOF) *m/z*: $[M + NH_4]^+$ Calcd for $C_{20}H_{28}NO_4$ 346.2013; Found 346.2011.

IR (neat): v 2965, 2895, 1681, 1159, 978 $cm^{-1}$

**Preparation of tertiary alcohols 64 and 94**

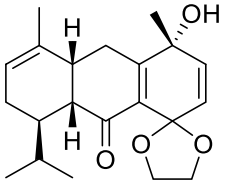


**94**

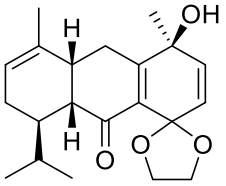


**64**

Methyl lithium (1.0 mL, 1.6 mmol, 1.6M in $Et_2O$) was added to a stirred solution of ketone **65** (493 mg, 1.5 mmol) in THF (15 mL) at -78 °C and stirred for 15 min. The reaction mixture was quenched with a solution of $NH_4Cl_{(aq)}$ and further extracted with EA. The combined organic phases were washed with brine, dried over anhydrous $MgSO_4$, filtered, concentrated and the resulting crude product was purified by column chromatography (15% EA in hexanes) to afford **64** (176 mg, 34%) and **94** (264 mg, 51%) (dr. 1:1.6) as a colorless liquid.

**Data for 94:**

$^1$H NMR (500 MHz, $CDCl_3$): $\delta$ 5.96 (d, $J$ = 10.0 Hz, 1H), 5.70 (d, $J$ = 10.0 Hz, 1H), 5.41 (m, 1H), 4.43 – 4.37 (m, 1H), 4.33–4.28 (m, 1H), 4.09–4.02 (m, 2H), 2.81 – 2.63 (m, 3H), 2.48 (dd, $J$ = 8.5 Hz, 4.7 Hz, 1H), 2.04–1.95 (m, 2H), 1.93 – 1.83 (m, 1H), 1.70 (s, 3H), 1.62 (m, 1H) 1.42 (s, 3H), 0.9 (d, $J$ = 6.8 Hz, 3H), 0.89 (d, $J$ = 7.0 Hz, 3H).

$^{13}$C NMR (101 MHz, $CDCl_3$): $\delta$ 200.3, 159.6, 134.3, 134.2, 129.8, 128.0, 122.9, 100.4, 68.1, 67.0, 66.2, 50.4, 36.9, 36.6, 27.9, 27.6, 27.5, 24.5, 21.5, 21.2, 17.5.

HRMS (ESI-TOF) *m/z*: $[M + NH_4]^+$ Calcd for $C_{21}H_{32}NO_4$ 362.2326; Found 362.2329.

IR (neat): v 3398, 2949, 1677, 1669, 1163, 965 $cm^{-1}$

**Data for 64:**

$^1$H NMR (500 MHz, $CDCl_3$): $\delta$ 5.90 (d, $J$ = 10.0 Hz, 1H), 5.67 (d, $J$ = 10.0 Hz, 1H), 5.41 (m, 1H), 4.41 (m, 1H), 4.31–4.26 (m, 1H), 4.08–4.02 (m, 2H), 3.07 (dd, $J$ = 5.6, 19.0 Hz, 1H), 2.56 (m, 1H), 2.42 (dd, $J$ = 4.7, 10.7 Hz, 1H), 2.34 (dd, $J$ = 10.2, 19.0 Hz, 1H), 2.31 (s, 1H), 2.02 (m, 1H), 1.93 – 1.84 (m, 2H), 1.72 (d, $J$ = 1.1 Hz, 3H), 1.37 (s, 3H), 0.88 (d, $J$ = 6.8 Hz, 3H), 0.87 (d, $J$ = 7.0 Hz, 3H).

$^{13}$C NMR (101 MHz, $CDCl_3$): $\delta$ 200.4, 159.9, 135.1, 133.8, 129.2, 127.8, 121.9, 100.6, 67.6, 67.0, 66.2, 50.5, 37.5, 35.5, 28.1, 27.9, 26.9, 24.7, 21.6, 21.4, 16.1.

HRMS (ESI-TOF) *m/z*: $[M + NH_4]^+$ Calcd for $C_{21}H_{32}NO_4$ 362.2326; Found 362.2325

IR (neat): v 3418, 2952, 2893, 1665, 1167, 959 $cm^{-1}$

**Preparation of carboxylic acid 462**

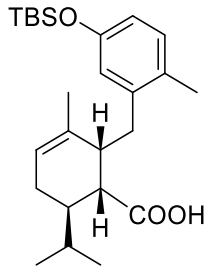


**462**

Using the same procedure depicted previously for **71**, the resulting crude product was purified by column chromatography (100% DCM) to afford carboxylic acid **462** (43% over 2 steps) as a colorless liquid.

$^1$H NMR (400 MHz, $CDCl_3$) $\delta$ 6.93 (d, *J* = 7.9 Hz, 1H), 6.60–6.55 (m, 2H), 5.37 (br s, 1H), 2.91–2.81 (m, 1H), 2.70–2.59 (m, 3H), 2.20 (s, 3H), 2.15–2.03 (m, 2H), 1.96–1.82 (m, 2H), 1.27 (s, 3H), 0.96 (s, 9H), 0.91 (d, *J* = 6.9 Hz, 3H), 0.78 (d, *J* = 6.8 Hz, 3H), 0.15 (s, 6H).

HRMS (ESI-TOF) *m/z*: $[M + NH_4]^+$ Calcd for $C_{25}H_{44}NO_3Si$ 434.3085; Found 434.3086.

**Preparation of tetralone 96**

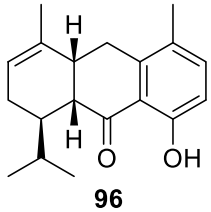


**96**

Using the same procedure depicted previously for **81**, the resulting crude product was purified by column chromatography (5% EA in pentane) to afford phenol **96** (71% over 2 steps) as a colorless liquid.

$^1$H NMR (400 MHz, $CDCl_3$) $\delta$ 12.57 (s, 1H), 7.25 (d, $J$ = 8.4 Hz, 1H), 6.73 (d, $J$ = 8.4 Hz, 1H), 5.42 (br s, 1H), 2.95 (dd, $J$ = 4.7, 17.3 Hz, 1H), 2.84 (dd, $J$ = 7.9, 17.3 Hz, 1H), 2.76–2.69 (m, 2H), 2.20 (s, 3H), 2.14–2.05 (m, 1H), 2.04–1.92 (m, 2H), 1.69 (s, 3H), 1.60 (m, 1H), 0.98 (d, $J$ = 6.7 Hz, 3H), 0.89 (d, $J$ = 6.8 Hz, 3H).

HRMS (ESI-TOF) *m/z*: $[M + NH_4]^+$ Calcd for $C_{19}H_{28}NO_2$ 302.2115; Found 302.2116.

**Preparation of tetralone 124**

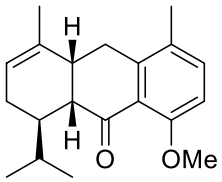


**124**

Potassium carbonate (0.58 g, 4.2 mmol) and MeI (1.04 mL, 16.8 mmol) were added to a stirred solution of tetralone **96** (300 mg, 1.05 mmol) in dry acetone (8.4 mL). The reaction was stirred at 70 °C for 24 h. The reaction mixture was quenched with a solution of $NH_4Cl_{(aq)}$ and further extracted with DCM. The combined organic phases were washed with brine, dried over anhydrous $MgSO_4$, filtered, concentrated and the resulting crude product was purified by column chromatography (16% EA in hexane) to afford tetralone **124** (240 mg, 70 %) as a colorless liquid.

$^1$H NMR (400 MHz, $CDCl_3$) $\delta$ 7.23 (d, $J$ = 8.3 Hz, 1H), 6.74 (d, $J$ = 8.3 Hz, 1H), 5.38 (br s, 1H), 3.85 (s, 3H), 2.98 (dd, $J$ = 8.8, 16.6 Hz, 1H), 2.80–2.67 (m, 2H), 2.63 (dd, $J$ = 4.5, 9.1 Hz, 1H), 2.21 (s, 3H), 2.03–1.88 (m, 3H), 1.69 (s, 3H), 1.63–1.57 (m, 1H), 0.91 (d, $J$ = 6.7 Hz, 3H), 0.87 (d, $J$ = 6.8 Hz, 3H).

HRMS (ESI-TOF) *m/z*: $[M + NH_4]^+$ Calcd for $C_{20}H_{30}NO_2$ 316.2271; Found 316.2266.

**Preparation of diketone 141**

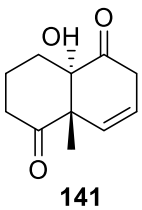


**141**

*m*CPBA (1.53 g, 6.83 mmol) was added to a stirred solution of diene **131** (1.61 g, 7.09 mmol) in methanol (160 mL) at rt and was stirred 1 h. The reaction mixture was

quenched with a solution of $Na_2S_2O_{3(aq)}$ and further extracted with EA. The combined organic phases were washed with brine, dried over anhydrous $MgSO_4$, filtered, concentrated and the resulting crude product was dissolved in THF (160 mL). A 1M HCl solution (30 mL) was added, and the resulting mixture was stirred for 1 h. The reaction mixture was quenched with a solution of pH 7 buffer and further extracted with EA. The combined organic phases were washed with brine, dried over anhydrous $MgSO_4$, filtered, concentrated and the resulting crude product was purified by column chromatography (15% EA in hexanes) to afford tertiary alcohol **141** (731 mg, 53 %) as a colorless liquid.

$^1$H NMR (400 MHz, $CDCl_3$) $\delta$ 6.42 (dt, $J$ = 2.2, 10.1 Hz, 1H), 5.94 (ddd, $J$ = 3.1, 4.1, 10.1 Hz, 1H), 3.31 (ddd, $J$ = 2.3, 4.1, 22.2 Hz, 1H), 2.85 (dt, $J$ = 2.3, 3.1, 22.2 Hz, 1H), 2.71 (s, 1H), 2.69–2.59 (m, 1H), 2.35 (m, 1H), 2.25–2.07 (m, 2H), 2.04–1.93 (m, 2H), 1.21 (s, 3H).

HRMS (ESI-TOF) *m/z*: $[M + NH_4]^+$ Calcd for $C_{11}H_{18}NO_3$ 212.1281; Found 212.1281.

**Preparation of diketone 143**

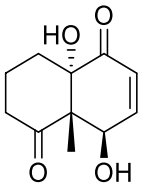


**143**

*m*CPBA (1.68 g, 9.72 mmol) was added to a stirred solution of diketone **141** (0.63 g, 3.2 mmol) in DCM (63 mL) at rt and was stirred for 48 h. The reaction mixture was quenched with a solution of $Na_2S_2O_{3(aq)}$ and further extracted with DCM. The combined organic phases were washed with brine, dried over anhydrous $MgSO_4$, filtered, concentrated and the resulting crude product was purified by column chromatography (25% EA in hexanes) to afford tertiary alcohol **143** (365 mg, 54 %) as a colorless liquid.

$^1$H NMR (500 MHz, $CDCl_3$) $\delta$ 6.87 (dd, $J$ = 5.6, 10.3 Hz, 1H), 6.17 (d, $J$ = 10.3 Hz, 1H), 5.30 (d, $J$ = 2.5 Hz, 1H), 4.61 (d, $J$ = 5.1 Hz, 1H), 4.40 (s, 1H), 2.68 (ddd, $J$ = 7.2, 13.6, 15.1 Hz, 1H), 2.39 (ddt, $J$ = 1.7, 5.0, 15.3 Hz, 1H), 2.24 (m, 1H), 2.12 (m, 1H), 2.05–1.98 (m, 1H), 1.90 (m, 1H).

HRMS (ESI-TOF) *m/z*: $[M + NH_4]^+$ Calcd for $C_{11}H_{18}NO_4$ 228.1230; Found 228.1235.

**Preparation of triol 144**

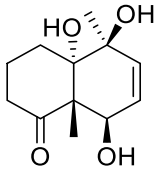

**144**

MeMgBr (400 µL, 0.71 mmol, 1.7M in THF) was added to a stirred solution of diketone **143** (50 mg, 0.238 mmol) in THF (3.5 mL) at -78 °C and stirred for 1 h. The reaction mixture was quenched with a solution of $NH_4Cl_{(aq)}$ and further extracted with EA. The combined organic phases were washed with brine, dried over anhydrous $MgSO_4$, filtered, concentrated and the resulting crude product was purified by column chromatography (1% DCM in MeOH) to afford tertiary alcohol **144** (24 mg, 45 %) as a colorless liquid.

$^1$H NMR (400 MHz, $CDCl_3$) $\delta$ 5.92 (dd, $J$ = 5.7, 10.2 Hz, 1H), 5.76 (d, $J$ = 10.2 Hz, 1H), 4.90 (br s, 1H), 4.38 (br s, 1H), 4.37 (d, $J$ = 5.7 Hz, 1H), 2.67 (ddd, $J$ = 7.3, 13.4, 14.9 Hz, 1H), 2.33 (ddt, $J$ = 1.8, 4.8, 15.2 Hz, 1H), 2.31–2.21 (m, 1H), 2.21–2.14 (m, 1H), 1.98–1.89 (m, H), 1.82 (m, 1H), 1.37 (s, 3H), 1.27 (s, 3H).

$^{13}$C NMR (101 MHz, $CDCl_3$) $\delta$ 214.6, 135.6, 124.3, 80.1, 69.6, 63.1, 54.3, 37.5, 25.7, 25.0, 21.8, 20.0.

HRMS (ESI-TOF) *m/z*: $[M + NH_4]^+$ Calcd for $C_{12}H_{22}NO_4$ 244.1543; Found 244.1545.

**Preparation of diketone 139**

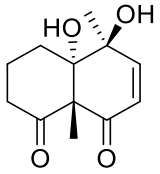

**139**

TPAP (40 mg, 0.11 mmol), NMO (153 mg, 1.3 mmol) and 4Å MS (25 mg) were added to a stirred solution of triol **144** (58 mg, 0.26 mmol) in DCM at rt and stirred overnight. The reaction mixture was filtered through a pad of silica and flushed with DCM/MeOH

(10/1). The filtrate was concentrated, and the resulting crude product was purified by column chromatography (5% DCM in MeOH) to afford diketone **139** (24 mg, 45 %) as a colorless liquid.

$^{1}$H NMR (600 MHz, $CDCl_3$) $\delta$ 6.51 (dd, $J$ = 10.3 Hz, 1H), 6.02 (d, $J$ = 10.3 Hz, 1H), 2.79 (dt, $J$ = 7.8, 13.2, 1H), 2.49 (ddd, $J$ = 6.2, 13.3, 14.1 Hz, 1H), 2.32 (m, 1H), 2.13–2.00 (m, 2H), 1.87 (m, 1H), 1.67 (s, 3H), 1.50 (s, 3H).

$^{13}$C NMR (151 MHz, $CDCl_3$) $\delta$ 206.8, 195.5, 147.1, 128.3, 81.0, 72.4, 63.2, 36.7, 25.3, 24.5, 23.9, 20.6.

HRMS (ESI-TOF) *m/z*: $[M + NH_4]^+$ Calcd for $C_{12}H_{20}NO_4$ 242.1387; Found 242.1387.

**Preparation of lactone 148**

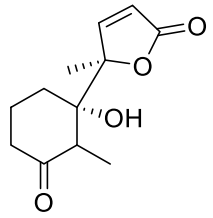


**148**

NaH (1.6 mg, 66.9 µmol) was added to a stirred solution of diketone **139** (15 mg, 66.9 µmol) in THF (1.5 mL) at 0 °C and stirred for 90 min. The reaction mixture was quenched with $H_2O$ and further extracted with EA. The combined organic phases were washed with brine, dried over anhydrous $MgSO_4$, filtered, concentrated and the resulting crude product was purified by column chromatography (5% MeOH in DCM) to afford lactone **148** (9.3 mg, 62 %) both as colorless liquids.

$^{1}$H NMR (600 MHz, $CDCl_3$) $\delta$ 7.57 (d, $J$ = 5.7 Hz, 1H), 6.13 (d, $J$ = 5.7 Hz, 1H), 2.64 (q, $J$ = 7.3 Hz, 1H), 2.51 (m, 1H), 2.24 (m, 1H), 2.05–1.98 (m, 1H), 1.93–1.86 (m, 2H), 1.51 (s, 3H), 1.32 (d, $J$ = 7.3 Hz, 3H).

$^{13}$C NMR (151 MHz, $CDCl_3$) $\delta$ 213.2, 172.4, 160.0, 121.2, 91.9, 79.6, 54.4, 36.1, 24.4, 19.6, 18.7, 15.0.

HRMS (ESI-TOF) *m/z*: $[M + NH_4]^+$ Calcd for $C_{12}H_{20}NO_4$ 242.1387; Found 242.1383.

**Preparation of carboxylic acid 463**

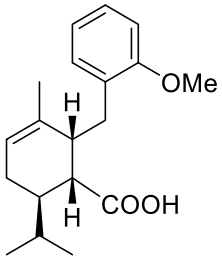


**463**

Using the same procedure depicted previously for **71**, the resulting crude product was purified by column chromatography (100% DCM) to afford carboxylic acid **463** (72% over 2 steps) as a colorless liquid.

$^1$H NMR (400 MHz, $CDCl_3$) $\delta$ 7.12 (dt, $J$ = 1.7, 8.1 Hz, 1H), 7.09 (dd, $J$ = 1.7, 7.5 Hz, 1H), 6.82 (dt, $J$ = 1.1, 7.5 Hz, 1H), 6.78 (dd, $J$ = 1.1, 8.1 Hz, 1H), 5.34 (br s, 1H), 3.76 (s, 3H), 3.02 (dd, $J$ = 5.3, 12.4, 1H), 2.80–2.68 (m, 2H), 2.15–1.96 (m, 3H), 1.93–1.84 (m, 1H), 1.45 (s, 3H), 1.26 (m, 1H), 0.87 (d, $J$ = 6.6 Hz, 3H), 0.80 (d, $J$ = 6.6 Hz, 3H).

HRMS (ESI-TOF) *m/z*: $[M + NH_4]^+$ Calcd for $C_{19}H_{30}NO_3$ 320.2220; Found 320.2221.

**Preparation of tetralone 124**

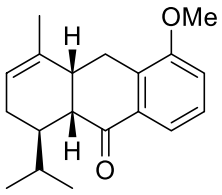


**124**

To a stirred solution of carboxylic acid **463** (2.26 g, 7.47 mmol) in DCM (104 mL) under $N_2$, was added DMF (60 µL, 0.75 mmol) followed by oxalyl chloride (1.95 mL, 28.4 mmol). After bubbling subsided, the reaction was stirred 1 h at rt before the solvent was removed in vacuo. The acyl chloride was directly used in the next step.

To an ice-cold solution (0 °C) of the previous crude in DCM (180 mL) was portion wise added $AlCl_3$ (1.1 g, 8.22 mmol). The resulting reaction mixture was stirred 5 min at 0 °C. The reaction mixture was quenched with an ice-cold water and pH was set to 7 using a solution of $NaHCO_{3(aq)}$, and further extracted with EA. The combined organic phases were dried over anhydrous $MgSO_4$, filtered, concentrated and the resulting crude

product was purified by column chromatography (1% $Et_2O$ and 0.5% $NEt_3$ in hexanes) to afford tetralone **124** (1.72 g, 67% over 2 steps) as a white solid.

$^1H$ NMR (400 MHz, $CDCl_3$) $\delta$ 7.61 (d, $J$ = 7.9 Hz, 1H), 7.26 (dd, $J$ = 7.9, 8.1 Hz, 1H), 7.01 (d, $J$ = 8.1 Hz, 1H), 5.40 (br s, 1H), 3.87 (s, 3H), 3.10 (dd, $J$ = 5.2, 17.7 Hz, 1H), 2.86 (dd, $J$ = 8.6, 17.7 Hz, 1H), 2.72 (m, 1H), 2.68 (dd, $J$ = 4.3, 8.6 Hz, 1H), 2.11–2.01 (m, 2H), 1.98–1.91 (m, 1H), 1.70 (s, 3H), 1.56 (m, 1H), 0.95 (d, $J$ = 6.7 Hz, 3H), 0.86 (d, $J$ = 6.8 Hz, 3H).

$^{13}C$ NMR (151 MHz, $CDCl_3$) $\delta$ 199.6, 156.9, 136.3, 134.6, 128.7, 128.5, 122.3, 119.5, 115.0, 55.8, 50.1, 39.9, 38.9, 29.6, 27.7, 26.5, 21.7, 21.0, 18.8.

HRMS (ESI-TOF) *m/z*: $[M + NH_4]^+$ Calcd for $C_{19}H_{28}NO_2$ 302.2115; Found 302.2118.

**Preparation of triene 154**

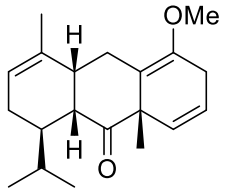


**154**

A dried 3-neck RBF was fitted with a cold finger and a stir bar. Tert-butanol (416 µL, 4.5 mmol) was added to a stirred solution of tetralone **124** (1.28 g, 4.50 mmol) in $Et_2O$ (8 mL). At -78 °C, $NH_{3(g)}$ (35 mL), was slowly condensed in the cold finger and was dropwise added to the reaction mixture. Potassium metal (0.77 g, 19.8 mmol) was added piece by piece in the reaction mixture. Solution turned blue, then yellow. Once all potassium was added, reaction was stirred 20 min at -78 °C. Flame-dried lithium bromide (0.84 g, 9.9 mmol) was added, and the reaction was stirred for 30 min. Finally, MeI (561 µL, 9.0 mmol) was added and the reaction mixture was stirred for 15 min more. The RBF was then left to stir at room temperature in the back of the fume hood until the ammonia was completely evaporated. After that, reaction mixture was diluted with $Et_2O$ and quenched with $H_2O$. The pH of the solution was carefully adjusted with a solution of $NaHCO_{3(aq)}$ till it reached pH 7 and further extracted with $Et_2O$. The combined organic phases were dried over anhydrous $MgSO_4$, filtered, concentrated and the resulting crude product was purified by column chromatography (0.5% $Et_2O$ and 0.5% $NEt_3$ in hexanes) to afford triene **154** (889 mg, 66%) as a colorless liquid.

$^{1}$H NMR (600 MHz, $C_6D_6$) $\delta$ 6.36 (td, $J$ = 2.0, 10.0 Hz, 1H), 5.43 (ddd, $J$ = 3.2, 4.5, 10.0 Hz, 1H), 5.26 (br s, 1H), 3.38 (dd, $J$ = 4.5, 14.9 Hz, 1H), 3.13 (s, 3H), 2.71 (t, $J$ = 5.4 Hz, 1H), 2.48 (m, 1H), 2.42 (m, 2H), 2.30 (m, 1H), 2.25 (m, 1H), 2.13 (m, 1H), 1.83–1.79 (m, 1H), 1.77 (s, 3H), 1.51 (m, 1H), 1.30 (s, 3H), 0.90 (d, $J$ = 6.6 Hz, 3H), 0.80 (d, $J$ = 6.7 Hz, 3H).

$^{13}$C NMR (151 MHz, $CDCl_3$) $\delta$ 214.7, 146.2, 134.9, 130.0, 122.3, 121.2, 115.2, 55.9, 51.1, 49.2, 38.1, 35.6, 29.0, 28.2, 25.8, 24.7, 23.9, 21.3, 21.0, 19.6.

HRMS (ESI-TOF) *m/z*: $[M + NH_4]^+$ Calcd for $C_{20}H_{32}NO_2$ 318.2428; Found 318.2427.

**Preparation of diketone 159**

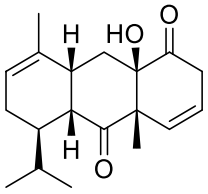


**159**

MMPP (182 mg, 372 µmol) was added to a stirred solution of triene **154** (124 mg, 413 µmol) in MeOH (8.4 mL) and pH 7 buffer solution (1.7 mL) at rt and the reaction was stirred for 45 min. The reaction mixture was quenched with an ice-cold water and pH was set to 7 using a solution of $Na_2S_2O_{3(aq)}$, and further extracted with EA. The combined organic phases were dried over anhydrous $MgSO_4$, filtered, concentrated and the resulting crude was dissolved in THF (5 mL). A 1M HCl solution (5 mL) was added, and the resulting mixture was stirred for 1 h. The reaction mixture was quenched with a solution of pH 7 buffer and further extracted with EA. The combined organic phases were washed with brine, dried over anhydrous $MgSO_4$, filtered, concentrated and the resulting crude product was purified by column chromatography (10% $Et_2O$ in hexanes) to afford diketone **159** (90 mg, 72 %) as a colorless liquid.

$^{1}$H NMR (400 MHz, $CDCl_3$) $\delta$ 5.75 (td, $J$ = 3.5, 10.0 Hz, 1H), 5.62 (ddd, $J$ = 1.4, 2.4, 10.0 Hz, 1H), 5.47 (br s, 1H), 3.27 (dt, $J$ = 3.0, 22.2 Hz, 1H), 3.06 (ddd, $J$ = 1.3, 3.5, 22.2 Hz, 1H), 2.83 (m, 1H), 2.68 (dd, $J$ = 5.5, 12.2 Hz, 1H), 2.42 (t, $J$ = 12.9 Hz, 1H), 2.11 (m, 1H), 1.99 (m, 1H), 1.83 (m, 1H), 1.71 (dd, $J$ = 3.5, 13.2 Hz, 1H), 1.66 (s, 3H), 1.57 (m, 1H), 1.43 (s, 1H), 1.01 (s, 3H), 0.92 (d, $J$ = 7.0 Hz, 3H), 0.88 (d, $J$ = 6.7 Hz, 3H).

$^{13}$C NMR (151 MHz, $CDCl_3$) $\delta$ 210.8, 209.0, 134.6, 132.0, 123.1, 122.2, 81.4, 57.5, 53.5, 37.8, 37.7, 36.3, 34.1, 28.9, 23.7, 21.6, 21.5, 19.6, 15.0.

HRMS (ESI-TOF) *m/z*: $[M + NH_4]^+$ Calcd for $C_{19}H_{30}NO_3$ 320.2220; Found 320.2220.

**Preparation of triketone 162**

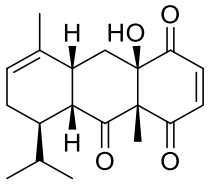


**162**

To a solution of diketone **159** (10 mg, 50 µmol) in DCM (1 mL) at °C were added 4Å MS (30 mg), $VO(acac)_2$ (2.7 mg, 10 µmol) and *t*-BuOH (36 µL, 200 µmol). The reaction was warmed up to rt and stirred 1 h. The reaction mixture was quenched with a solution of $Na_2SO_{3(aq)}$ and further extracted with EA. The combined organic phases were washed with brine, dried over anhydrous $MgSO_4$, filtered, concentrated and the resulting crude product was purified by column chromatography (30% EA in hexanes) to afford triketone **162** (2 mg, 20%) as a colorless liquid.

$^1$H NMR (500 MHz, $CDCl_3$) $\delta$ 6.97 (d, $J$ = 10.6 Hz, 1H), 6.49 (d, $J$ = 10.6 Hz, 1H), 5.46 (br s, 1H), 3.71 (s, 1H), 2.85 (m, 2H), 2.34 (t, $J$ = 13.3 Hz, 1H), 2.02 (m, 1H), 1.87 (m, 2H), 1.73 (dd, $J$ = 3.8, 13.7 Hz, 1H), 1.64 (s, 3H), 1.55 (m, 1H), 1.28 (s, 3H), 0.94 (d, $J$ = 7.1 Hz, 3H), 0.91 (d, $J$ = 6.7 Hz, 3H).

HRMS (ESI-TOF) *m/z*: $[M + H]^+$ Calcd for $C_{19}H_{25}O_4$ 317.1747; Found 317.1743.

**Preparation of enone 170**

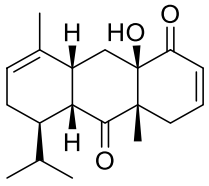


**170**

DBU (50 µL, 0.34 mmol) was added to a stirred solution of diketone **159** (30 mg, 0.11 mmol) in DCM (4 mL) at rt and stirred for 15 min. The reaction mixture was quenched with a solution of $Na_2H_2PO_{4(aq)}$ and further extracted with DCM. The combined organic

phases were washed with brine, dried over anhydrous $MgSO_4$, filtered, concentrated and the resulting crude product was purified by column chromatography (25% $Et_2O$ in hexanes) to afford alcohol enone **170** (27 mg, 90%) as a colorless liquid.

$^1$H NMR (400 MHz, $CDCl_3$) $\delta$ 6.89 (ddd, $J$ = 2.4, 5.5, 10.1 Hz, 1H), 6.17 (ddd, $J$ = 0.7, 3.2, 10.1 Hz, 1H), 5.50 (br s, 1H), 3.01–2.90 (m, 2H), 2.75 (dd, $J$ = 6.3, 11.4 Hz, 1H), 2.28 (dd, $J$ = 5.5, 19.8 Hz, 1H), 2.07–1.96 (m, 3H), 1.89–1.81 (m, 2H), 1.74 (dd, $J$ = 4.2, 13.7 Hz, 1H), 1.66 (s, 3H), 1.54 (m, 1H), 1.12 (s, 3H), 0.95 (d, $J$ = 7.0 Hz, 3H), 0.92 (d, $J$ = 6.7 Hz, 3H).

$^{13}$C NMR (101 MHz, $CDCl_3$): $\delta$ 211.7, 200.2, 148.1, 134.5, 126.2, 122.5, 79.1, 53.8, 52.8, 40.0, 36.8, 34.8, 34.2, 28.5, 24.6, 21.8, 21.6, 16.3, 15.7.

HRMS (ESI-TOF) *m/z*: $[M + H]^+$ Calcd for $C_{19}H_{27}O_3$ 303.1955; Found 303.1956.

**Preparation of diazonium 166**

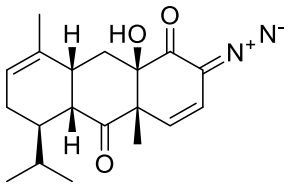


**166**

Para-acetamidobenzenesulfonyl azide (5.4 mg, 23 μmol) was added to a stirred solution of diketone **159** (5.7 mg, 19 μmol) in MeCN (150 μL) at rt. DBU (3.30 μL, 26.3 μmol) was added dropwise. After 5 min, TLC showed complete disappearance of starting material and the reaction mixture was concentrated *in vacuo*. The crude was dissolved in DCM and purified by column chromatography (20% $Et_2O$ in hexanes) to afford α-diazocarbonyl **166** (6.1 mg, 100 %) as a colorless liquid.

$^1$H NMR (400 MHz, $CDCl_3$) $\delta$ 6.14 (d, $J$ = 10.0 Hz, 1H), 5.46 (br s, 1H), 5.25 (d, $J$ = 10.0 Hz, 1H), 3.63 (s, 1H), 2.83–2.75 (m, 1H), 2.66 (dd, $J$ = 5.5, 12.2 Hz, 1H), 2.20 (t, $J$ = 13.2 Hz, 1H), 2.11–1.92 (m, 2H), 1.87–1.76 (m, 1H), 1.67 (m, 1H), 1.65 (s, 3H), 1.57 (m, 1H), 1.12 (s, 3H), 0.92 (d, $J$ = 7.0 Hz, 3H), 0.89 (d, $J$ = 6.7 Hz, 3H).

**Preparation of triene 174**

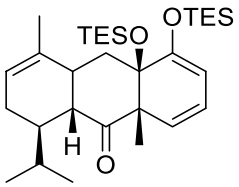


**174**

N-butyllithium (47.3 µL, 0.12 mmol, 2.5M in hexanes) was added to a stirred solution of diisopropylamine (18.6 µL, 0.13 mmol) in THF (1.4 mL) at -78 °C and stirred for 30 min. Diketone **159** (14.3 mg, 47.3 µmol) in THF (0.5 mL) was dropwise added to the reaction mixture. Right after, TESCl (19.8 µL, 0.12 mmol) was added too. The reaction was allowed to warm up to rt and stirred 30 min. The reaction mixture was quenched by pouring it into a solution of $NH_4Cl_{(aq)}$ and further extracted with $Et_2O$. The combined organic phases were washed with brine, dried over anhydrous $MgSO_4$, filtered, concentrated and the resulting crude product **174** was used directly into the next step.

$^1$H NMR (400 MHz, $CDCl_3$) $\delta$ 5.71 (dd, $J$ = 6.2, 9.5 Hz, 1H), 5.44 (br s, 1H), 5.22 (d, $J$ = 9.5 Hz, 1H), 4.99 (d, $J$ = 6.2 Hz, 1H), 2.59–2.47 (m, 2H), 2.19 (m, 1H), 2.08 (t, $J$ = 13.7 Hz, 1H), 1.98–1.87 (m, 2H), 1.78 (m, 1H), 1.67 (s, 3H), 1.62 (m, 1H), 1.15 (s, 3H), 1.00 (t, $J$ = 7.9 Hz, 9H), 0.91 (t, $J$ = 7.9 Hz, 9H), 0.89 (d, $J$ = 7.0 Hz, 3H), 0.86 (d, $J$ = 6.7 Hz, 3H), 0.85–0.79 (m, 6H), 0.74–0.56 (m, 6H).

**Preparation of cyclobutanone 185**

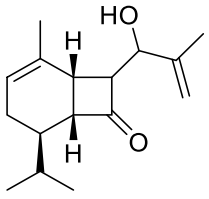


**185**

Lithium hexamethyldisilane (3.64 mL, 3.64 mmol, 1M in THF) was added to a stirred solution of cyclobutanone **68** in THF (40 mL) at -78 °C and stirred for 30 min. Then, methacrolein **184** (0.29 g, 4.2 mmol) in THF (10 mL) was dropwise added to the reaction mixture at the same temperature and stirred for 2 h. The reaction mixture was quenched with a solution of $NH_4Cl_{(aq)}$ and further extracted with EA. The combined organic phases were washed with brine, dried over anhydrous $MgSO_4$, filtered, concentrated and the resulting crude product was purified by column chromatography

(25% $Et_2O$ in hexanes) to afford alcohol **185** (0.38 g, 54%) as a mixture of diastereoisomers (1:1) as a colorless liquid.

$^1$H NMR (400 MHz, $CDCl_3$) $\delta$ 5.55 (br s, 1H), 5.05 (s, 1H), 4.95 (s, 1H), 4.30 (dd, $J$ = 3.0, 7.7 Hz, 1H), 3.29 (dt, $J$ = 2.8, 8.9 Hz, 1H), 3.22 (m, 1H), 2.56–2.49 (m, 2H), 2.05 (m, 1H), 1.79 (m, 1H), 1.77 (s, 3H), 1.70 (m, 1H), 1.65 (s, 3H), 1.63 (m, 1H), 0.94 (d, $J$ = 6.7 Hz, 3H), 0.87 (d, $J$ = 6.6 Hz, 3H).

$^{13}$C NMR (126 MHz, $CDCl_3$): $\delta$ 213.3, 144.4, 133.6, 123.0, 113.6, 76.7, 67.8, 58.8, 38.7, 32.4, 30.8, 25.0, 21.3, 20.9, 19.3, 17.5.

HRMS (ESI-TOF) *m/z*: $[M + H]^+$ Calcd for $C_{16}H_{25}O_2$ 249.1849; Found 249.1850.

**Preparation of diketone 183**

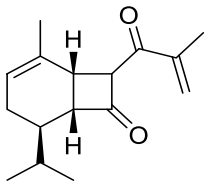


**183**

Dess-Martin periodinane (768 mg, 1.81 mmol) was added to a stirred solution of alcohol **185** (376 mg, 1.51 mmol) in DCM (15 mL) at rt and stirred for 30 min. The reaction mixture was quenched with a 1/3:1/3:1/3 mixture of $H_2O$/$NaHCO_{3(aq)}$/$Na_2S_2O_{3(aq)}$ and further extracted with EA. The combined organic phases were washed with brine, dried over anhydrous $MgSO_4$, filtered, concentrated and the resulting crude product was purified by column chromatography (5% $Et_2O$ in hexanes) to afford diketone **183** (244 mg, 66%) as a colorless liquid.

$^1$H NMR (500 MHz, $CDCl_3$) $\delta$ 6.12 (s, 1H), 6.03 (s, 1H), 5.58 (br s, 1H), 4.52 (dd, $J$ = 2.3, 5.8 Hz, 1H), 3.44 (m, 1H) 3.37 (m, 1H), 2.12 (m, 1H), 1.92 (s, 3H), 1.82 (m, 1H), 1.69 (m, 2H), 1.65 (s, 3H), 0.94 (d, $J$ = 6.6 Hz, 3H), 0.87 (d, $J$ = 6.4 Hz, 3H).

HRMS (ESI-TOF) *m/z*: $[M + NH_4]^+$ Calcd for $C_{16}H_{26}NO_2$ 264.1958; Found 264.1953.

**Preparation of enone 186**

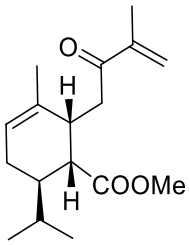


**186**

NaOMe (4.7 mg, 87 μmol) was added to a stirred solution of diketone **183** (214 mg, 870 μmol) in MeOH (43 mL) at 0 °C for 5 min. The reaction mixture was quenched with AcOH, and further extracted with EA. The combined organic phases were washed with brine, dried over anhydrous $MgSO_4$, filtered, concentrated and the resulting crude product was purified by column chromatography (10% $Et_2O$ in hexanes) to afford ester **186** (240 mg, 99%) as a colorless liquid.

$^1H$ NMR (400 MHz, $CDCl_3$) $\delta$ 5.95 (s, 1H), 5.72 (s, 1H), 5.42 (br s, 1H), 3.55 (d, 3H), 3.26 (dd, $J$ = 8.6, 18.2 Hz, 1H), 3.12 (m, 1H), 2.63 (dd, $J$ = 4.8, 11.0 Hz, 1H), 2.48 (dd, $J$ = 2.5, 18.2 Hz, 1H), 1.97 (m, 1H), 1.90 (m, H), 1.87 (s, 3H), 1.86–1.76 (m, 2H), 1.64 (s, 3H), 0.90 (d, $J$ = 6.8 Hz, 3H), 0.73 (d, $J$ = 6.7 Hz, 3H).

$^{13}C$ NMR (126 MHz, $CDCl_3$): $\delta$ 200.3, 172.1, 143.5, 132.4, 124.7, 123.0, 51.2, 45.6, 40.0, 39.1, 37.2, 28.1, 23.8, 22.1, 20.5, 18.8, 18.0.

HRMS (ESI-TOF) *m/z*: $[M + H]^+$ Calcd for $C_{17}H_{27}O_3$ 279.1955; Found 279.1956.

**Preparation of methyl ester 187**

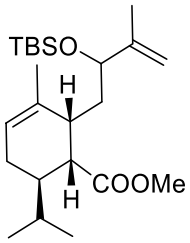


**187**

$NaBH_4$ (48 mg, 0.8 mmol) was added to a stirred solution of enone **186** (113 mg, 0.40 mmol) and $CeCl_3.7H_2O$ (287 mg, 0.60 mmol) in MeOH (8.0 mL) at 0 °C and stirred for 15 min. The reaction mixture was quenched with $H_2O$, and further extracted with EA. The combined organic phases were washed with brine, dried over anhydrous $MgSO_4$,

filtered, concentrated and the resulting crude product was used directly into the next step.

TBSOTf (122 µL, 0.40 mmol) was added to a stirred solution of the corresponding allylic alcohol (113 mg, 0.40 mmol) and lutidine (70 µL, 0.6 mmol) in DCM (8 mL) at 0 °C and stirred for 30 min. The reaction mixture was quenched with $NH_4Cl_{(aq)}$, and further extracted with DCM. The combined organic phases were washed with brine, dried over anhydrous $MgSO_4$, filtered, concentrated and the resulting crude product was purified by column chromatography (1% $Et_2O$ in hexanes) to afford ester **187** (139 mg, 87% over 2 steps) as colorless liquid.

$^1$H NMR (400 MHz, $CDCl_3$) $\delta$ 5.31 (br s, 1H), 4.79 (s, 2H), 4.00 (s, 3H), 3.67 (t, $J$ = 7.2 Hz, 1H), 2.62 (dd, $J$ = 4.7, 9.6 Hz, 1H), 2.22 (q, $J$ = 5.2 Hz, 1H), 2.00–1.76 (m, 5H), 1.70 (s, 3H), 1.67 (s, 3H), 1.49 (ddd, $J$ = 5.1, 7.2, 14.1 Hz, 1H), 0.89 (d, $J$ = 6.9 Hz, 3H), 0.88 (s, 9H), 0.73 (d, $J$ = 6.8 Hz, 3H), 0.06 (s, 3H), 0.00 (s, 3H).

HRMS (ESI-TOF) *m/z*: $[M + H]^+$ Calcd for $C_{23}H_{43}O_3Si$ 395.2976; Found 395.2977.

**Preparation of alcohol 188**

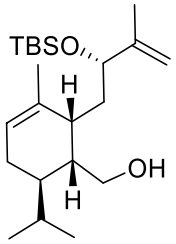


**188**

Lithium aluminum hydride (0.64 mL, 0.64 mmol, 1M solution in THF) was added to a stirred solution of ester **187** (126 g, 0.32 mmol) in THF (3.6 mL) at 0 °C and stirred for 2 h. At 0 °C, 24.2 µL of $H_2O$ was added followed by 24.2 µL of NaOH(aq) (15%) and 72.6 µL of $H_2O$. The reaction was allowed to warm up to room temperature and stirred 15 min. Magnesium sulfate was added to the reaction mixture and left to stir for another 30 min. The reaction mixture was filtered and concentrated to obtain the crude alcohol as a pale-yellow liquid. The resulting crude product was purified by column chromatography (5% $Et_2O$ in hexanes) to afford primary alcohol **188** (81 mg, 69%) as a colorless liquid.

$^1$H NMR (400 MHz, $CDCl_3$) $\delta$ 5.31 (br s, 1H), 4.92 (s, 1H), 4.79 (s, 1H), 4.30 (dd, $J$ = 2.9, 10.9 Hz, 1H), 3.78 (dt, $J$ = 5.9, 11.7 Hz, 1H), 3.63 (m, 1H), 3.37 (dd, $J$ = 3.0, 11.0 Hz, 1H), 2.28 (m, 1H), 1.92–1.80 (m, 3H), 1.78 (s, 3H), 1.72 (s, 3H), 1.69 (m, 1H), 1.39–1.23 (m, 3H), 0.94 (s, 9H), 0.86 (d, $J$ = 6.9 Hz, 3H), 0.78 (d, $J$ = 6.8 Hz, 3H), 0.14 (s, 3H), 0.08 (s, 3H).

HRMS (ESI-TOF) *m/z*: $[M + H]^+$ Calcd for $C_{22}H_{43}O_2Si$ 367.3027; Found 367.3023.

**Preparation of aldehyde 189**

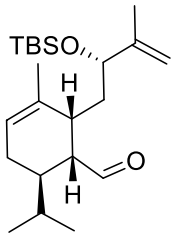


**189**

Dess-Martin periodinane (114 mg, 0.27 mmol) was added to a stirred solution of alcohol **188** (76 mg, 0.21 mmol) and $NaHCO_3$ (70 mg, 0.83 mmol) in DCM (2.1 mL) at rt and stirred for 30 min. The reaction mixture was quenched with a 1/3:1/3:1/3 mixture of $H_2O$/$NaHCO_{3(aq)}$/$Na_2S_2O_{3(aq)}$ and further extracted with EA. The combined organic phases were washed with brine, dried over anhydrous $MgSO_4$, filtered, concentrated and the resulting crude product was purified by column chromatography (15% $Et_2O$ in hexanes) to afford aldehyde **189** (51 mg, 61%) as a colorless liquid.

$^1$H NMR (400 MHz, $CDCl_3$) $\delta$ 9.80 (s, 1H), 5.38 (br s, 1H), 4.86 (s, 1H), 4.82 (s, 1H), 4.11 (t, $J$ = 7.1 Hz, 1H), 2.53 (m, 1H), 2.23 (m, 1H), 2.03 (m, 1H), 1.92 (m, 1H), 1.83–1.75 (m, 2H), 1.73 (s, 3H), 1.71 (m, 1H), 1.68 (s, 3H), 0.90 (d, $J$ = 6.6 Hz, 3H), 0.87 (s, 9H), 0.82 (d, $J$ = 6.5 Hz, 3H), 0.03 (s, 3H), 0.00 (s, 3H).

**Preparation of bromo cyano alkenes 199 and 200**

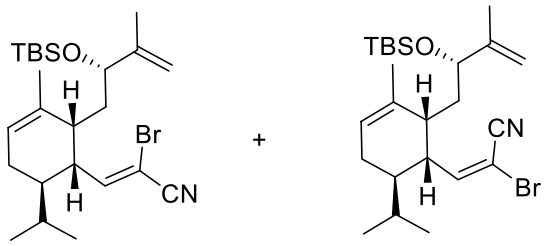


desired
**199**

undesired
**200**

Phosphonate **198** (10.2 mg, 40 µmol), LiCl (1.3 mg, 30 µmol) and DBU (3.7mg, 24 µmol) were successively added to a stirred solution of aldehyde **189** (7.3 mg, 20 µmol) in MeCN (0.2 mL) at 0 °C and stirred for 2h. The reaction mixture was quenched with $H_2O$ and further extracted with EA. The combined organic phases were washed with brine, dried over anhydrous $MgSO_4$, filtered, concentrated and the resulting crude product was purified by column chromatography (3 times) (0.5% $Et_2O$ in hexanes) to afford unsaturated nitrile **199** (2.3 mg, 25%) and **200** (4.6 mg, 50%) both as colorless liquids.

**Data for 199:**

$^1$H NMR (500 MHz, $CDCl_3$) $\delta$ 7.02 (d, $J$ = 9.9 Hz, 1H), 5.38 (br s, 1H), 4.92 (br s, 1H), 4.87 (br s, 1H), 4.03 (dd, $J$ = 5.5, 9.4 Hz, 1H), 3.0 (m, 1H), 2.03 (m, 1H), 1.95 (m, 2H), 1.82 (ddd, $J$ = 4.2, 9.4, 13.9 Hz, 1H), 1.68 (s, 6H), 1.56 (m, 1H), 1.41 (m, 1H), 1.28 (ddd, $J$ = 5.6, 9.7, 14.7 Hz, 1H), 0.92 (d, $J$ = 6.7 Hz, 3H), 0.88 (s, 9H), 0.82 (d, $J$ = 6.6 Hz, 3H), 0.06 (s, 3H), 0.02 (s, 3H).

HRMS (ESI-TOF) *m/z*: $[M + H]^+$ Calcd for $C_{24}H_{41}BrNOSi$ 466.2135; Found 466.2137.

**Data for 200:**

$^1$H NMR (500 MHz, $CDCl_3$) $\delta$ 5.93 (d, $J$ = 11.2 Hz, 1H), 5.37 (br s, 1H), 4.94 (br s, 1H), 4.88 (br s, 1H), 4.11 (dd, $J$ = 5.6, 9.3 Hz, 1H), 2.96 (m, 1H), 2.04 (m, 1H), 1.96 (m, 2H), 1.78 (ddd, $J$ = 3.8, 9.4, 13.8 Hz, 1H), 1.69 (s, 3H), 1.67 (s, 3H), 1.56 (m, 1H), 1.46 (m, 1H), 1.34 (ddd, $J$ = 5.5, 9.6, 14.7 Hz, 1H), 0.93 (d, $J$ = 6.7 Hz, 3H), 0.88 (s, 9H), 0.83 (d, $J$ = 6.6 Hz, 3H), 0.08 (s, 3H), 0.03 (s, 3H).

HRMS (ESI-TOF) *m/z*: $[M + H]^+$ Calcd for $C_{24}H_{41}BrNOSi$ 466.2135; Found 466.2130.

**Preparation of unsaturated lactone 228**

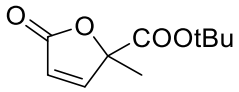


**228**

Lindlar catalyst (21mg, 12% wt) was added to a stirred solution of tertiary alcohol (169 mg, 0.74 mmol) and quinoline (88 µL, 0.74 mmol) in toluene (6 mL) at rt. The reaction mixture was flushed with a balloon of $H_2$ and stirred for 3h. The reaction mixture was filtered through a plug of celite and flushed with EA. The filtrate was washed with a 1M solution of HCl and further extracted with EA. The combined organic phases were washed with brine, dried over anhydrous $MgSO_4$, filtered, concentrated and the resulting crude product was purified by column chromatography (15% $Et_2O$ in hexanes) to afford lactone **228** (120 mg, 82%) as a colorless liquid.

$^1$H NMR (500 MHz, $CDCl_3$) $\delta$ 7.42 (d, $J$ = 5.6 Hz, 1H), 6.12 (d, $J$ = 5.6 Hz, 1H), 1.69 (s, 3H), 1.47 (s, 9H).

$^{13}$C NMR (126 MHz, $CDCl_3$): $\delta$ 172.4, 168.2, 151.0, 119.7, 87.2, 82.1, 28.1, 23.2.

HRMS (ESI-TOF) *m/z*: $[M + H]^+$ Calcd for $C_{10}H_{15}O_4$ 199.0965; Found 199.0967.

**Preparation of unsaturated lactone 229**

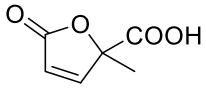


**229**

TFA (5 mL) was added to a stirred solution of ester **228** (61 mg, 0.31 mmol) in DCM (5 mL) at rt and stirred for 1 h. The reaction was evaporated, and the crude directly used in the next step.

$^1$H NMR (400 MHz, $CDCl_3$) $\delta$ 7.52 (d, $J$ = 5.6 Hz, 1H), 6.23 (d, $J$ = 5.6 Hz, 1H), 1.79 (s, 3H).

$^{13}$C NMR (151 MHz, $CDCl_3$): $\delta$ 172.8, 170.1, 152.6, 120.0, 89.5, 23.3.

**Preparation of cyclobutanone 231**

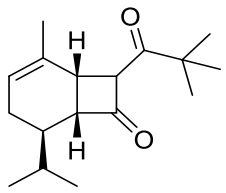

**231**

LiHMDS (74 µL, 74 µmol, 1M in hexanes) was added to a stirred solution of cyclobutanone **68** (12 mg, 67 µmol) in toluene (0.7 mL) at -78 °C and stirred for 30 min. Then, pivaloyl chloride **230** (11 µL, 88 µmol) in toluene (0.3 mL) was added to the reaction mixture. After 20 min, the reaction mixture was quenched with a solution of $NH_4Cl_{(aq)}$ and further extracted with EA. The combined organic phases were washed with brine, dried over anhydrous $MgSO_4$, filtered, concentrated and the resulting crude product was purified by column chromatography (10% $Et_2O$ in hexanes) to afford diketone **231** (10.4 mg, 60%) as a colorless liquid.

$^1$H NMR (500 MHz, $CDCl_3$) $\delta$ 5.56 (br s, 1H), 4.41 (dd, $J$ = 2.4, 5.6 Hz, 1H), 3.51 (ddd, $J$ = 2.3, 6.6, 9.3 Hz, 1H), 3.15 (dd, $J$ = 6.6, 9.6 Hz, 1H), 2.11 (m, 1H), 1.84 (m, 1H), 1.69 (m, 1H), 1.66 (m, 1H), 1.62 (s, 3H), 1.18 (s, 9H), 0.93 (d, $J$ = 6.7 Hz, 3H), 0.87 (d, $J$ = 6.5 Hz, 3H).

$^{13}$C NMR (151 MHz, $CDCl_3$): $\delta$ 211.6, 206.9, 133.2, 121.3, 67.6, 56.6, 46.6, 39.7, 34.5, 30.4, 25.8, 25.7, 21.3, 20.4, 17.3.

HRMS (ESI-TOF) *m/z*: $[M + H]^+$ Calcd for $C_{17}H_{27}O_2$ 263.2006; Found 263.2007.

**Preparation of alcohol 237**

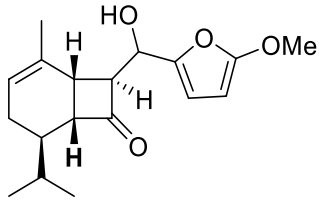

**237**

LiHMDS (4.43 mL, 4.43 mmol, 1M in hexanes) was added to a stirred solution of cyclobutanone **68** (608 mg, 3.41 mmol) in THF (48 mL) at 0 °C and stirred for 30 min. Then, aldehyde **236** (430 mg, 3.41 mmol) in THF (13 mL) was added to the reaction

mixture. After 2 h, the reaction mixture was quenched with a solution of $NH_4Cl_{(aq)}$ and further extracted with EA. The combined organic phases were washed with brine, dried over anhydrous $MgSO_4$, filtered, concentrated and the resulting crude product was purified by column chromatography (15% EA in hexanes) to afford alcohol **237** (327 mg, 67%) as a mixture of diastereoisomers (1:1) both as a white solid. Those diastereoisomers were not isolated and directly used in the next step.

**Preparation of methyl ester 233**

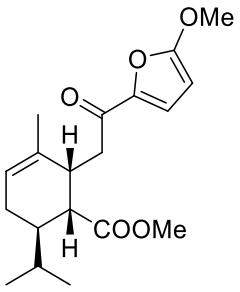


**233**

NMO (145 mg, 1.24 mmol), and TPAP (32 mg, 93 µmol) were successfully added to a stirred solution of alcohol **237** (188 mg, 0.62 mmol) with MS 4Å (309 mg) in DCM (12.4 mL) at rt and was stirred for 48 h. The reaction mixture was filtered through a plug of celite, flushed with EA, evaporated, and directly used into the next step.

Sodium methoxide (4 mg, 6.2 µmol) was added to a stirred solution of crude diketone in MeOH (6 mL) at 0 °C and was stirred for 5 min. The reaction mixture was quenched with a solution of $NH_4Cl_{(aq)}$ and further extracted with EA. The combined organic phases were washed with brine, dried over anhydrous $MgSO_4$, filtered, concentrated and the resulting crude product was purified by column chromatography (15% EA in hexanes) to afford a ester **233** (45 mg, 22% over 2 steps) as a white solid.

$^1$H NMR (400 MHz, $CDCl_3$) $\delta$ 7.14 (d, $J$ = 3.7 Hz, 1H), 5.41 (br s, 1H), 5.35 (d, $J$ = 3.7 Hz, 1H), 3.95 (s, 3H), 3.54 (s, 3H), 3.23 (dd, $J$ = 8.0, 17.4 Hz, 1H), 3.18–3.13 (m, 1H), 2.66 (dd, $J$ = 4.6, 10.6 Hz, 1H), 2.59 (dd, $J$ = 2.9, 17.4 Hz, 1H), 2.03–1.77 (m, 4H), 1.65 (s, 3H), 0.91 (d, $J$ = 6.7 Hz, 3H), 0.74 (d, $J$ = 6.8 Hz, 3H).

$^{13}$C NMR (126 MHz, $CDCl_3$): $\delta$ 187.0, 172.0, 161.7, 152.9, 131.9, 123.0, 115.1, 85.1, 57.9, 51.2, 45.7, 40.3, 40.2, 37.2, 28.3, 23.8, 22.1, 20.5, 18.0.

HRMS (ESI-TOF) *m/z*: $[M + NH_4]^+$ Calcd for $C_{19}H_{30}NO_5$ 352.2118; Found 352.2119.

**Preparation of aldehyde 244 and side-product 243**

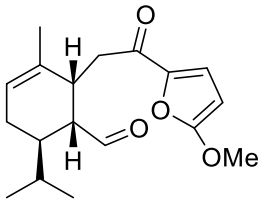

**244**

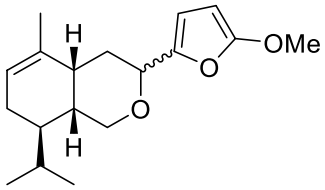

**243**

Lithium aluminum hydride (3.84 mL, 3.84 mmol, 1M solution in THF) was added to a stirred solution of ester **233** (214 mg, 0.64 mmol) in THF (10 mL) at -15 °C and stirred for 2 h. At -15 °C, the reaction mixture was quenched with a mixture of $Et_2O$:Acetone (4:1) (10 mL) and $H_2O$ (10 mL) and was further extracted with $Et_2O$. The combined organic phases were washed with brine, dried over anhydrous $MgSO_4$, filtered, diluted with DCE and concentrated until it remained about 10 mL of DCE in the flash. The resulting crude product was directly used into the next step.

TPAP (63 mg, 0.18 mmol), NMO (281 mg, 2.4 mmol) and 4Å MS (300 mg) were added to a stirred solution of previous crude diol **242** in DCE (30 mL) at rt and stirred overnight. The reaction mixture was filtered through a pad of silica and flushed with DCM. The filtrate was concentrated, and the resulting crude product was purified by column chromatography (5% DCM in MeOH) to afford ketoaldehyde **244** (34 mg, 15 % over 2 steps) as a colorless liquid.

**Data for 244:**

$^1$H NMR (400 MHz, $CDCl_3$) $\delta$ 9.70 (d, $J$ = 2.7 Hz, 1H), 7.17 (d, $J$ = 3.7 Hz, 1H), 5.41 (br s, 1H), 5.38 (d, $J$ = 3.7 Hz, 1H), 3.97 (s, 3H), 3.07 (dd, $J$ =8.7, 16.4 Hz, 1H), 2.84 (dd, $J$ = 4.1, 16.4 Hz, 1H), 2.72 (m, 1H), 2.02 (m, 1H), 1.92–1.81 (m, 2H), 1.69 (s, 3H), 1.66 (m, 1H), 1.51 (m, 1H), 0.96 (d, $J$ = 6.6 Hz, 3H), 0.83 (d, $J$ = 6.5 Hz, 3H).

HRMS (ESI-TOF) *m/z*: $[M + NH_4]^+$ Calcd for $C_{18}H_{28}NO_4$ 322.2013; Found 322.2011.

**Data for 243:**

$^1$H NMR (400 MHz, $CDCl_3$) $\delta$ 6.15 (d, $J$ = 3.3 Hz, 1H), 5.42 (br s, 1H), 5.07 (d, $J$ = 3.3 Hz, 1H), 4.26 (dd, $J$ = 2.4, 11.6 Hz, 1H), 4.24 (d, $J$ = 12.0 Hz, 1H) 3.82 (s, 3H), 3.58 (dd,

*J* = 2.7, 12.0 Hz, 1H), 2.23–2.10 (m, 2H), 2.05–1.91 (m, 3H), 1.84–1.71 (m, 2H), 1.67 (s, 3H), 1.49 (m, 1H), 0.92 (d, *J* = 6.9 Hz, 3H), 0.72 (d, *J* = 6.8 Hz, 3H).

$^{13}$C NMR (101 MHz, $CDCl_3$) *δ* 161.3, 144.8, 136.1, 121.8, 108.1, 79.9, 73.3, 68.5, 57.7, 40.4, 36.0, 32.9, 30.9, 25.8, 24.1, 21.2, 21.2, 14.4.

HRMS (ESI-TOF) *m/z*: $[M + NH_4]^+$ Calcd for $C_{18}H_{30}NO_3$ 308.2220; Found 308.2218.

**Preparation of bromo cyano alkenes 245 and 246**

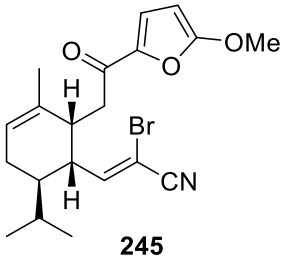


**245**

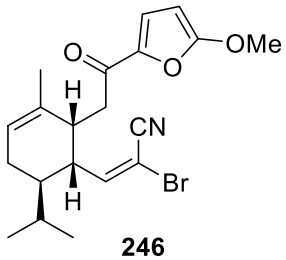


**246**

Phosphonate **198** (135 mg, 0.53 mmol), LiCl (16.7 mg, 0.40 mmol) and DBU (59 µL, 0.40 mmol) were successively added to a stirred solution of aldehyde **232** (80 mg, 0.26 mmol) in MeCN (3 mL) at 0 °C and stirred for 2h. The reaction mixture was quenched with $H_2O$ and further extracted with EA. The combined organic phases were washed with brine, dried over anhydrous $MgSO_4$, filtered, concentrated and the resulting crude product was purified by column chromatography (10% EA in hexanes) to afford the mixture of bromo cyano alkenes **245** and **246** as a mixture of 1:2 respectively (95 mg, 89%) as colorless liquids. These products were not separated.

$^1$H NMR (400 MHz, $CDCl_3$) *δ* 7.22–7.19 (m, 1H), 6.88 (d, *J* = 9.7 Hz, 0.33H), 6.77 (d, *J* = 11.1 Hz, 0.67H), 5.46–5.41 (m, 2H), 3.99 (s, 3H), 3.08–2.87 (m, 2H), 2.75–2.68 (m, 2H), 2.02–1.92 (m, 2H), 1.68 (s, 3H), 1.67–1.59 (m, 2H), 1.00–0.96 (m, 3H), 0.82 (d, *J* = 6.4 Hz, 2H), 0.81 (d, *J* = 6.6 Hz, 1H).

HRMS (ESI-TOF) *m/z*: $[M + H]^+$ Calcd for $C_{20}H_{25}BrNO_3$ 406.1012; Found 406.1007.

**Preparation of aldehyde 263**

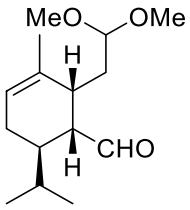


**263**

Dess-Martin periodinane (2.08 g, 4.9 mmol) was added to a stirred solution of the corresponding alcohol (1.04 g, 4.1 mmol) and $NaHCO_3$ (1.03 g, 12.2 mmol) in DCM (41 mL) at rt and stirred for 30 min. The reaction mixture was quenched with a 1/3:1/3:1/3 mixture of $H_2O$/$NaHCO_{3(aq)}$/$Na_2S_2O_{3(aq)}$ and further extracted with EA. The combined organic phases were washed with brine, dried over anhydrous $MgSO_4$, filtered, concentrated and the resulting crude product was purified by column chromatography (20% $Et_2O$ in hexanes) to afford aldehyde **263** (560 mg, 54%) as a colorless liquid.

$^1$H NMR (500 MHz, $CDCl_3$) $\delta$ 9.78 (d, $J$ = 3.4 Hz, 1H), 5.39 (br s, 1H), 4.37 (dd, $J$ = 5.1, 6.5 Hz, 1H), 3.32 (s, 3H), 3.31 (s, 3H), 2.57 (m, 1H), 2.40 (m, 1H), 2.03 (m, 1H), 1.98–1.74 (m, 5H), 1.73 (s, 3H), 0.93 (d, $J$ = 6.8 Hz, 3H), 0.84 (d, $J$ = 6.7 Hz, 3H).

**Preparation of bromo cyano alkenes 264 and 265**

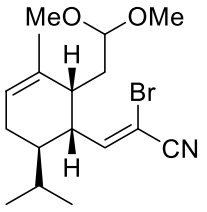


**264**

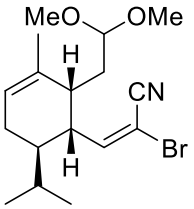


**265**

Phosphonate **198** (1.01 g, 3.96 mmol), LiCl (126 mg, 2.97 mmol) and DBU (359 µL, 2.38 mmol) were successively added to a stirred solution of aldehyde **263** (500 mg, 1.98 mmol) in MeCN (20 mL) at 0 °C and stirred for 2h. The reaction mixture was quenched with $H_2O$ and further extracted with $Et_2O$. The combined organic phases were washed with brine, dried over anhydrous $MgSO_4$, filtered, concentrated and the resulting crude product was purified by column chromatography (15% $Et_2O$ in hexanes) to afford unsaturated nitrile **264** (192 mg, 27%) and **265** (363 mg, 54%) both as colorless liquids.

**Data for 264:**

$^1$H NMR (500 MHz, $CDCl_3$) $\delta$ 7.01 (d, $J$ = 9.8 Hz, 1H), 5.41 (br s, 1H), 4.31 (dd, $J$ = 4.4, 7.3 Hz, 1H), 3.35 (s, 3H), 3.33 (s, 3H), 2.97 (ddd, $J$ = 4.6, 6.9, 9.8 Hz, 1H), 2.32 (s, 1H), 1.96 (m, 2H), 1.86 (ddd, $J$ = 4.6, 7.3, 14.5 Hz, 1H), 1.69 (s, 3H), 1.62 (m, 1H), 1.54 (m, 1H), 1.45 (ddd, $J$ = 4.4, 9.3, 14.5 Hz, 1H), 0.96 (d, $J$ = 6.7 Hz, 3H), 0.83 (d, $J$ = 6.6 Hz, 3H).

HRMS (ESI-TOF) *m/z*: $[M + H]^+$ Calcd for $C_{17}H_{27}BrNO_2$ 356.1220; Found 356.1222.

**Data for 265:**

$^1$H NMR (500 MHz, $CDCl_3$) $\delta$ 6.93 (d, $J$ = 11.2 Hz, 1H), 5.40 (br s, 1H), 4.34 (dd, $J$ = 4.6, 6.9 Hz, 1H), 3.37 (s, 3H), 3.35 (s, 3H), 2.93 (ddd, $J$ = 4.7, 7.7, 11.3 Hz, 1H), 2.29 (s, 1H), 1.96 (m, 2H), 1.81 (ddd, $J$ = 4.2, 6.9, 14.5 Hz, 1H), 1.69 (s, 3H), 1.63–1.50 (m, 3H), 0.96 (d, $J$ = 6.7 Hz, 3H), 0.83 (d, $J$ = 6.6 Hz, 3H).

HRMS (ESI-TOF) *m/z*: $[M + H]^+$ Calcd for $C_{17}H_{27}BrNO_2$ 356.1220; Found 356.1219.

**Preparation of vinyl bromide 266**

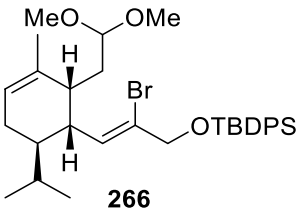


**266**

DiBAlH (1.25 mL, 1.25 mmol, 1M solution in hexanes) was added to a stirred solution of nitrile **264** (370 mg, 1.04 mmol) in petroleum ether (10.4 mL) at -78 °C and stirred for 1 h. Then, the reaction mixture was quenched with a 10% citric acid solution (10 mL) and further stirred overnight at room temperature. The reaction mixture was extracted with $Et_2O$ and the combined organic phases were washed with brine, dried over anhydrous $MgSO_4$, filtered and concentrated. The resulting crude product was directly used into the next step.

The crude mixture was dissolved in MeOH (9.5 mL) at 0 °C. Sodium borohydride (36 mg, 0.95 mmol) was added. After 30 min, the reaction was quenched with water and extracted with EA. The combined organic phases were washed with brine, dried over

anhydrous $MgSO_4$, filtered and concentrated. The resulting crude product was directly used into the next step.

Imidazole (97 mg, 1.43 mmol) and TBDPSCl (300 µL, 1.15 mmol) were added to a stirred solution of the corresponding free allylic alcohol crude in DCM (4.8 mL) at rt and stirred overnight. The reaction mixture was quenched with a solution of $NaHCO_3$ and further extracted with DCM. The combined organic phases were washed with brine, dried over anhydrous $MgSO_4$, filtered, concentrated and the resulting crude product was purified by column chromatography (15% $Et_2O$ in hexanes) to afford TBDPS-protected alcohol **266** (482 mg, 90% over 3 steps) as a colorless liquid.

$^1$H NMR (400 MHz, $CDCl_3$) $\delta$ 7.69–7.64 (m, 4H), 7.44–7.35 (m, 6H), 6.22 (d, $J$ = 9.5 Hz, 1H), 5.36 (br s, 1H), 4.45 (dd, $J$ = 3.8, 8.3 Hz, 1H), 4.29 (s, 2H), 3.38 (s, 3H), 3.29 (s, 3H), 2.91 (ddd, $J$ = 5.1, 6.8, 9.6 Hz, 1H), 2.31 (m, 1H), 1.94 (m, 2H), 1.82 (ddd, $J$ = 4.7, 8.2, 14.0 Hz, 1H), 1.68 (s, 3H), 1.64 (m, 1H), 1.54–1.44 (m, 2H), 1.06 (s, 9H), 0.97 (d, $J$ = 6.8 Hz, 3H), 0.83 (d, $J$ = 6.6 Hz, 3H).

HRMS (ESI-TOF) *m/z*: $[M + NH_4]^+$ Calcd for $C_{33}H_{51}BrNO_3Si$ 616.2816; Found 616.2816.

**Preparation of the aldehyde 464**

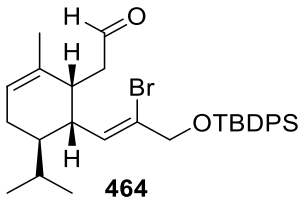


**464**

PTSA.$H_2O$ (56 mg, 0.30 mmol) was added to a stirred solution of the corresponding ketal **266** (167 mg, 0.27 mmol) in acetone (2.7 mL) at rt and stirred for 4 h. The reaction mixture was quenched with a solution of $NaHCO_3$ and further extracted with EA. The combined organic phases were washed with brine (20 mL), dried over anhydrous $MgSO_4$, filtered, concentrated and the resulting crude product was purified by column chromatography (25% DCM in hexanes) to afford aldehyde **464** (136 mg, 92%) as a colorless liquid.

$^1$H NMR (500 MHz, $CDCl_3$) $\delta$ 9.70 (t, $J$ = 2.3 Hz, 1H), 7.68–7.64 (m, 4H), 7.46–7.36 (m, 6H), 6.04 (d, $J$ = 9.3 Hz, 1H), 5.46 (br s, 1H), 4.27 (m, 2H), 2.90–2.79 (m, 2H), 2.44 (ddd, $J$ = 2.7, 7.6, 16.7 Hz, 1H), 2.35 (ddd, $J$ = 2.1, 4.9, 16.7 Hz, 1H), 1.97 (m, 1H), 1.88

(m, 1H), 1.72 (m, 1H), 1.67 (s, 3H), 1.57 (m, 1H), 1.07 (s, 9H), 0.93 (d, *J* = 6.9 Hz, 3H), 0.76 (d, *J* = 6.8 Hz, 3H).

HRMS (ESI-TOF) *m/z*: $[M + H]^+$ Calcd for $C_{31}H_{42}BrO_2Si$ 553.2132; Found 553.2130.

**Preparation of alcohol 267**

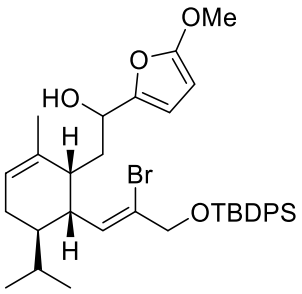


**267**

*Sec*-BuLi (1.55 mL, 2.17 mmol, 1.4M in hexanes) was added to a stirred solution of 2-methoxyfuran (215 µL, 2.33 mmol) in THF (1.3 mL) at -78 °C and stirred for 30 min. Then, aldehyde **464** (432 mg, 0.78 mmol) in THF (0.7 mL) was added and the resulting mixture was stirred 2 h at -78 °C. The reaction mixture was quenched with a solution of $NH_4Cl_{(aq)}$ and further extracted with EA. The combined organic phases were washed with brine (20 mL), dried over anhydrous $MgSO_4$, filtered, concentrated and the resulting crude product was purified by column chromatography (10% EA in hexanes) to afford **267** as a mixture of diastereoisomers (1:1) (261 mg, 52%) as a colorless liquid. They were non isolated and consequently non characterized.

HRMS (ESI-TOF) *m/z*: $[M + NH_4]^+$ Calcd for $C_{36}H_{51}BrNO_4Si$ 668.2765; Found 668.2762.

**Preparation of ketone 268**

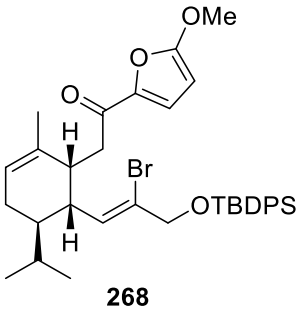


**268**

TPAP (17 mg, 47 µmol), NMO (73 mg, 0.62 mmol) and MS 4Å (155 mg) were added to a stirred solution of furfuryl alcohol **267** (202 mg, 0.31 mmol) in DCM (6.2 mL) at rt and

stirred overnight. The reaction mixture was filtered through a pad of silica and flushed with DCM. The filtrate was concentrated, and the resulting crude product was purified by column chromatography (10% EA in hexanes) to afford ketoaldehyde **268** (76 mg, 38%) as a colorless liquid.

$^{1}$H NMR (500 MHz, $CDCl_3$) $\delta$ 7.70–7.65 (m, 4H), 7.44–7.36 (m, 6H), 7.13 (d, $J$ = 3.7 Hz, 1H), 5.96 (d, $J$ = 10.3 Hz, 1H), 5.38 (br s, 1H), 5.31 (d, $J$ = 3.7 Hz, 1H), 4.33 (d, $J$ = 12.6 Hz, 1H), 4.07 (d, $J$ = 12.6 Hz, 1H), 3.91 (s, 3H), 2.78 (dd, $J$ = 8.2, 15.4 Hz, 1H), 2.63 (m, 1H), 2.57 (dd, $J$ = 5.0, 15.4 Hz, 1H), 2.00 (m, 1H), 1.84 (m, 1H), 1.72–1.64 (m, 2H), 1.60 (s, 3H), 1.36 (m, 1H), 1.03 (s, 9H), 0.86 (d, $J$ = 6.8 Hz, 3H), 0.74 (d, $J$ = 6.7 Hz, 3H).

$^{13}$C NMR (101 MHz, $CDCl_3$) $\delta$ 185.2, 161.7, 149.4, 135.8, 134.3, 133.9, 133.6, 129.7, 127.7, 121.7, 121.3, 115.2, 85.1, 70.7, 57.9, 42.6, 42.2, 40.5, 39.5, 26.8, 24.3, 20.2, 19.1, 19.1, 19.0.

HRMS (ESI-TOF) *m/z*: $[M + NH_4]^+$ Calcd for $C_{36}H_{49}BrNO_4Si$ 666.2609; Found 666.2604.

**Preparation of alcohol 272**

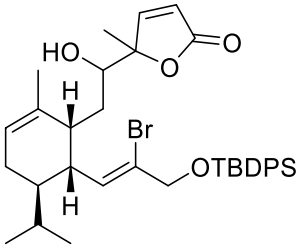


**272**

Potassium *tert*-butoxide (101 mg, 0.90 mmol) was added to a stirred solution of aldehyde **270** (198 mg, 0.36 mmol) and α-angelicalactone **271** (161 µL, 1.79 mmol) in THF (4 mL) at 0°C and stirred for 15 min. The reaction mixture was quenched with a solution of $NH_4Cl_{(aq)}$ and further extracted with EA. The combined organic phases were washed with brine (20 mL), dried over anhydrous $MgSO_4$, filtered, concentrated and the resulting crude product was purified by column chromatography (10% EA in hexanes) to afford an only diastereoisomer alcohol **272** (98 mg, 42%) as a colorless liquid.

$^{1}$H NMR (400 MHz, $CDCl_3$) $\delta$ 7.68–7.62 (m, 4H), 7.45–7.36 (m, 6H), 7.31 (d, $J$ = 5.7 Hz, 1H), 6.15 (d, $J$ = 9.8 Hz, 1H), 6.01 (d, $J$ = 5.7 Hz, 1H), 5.40 (br s, 1H), 4.30 (s, 2H), 3.84

(dd, *J* = 6.4, 11.1 Hz, 1H), 3.02 (m, 1H), 2.51 (m, 1H), 1.95 (m, 2H), 1.89 (d, *J* = 6.4 Hz, 1H), 1.69 (m, 2H), 1.65 (s, 3H), 1.61 (m, 1H), 1.41 (s, 3H), 1.38 (m, 1H), 1.07 (s, 9H), 0.98 (d, *J* = 6.8 Hz, 3H), 0.84 (d, *J* = 6.6 Hz, 3H).

HRMS (ESI-TOF) *m/z*: $[M + H]^+$ Calcd for $C_{36}H_{48}BrO_4Si$ 651.2500; Found 651.2499.

**Preparation of alcohol 282**

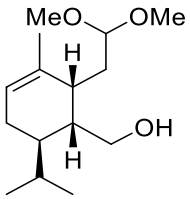


**282**

Lithium aluminum hydride (27.6 mL, 27.6 mmol, 1M solution in THF) was added to a stirred solution of ester **262** (5.2 g, 18.4 mmol) in diethyl ether (184 mL) at 0 °C and stirred for 2 h. At 0 °C, 1.2 mL of $H_2O$ was added followed by 1.2 mL of NaOH(aq) (15%) and 3.6 mL of $H_2O$. The reaction was allowed to warm up to room temperature and stirred 15 min. Magnesium sulfate was added to the reaction mixture and left to stir for another 30 min. The reaction mixture was filtered and concentrated to obtain the crude alcohol as a pale-yellow liquid. The resulting crude product was purified by column chromatography (20% EA in hexanes) to afford alcohol **282** (4.81 g, 92%) as a colorless liquid.

$^1$H NMR (600 MHz, $C_6D_6$) $\delta$ 5.30 (s, 1H), 4.44 (dd, *J* = 4.1, 7.3 Hz, 1H), 3.82 (ddd, *J* = 5.2, 8.9, 11.7 Hz, 1H), 3.56 (dt, *J* = 4.1, 11.1 Hz, 1H), 3.10 (s, 3H), 3.07 (s, 3H), 2.89 (m, 1H), 2.38 (m, 1H), 1.98–1.91 (m, 2H), 1.83 (m, 1H), 1.75–1.72 (m, 1H), 1.71 (s, 3H), 1.67–1.61 (m, 1H), 1.51 (ddd, *J* = 4.2, 5.2, 14.7 Hz, 1H), 1.41–1.34 (m, 1H), 0.81 (d, *J* = 6.9 Hz, 3H), 0.73 (d, *J* = 6.8 Hz, 3H).

$^{13}$C NMR (151 MHz, $C_6D_6$) $\delta$ 128.3, 121.0, 105.6, 61.7, 54.2, 52.0, 42.1, 36.6, 34.9, 33.6, 26.8, 24.7, 23.0, 21.3, 15.7.

HRMS (ESI-TOF) *m/z*: $[M + H]^+$ Calcd for $C_{15}H_{29}O_3$ 257.2111; Found 257.2112.

IR (neat): v 3426, 2956, 2899, 1456, 1369, 1131, 1054 $cm^{-1}$

$[\alpha]_D^{20}$ = + 93.4 (c = 2.37) in $C_6H_6$

**Preparation of acetal 465**

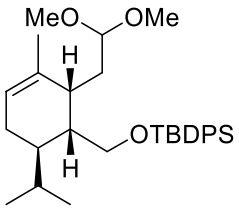


**465**

Imidazole (2.5 g, 36.6 mmol) and TBDPSCl (7.59 mL, 29.2 mmol) were added to a stirred solution of ketal **282** (6.2 g, 24.4 mmol) in DCM (122 mL) at rt and stirred overnight. The reaction mixture was quenched with a solution of $NaHCO_3$ and further extracted with DCM. The combined organic phases were washed with brine, dried over anhydrous $MgSO_4$, filtered, concentrated and the resulting crude product was purified by column chromatography (5% EA in hexanes) to afford ketal **465** (11.8 g, 98%) as a colorless liquid.

$^1$H NMR (400 MHz, $CDCl_3$) $\delta$ 7.74–7.66 (m, 4 H), 7.48–7.36 (m, 6 H), 5.30 (s, 1 H), 4.45 (dd, *J* = 5.5, 6.3 Hz, 1 H), 3.69 (d, *J* = 7.4 Hz, 2H), 3.25 (s, 3 H), 3.18 (s, 3 H), 2.39 (m 1 H), 2.12 (m, 1 H), 1.86 (m, 1 H), 1.78 (m, 1 H), 1.66 (s, 3 H), 1.63–1.48 (m, 4 H), 1.04 (s, 9 H), 0.82 (d, *J* = 6.6 Hz, 3 H), 0.62 (d, *J* = 6.5 Hz, 3 H).

$^{13}$C NMR (126 MHz, $CDCl_3$) $\delta$ 137.0, 135.6, 132.9, 129.7, 127.6, 122.4, 105.0, 65.0, 55.0, 41.9, 41.5, 36.4, 34.2, 28.1, 26.9, 23.7, 21.0, 19.2, 17.2, 15.2.

HRMS (ESI-TOF) *m/z*: $[M + H]^+$ Calcd for $C_{31}H_{47}O_3Si$ 495.3289; Found 495.3291.

IR (neat): v 2956, 2919, 2889, 2852, 1423, 1114, 1057 $cm^{-1}$

$[\alpha]_D^{20}$ = + 15.9 (c = 2.19) in $C_6H_6$

**Preparation of aldehyde 283**

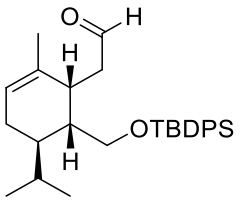


**283**

PTSA.$H_2O$ (422 mg, 2.22 mmol) was added to a stirred solution of ketal **465** (1 g, 2.02 mmol) in acetone (21 mL) at rt and stirred for 4 h. The reaction mixture was quenched with a solution of $NaHCO_3$ and further extracted with EA. The combined organic phases were washed with brine (20 mL), dried over anhydrous $MgSO_4$, filtered, concentrated and the resulting crude product was purified by column chromatography (10% DCM in hexane) to afford aldehyde **283** (822 mg, 91%) as a colorless liquid.

$^1$H NMR (400 MHz, $CD_3CN$) $\delta$ 9.87 (t, $J$ = 2.8 Hz, 1 H), 7.67–7.62 (m, 4 H), 7.44–7.34 (m, 6 H), 5.40 (m, 1 H), 3.74 (dd, $J$ = 5.1, 10.9 Hz, 1 H), 3.51 (t, $J$ = 10.6 Hz, 1 H), 3.01 (m, 1 H), 2.60 (ddd, $J$ = 3.1, 6.8, 16.2 Hz, 1 H), 2.33 (ddd, $J$ = 2.6, 5.2, 16.2 Hz, 1 H), 1.92–1.82 (m, 2 H), 1.72 (s, 3 H), 1.70 (m, 1 H), 1.49–1.34 (m, 2 H), 1.27 (m, 1 H), 1.05 (s, 9 H), 0.76 (d, $J$ = 6.8 Hz, 3 H), 0.43 (d, $J$ = 6.8 Hz, 3 H).

$^{13}$C NMR (126 MHz, $CD_3CN$) $\delta$ 202.1, 135.6, 134.4, 132.9, 129.7, 127.6, 122.6, 63.9, 44.4, 43.4, 36.5, 36.0, 27.9, 26.9, 23.4, 22.4, 19.2, 17.0, 15.0.

HRMS (ESI-TOF) *m/z*: $[M + H]^+$ Calcd for $C_{29}H_{41}O_2Si$ 449.2870; Found 449.2871.

IR (neat): v 2949, 2926, 2882, 2852, 1721, 1430, 1111, 1064 $cm^{-1}$

$[\alpha]_D^{20}$ = + 33.5 (c = 1.49) in $C_6H_6$

**Preparation of diene 311**

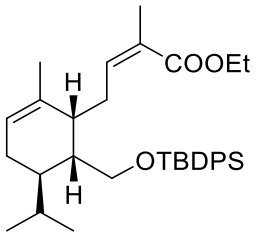


**311**

To a solution of phosphonate **310** (2.70 g, 8.13 mmol) and 18-C-6 crown ether (8.27 g, 31.3 mmol) in THF (101 mL) was slowly added a 1M solution of KHMDS (6.88 mL, 6.88 mmol, 1M solution in THF) at -78 °C. After 30 min, aldehyde **283** (2.77 g, 6.25 mmol) in THF (10 mL) was slowly added to the reaction mixture and stirred for 4 h at the same temperature. After completion, the reaction was quenched with an aqueous solution of $NH_4Cl$ and further extracted with EA. The combined organic phases were washed with brine (20 mL), dried over anhydrous $MgSO_4$, filtered, concentrated and the resulting crude product was purified by column chromatography (10% DCM in hexane) to afford α,β-unsaturated ester **311** (2.95 g, 92%) as a colorless viscous liquid.

$^1$H NMR (600 MHz, $CDCl_3$) $\delta$ 7.68–7.65 (m, 4H), 7.43–7.34 (m, 6H), 6.18 (t, *J* = 7.1 Hz, 1H), 5.34 (m, 1H), 4.16 (q, *J* = 7.1 Hz, 2H), 3.71 (dd, *J* = 5.9, 10.5 Hz, 1H), 3.61 (t, *J* = 10.1 Hz, 1H), 2.72 (m, 1H), 2.60 (m, 1H), 2.51 (m, 1H), 1.93–1.82 (m, 5H), 1.77–1.69 (m, 4H), 1.53 (m, 1H), 1.47 (m, 1H), 1.26 (t, *J* = 7.1 Hz, 3H), 1.04 (s, 9H), 0.76 (d, *J* = 6.7 Hz, 3H), 0.49 (d, *J* = 6.6 Hz, 3H).

$^{13}$C NMR (151 MHz, $CDCl_3$) $\delta$ 168.3, 144.5, 136.7, 135.6, 135.5, 134.0, 133.8, 129.6, 129.5, 127.7, 127.6, 125.9, 121.4, 63.0, 60.0, 41.5, 39.7, 36.0, 29.7, 26.9, 26.6, 24.2, 22.9, 21.0, 20.8, 19.3, 15.6, 14.3.

HRMS (ESI-TOF) *m/z*: $[M + H]^+$ Calcd for $C_{33}H_{47}O_3Si$ 519.3289; Found 519.3284.

IR (neat): v 2953, 2923, 2882, 2852, 1711, 1423, 1201, 1107, 1064 $cm^{-1}$

$[\alpha]_D^{20}$ = + 39.5 (c = 2.33) in $CHCl_3$

**Preparation of allylic alcohol 466**

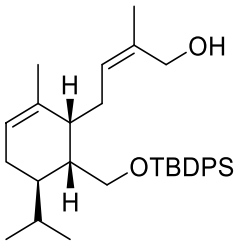


**466**

Lithium aluminum hydride (14.8 mL, 14.8 mmol, 1M solution in THF) was added to a stirred solution of ester **311** (3.8 g, 7.4 mmol) in diethyl ether (74 mL) at 0 °C and stirred for 1 h. At 0 °C, the reaction mixture was quenched with a Rochelle salt solution and was further extracted with EA. The combined organic phases were washed with brine (20 mL), dried over anhydrous $MgSO_4$, filtered, concentrated and the resulting crude product was purified by column chromatography (15% EA in hexanes) to afford allyl alcohol **466** (3.63 g, 100%) as a pale-yellow viscous liquid.

$^1$H NMR (600 MHz, $CDCl_3$) $\delta$ 7.71–7.64 (m, 4H), 7.45–7.34 (m, 6H), 5.43 (t, *J* = 7.5 Hz, 1H), 5.37 (s, 1H), 4.06 (dd, *J* = 5.8, 11.8 Hz, 1H), 3.99 (dd, *J* = 6.0, 11.8 Hz, 1H), 3.74 (dd, *J* = 6.1, 10.4 Hz, 1H), 3.57 (t, *J* = 10.0 Hz, 1H), 2.44 (m, 1H), 2.20 (m, 2H), 1.92 (m, 1H), 1.85 (m, 1H), 1.77 (s, 3H), 1.73 (m, 1H), 1.69 (s, 3H), 1.59–1.54 (m, 2H), 1.50 (m, 1H), 1.05 (s, 9H), 0.77 (d, *J* = 6.8 Hz, 3H), 0.55 (d, *J* = 6.7 Hz, 3H).

$^{13}$C NMR (151 MHz, $CDCl_3$) $\delta$ 137.5, 135.7, 135.7, 134.1, 133.9, 133.8, 129.8, 129.7, 129.0, 127.8, 127.8, 121.8, 63.3, 61.8, 41.2, 39.4, 36.1, 27.7, 27.0, 26.9, 24.3, 23.5, 21.7, 21.1, 19.4, 15.8.

HRMS (ESI-TOF) *m/z*: $[M + NH_4]^+$ Calcd for $C_{32}H_{50}NO_2Si$ 508.3605; Found 508.3607.

IR (neat): v 3342, 2963, 2926, 2889, 2852, 1430, 1114, 1067 $cm^{-1}$

$[\alpha]_D^{20}$ = + 53.9 (c = 1.93) in $CHCl_3$

**Preparation of allylic bromide 312**

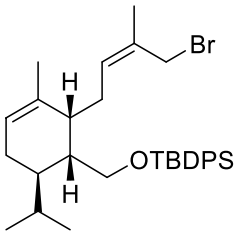


**312**

Phosphorus tribromide (103 µL, 1.02 mmol) was added to a stirred solution of allyl alcohol **466** (1.0 g, 2.04 mmol) in THF (5.1 mL) at -20 °C and stirred for 2 h. At -20 °C, the reaction mixture was quenched with iced-cold water, $NaHCO_{3(aq)}$, and was further extracted with $Et_2O$. The combined organic phases were washed with brine (20 mL), dried over anhydrous $MgSO_4$, filtered, concentrated and the resulting crude product was directly used for the next step without purification affording allyl bromide **312** (1.05 g, 92%) as a pale-yellow liquid.

$^1$H NMR (500 MHz, $CDCl_3$) $\delta$ 7.71–7.64 (m, 4H), 7.44–7.34 (m, 6H), 5.55 (t, *J* = 7.3 Hz, 1H), 5.37 (s, 1H), 3.95 (d, *J* = 9.6 Hz, 1H), 3.91 (d, *J* = 9.6 Hz, 1H), 3.75 (dd, *J* = 6.0, 10.6 Hz, 1H), 3.61 (t, *J* = 10.2 Hz, 1H), 2.51 (m, 1H), 2.22 (m, 2H), 1.91 (m, 1H), 1.84 (m, 1H) 1.79 (s, 3H), 1.76 (m, 1H), 1.70 (s, 3H), 1.60–1.46 (m, 2H), 1.06 (s, 9H), 0.76 (d, *J* = 6.8 Hz, 3H), 0.51 (d, *J* = 6.6 Hz, 3H).

$^{13}$C NMR (126 MHz, $CDCl_3$) $\delta$ 136.9, 135.8, 135.7, 134.1, 134.0, 132.5, 130.4, 129.8, 129.7, 127.8, 127.8, 121.9, 66.0, 63.4, 41.6, 39.4, 36.1, 33.1, 28.1, 27.1, 26.8, 24.4, 23.2, 22.1, 21.1, 19.4, 15.6, 15.4.

HRMS (ESI-TOF) *m/z*: $[M + H]^+$ Calcd for $C_{32}H_{46}BrOSi$ 553.2496; Found 553.2498

**Preparation of ketoester 313**

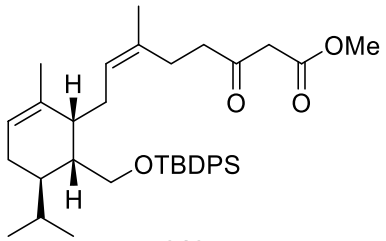


**313**

Methyl acetoacetate (29.2 µL, 0.27 mmol) was added to a stirred solution of NaH (11.6 mg, 0.29 mmol) in THF (0.8 mL) at 0 °C and stirred for 10 min. Then, *n*-butyllithium (117 µL, 0.28 mmol, 2.39M in hexanes) was added dropwise to the reaction mixture at 0 °C and left to stir for 30 min. Allyl bromide **312** (50 mg, 0.09 mmol) in THF (0.5 mL) was finally added, and the reaction was allowed to warm up to rt and stirred for 3 h. The reaction mixture was quenched with $NH_4Cl_{(aq)}$, and was further extracted with EA. The combined organic phases were washed with brine (20 mL), dried over anhydrous $MgSO_4$, filtered, concentrated and the resulting crude product was purified by column chromatography (10% EA in hexanes) to afford ketoester **313** (27 mg, 50%) as a colorless viscous liquid.

$^1$H NMR (400 MHz, $CDCl_3$) $\delta$ 11.99 (s, 0.25H), 7.70–7.64 (m, 4H), 7.44–7.34 (m, 6H), 5.35–5.30 (m, 2H), 4.96 (m, 0.25H), 3.75–3.69 (m, 4H), 3.58 (t, $J$ = 9.9 Hz, 1H), 3.4 (s, 1.5H), 2.51 (m, 1.5H), 2.41 (m, 1H), 2.28–2.18 (m, 2.5H), 2.10 (m, 1.75H), 1.97–1.81 (m, 2.25H), 1.80–1.71 (m, 1.25H), 1.68 (s, 2.75H), 1.65 (s, 0.75H), 1.63 (s, 2.5H), 1.61–1.55 (m, 0.75H), 1.53–1.46 (m, 1H), 1.04 (s, 9H), 0.78 (d, $J$ = 6.8 Hz, 3H), 0.56 (d, $J$ = 6.6 Hz, 3H).

$^{13}$C NMR (101 MHz, $CDCl_3$) $\delta$ 202.5, 178.8, 167.7, 137.5, 135.7, 135.7, 134.3, 134.1, 132.2, 129.7, 129.7, 127.8, 127.8, 127.7, 127.4, 121.4, 88.9, 66.0, 63.4, 52.4, 49.2, 41.4, 41.3, 39.4, 36.3, 28.9, 28.0, 27.0, 25.9, 24.4, 23.3, 23.3, 21.1, 19.4, 16.2, 15.4.

HRMS (ESI-TOF) *m/z*: $[M + NH_4]^+$ Calcd for $C_{37}H_{56}NO_4Si$ 606.3973; Found 606.3975.

**Preparation of ketoester 314**

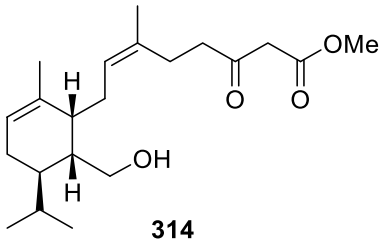


**314**

HF.pyr (4.3 mL, 159 mmol) was added to a stirred solution of **313** (938 mg, 1.59 mmol) in THF (8.6 mL) and pyridine (12.9 mL) at rt and stirred for 48 h. The reaction mixture was quenched with $NaHCO_{3(aq)}$, and was further extracted with EA. The combined organic phases were dried over anhydrous $MgSO_4$, filtered, concentrated and the resulting crude product was purified by column chromatography (20% EA in hexanes) to afford primary alcohol **314** (525 mg, 94%) as a colorless viscous liquid.

$^1$H NMR (400 MHz, $CDCl_3$) $\delta$ 12.02 (s, 0.1H), 5.37–5.28 (m, 2H), 5.01 (s, 0.1H), 3.77–3.70 (m, 4H), 3.56 (dd, $J$ = 9.3, 11.0 Hz, 1H), 3.47 (s, 1.75H), 2.62 (m, 2H), 2.36 (m, 2H), 2.22 (m, 1H), 2.12 (m, 2H), 1.97 (m, 1H), 1.84 (m, 2H), 1.76–1.64 (m, 7H), 1.57 (m, 2H), 0.89 (d, $J$ = 6.8 Hz, 3H), 0.82 (d, $J$ = 6.7 Hz, 3H).

$^{13}$C NMR (151 MHz, $CDCl_3$) $\delta$ 202.6, 167.8, 138.9, 133.8, 126.8, 121.6, 62.5, 52.8, 49.2, 41.3, 41.0, 39.7, 36.4, 27.8, 27.1, 25.9, 24.4, 23.3, 23.1, 21.2, 16.6.

HRMS (ESI-TOF) *m/z*: $[M + H]^+$ Calcd for $C_{21}H_{35}O_4$ 351.2530; Found 351.2531.

**Preparation of aldehyde 315**

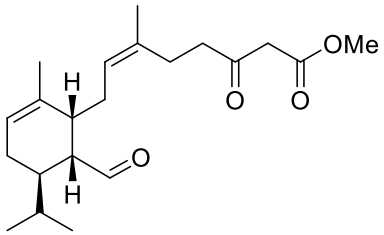


**315**

Dess-Martin Periodinane (182 mg, 428 µmol) was added to a stirred solution of alcohol **314** (125 mg, 357 µmol) and sodium bicarbonate (150 mg, 1.79 mmol) in DCM (3.6 mL) at rt and stirred for 1 h. The reaction mixture was quenched with a mixture of

$H_2O$:$NaHCO_{3(aq)}$:$Na_2S_2O_3$ (1/3:1/3:1/3) and was further extracted with DCM. The combined organic phases were washed with brine, dried over anhydrous $MgSO_4$, filtered, concentrated and the resulting crude product was purified by column chromatography (15% EA in hexanes) to afford aldehyde **315** (80 mg, 64%) as a pale-yellow viscous liquid.

$^1$H NMR (500 MHz, $CDCl_3$) $\delta$ 9.73 (d, $J$ = 4.1 Hz, 1H), 5.40 (br s, 1H), 5.10 (t, $J$ = 6.9 Hz, 1H), 3.74 (s, 3H), 3.47 (s, 2H), 2.59 (dd, $J$ = 7.5, 8.7 Hz, 2H), 2.47 (m, 1H), 2.35–2.21 (m, 5H), 2.03–1.95 (m, 2H), 1.89 (m, 1H), 1.78 (m, 1H), 1.72 (s, 3H), 1.66 (s, 3H), 0.92 (d, $J$ = 6.9 Hz, 3H), 0.79 (d, $J$ = 6.7 Hz, 3H).

$^{13}$C NMR (151 MHz, $CDCl_3$) $\delta$ 207.1, 202.4, 167.7, 135.6, 134.6, 125.5, 122.0, 52.6, 52.5, 49.2, 41.1, 40.3, 36.4, 28.4, 28.3, 25.8, 24.2, 23.3, 22.3, 20.9, 17.3.

HRMS (ESI-TOF) *m/z*: $[M + H]^+$ Calcd for $C_{21}H_{33}O_4$ 349.2373; Found 349.2373

**Preparation of macrocycle 316**

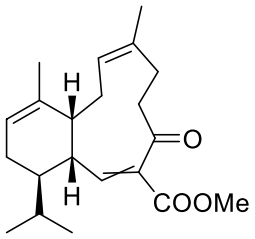


**316**

β-alanine (27.6 mg, 310 μmol) was added to a stirred solution of aldehyde **315** (25 mg, 77.5 μmol) in DMSO (1.9 mL) at rt and was stirred at 70°C for 2 days. The reaction mixture was quenched with brine and was further extracted with $Et_2O$. The combined organic phases were washed with brine, dried over anhydrous $MgSO_4$, filtered, concentrated and the resulting crude product was purified by column chromatography (6 to 15% EA in hexanes) to afford a mixture of diastereoisomers of the 10-membered ring **316** (2.5 mg, 10%) as a white solid.

$^1$H NMR (500 MHz, $CDCl_3$) $\delta$ 7.18 (d, $J$ = 12.4 Hz, 0.4H), 7.06 (d, $J$ = 12.2 Hz, 1H), 5.45 (br s, 0.4H), 5.40 (br s, 1H), 5.01 (dd, $J$ = 4.1, 11.8 Hz, 1H), 4.88 (dd, $J$ = 4.9, 10.8 Hz, 0.4H), 3.81 (s, 1.2H), 3.78 (s, 3H), 3.13–3.06 (m, 1.4H), 2.96–2.79 (m, 2.4H), 2.69–2.56 (m, 1.8H), 2.32–1.96 (m, 6.2H), 1.95–1.81 (m, 2.8H), 1.73 (s, 3H), 1.70 (s, 1.2H), 1.68

(s, 4.2H), 1.69–1.62 (m, 0.8H), 1.53–1.46 (m, 1.4H) 0.92 (d, *J* = 6.8 Hz, 1.2H), 0.91 (d, *J* = 6.8 Hz, 3H), 0.84 (d, *J* = 6.7 Hz, 4.2H).

HRMS (ESI-TOF) *m/z*: $[M + NH_4]^+$ Calcd for $C_{21}H_{34}NO_3$ 348.2533; Found 348.2536.

**Preparation of ester 323**

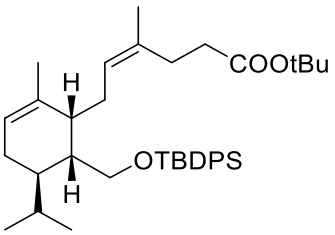


**323**

LiHMDS (6.34 mL, 6.34 mmol, 1M in hexanes) was added to a stirred solution of tert-butyl acetate (947 mg, 8.15 mmol) in THF (18 mL) at -78 °C and stirred for 30 min. Then, allyl bromide **312** (1 g, 1.81 mmol) in THF (6.2 mL) was added dropwise to the reaction mixture at -78 °C and left to stir for 2 h. The reaction mixture was quenched with $NH_4Cl_{(aq)}$, and was further extracted with EA. The combined organic phases were washed with brine, dried over anhydrous $MgSO_4$, filtered, concentrated and the resulting crude product was purified by column chromatography (4% $Et_2O$ in hexanes) to afford tert-butyl ester **323** (650 mg, 61%) as a colorless viscous liquid.

$^1$H NMR (600 MHz, $CDCl_3$) *δ* 7.70–7.62 (m, 4H), 7.45–7.35 (m, 6H), 5.34–5.29 (m, 2H), 3.71 (dd, *J* = 6.3, 10.4 Hz, 1H), 3.60 (t, *J* = 9.9 Hz, 1H), 2.42 (m, 1H), 2.24 (m, 4H), 2.13 (m, 2H), 1.92 (m, 1H), 1.79–1.72 (m, 2H), 1.69 (s, 3H), 1.65 (s, 3H), 1.59 (m, 1H), 1.51 (m, 1H), 1.44 (s, 9H), 1.05 (s, 9H), 0.78 (d, *J* = 6.8 Hz, 3H), 0.56 (d, *J* = 6.6 Hz, 3H).

$^{13}$C NMR (151 MHz, $CDCl_3$) *δ* 173.1, 137.6, 135.7, 135.7, 134.2, 134.0, 132.3, 129.7, 129.6, 127.8, 127.8, 127.7, 127.0, 121.3, 63.3, 41.3, 39.4, 36.2, 34.1, 28.2, 27.9, 27.5, 27.0, 26.9, 24.3, 23.3, 23.3, 21.1, 19.4, 16.1.

HRMS (ESI-TOF) *m/z*: $[M +]^+$ Calcd for $C_{38}H_{60}NO_3Si$ 606.4337; Found 606.4338.

IR (neat): v 2956, 2926, 2889, 2852, 1725, 1426, 1392, 1141, 1107, 1071 $cm^{-1}$

$[\alpha]_D^{20}$ = + 43.6 (c = 2.34) in $CHCl_3$

**Preparation of ketonitrile 322**

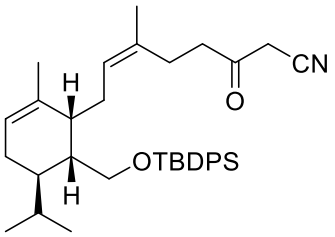


**322**

LiHMDS (2.2 mL, 2.2 mmol, 1M in hexanes) was added to a stirred solution of acetonitrile (226 mg, 287 µmol) in THF (20 mL) at -78 °C and stirred for 5 min. Then, tert-butyl ester **323** (650 mg, 1.10 mmol) in THF (5 mL) was added dropwise to the reaction mixture at -78 °C and left to stir for 3 h. After that, 5 more equivalents of acetonitrile and 2 more equivalents of LiHMDS were added and the reaction mixture was stirred for another hours. Then, the reaction mixture was quenched with $NH_4Cl_{(aq)}$, and was further extracted with EA. The combined organic phases were washed with brine, dried over anhydrous $MgSO_4$, filtered, concentrated and the resulting crude product was purified by column chromatography (4% $Et_2O$ in hexanes) to afford tert-butyl ester **322** (550 mg, 90%) as a colorless viscous liquid and 10% of remaining tarting material.

$^1$H NMR (600 MHz, $CDCl_3$) $\delta$ 7.69–7.64 (m, 4H), 7.45–7.35 (m, 6H), 5.36–5.32 (m, 2H), 3.74 (dd, *J* = 6.3, 10.4 Hz, 1H), 3.56 (t, *J* = 9.8 Hz, 1H), 3.34 (s, 2H), 2.56 (dd, *J* = 6.9, 8.8 Hz, 2H), 2.42 (m, 1H), 2.28–2.24 (m, 2H), 2.12–2.07 (m, 2H), 1.93 (m, 1H), 1.87 (m, 1H), 1.76 (m, 1H), 1.69 (s, 3H), 1.63 (s, 3H), 1.58 (m, 1H), 1.52 (m, 1H), 1.04 (s, 9H), 0.79 (d, *J* = 6.8 Hz, 3H), 0.57 (d, *J* = 6.7 Hz, 3H).

$^{13}$C NMR (151 MHz, $CDCl_3$) $\delta$ 197.3, 137.3, 135.7, 135.7, 134.2, 134.0, 131.4, 129.8, 129.7, 128.0, 127.8, 121.6, 113.8, 63.4, 41.1, 39.3, 36.2, 32.1, 28.0, 27.0, 26.9, 25.7, 24.3, 23.4, 23.3, 21.1, 19.4, 16.1.

HRMS (ESI-TOF) *m/z*: $[M + NH_4]^+$ Calcd for $C_{38}H_{49}NO_2Si$ 573.3871; Found 573.3870.

IR (neat): v 2956, 2926, 2889, 2849, 2255, 1735, 1430, 1107, 1067 $cm^{-1}$

$[\alpha]_D^{20}$ = + 53.3 (c = 2.23) in $CHCl_3$

**Preparation of alcohol 467**

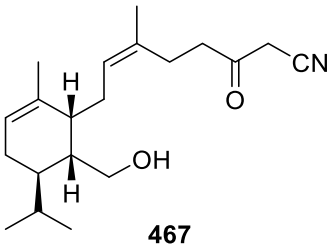


**467**

HF.pyr (5.1 mL, 194.2 mmol) was added to a stirred solution of **322** (540 mg, 0.971 mmol) in THF (2.2 mL) and pyridine (5.1 mL) at rt and stirred for 2 h. The reaction mixture was quenched with $NaHCO_{3(aq)}$, and was further extracted with EA. The combined organic phases were dried over anhydrous $MgSO_4$, filtered, concentrated and the resulting crude product was purified by column chromatography (20% EA in hexanes) to afford primary alcohol **467** (250 mg, 81%) as a colorless viscous liquid.

$^1$H NMR (600 MHz, $CDCl_3$) $\delta$ 5.37–5.33 (m, 2H), 3.75 (dd, *J* = 5.8, 11.0 Hz, 1H), 3.54 (dd, *J* = 9.1, 11.0 Hz, 1H), 3.47 (s, 2H), 2.69 (dt, *J* = 1.7, 7.5 Hz, 2H), 2.40–2.36 (m, 2H), 2.23 (m, 1H), 2.16 (m, 1H), 2.08 (m, 1H), 1.96 (m, 1H), 1.87–1.78 (m, 2H), 1.73–1.69 (m, 1H), 1.69 (s, 3H), 1.68 (s, 3H), 1.58–1.53 (m, 1H), 0.89 (d, *J* = 6.9 Hz, 3H), 0.81 (d, *J* = 6.7 Hz, 3H).

$^{13}$C NMR (151 MHz, $CDCl_3$) $\delta$ 197.5, 136.8, 132.8, 127.5, 121.7, 113.9, 62.6, 41.0, 40.5, 39.6, 36.4, 32.2, 27.8, 27.1, 25.8, 24.4, 23.3, 23.2, 21.2, 16.5.

HRMS (ESI-TOF) *m/z*: $[M + NH_4]^+$ Calcd for $C_{20}H_{35}N_2O_2$ 335.2693; Found 335.2695.

IR (neat): v 3379, 2956, 2889, 2265, 2198, 1725, 1430, 1390, 1040 $cm^{-1}$

$[\alpha]_D^{20}$ = + 100.4 (c = 1.88) in $CHCl_3$

**Preparation of aldehyde 321**

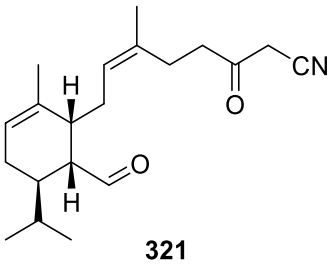


**321**

PCC (2.05 g, 9.50 mmol) was added to a stirred solution of alcohol **467** (2.50 g, 7.90 mmol) and 4Å MS (3.80 g) in DCM (79 mL) and stirred for 1 h. Diethyl ether was added, and the resulting mixture filtered through a pad of silica gel and further flushed with $Et_2O$. The resulting crude product was purified by column chromatography (15% EA in hexanes) to afford aldehyde **321** (1.24 g, 50%) as a light-yellow viscous liquid.

$^1$H NMR (600 MHz, $CDCl_3$) $\delta$ 9.72 (d, $J$ = 3.9 Hz, 1H), 5.41 (br s, 1H), 5.12 (t, $J$ = 7.1 Hz, 1H), 3.49 (s, 2H), 2.66 (m, 2H), 2.49 (m, 1H), 2.36–2.21 (m, 5H), 2.03 (m, 1H), 1.97–1.88 (m, 2H), 1.79 (m, 1H), 1.72 (s, 3H), 1.67 (s, 3H), 0.92 (d, $J$ = 6.9 Hz, 3H), 0.80 (d, $J$ = 6.7 Hz, 3H).

$^{13}$C NMR (151 MHz, $CDCl_3$) $\delta$ 207.0, 197.3, 135.4, 133.9, 125.9, 122.1, 113.9, 52.4, 40.2, 39.7, 36.7, 32.2, 28.5, 28.2, 25.7, 24.3, 23.2, 22.3, 20.8, 17.5.

HRMS (ESI-TOF) *m/z*: $[M + NH_4]^+$ Calcd for $C_{20}H_{33}N_2O_2$ 333.2537; Found 333.2539.

**Preparation of macrocycle 324**

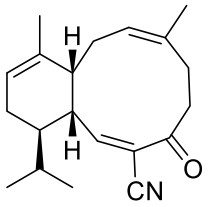


**324**

β-alanine (28.3 mg, 317 μmol) was added to a stirred solution of aldehyde **321** (25 mg, 79.2 μmol) in DMSO (30 mL) at rt and was stirred at rt for 30 h. The reaction mixture was quenched with brine and was further extracted with DCM. The combined organic phases were washed with brine, $LiCl_{(aq)}$, dried over anhydrous $MgSO_4$, filtered, concentrated and the resulting crude product was purified by column chromatography

(6 to 12% EA in hexanes) to afford a mixture of diastereoisomers of the 10-membered ring **324** (4 mg, 15%) as a white solid. Due to rotamers, $^{13}C$ NMR spectroscopy was not acquired.

$^{1}H$ NMR (400 MHz, 60°C, $CDCl_3$) $\delta$ 6.82 (d, $J$ = 11.0 Hz, 1H), 5.24 (s, 1H), 5.05 (t, $J$ = 8.1 Hz, 1H), 3.11 (m, 1H), 2.57 (m, 1H), 2.33–2.14 (m, 2H), 2.14–1.98 (m, 1H), 1.90 (m, 2H), 1.80–1.69 (m, 1H), 1.69–1.58 (m, 1H), 1.50 (s, 3H), 1.46 (s, 3H), 1.41–1.16 (m, 3H), 0.85 (d, $J$ = 6.8 Hz, 3H), 0.65 (d, $J$ = 6.7 Hz, 3H).

HRMS (ESI-TOF) *m/z*: $[M + NH_4]^+$ Calcd for $C_{20}H_{31}N_2O$ 315.2431; Found 315.2427.

$[\alpha]_D^{20}$ = + 83.0 (c = 0.57) in $C_6D_6$

IR (neat): v 2956, 2926, 2865, 2228, 2194, 1674, 1460, 1242, 729 $cm^{-1}$

**Preparation of dimer 325**

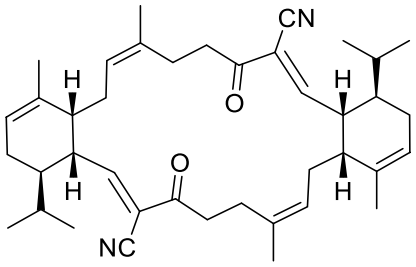


**325**

$^{1}H$ NMR (600 MHz, $CDCl_3$) $\delta$ 6.84 (d, $J$ = 12.1 Hz, 2H), 5.42 (s, 2H), 5.04 (m, 2H), 3.13 (ddd, $J$ = 3.1, 4.1, 12.1 Hz, 2H), 3.09 (dt, $J$ = 4.2, 12.9 Hz, 2H), 2.94 (dt, $J$ = 3.8, 13.8 Hz, 2H), 2.60 (dt, $J$ = 4.1, 13.2 Hz, 2H), 2.27 (m, 4H), 2.15 (m, 4H), 2.06 (m, 2H), 1.86 (q, $J$ = 12.8 Hz, 2H), 1.74 (s, 6H), 1.69 (s, 6H), 1.53 (m, 2H), 1.32 (m, 2H), 0.95 (d, $J$ = 6.5 Hz, 6H), 0.88 (d, $J$ = 6.6 Hz, 6H).

$^{13}C$ NMR (151 MHz, $CDCl_3$) $\delta$ 198.0, 160.9, 134.0, 132.8, 126.0, 121.6, 117.1, 116.7, 42.0, 39.2, 38.3, 37.1, 29.0, 28.7, 28.1, 25.2, 22.6, 21.8, 21.7, 20.1.

HRMS (ESI-TOF) *m/z*: $[M + NH_4]^+$ Calcd for $C_{40}H_{58}N_3O_2$ 612.4524; Found 612.4526.

**Preparation of diol 327**

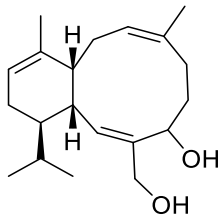


**327**

DiBALH (2.66 mL, 2.66 mmol, 1M in hexanes) was added to a stirred solution of ketonitrile **324** (360 mg, 1.21 mmol) in toluene (12.1 mL) at -78 °C and the reaction mixture was stirred for 5 h. The reaction mixture was quenched with $H_2O$ and was further extracted with EA. The combined organic phases were washed with brine, dried over anhydrous $MgSO_4$, filtered, concentrated and the resulting crude product was directly used into the next step.

$NaBH_4$ (48 mg, 1.03 mmol) was added to a stirred solution of aldehyde (155 mg, 0.51 mmol) and $CeCl_3.7H_2O$ (287 mg, 0.77 mmol) in MeOH (10.2 mL) at 0 °C and stirred for 15 min. The reaction mixture was quenched with $H_2O$, and further extracted with EA. The combined organic phases were washed with brine, dried over anhydrous $MgSO_4$, filtered, concentrated and the resulting crude product was purified by column chromatography (25% EA in hexanes) to afford primary alcohol **327** (84 mg, 23% over 2 steps) as a white solid.

$^1$H NMR (600 MHz, $CDCl_3$) $\delta$ 5.85 (d, $J$ = 9.4 Hz, 1H), 5.38 (br s, 1H), 5.12 (dd, $J$ = 4.8, 11.8 Hz, 1H), 4.63 (br s, 1H), 4.15 (d, $J$ = 12.0 Hz, 1H), 3.90 (d, $J$ = 12.0 Hz, 1H), 2.70–2.63 (m, 2H), 2.30 (ddd, $J$ = 8.2, 12.0, 14.1 Hz, 1H), 2.02 (m, 1H), 1.97 (m, 1H), 1.91–1.78 (5H), 1.67 (s, 3H), 1.65 (s, 3H), 1.55 (m, 1H), 1.34 (m, 1H), 0.96 (d, $J$ = 6.8 Hz, 3H), 0.77 (d, $J$ = 6.7 Hz, 3H).

$^{13}$C NMR (151 MHz, $CDCl_3$) $\delta$ 138.5, 135.9, 135.3, 128.2, 126.4, 121.0, 71.4, 60.6, 42.2, 39.7, 36.6, 30.0, 29.2, 27.4, 24.1, 23.5, 23.4, 21.8. 21.3, 18.6.

HRMS (ESI-TOF) *m/z*: $[M + NH_4]^+$ Calcd for $C_{20}H_{36}NO_2$ 322.2741; Found 322.2738.

**Preparation of ketone 329**

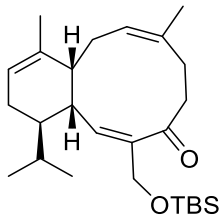


**329**

Imidazole (30 mg, 0.44 mmol) and TBSCl (48 mg, 0.32 mmol) were added to a stirred solution of diol **327** (74 mg, 0.24 mmol) in DMF (1.5 mL) at 0 °C and stirred for 30 min. The reaction mixture was quenched with a solution of $NaHCO_3$ and further extracted with $Et_2O$. The combined organic phases were washed with brine, dried over anhydrous $MgSO_4$, filtered, concentrated and the resulting crude product was directly used into the next step.

Dess-Martin Periodinane (140 mg, 331 µmol) was added to a stirred solution previous crude of allylic alcohol **328** and $NaHCO_3$ (116 mg, 1.38 mmol) in DCM (2.8 mL) at 0 °C and stirred for 1 hour. The reaction mixture was quenched with a mixture of $H_2O$:$NaHCO_{3(aq)}$:$Na_2S_2O_3$ (1:1:1) and was further extracted with DCM. The combined organic phases were washed with brine, dried over anhydrous $MgSO_4$, filtered, concentrated and the resulting crude product was purified by column chromatography (4% $Et_2O$ in hexanes) to afford enone **329** (98 mg, 85% over 2 steps) as a white solid.

$^1$H NMR (600 MHz, $CDCl_3$) $\delta$ 6.65 (d, $J$ = 10.2 Hz, 1H), 5.44 (br s, 1H), 5.23 (dd, $J$ = 6.9, 9.5 Hz, 1H), 4.37 (d, $J$ = 11.5 Hz, 1H), 4.21 (d, $J$ = 11.5 Hz, 1H), 3.02–2.92 (m, 2H), 2.77 (m, 1H), 2.27–2.09 (m, 3H), 1.95 (m, 1H), 1.88–1.73 (m, 3H), 1.70 (s, 3H), 1.65–1.58 (m, 2H), 1.57 (s, 3H), 0.95 (d, $J$ = 6.9 Hz, 3H), 0.87 (s, 9H), 0.71 (d, $J$ = 6.8 Hz, 3H), 0.06 (s, 3H), 0.05 (s, 3H).

$^{13}$C NMR (151 MHz, $CDCl_3$) $\delta$ 202.2, 150.1, 138.4, 135.8, 131.4, 129.2, 121.6, 57.3, 44.3, 39.7, 38.6, 38.6, 28.9, 28.8, 28.6, 26.1, 23.5, 23.3, 21.8, 21.4, 18.4, 15.9, -5.3, -5.5.

HRMS (ESI-TOF) *m/z*: $[M + H]^+$ Calcd for $C_{26}H_{45}O_2Si$ 417.3183; Found 417.3181.

$[\alpha]_D^{20}$ = - 10.6 (c = 0.52) in $CHCl_3$

IR (neat): v 2960, 2920, 2856, 2352, 1651, 1470, 1248, 1078, 829 $cm^{-1}$

**Preparation of diol 333**

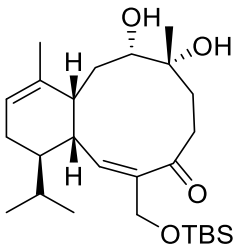


**333**

$RuCl_3.xH_2O$ (0.26 mg, 1.0 μmol) and $NaIO_4$ (3.1 mg, 14.7 μmol) were added to a stirred solution of enone **329** (5.6 mg, 13.4 μmol) in a 1:1:1 mixture of EA:MeCN:$H_2O$ (1.5 mL) at 0 °C and stirred for 30 min. The reaction mixture was quenched with $H_2O$, and further extracted with EA. The combined organic phases were washed with brine, dried over anhydrous $MgSO_4$, filtered, concentrated and the resulting crude product was purified by column chromatography (15% EA in hexanes) to afford diol **333** (3.1 mg, 52%) as a white solid.

$^1$H NMR (600 MHz, $CDCl_3$) *δ* 6.74 (d, *J* = 10.0 Hz, 1H), 5.46 (br s, 1H), 4.49 (d, *J* = 10.8 Hz, 1H), 4.20 (d, *J* = 10.8 Hz, 1H), 3.82 (t, *J* = 5.5 Hz, 1H), 3.00–2.93 (m, 2H), 2.70 (ddd, *J* = 6.7, 12.4, 16.8 Hz, 1H), 2.55 (ddd, *J* = 6.3, 12.4, 15.4 Hz, 1H), 2.41 (t, *J* = 7.3 Hz, 1H), 2.05 (m, 2H), 1.95 (dt, *J* = 4.5, 17.2 Hz, 1H), 1.89 (ddd, *J* = 3.1, 6.6, 15.3 Hz, 1H), 1.86–1.80 (m, 1H), 1.80–1.74 (m, 1H), 1.71 (s, 3H), 1.65 (m, 1H), 1.55 (s, 1H), 1.26 (m, 1H), 1.19 (s, 3H), 0.96 (d, *J* = 6.9 Hz, 3H), 0.89 (s, 9H), 0.70 (d, *J* = 6.9 Hz, 3H), 0.10 (s, 3H), 0.08 (s, 3H).

$^{13}$C NMR (151 MHz, $CDCl_3$) *δ* 200.7, 152.5, 138.5, 135.6, 121.6, 79.4, 75.8, 57.4, 45.0, 40.6, 39.7, 38.2, 38.0, 33.2, 29.0, 25.9, 24.3, 23.6, 21.4, 21.4, 18.3, 15.4, -5.3, -5.5.

HRMS (ESI-TOF) *m/z*: $[M + H]^+$ Calcd for $C_{26}H_{47}O_4Si$ 451.3238; Found 451.3239.

**Preparation of epoxide 334**

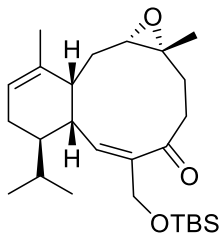


**334**

*M*-CPBA (39 mg, 0.17 mmol) was added to a stirred solution of enone **329** (60 mg, 0.14 mmol) in DCM (2.9 mL) at -20 °C and stirred for 30 min. The reaction mixture was quenched with a solution of $Na_2S_2O_{3(aq)}$ and was further extracted with DCM. The combined organic phases were washed with brine, dried over anhydrous $MgSO_4$, filtered, concentrated and the resulting crude product was purified by column chromatography (10% $Et_2O$ in hexanes) to afford epoxide **334** (31.7 mg, 85%) as a white solid.

$^1$H NMR (600 MHz, $CDCl_3$) *δ* 6.70 (d, *J* = 10.1 Hz, 1H), 5.45 (br s, 1H), 4.57 (d, *J* = 10.6 Hz, 1H), 4.13 (d, *J* = 10.6 Hz, 1H), 3.05 (dd, *J* = 8.6, 17.3 Hz, 1H), 2.85 (dt, *J* = 6.0, 11.0 Hz, 1H), 2.77–2.70 (m, 2H), 2.38 (t, *J* = 6.6 Hz, 1H), 2.10 (dd, *J* = 8.8, 15.1 Hz, 1H), 2.00–1.89 (m, 3H), 1.85–1.78 (m, 1H), 1.74 (m, 1H), 1.72 (s, 3H), 1.63 (m, 1H), 1.40 (ddd, *J* = 7.6, 10.9, 15.6, 1H), 1.16 (s, 3H), 0.94 (d, *J* = 7.0 Hz, 3H), 0.88 (s, 9H), 0.67 (d, *J* = 6.9 Hz, 3H), 0.09 (s, 3H), 0.06 (s, 3H).

$^{13}$C NMR (151 MHz, $CDCl_3$) *δ* 201.9, 151.8, 138.3, 135.6, 121.8, 68.7, 61.9, 56.6, 43.3, 40.0, 38.1, 37.6, 29.4, 29.1, 29.1, 26.1, 23.6, 22.4, 21.6, 21.3, 18.5, 15.2, -5.2, -5.5.

HRMS (ESI-TOF) *m/z*: $[M + H]^+$ Calcd for $C_{26}H_{45}O_3Si$ 433.3132; Found 433.3131.

$[\alpha]_D^{20}$ = - 8.8 (c = 1.0) in $CH_2Cl_2$

IR (neat): v 2949, 2919, 2849, 1664, 1426, 1101, 701 $cm^{-1}$

**Preparation of phenylseleno ketone 340**

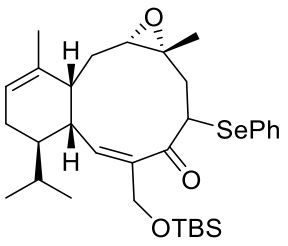


**340**

LiHMDS (46 µL, 46 µmol, 1M in hexanes) was added to a stirred solution of enone **334** (10 mg, 23 µmol) in THF (2.5 mL) at -78 °C and stirred for 1 h. After that, phenylselenyl chloride (8.8 mg, 46 µmol) was added in the minimum of THF and the reaction was stirred for 30 min more at the same temperature. The reaction mixture was quenched with a solution of $Na_2S_2O_{3(aq)}$ and was further extracted with EA. The combined organic phases were washed with brine, dried over anhydrous $MgSO_4$, filtered, concentrated and the resulting crude product was purified by column chromatography ( EA in hexanes) to afford phenylseleno ketone **340** (12.4 mg, 92%) as a white solid.

$^1$H NMR (500 MHz, $CDCl_3$) $\delta$ 7.63–7.59 (m, 3H), 7.33–7.30 (m, 2H), 7.00 (d, $J$ = 10.1 Hz, 1H), 5.45 (br s, 1H), 4.55 (d, $J$ = 10.6 Hz, 1H), 4.12 (d, $J$ = 10.6 Hz, 1H), 4.04 (dd, $J$ = 8.3, 11.6 Hz, 1H), 2.82 (ddd, $J$ = 6.0, 10.7, 11.5, 1H), 2.72 (dd, $J$ = 2.3, 11.0 Hz, 1H), 2.57 (dd, $J$ = 8.4, 15.0 Hz, 1H), 2.38 (m, 1H), 1.97 (m, 1H), 1.92 (m, 1H), 1.87–1.78 (m, 3H), 1.71 (s, 3H), 1.67 (m, 1H), 1.37 (ddd, $J$ = 7.7, 11.1, 15.6 Hz, 1H), 1.15 (s, 3H), 0.99 (d, $J$ = 6.9 Hz, 3H), 0.87 (s, 9H), 0.73 (d, $J$ = 6.9 Hz, 3H), 0.07 (s, 3H), 0.03 (s, 3H).

HRMS (ESI-TOF) *m/z*: $[M + H]^+$ Calcd for $C_{32}H_{49}O_3SeSi$ 589.2611; Found 589.2608.

**Preparation of triene 341**

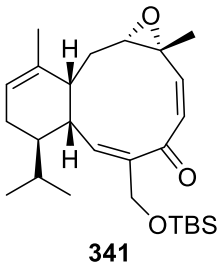


**341**

*M*CPBA (39 mg, 0.17 mmol) was added to a stirred solution of phenylseleno ketone **340** (60 mg, 0.14 mmol) in DCM (2.9 mL) at -20 °C and stirred for 30 min. The reaction

mixture was quenched with a solution of $Na_2S_2O_{3(aq)}$ and was further extracted with DCM. The combined organic phases were washed with brine, dried over anhydrous $MgSO_4$, filtered, concentrated and the resulting crude product was purified by column chromatography (10% $Et_2O$ in hexanes) to afford epoxide **341** (31.7 mg, 85%) as a white solid.

$^1$H NMR (600 MHz, $CDCl_3$) $\delta$ 7.00 (d, $J$ = 10.9 Hz, 1H), 6.37 (d, $J$ = 12.6 Hz, 1H), 6.22 (d, $J$ = 12.6 Hz, 1H), 5.48 (br s, 1H), 4.60 (d, $J$ = 11.0 Hz, 1H), 4.22 (d, $J$ = 11.0 Hz, 1H), 2.86 (dt, $J$ = 6.2, 11.1 Hz, 1H), 2.81 (dd, $J$ = 2.1, 11.1, 1H), 2.29 (m, 1H), 2.04 (d, $J$ = 15.2 Hz, 1H), 1.93 (m, 1H), 1.80 (m, 1H), 1.72 (s, 3H), 1.62 (m, 1H), 1.52 (m, 1H), 1.32 (ddd, $J$ = 7.1, 11.0, 15.1 Hz, 1H), 1.28 (s, 3H), 0.90 (d, $J$ = 6.9 Hz, 3H), 0.89 (s, 9H), 0.66 (d, $J$ = 6.8 Hz, 3H), 0.10 (s, 3H), 0.08 (s, 3H).

$^{13}$C NMR (151 MHz, $CDCl_3$) $\delta$ 198.2, 158.3, 139.3, 138.7, 135.0, 132.9, 122.2, 70.1, 62.8, 56.0, 43.2, 39.7, 38.4, 30.1, 29.1, 26.1, 23.4, 21.6, 21.3, 18.5, 15.4, -5.3, -5.5.

HRMS (ESI-TOF) *m/z*: $[M + H]^+$ Calcd for $C_{26}H_{43}O_3Si$ 431.2976; Found 431.2978.

$[\alpha]_D^{20}$ = - 5.5 (c = 0.1) in $CHCl_3$

IR (neat): v 2959, 2926, 2855, 1658, 1453, 1248, 1057, 826 $cm^{-1}$

# Chapter 3.

# Carbafucose Project

## 3.1. Introduction

Antibody-dependent cell-mediated cytotoxicity (ADCC) is an essential cell-mediated immune defense mechanism in which an effector cell is recruited to eradicate a target through the formation of an antibody-antigen complex. ADCC's activation usually involves immunoglobulin G, although immunoglobulin E can be observed on specific pathogen surfaces (e.g., parasites).[141] This process is part of the humoral immune response where antibodies have the main objective of containing infections. First and foremost, white blood cells (e.g., B-cells) produce antibodies directed towards a specific antigen present on the cell membranes of an invader (e.g., cancer, bacteria, virus, parasite). Once these antibodies encounter their target, they form an antigen/antibody complex. From there, the constant region of the antibody (i.e., Fc region) is recognized by specific effector cells (e.g., natural killers (NK), macrophages, neutrophils and eosinophils) via the Fc receptors on their surface. Finally, effector cells release various chemicals that lyse and ultimately kill the cell bound to the antibody. One of the most common mechanisms operates through a calcium-dependent process, that once activated, triggers an exocytic cascade that ultimately releases several chemicals. For instance, the release of perforin creates a pore in the cell membrane to allow for the subsequent leakage of granzymes, a family of pro-apoptotic proteases that actively destroy the target through DNA fragmentation thus leading to lysis.[142] Other mechanisms of destruction exploit reactive oxygen species or Fas ligands which similarly lead to cell death.

### 3.1.1. Afucosylated Monoclonal Antibodies

After transcription, gene expression takes place in the cytoplasm. Specifically, the role of ribosomes is to decode and translate the messenger ribonucleic acid (mRNA) into corresponding proteins. The latter subsequently undergo several post-translational modifications (PTMs) that increase the proteome's functional diversity.

This process is performed through numerous chemical modifications (e.g., covalent additions, cleavage, or degradation). An important class of PTMs involves glycosylation of eukaryotic proteins which are known to play essential roles in a wide range of biological processes (e.g., stability, activity, protein folding). Specifically, glycosylation of antibodies has a dramatic impact on their potency, biodistribution, and recycling.[143] In 2002, the Shields research group made a discovery that revolutionized the research around antibodies for cancer therapy. Indeed, researchers have reported that *N*-glycosylation at Asn297 in the $CH_2$ domain of $IgG_1$ had a significant effect on the interaction between the antibody Fc region and the Fcy receptor (Fcy RIIIa) expressed on natural killer (NK) cells.[144] More precisely, fucosylation of this glycan had a deleterious impact on Fc receptor binding due to a steric barrier that prevents the alignment with the $IgG_1$ binding site. Moreover, their research showed that the loss of fucose in the glycan led to a ~50-fold increase in ADCC. Following this discovery, a rise in interest in the development of fucose-deficient (FD)-antibodies was immediately noticed.

### 3.1.2. How to Produce Afucosylated Antibodies

Currently, there are five different approaches to make afucosylated antibodies. Manipulating cell-growth conditions to decrease core fucosylation is one way to reach this objective. Indeed, several parameters such as $CO_2$ partial pressure, media hold duration (37 °C) and the presence of manganese have shown an influence on the formation of afucosylated antibodies.[145] Genetically engineered cell lines to impair fucose utilization represent another method to decrease the fucosylation of antibodies. For example, disruption of both FUT8 alleles in Chinese hamster ovary (CHO) cell lines allowed for the production of completely afucosylated recombinant antibodies.[146] Editing glycosylation after antibody purification illustrates a different perspective in the generation of afucosylated antibodies using chemoenzymatic glycoengineering.[147] Another approach uses the transgenic heterologous expression of bacterial enzymes that consume the building blocks required for the *de novo* synthesis of fucose leading to the incapacity of producing fucosylated antibodies.[148] Finally, the synthesis of small molecules that inhibit antibody fucosylation (i.e., via enzyme inhibition) has become popular in the scientific community as depicted with deoxymannojirimycin discovery, a known inhibitor of mannosidase.[149] Currently, 30 FD-antibodies are being investigated

in clinical trials while 3 afucosylated antibodies were approved by the FDA. These ongoing investigations further emphasize the general interest in producing antibodies that are capable of improving ADCC.

### 3.1.3. Background of Small Molecule Inhibitors

Small molecule inhibitors are particularly attractive given that they represent a significantly cheaper alternative for the production of FD-antibodies. Indeed, this method of production does not require the development of specific cell lines or expensive purification processes.[150,151] In 2008, Zhou's group showed that the natural product known as kifunensine was modulating the glycosylation of human monoclonal antibodies. More specifically, inhibition of mannosidase I led to the formation of oligomannose-type *N*-glycans.[152] Although these efforts resulted in the formation of FD-antibodies that showed an improved ADCC (~ 8-fold), the oligomannose structure was rapidly cleared from the body thus preventing its use as an immunotherapeutic.[153]

More recently, several additional inhibitors of antibody fucosylation have been reported.[151] These carbohydrate analogs are metabolized into their GDP-derivatives and act by inhibiting GDP-mannose-4,6-dehydratase (GMD) and/or α-1,6-fucosyltransferase (FUT8). Amongst these recent advances, Seattle Genetics discovered that 2-fluorofucose **358** and 5-alkynylfucose **359** partly blocked antibody fucosylation in the Chinese hamster ovary (CHO). Unfortunately, incorporation of these synthetic compounds into glycoproteins (i.e., between 0.5 to 3%) raised important health concerns as it could trigger an unwanted immune response.[151,154,155] Similarly, ethynyl **360**, nitrile **361**, ester **362**, alkyl bromide **363**, and difluoromethane **364** fucose analogues all inhibited antibody fucosylation while also presenting a high rate of *N*-glycan incorporation (i.e., >50%) (Figure 3.1a).[151,154,155] Three years later, Amgen reported a series of additional promising compounds. Indeed, they disclosed that 6,6,6-trifluoromethylfucose **365** efficiently blocked IgG1 mAbs fucosylation expressed in CHO cells but again was similarly incorporated at a level of 0.5% in the antibody glycan. Interestingly, it was found that fucophosphonate **366** not only blocked the fucosylation but also did not transfer onto the *N*-glycan. Unfortunately, stability problems combined with high cellular toxicity and decreased potency (~10-fold less potent) forced Amgen to halt further use of this compound (Figure 3.1b).[150] Interestingly, Toyokuni showed that GDP-carbafucose **367** inhibited antibody fucosylation *in vitro* demonstrating that the

endocyclic oxygen was not mandatory to display activity (Figure 3.1c).[156] This discovery was further confirmed when the synthesis of 5-thiofucose **368** was performed and the subsequent metabolization of **368** into its GDP analog **369** led to fucosyltransferase inhibition (Figure 3.1d).[157]

**a) Seattle Genetics inhibitors**[151,154,155]

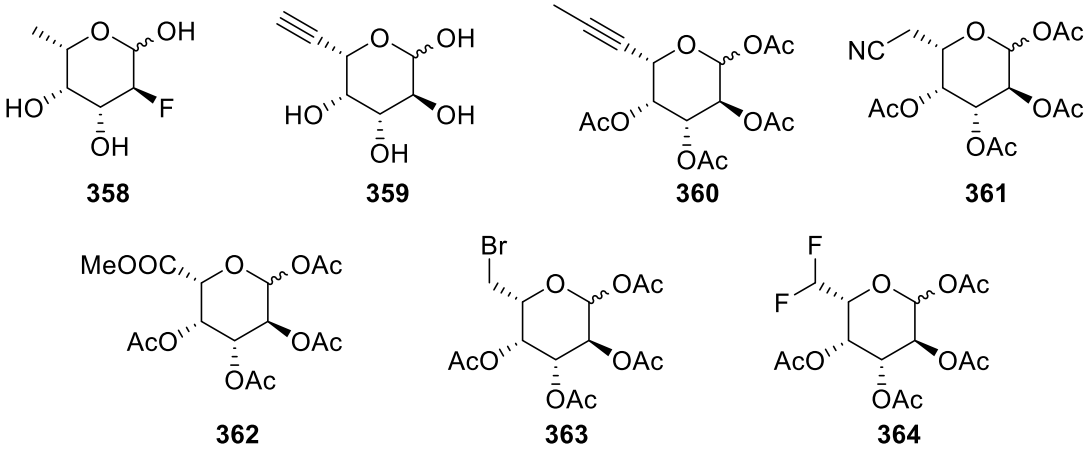


**b) Amgen inhibitors**[150]

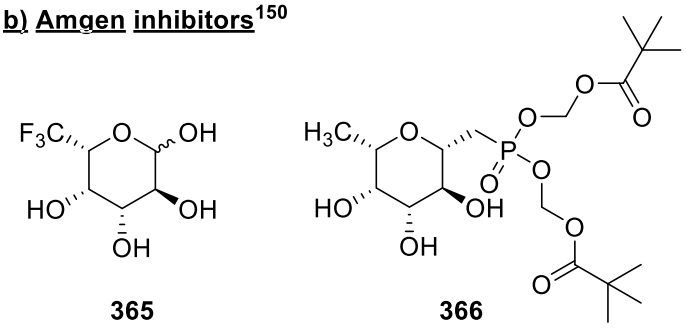


**c) Toyokuni's inhibitor**[156]

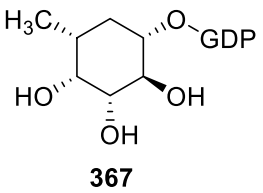


**d) Intracyclic sulfur analogue**[157]

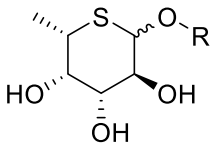

**368** : X = H
**369** : X = GDP

**Figure 3.1. Seattle Genetics', Amgen's and Toyokuni's inhibitors**

## 3.1.4. Objectives

Unfortunately, apart from fucophosphonate **366** (highly toxic), all tested compounds in the production of FD-antibodies displayed significant incorporation in the

antibody *N*-glycan. To cope with this problem, we aimed to develop new potent inhibitors of fucosyltransferase that cannot be incorporated into the *N*-glycan. Replacement of the endocyclic oxygen with a methylene unit was anticipated to prevent the incorporation of the inhibitors since the oxocarbenium ion intermediate involved in enzymatic glycosylation processes would be avoided.[158,159] Combining the knowledge acquired from Amgen's, Seattle Genetics' and Toyokuni's investigations, we aimed to synthesize a series of carbafucose derivatives that will be evaluated *in vitro*.

## 3.2. Britton's and Vocadlo's Investigations

### 3.2.1. Preliminary Work

#### *Synthesis of Carbafucose Analogs*

To support the testing of carbafucose **377** and 2-fluorocarbafucose **384**, a concise, efficient and scalable synthesis was required. Using Britton's methodology involving the organocatalytic α-chlorination/aldol and α-fluorination/aldol reactions, chlorohydrin **371** and fluorohydrin **380** were synthesized in decent yields displaying impressive diastereoselectivity.[160,161] To ultimately generate carbafucose **377**, Julia olefination was performed on **371** and delivered diene **373**. Subsequent deprotection of **373** followed by ring-closing metathesis (RCM) yielded carbacyclic cyclohexene **374** in modest yield. Treatment with a NaOH aqueous solution at reflux delivered unsaturated carbafucose **376** which was finally submitted to hydrogenation conditions to generate a mixture of carbafucose **377** and **378** (Scheme 3.1a). In a similar fashion, 2-deoxy-2-fluorocarbofucose **383** and **384** were prepared (Scheme 3.1b). To further increase cell-permeability, the per-acetylated counterparts **385** and **386** were also prepared (Scheme 3.1c).

**a) α-chlorination/aldol synthetic route to carbafucose 377**

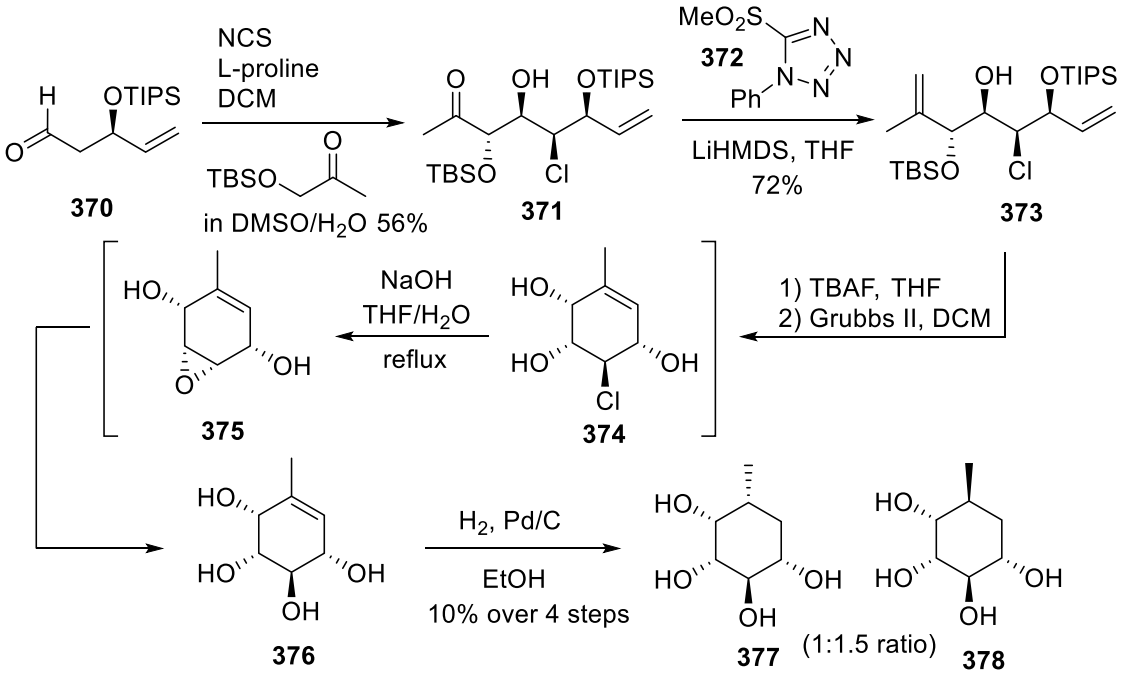


**b) α-fluorination/aldol synthetic route to 2-fluorocarbafucose 384**

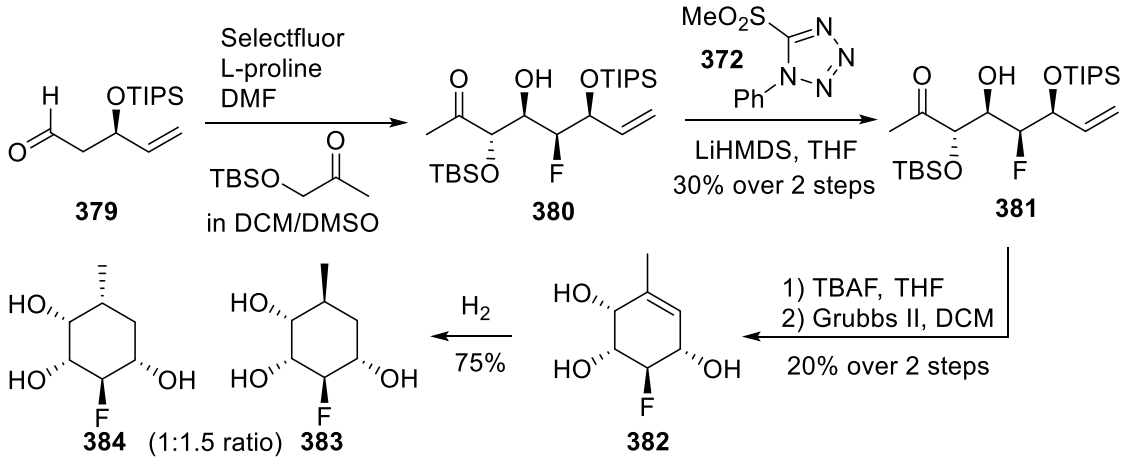


**c) peracetylation of carbafucose 377 and 2-fluorocarbafucose 384**

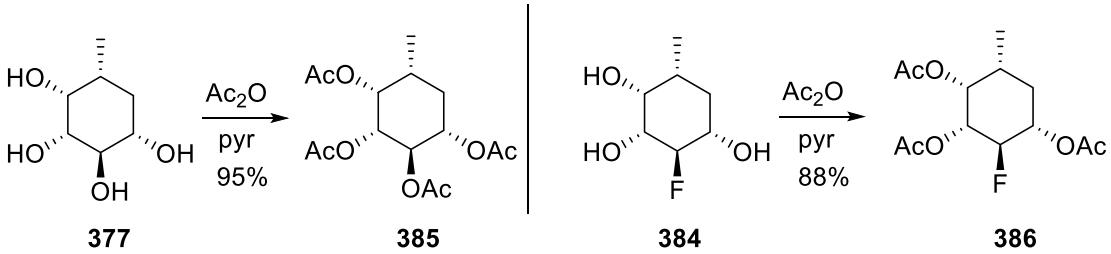


**Scheme 3.1. α-chlorination/aldol and α-fluorination/aldol strategies**

### *Bioactivity and Mechanism of Action of Carbafucose Analogs*

In our initial experiments, 8 compounds (4 fucose analogs and their 4 peracetates) were tested to assess their efficiency in inhibiting antibody fucosylation (Table 3.1). Cultures of ExpiCHO cells were incubated with each compound at a concentration of 0.1 mM. After 8 days, the cells were collected, and the antibodies were purified and deglycosylated. Subsequently, the glycans were purified and analyzed by capillary electrophoresis-laser-induced fluorescence (E-LIF). In the control experiment, two structures of glycans were mainly found on therapeutic Her2 antibody: FA2G2S1 (16.8%) and FA2 (78.7%), both possessing a fucose unit. The A2 structure represents a glycan without any fucose unit. Only carbafucose and its peracetylated counterpart showed a significant increase in fucose deficient antibodies. Indeed, antibodies expressed in the presence of carbafucose **377** showed a >70% increase in FD-antibodies.

**Table 3.1.** **Structure of glycans commonly found on therapeutic Her2 antibody expressed at a contract research organization (CRO, Catalent) and the fraction of each found when using our first set of candidate carbafucose analogues**

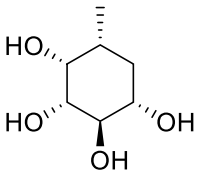


**377**

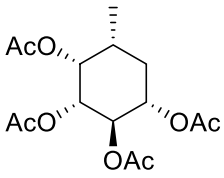


**385**

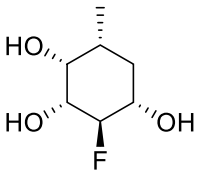


**384**

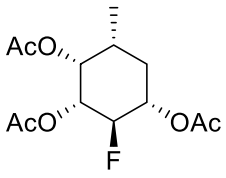


**386**

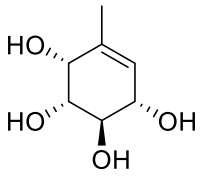


**376**

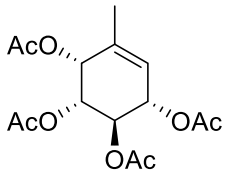


**387**

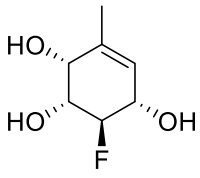


**382**

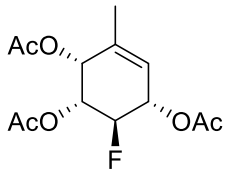


**388**

| glycan | ctrl(%) | 376(%) | 387(%) | 382(%) | 388(%) | 377(%) | 385(%) | 384(%) | 386(%) |
|---|---|---|---|---|---|---|---|---|---|
| **FA2G2S2** | 0.0 | 0.0 | 0.0 | 0.0 | 0.0 | 3.3 | 0.0 | 0.0 | 0.0 |
| **FA2(6)G1S1** | 0.0 | 0.9 | 0.8 | 0.9 | 0.0 | 17.2 | 5.4 | 0.0 | 0.0 |
| **A2** | 0.0 | 0.0 | 0.0 | 0.0 | 0.0 | 70.6 | 33.2 | 0.0 | 0.0 |
| **FA2G2S1** | 16.8 | 16.4 | 15.9 | 17.0 | 16.6 | 0.0 | 0.0 | 16.8 | 16.4 |
| **FA2** | 78.7 | 76.8 | 77.7 | 77.3 | 79.5 | 8.8 | 57.0 | 79.3 | 78.9 |
| **FA2(6)G1** | 0.0 | 4.4 | 4.1 | 3.9 | 3.9 | 0.0 | 3.6 | 3.9 | 3.9 |
| **FA2(3)G1** | 0.0 | 0.7 | 0.6 | 0.0 | 0.0 | 0.0 | 0.0 | 0.0 | 0.0 |
| **A2BG2** | 0.0 | 0.8 | 0.8 | 0.8 | 0.0 | 0.0 | 0.8 | 0.0 | 0.8 |
| **F-glycan** | 100 | 99.2 | 99.2 | 99.2 | 100 | 29.4 | 66 | 100 | 99.2 |

Note: Structures of N-glycans are shown at top using the Consortium for Functional Glycomics (CFG) image notation for monosaccharides showing the N-glycans commonly found on antibodies and annotated using the Oxford Notation. Strikingly, in these unoptimized experiments we found that carbafucose resulted in marked production of A2 N-glycan, which represents FD antibody. FD-antibody glycans are shows at top in the blue box and lack the red triangle that represents fucose.

Unfortunately, this assay was performed by Catalent and represented a significant expense (about $3,000 per compound) ultimately forcing us to develop our own in-house bioassay. Using CHO-K1 cell lines that solely express one fucosyltransferase (i.e., FUT8), the Vocadlo group was able to determine the percentage of fucosylation for each inhibitor depending on their concentration. The cells were incubated with a specific lectin (i.e., *Aleuria aurantia lectin* (AAL)) that is linked to a fluorophore (i.e., FITC). The lectin protein recognizes and binds to *N*-glycans that are core-fucosylated thus emitting a fluorescent signal. The cells are washed to remove the extra lectin and subsequently analyzed by fluorescence microscopy. Using this bioassay, it was found that dose-dependent effects were greater for 2-fluorocarbafucose **384** ($IC_{50}$ = 15 μM) than the 2-fluorofucose counterpart **358** ($IC_{50}$ =

110 μM). These results further emphasized the potential of carbafucose analogs over their fucose counterparts and showed that fucosylation inhibitors can be produced that are incapable of transfer to the *N*-glycan.

## 3.2.2. Previous work

My co-worker Dr. Wang was the first member of the Britton group to work on the synthetic aspect of the project. Dr. Wang commenced the synthesis of the carbafucose counterparts of the main fucosyl transferase inhibitors reported by Seattle Genetics and Amgen (Figure 3.2).

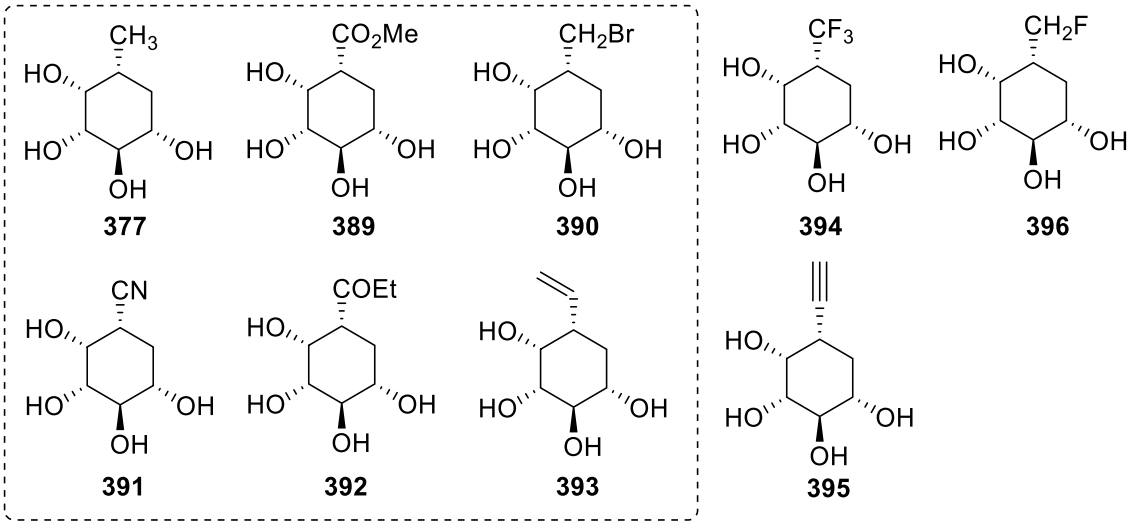


**Figure 3.2. Carbafucose counterparts of known inhibitors**
Note: these compounds were made by Dr. Wang (squared)

Dr. Wang expected to produce these targets through a common intermediate: aldehyde **397** (Figure 3.3). Indeed, a series of synthetic modifications of the carbonyl moiety were thought to provide access to several targeted molecules (e.g., Grignard addition, Appel reaction, Wittig olefination, or Seyferth-Gilbert homologation).

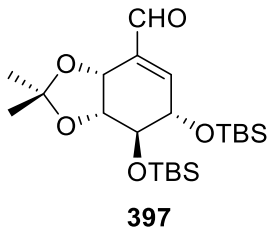


**Figure 3.3. Molecular structure of precursor 397**

As an alternative synthesis of carbafucose, we initiated with the chiral pool material L-Quebrachitol (**398**), a cheap and commercially available carbasugar. First, bis-acetonide protection of **398** was performed and the remaining alcohol was then oxidized into the corresponding ketone to provide **400**. Subsequent Wittig olefination offered vinyl ether **401** in poor yield. Finally, submission to acidic conditions delivered **397** in a 54% yield step (Scheme 3.2).

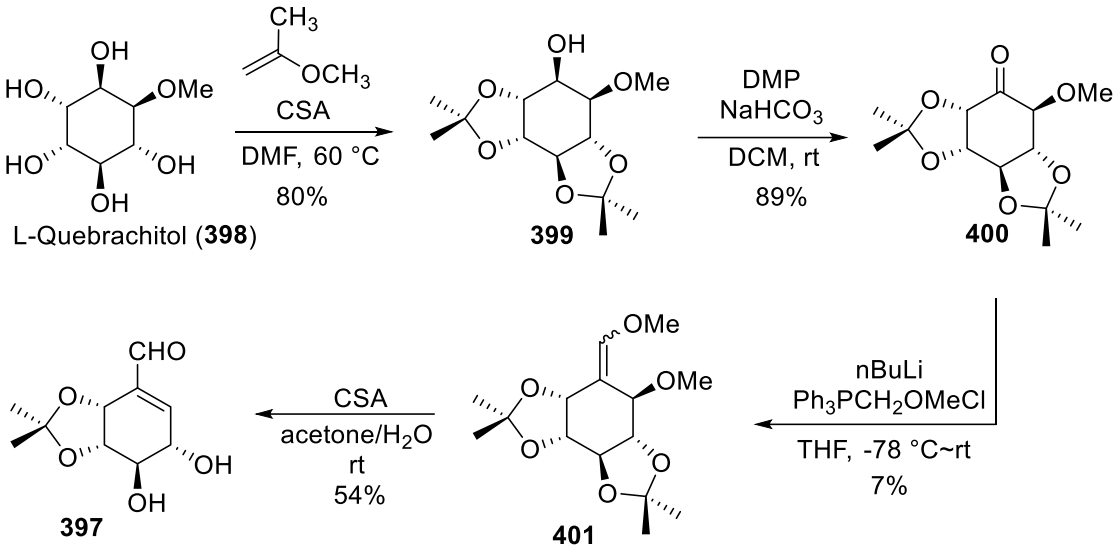


**Scheme 3.2. Synthesis of aldehyde 397**

With aldehyde **397** in hand, the synthesis of several analogs commenced. Protection of diol was performed followed by the Grignard addition of ethyl magnesium bromide to deliver alcohol **403**. A sequence of oxidation/hydrogenation/deprotection steps led to 5-ethyl ketone carbafucose **392** (Scheme 3.3).

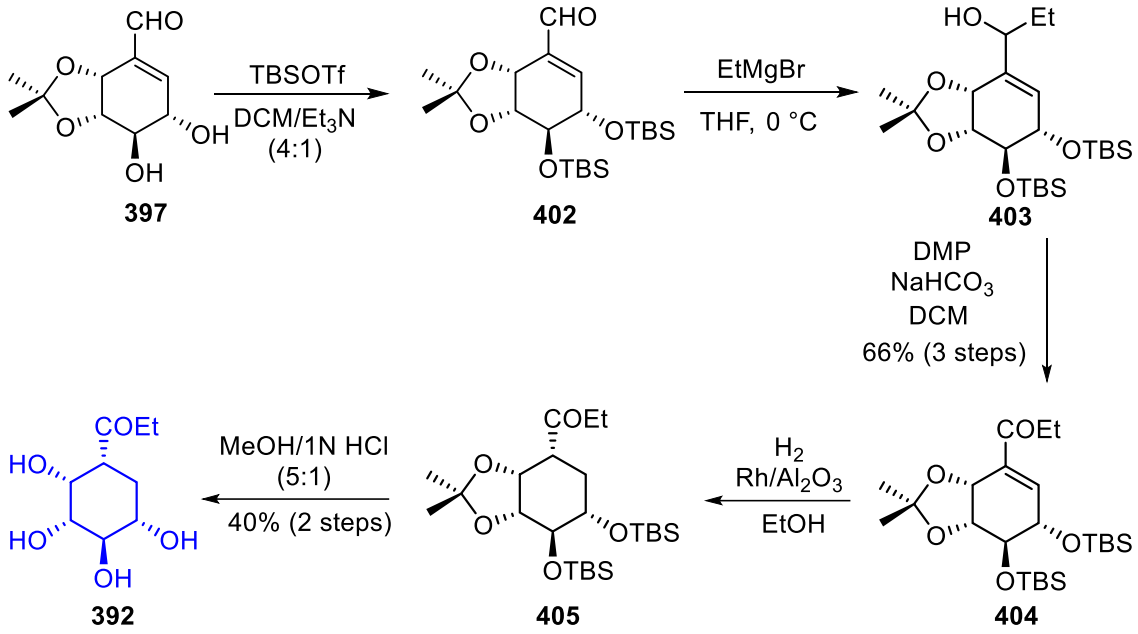


**Scheme 3.3. Synthesis of 5-ethyl ketone carbafucose 392**

To generate carbafucose methyl ester **389**, the initial protection step was repeated followed by oxidation of aldehyde **402** into the corresponding carboxylic acid **406**. Subsequent esterification with TMS-diazomethane provided α,β-unsaturated ester **407** that was in turn hydrogenated to yield **408**. Final alcohol deprotection delivered the second target **389** (Scheme 3.4).

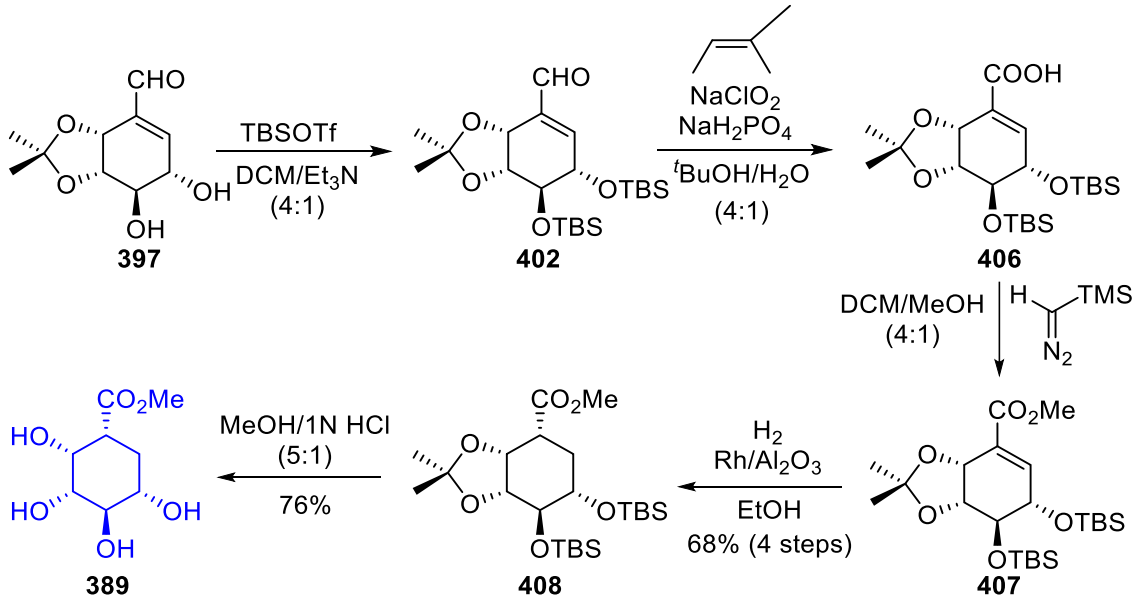


**Scheme 3.4. Synthesis of 5-methyl ester carbafucose 389**

To accomplish the synthesis of 5-cyanocarbafucose, protected aldehyde **402** was immediately transformed into the nitrile counterpart **409** in 45% yield over 2 steps. A subsequent sequence of hydrogenation/deprotection steps generated **391** (Scheme 3.5).

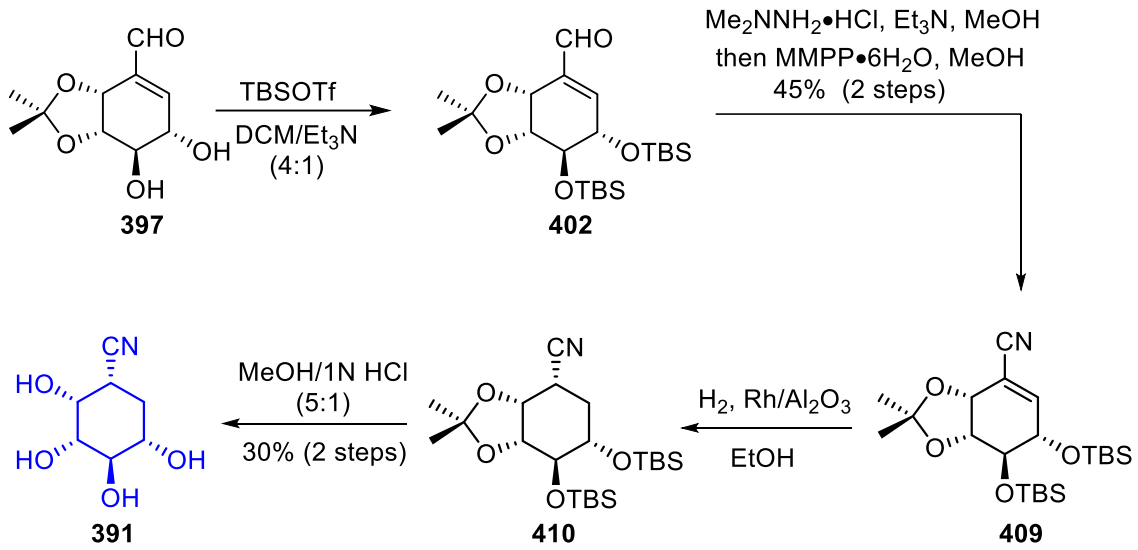


**Scheme 3.5. Synthesis of 5-cyanocarbafucose 391**

For the synthesis of the remaining targets, protected carbafucose methyl ester **389** was used as the common intermediate. Reduction of the ester into primary alcohol **411** followed by Appel reaction and deprotection provided 5-bromomethyl carbafucose **390** in good yield (Scheme 3.6).

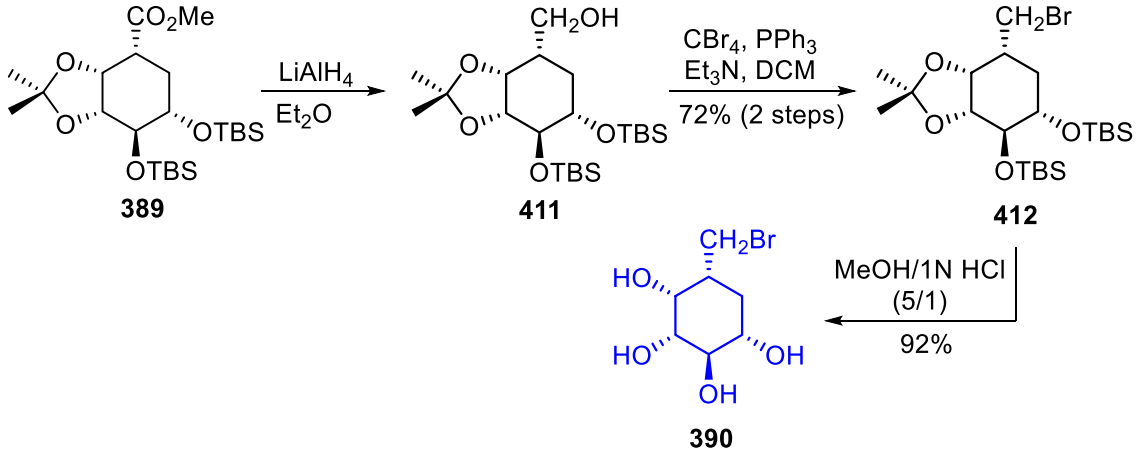


**Scheme 3.6. Synthesis of 5-bromomethyl carbafucose 390**

Similarly, protected carbafucose methyl ester **389** was reduced and subsequently converted into mesylate **413**. Submission to super-hydride (lithium triethyl borohydride) followed by global deprotection led to the formation of carbafucose **377** in good overall yield (60% over 4 steps). Thus, this route provided complimentary access to our lead inhibitor (Scheme 3.7).

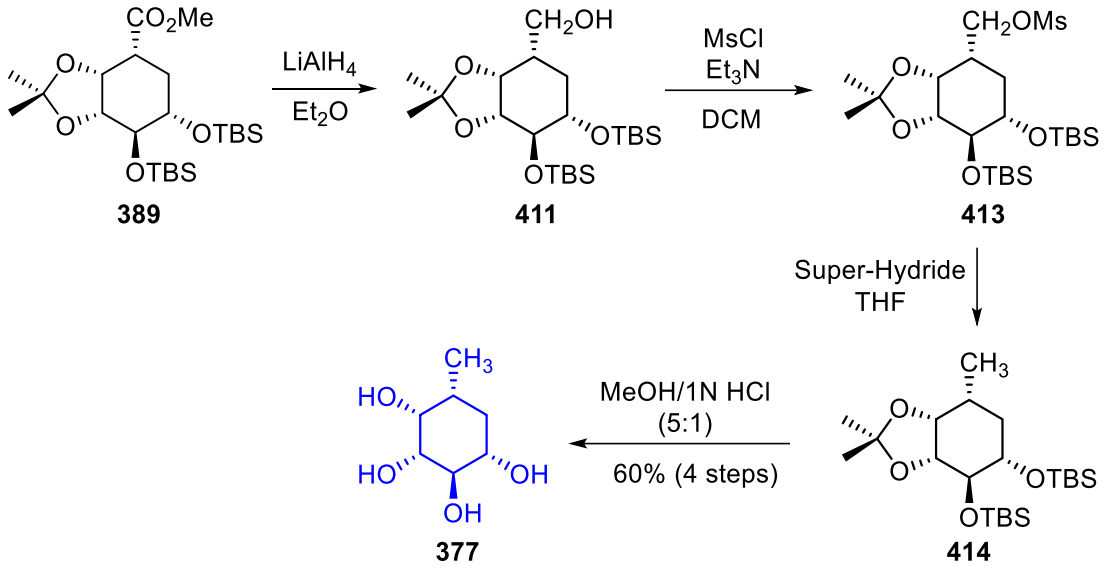


**Scheme 3.7. Synthesis of carbafucose 377**

To synthesize the final target, Dr. Wang performed a sequence of reduction/oxidation steps to deliver aldehyde **415**. Subsequent Wittig reaction allowed for the formation of protected vinyl carbafucose **416** that was further deprotected to yield the alkene **393** (Scheme 3.8).

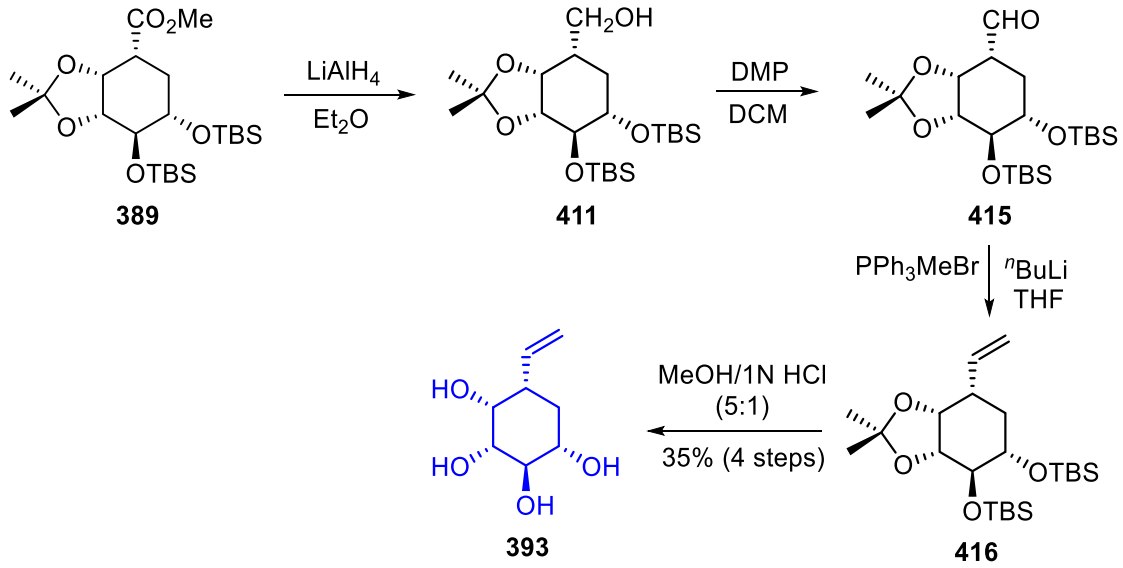


**Scheme 3.8. Synthesis of 5-vinyl carbafucose 393**

## 3.2.3. Dr. Wang's Remaining Targets

As I joined the project, remaining efforts were directed toward the synthesis of alkynyl carbafucose **395**, 6,6,6-trifluorocarbafucose **394** and 6-flurocarbafucose **396** (Figure 3.4).

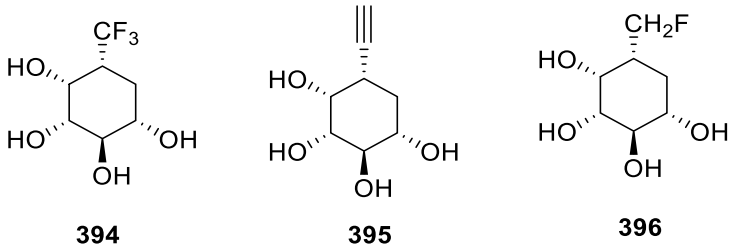


**Figure 3.4. Remaining targets 394, 395 and 396**

We anticipated that these analogs could be generated through the deoxygenation of different tertiary alcohol analogues (**420**, **421**, and **422**). Further disconnection would lead to ketone **423**, which would be submitted to the addition of different nucleophiles. Finally, we envisioned that ketone **423** could be traced back to vinyl bromide **424**, a functional intermediate synthesized from commercially available diene **425** (Scheme 3.9).

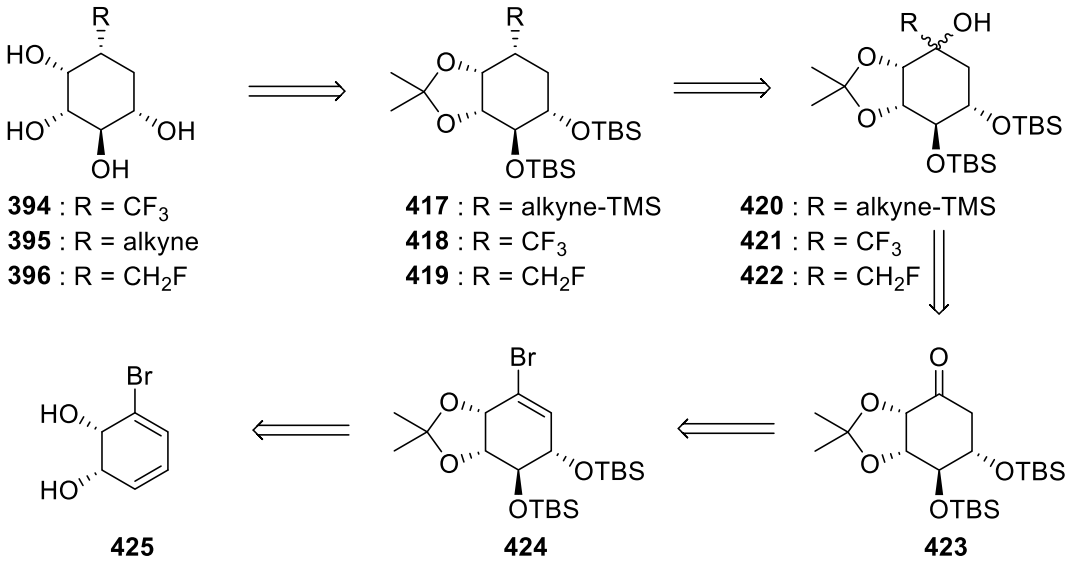


**Scheme 3.9. Retrosynthetic disconnections**

Excitedly, we commenced the investigation with the protection of commercially available **425** to generate acetonide **426** in excellent yield. Next, selective epoxidation provided vinyl bromide **427** in modest yield. We believed that the bicyclic conformation favored the *m*CPBA attack on the top face thus leading to a single diastereoisomer. Further epoxide opening provided **428** that was subsequently deprotected to deliver diol **429**.[162] Finally, TBS-protection yielded vinyl bromide **424**, the first target of this retrosynthetic approach[163] (Scheme 3.10).

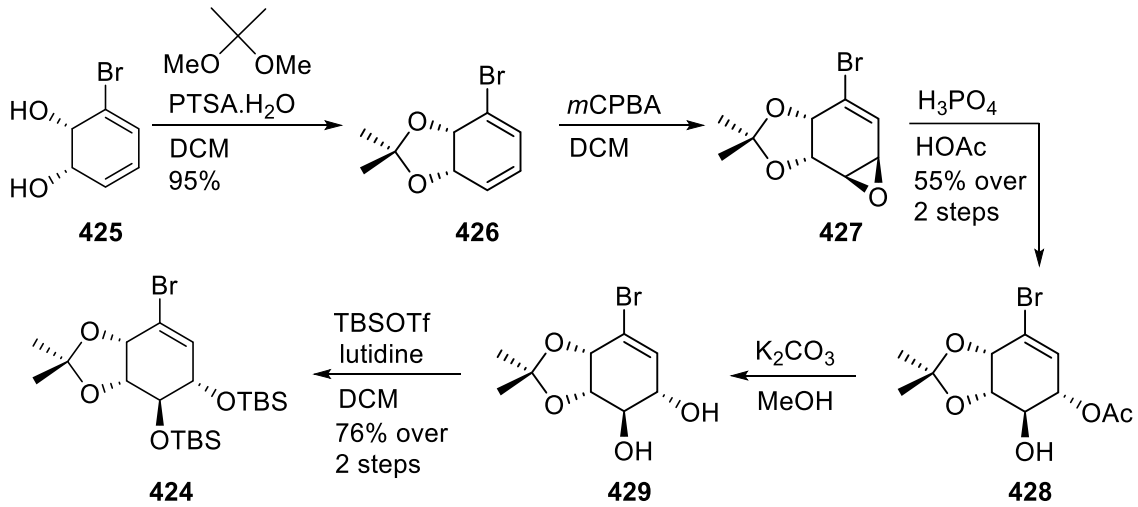


**Scheme 3.10. Synthesis of vinyl bromide 424**

With **424** in hand, we attempted the replacement of C5-bromine by a hydroxyl group to further deliver ketone **423**. We anticipated that a palladium-catalyzed coupling

between vinyl bromide **424** and piperidine could provide the desired ketone via enamine formation (Scheme 3.11). Unfortunately, the yield of the reaction was very poor (8% to 12%) which led us to seek alternative routes to ketone **411**. Thus, formation of a vinyl anion through a lithium-bromide exchange and subsequent reaction with a borate furnished the boronic ester *in situ*. Subsequent oxidative cleavage of the carbon-boron bond delivered the corresponding ketone **411**, which led to a significant improvement in the yield (i.e., 78% vs 10%). With a considerable amount of **411** in hand, we assessed the feasibility of our strategy. The addition of trimethylsilyl acetylene on ketone **411** yielded a diastereoisomerically pure tertiary alcohol **408** that was not characterized due to future racemization (Scheme 3.11).

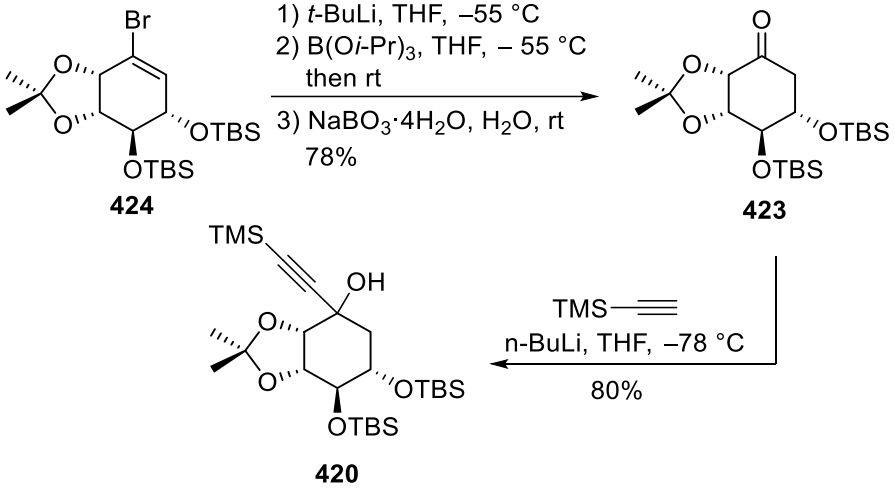


**Scheme 3.11. formation of ketone 423 and subsequent alkyne formation**
Note: The ketone synthesis was performed by my colleague Dr. Narasimha Thota

We first subjected the tertiary alcohol **420** to sodium cyanoborohydride in the presence of zinc iodide, which provided the asymmetric acetonide opened product **431.**[164] A similar outcome was observed when using boron trifluoride and $Et_3SiH$ ultimately providing the TES-protected counterpart **432**.[165] Finally, the use of tungstophosphoric acid was also fruitless, leaving starting material **430** unreacted despite prolonged reaction times and heating (Scheme 3.12).[166]

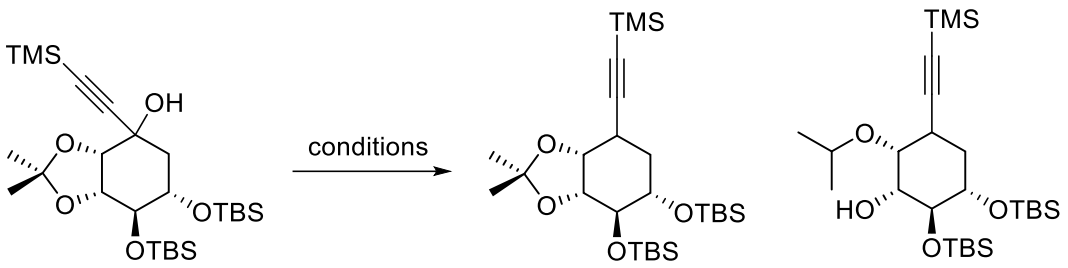


**420** **430** **431** : R = H
**432** : R = TES

**Scheme 3.12. Deoxygenation of tertiary alcohol 420**

We next explored Barton-McCombie reaction, which involves two consecutive steps: esterification and deoxygenation. Although several esters can be used, two parameters are crucial for carrying out a radical reaction in the optimum conditions: a dry and oxygen free reaction medium. Indeed, the presence of water or oxygen can dramatically reduce the lifetime of the radicals thus preventing the reaction from occurring, and ultimately leading to ester hydrolysis (Scheme 3.13).

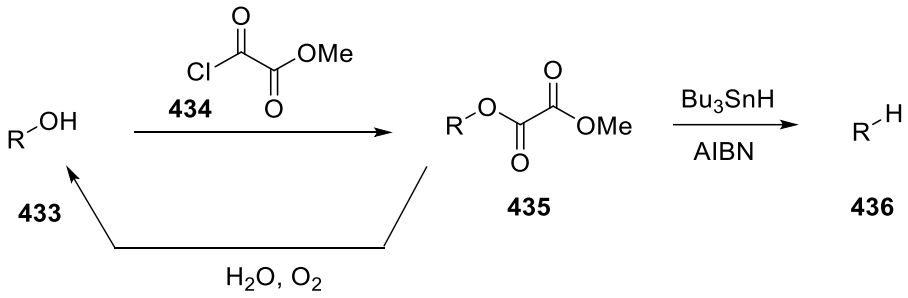


**Scheme 3.13. Classic Barton-McCombie pathway**

Toward this goal, methyl chlorooxoacetate **434** and DMAP were employed to protect tertiary alcohol **420** thus yielding the corresponding ester **437** in good yield. Notably, the purification of **437** must be performed rapidly to prevent hydrolysis. With ester **437** in hand, we modified the standard operating procedure of the deoxygenation step to fulfill the criteria (i.e., dryness and absence of oxygen). Reagents were split into two different reactors i) ester **437**, AIBN and toluene and ii) tributyltin hydride. Toluene and tin reagents were initially dried on molecular sieves (MS 4Å) overnight. Each solution was sparged with a strong flow of nitrogen gas for 30 minutes. Thereafter, the reaction was performed and delivered the deoxygenated product in 52% yield over 2 steps as a mixture of diastereoisomers **417** and **438** (d.r. = 1:4) (Scheme 3.14).

Unfortunately, the diastereoisomeric ratio was in favor of undesired isomer **438** after careful analysis of 1D NOESY experiments.

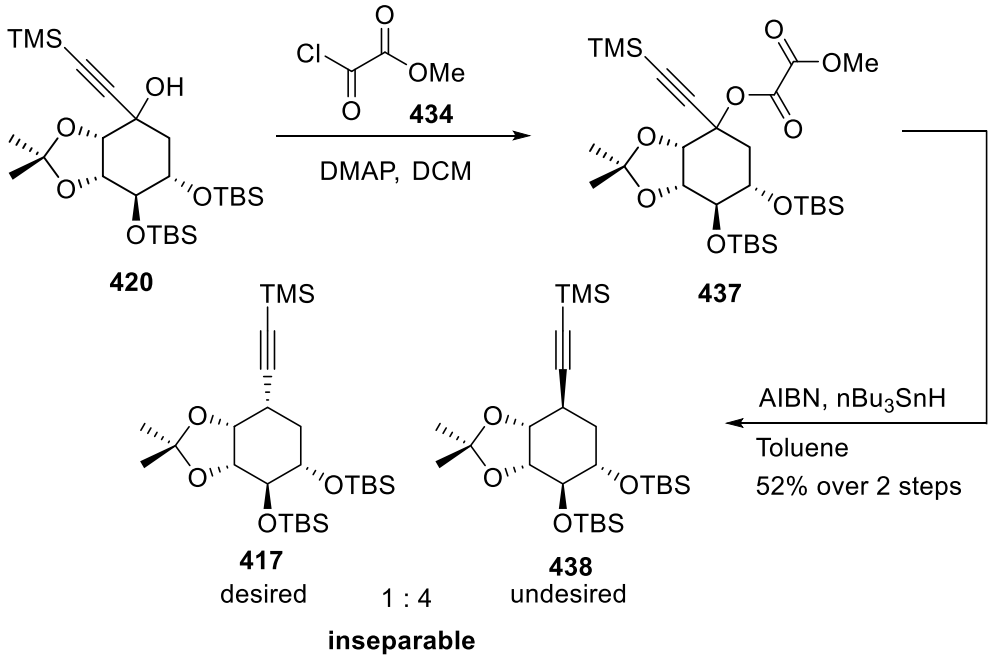


**Scheme 3.14. Deoxygenation sequence on alkynyl 420**

Although these diastereoisomers were not separable, we anticipated that TMS-deprotection would facilitate separation. Thus, treatment of the mixture of isomers **417** and **438** with potassium carbonate in methanol, enabled selective removal of the TMS group, and yielded a mixture of separable diastereoisomers **439** and **440**. We concluded that the diastereoisomeric ratio was 3:1 in favor of the undesired isomer **440**. Finally, deprotection of the TBS and acetonide groups under acidic conditions delivered the 5-alkynylcarbafucose **395** (Scheme 3.15).

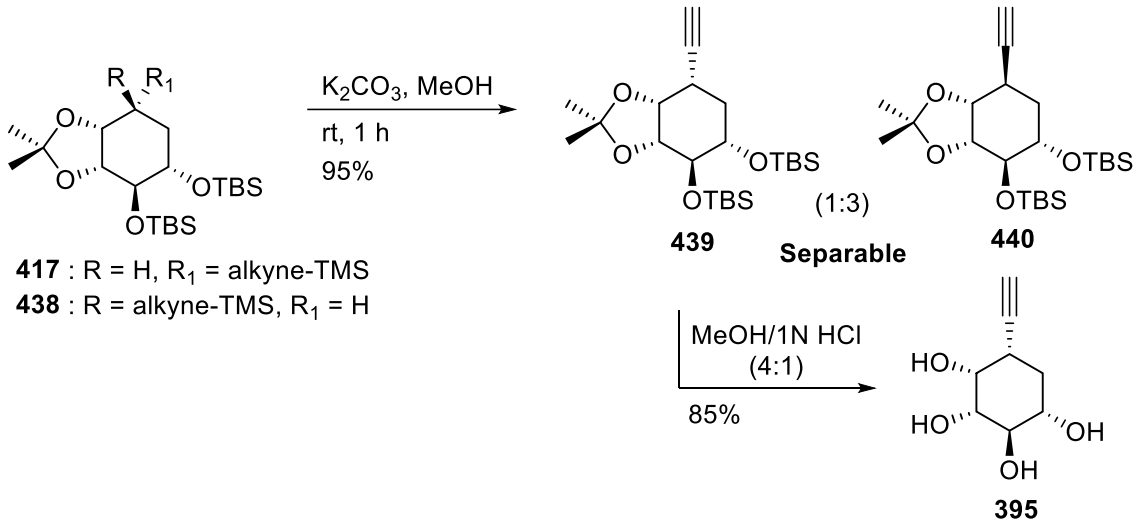


**417** : R = H, $R_1$ = alkyne-TMS
**438** : R = alkyne-TMS, $R_1$ = H

**Scheme 3.15. Synthesis of 5-alkynyl carbafucose 395**

Delighted with the success of this approach, we sought to adapt this sequence for the synthesis of 5-trifluoromethyl carbafucose. However, to apply a similar strategy, a nucleophilic source of the "$CF_3^-$" anion was required. Fortunately, the Olah group previously reported that TMS-$CF_3$ was easily added to ketones and aldehydes with a catalytic amount of TBAF.[167] The mechanism involves two steps: induction and propagation. First, a small amount of '$CF_3^-$' is released by the action of fluoride which then reacts on ketone **441** to form the corresponding alkoxide **443** (i.e., induction step). The newly-formed alkoxide then triggers the formation of a second '$CF_3^-$' by itself reacting with the "Si" center in the reagent. Finally, a slightly acidic workup results in hydrolytic cleavage of the TMS group to generate the corresponding free alcohol **446** (Scheme 3.16).

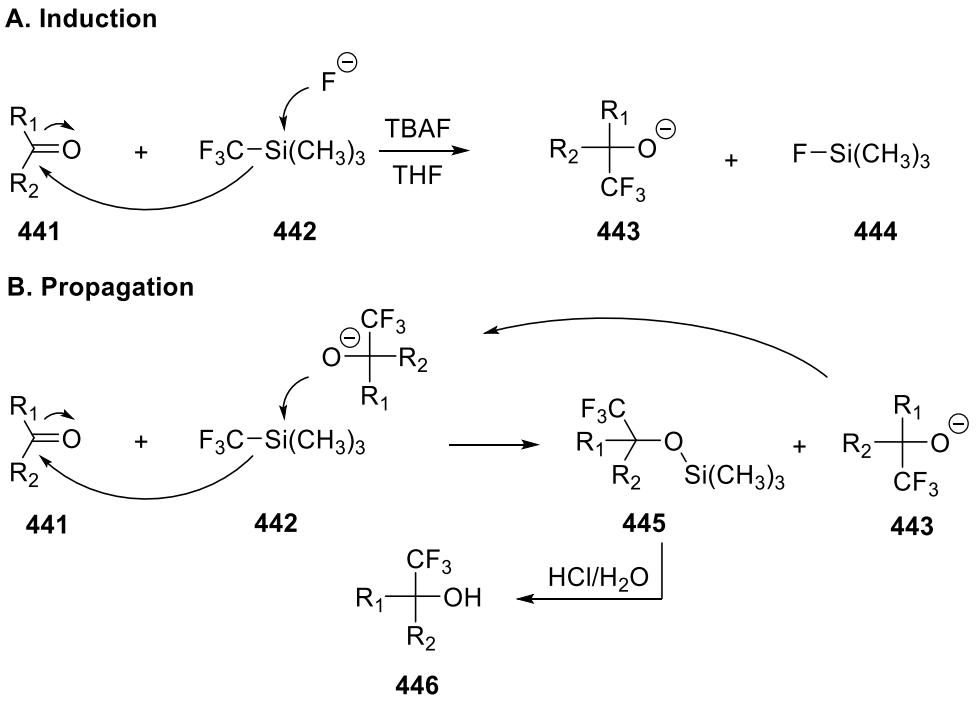


**Scheme 3.16. Mechanism of the "$CF_3^-$" addition**

Although the scope of the reaction reported by Olah was very narrow (i.e., limited to aliphatic and/or unhindered ketones and aldehydes), we applied these conditions to substrate **423**. Fortunately, the reaction smoothly delivered the desired TMS-protected tertiary alcohol which was further deprotected to deliver **421** as a mixture of diastereoisomers. The corresponding oxalyl ester was synthesized but appeared to be even more unstable than the alkyne counterpart **437**. After rapid work-up and a flash chromatography, a significant amount of starting material **421** was observed by TLC analysis and NMR spectroscopy. Immediately, the deoxygenation was carried out and delivered a mixture of diastereoisomers **418** and **447** in low yield (1.2:1 in favor of **447**). The remaining starting material was recovered and resubmitted to the same sequence of reactions. Similar to the alkynyl products, the $CF_3$ diastereoisomers were not isolable at this stage. To facilitate separation, the TBS groups were selectively removed and the products **448** and **449** were separated and isolated. Finally, acetonide deprotection provided both 6,6,6-trifluorocarbafucose **394** and **450** (Scheme 3.17).

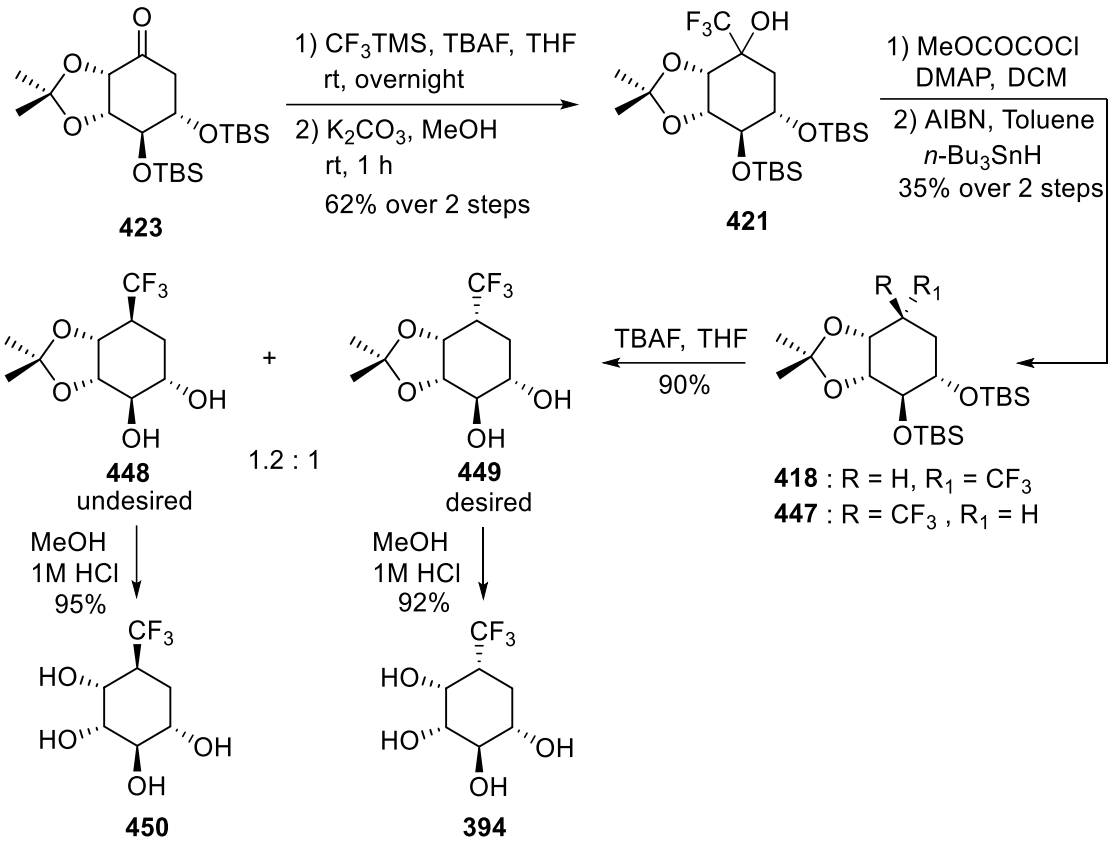


**Scheme 3.17. Synthesis of trifluoromethyl carbafucose 450 and 394**

Preliminary results showed that 6,6,6-trifluorocarbafucose **394** was moderately active in comparison to carbafucose **377** (i.e., **394**: $IC_{50}$ = 320 μM vs **377**: $IC_{50}$ = 15 μM). To further assess the impact of the fluorine on the C6 methyl group, we decided to synthesize 6-fluorocarbafucose **396**, which could be prepared in a similar manner to the trifluoromethyl carbafucose but required a nucleophilic source of "$FCH_2^-$". Fortunately, Luisi's group developed a robust methodology that was anticipated to provide the desired compound.[168] We applied this methodology to ketone **423** which provided the corresponding alcohol **422** as a mixture of isomers in good yield. Carrying out the same sequence of reactions, both 6-fluorocarbafucose isomers **396** and **454** were synthesized. Finally, peracetylation of **396** was performed to generate tetraacetate **455** in 85% yield (Scheme 3.18).

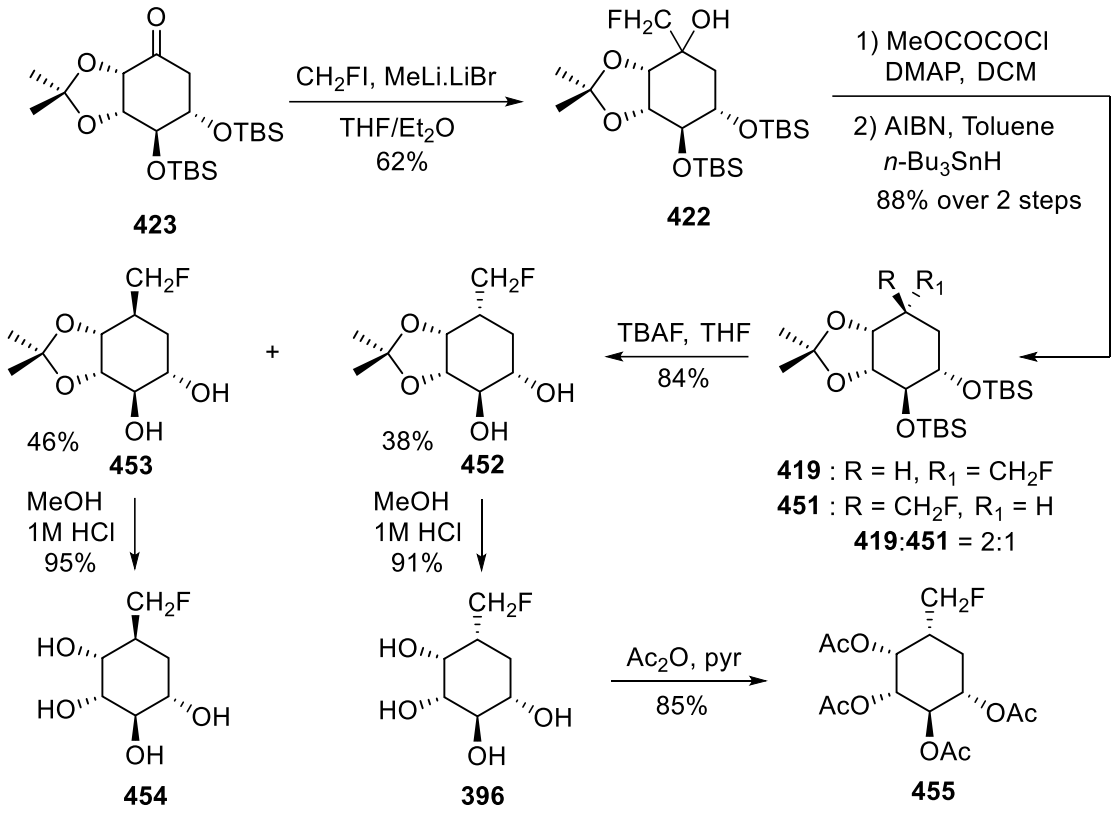


**Scheme 3.18. Synthesis of 454, 396 and 455**

Unfortunately, none of these compounds showed an improved inhibition of protein fucosylation when compared to carbafucose **377** (Figure 3.5). Thus, we envisioned taking a different approach by focusing on modifications of carbafucose **377**.

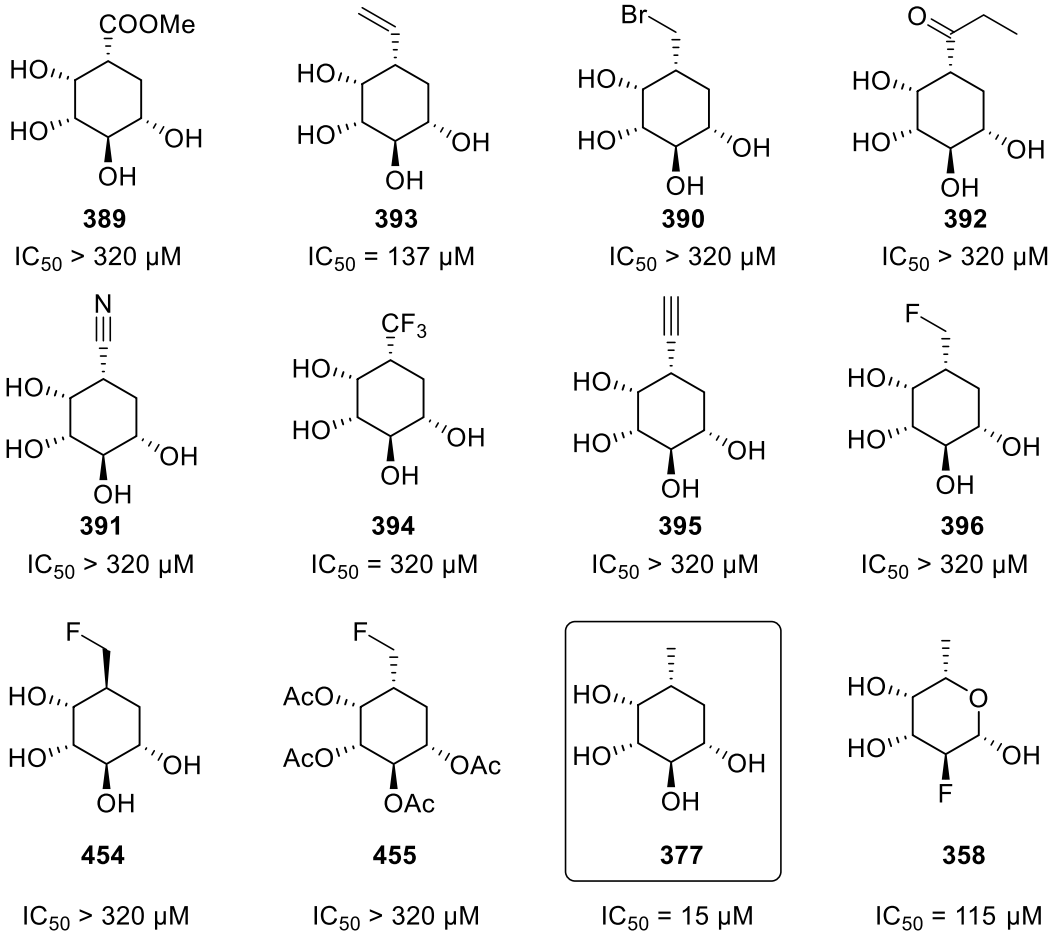


**Figure 3.5. Inhibitors and their $IC_{50}$ value**

## 3.2.4. New targets

At this point, expecting an increased demand for carbafucose, the development of a more efficient synthesis of **377** was set as a top priority. Indeed, generating a sufficient amount of carbafucose **377** would allow us to synthesize several additional derivatives. Moreover, a robust synthesis might be required in the future for the industrial production of large batches of afucosylated antibodies. Trisubstituted alkene **456** was envisioned to be a logical common intermediate accessible from the corresponding vinyl bromide **424** (Scheme 3.19).

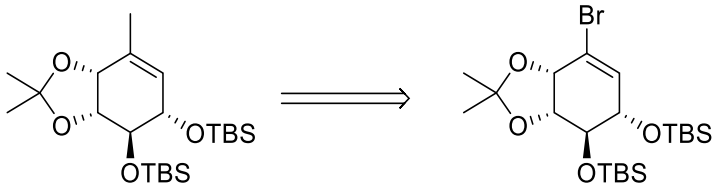


**456** **424**

**Scheme 3.19. Retrosynthetic approach to synthesize 456**

Vinyl bromide **424** was treated with *tert*-butyllithium which triggered a lithium-halogen exchange that was immediately subjected to iodomethane to deliver alkene **456** in a concise and high-yielding manner. Unfortunately, hydrogenation of alkene **456** failed to provide the protected carbafucose **414** in an acceptable yield. The conversion was poor even when the reaction was performed under high pressure (i.e., 50 psi). The major side-product was found to be substrate **457** arising from the allylic deoxygenation of **456** (Scheme 3.20).

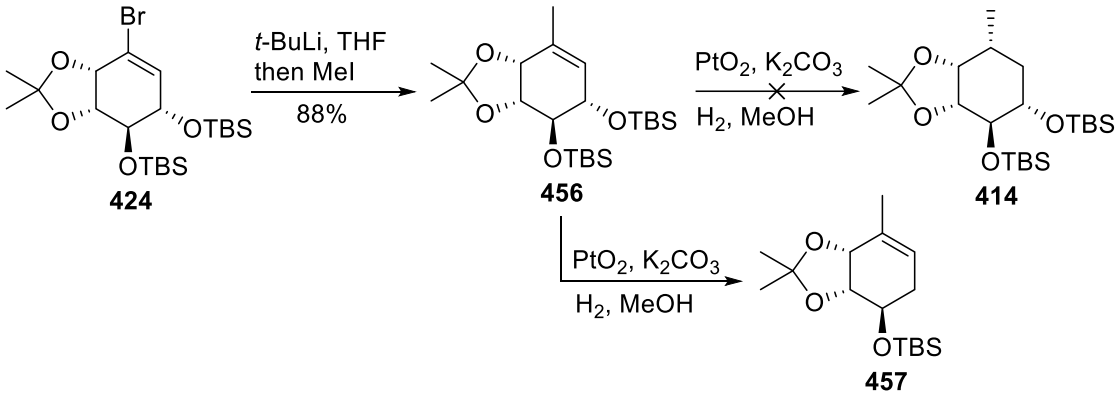


**Scheme 3.20. Failed hydrogenation attempt on 456**

We envisioned that the presence of the TBS groups impacted the hydrogenation. To assess our theory, alkene **456** was submitted to TBAF and delivered the corresponding diol **458**. Fortunately, subsequent hydrogenation provided saturated diol **459** and **460** in good yield as a mixture of separable isomers (i.e., 5:1 in favor of **459**) (Scheme 3.21).

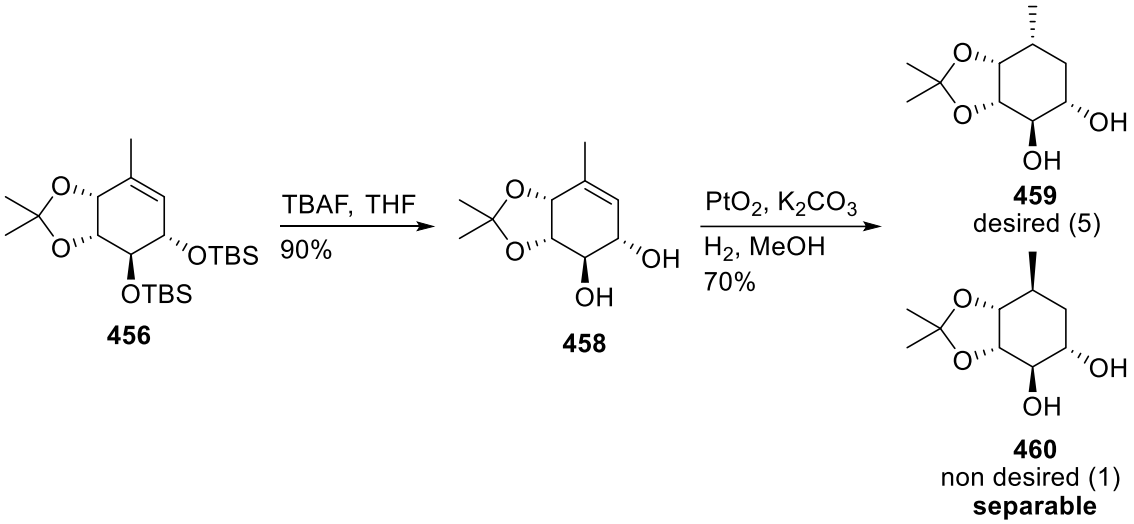


**Scheme 3.21. Hydrogenation success**

After isolation, both diastereoisomers **459** and **460** were independently submitted to a methanolic solution of HCl to provide carbafucose **377** and the epimer **378**. Finally, peracetylation of carbafucose **377** was performed and delivered tetraacetate carbafucose **461** (Scheme 3.22).

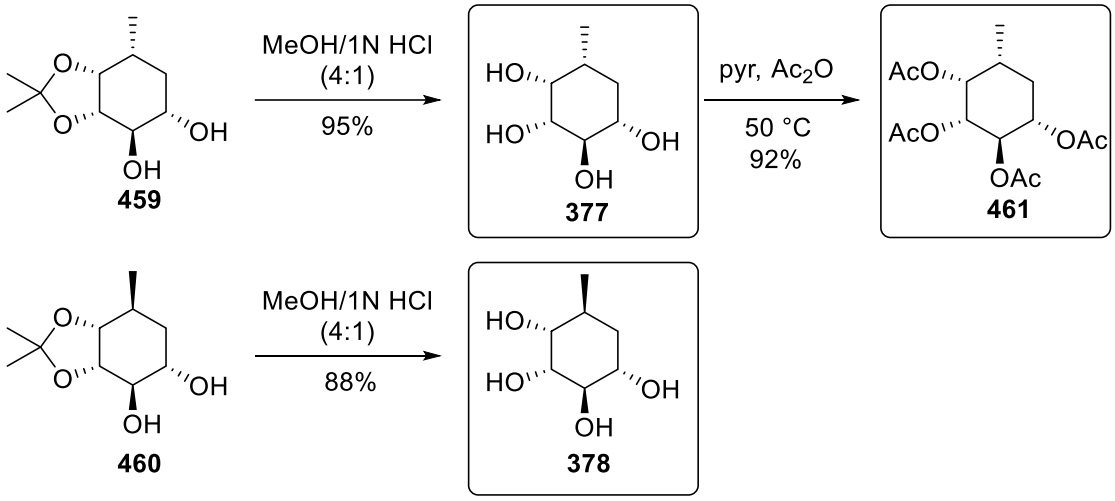


**Scheme 3.22. Synthesis of carbafucose 377, isomer 378 and peracetylate 461**

## 3.3. Future Direction

Given that carbafucose **377** appeared to be the best inhibitor among all the analogs assessed in our own in-house bioassay, further modifications at C6 may not prove useful. However, in combination with phosphorylation at C1-OH the existing

modified carbafucose analogs may prove to have enhanced activity and is a pathway that should be explored.

Ultimately, the development of a more robust and scalable synthesis of carbafucose is necessary. Indeed, the currently employed strategy is inadequate for producing large amounts of carbafucose. More specifically, the cost and the safety profile of the reagents combined with the long and fastidious process that involves several selectivity issues rendered the implementation of this synthesis impossible on a larger scale.

## 3.4. Conclusion

In conclusion, *Chapter 3* has presented the development of several syntheses to perform a thorough structure-activity-relationships study to generate potent inhibitors for the production of FD-antibodies. Although none of the synthesized compounds displayed better activity than carbafucose **377**, this study paved the path for the synthesis of potential inhibitors with C1 modifications. Indeed, the robust method developed to synthesize a decent amount of carbafucose **377** will allow further screening of the impact of several protected phosphoric acids at C1.

## 3.5. Experimental

**General:**

All reactions described were performed under an atmosphere of dry argon using oven dried glassware. Tetrahydrofuran was distilled over Na/benzophenone and dichloromethane was dried by distillation over $CaH_2$. All other solvents were used directly from EMD drysolv septum sealed bottles unless otherwise specified. Cold temperatures were maintained using following reaction baths: -115 °C, EtOH-$N_2$(l); -78 °C, acetone-dry ice; temperatures between -40 °C to -20 °C were maintained with a Polyscience VLT-60A immersion chiller.

All reagents and starting materials were purchased from Sigma Aldrich, Alfa Aesar, TCI America, Arcos or Carbosynth and were used without further purification. All solvents were purchased from Sigma Aldrich, EMD, Anachemia, Caledon, Fisher or ACP and used without further purification unless otherwise specified.

Flash chromatography was carried out with 230-400 mesh silica gel (E. Merck, Silica Gel 60) following the technique described by Still.[174] Thin layer chromatography was carried out on commercial aluminum backed silica gel 60 plates (E. Merck, type 5554, thickness 0.2 mm). Visualization of chromatograms was accomplished using ultraviolet light (254 nm) followed by heating the plate after staining with one of the following solutions: (a) *p*-anisaldehyde in sulphuric acid-ethanol mixture (5% anisaldehyde v/v and 5% sulphuric acid v/v in ethanol); (b) 1% potassium permanganate w/v, 6.6% potassium carbonate w/v, and 1% v/v 10% sodium hydroxide in water. Concentration and removal of trace solvents was done via a Büchi rotary evaporator using acetone-dry-ice condenser and a Welch vacuum pump.

Nuclear magnetic resonance (NMR) spectra were recorded using $CDCl_3$ or $CD_3OD$. Signal positions (δ) are given in parts per million from tetramethylsilane (δ 0) and were measured relative to the signal of the solvent ($^1$H NMR: $CDCl_3$: *δ* 7.26, $CD_3OD$: *δ* 3.31, $D_2O$: *δ* 4.79; $^{13}$C NMR: $CDCl_3$: *δ* 77.16, $CD_3OD$: *δ* 49.00). Coupling constants (*J* values) are given in Hertz (Hz) and are reported to the nearest 0.1 Hz. $^1$H NMR spectral data are tabulated in the order: multiplicity (s, singlet; d, doublet; t, triplet; q, quartet; m, multiplet; br., broad), coupling constants, number of protons. Proton nuclear magnetic resonance ($_1$H NMR) spectra were recorded on a Bruker Avance II 600 equipped with a

QNP or TCI cryoprobe (600 MHz), Varian Inova 500 (500 MHz), Bruker Avance III 500 (500 MHz), or Bruker Avance III 400 (400 MHz). Carbon nuclear magnetic resonance ($_{13}$C NMR) spectra were recorded on a Bruker Avance 600 equipped with a QNP or TCI cryoprobe (150 MHz), Bruker Avance III 500 (125 MHz), or Bruker Avance III 400 (100 MHz). Assignments of $^{1}$H and $^{13}$C NMR spectra are based on analysis of $^{1}$H-$^{1}$H COSY, HSQC, HMBC and nOe spectra.

Infrared (IR) spectra were recorded on a MB-series Bomem/Hartman & Braun Fourier transform spectrophotometer with internal calibration as films between sodium chloride plates. Only selected, characteristic absorption data are provided for each compound.

High resolution mass spectra were performed on an Agilent 6210 TOF LC/MS using ESI-MS technique.

Optical rotation was measured on a Perkin Elmer 341 Polarimeter at 589 nm.

**Preparation of vinyl bromide 424**

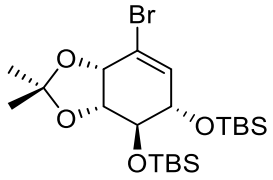


**424**

Potassium carbonate (200 mg, 1.45 mmol) was added to a stirred solution of acetate **428** (402 mg, 1.31 mmol) in methanol (5 mL) and stirred for 1 h. The reaction mixture was concentrated under reduced pressure. The solid mass thus obtained was treated with saturated aq $NH_4Cl$ solution (10 mL) and extracted with ethyl acetate (20 mL). The aqueous layer was separated and further extracted with EtOAc (2 × 20 mL). The combined organic phases were washed with brine (20 mL), dried over anhydrous $Na_2SO_4$, filtered and concentrated to obtain the crude diol **429** as a pale-yellow viscous liquid.

Without further purification, the crude diol was dissolved in $CH_2Cl_2$ (5 mL) and cooled to 0 °C. Triethylamine (1.25 mL, 8.97 mmol) followed by *tert*-butyldimethylsilyl trifluoromethanesulfonate (0.90 mL, 3.92 mmol) was added dropwise. Ice bath was removed, and the reaction mixture was warmed to room temperature. After stirring for

10 h, reaction mixture was treated with saturated aq $NH_4Cl$ solution (10 mL) and extracted with $Et_2O$ (20 mL). The aqueous layer was separated and further extracted with $Et_2O$ (2 × 20 mL). The combined organic phases were washed with brine (20 mL), dried over anhydrous $Na_2SO_4$, filtered, concentrated and the resulting crude product was purified by column chromatography (10% $Et_2O$ in hexane) to afford **424** (491 mg, 76% over 2 steps) as a white solid.

$^1$H NMR (500 MHz, $CDCl_3$) $\delta$ 6.06 (d, $J$ = 3.4 Hz, 1H), 4.61 (d, $J$ = 6.4 Hz, 1H), 4.16 (t, $J$ = 6.2 Hz, 1H), 4.03 (m, 1H), 3.81 (t, $J$ = 5.6 Hz, 1H), 1.49 (s, 3H), 1.39 (s, 3H), 0.90 (s, 9H), 0.89 (s, 9H), 0.12 (s, 6H), 0.10 (s, 3H), 0.09 (s, 3H).

**Preparation of ketone 423**

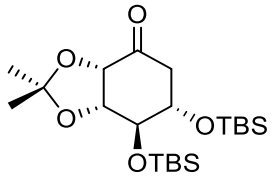


**423**

A flame-dried 50-mL flask equipped with a magnetic stirring bar, an argon inlet, and a septum was charged with vinyl bromide **424** (565 mg, 1.14 mmol) and THF (6 mL). The mixture was cooled to –55 °C using dry-ice and acetone bath, then *tert*-butyllithium (1.45 M in pentane, 1.25 mL, 1.81 mmol) was added dropwise. The reaction mixture was stirred at –55 °C for 30 min, then triisopropylborate (neat, 1.10 mL, 4.77 mmol) was added dropwise. The dry-ice and acetone bath was removed, and the reaction mixture was slowly warmed up to room temperature and stirred for 60 h. Then $NaBO_3 \cdot 4H_2O$ (1.77 g, 11.5 mmol) and $H_2O$ (6 mL) was added. After the mixture had been stirred at rt for 24 h, it was poured into water (20 mL), extracted with $Et_2O$ (30 mL). The aqueous layer was separated and further extracted with $Et_2O$ (2 × 30 mL). The combined organic phases were washed with brine (20 mL), dried over anhydrous $Na_2SO_4$, filtered, concentrated and the resulting crude product was purified by column chromatography (20% $Et_2O$ in hexane) to afford **423** (386 mg, 78% over the three steps) as a white solid.

$^{1}$H NMR (500 MHz, $CDCl_3$) $\delta$ 4.42 (m, 2H), 4.19 (m, 1H), 4.12 (m, 1H), 2.94 (dd, $J$ = 13.6, 2.9 Hz, 1H), 2.38 (dd, $J$ = 13.6, 3.8 Hz, 1H), 1.41 (s, 3H), 1.36 (s, 3H), 0.92 (s, 9 H), 0.86 (s, 9H), 0.16 (s, 3H), 0.13 (s, 3 H), 0.11 (s, 3H), 0.10 (s, 3H);

$^{13}$C NMR (126 MHz, $CDCl_3$) $\delta$ 206.2, 110.6, 82.3, 78.1, 74.6, 70.3, 42.8, 27.3, 25.9, 25.7, 25.6, 18.0, 17.9, –4.88, –4.91, –5.1.

HRMS (ESI-TOF) *m/z*: $[M + NH_4]^+$ Calcd for $C_{21}H_{46}NO_5Si_2$ 448.2909; Found 448.2913.

IR (neat): ν 2953, 2926, 2886, 2852, 1731, 1362, 1248, 1081, 825 cm$^{-1}$

$[\alpha]_D^{20}$ = +30.4 (c = 0.83) in $CHCl_3$

**Preparation of alcohol 420**

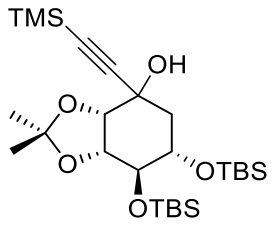


**420**

To a stirred solution of ethynyltrimethylsilane (0.25 mL, 1.77 mmol) in THF (1 mL) under Ar atmosphere at –15 °C was added *n*-butyllithium (2.41 M in hexane, 600 µL, 1.45 mmol). The reaction mixture was allowed to stir at –15 °C for 30 min, and then was cooled to –50 °C. Ketone **423** (201 mg, 0.467 mmol) in THF (2 mL) was added dropwise to the above reaction mixture and allowed to stir for 3 h between –50 °C and –30 °C. Excess lithium trimethylsilylethanide was quenched by the addition of saturated aq $NH_4Cl$ solution (10 mL) and extracted with EtOAc (20 mL). The aqueous layer was separated and further extracted with EtOAc (2 × 20 mL). The combined organic phases were washed with brine (20 mL), dried over anhydrous $Na_2SO_4$, filtered, concentrated and the resulting crude product was purified by column chromatography (20% $Et_2O$ in hexane) to afford **420** (235 mg, 95%) as a white solid.

$^{1}$H NMR (500 MHz, $CDCl_3$) $\delta$ 4.23 (d, $J$ = 5.4 Hz, 1H), 3.99 (t, $J$ = 5.6 Hz, 1H), 3.77 (m, 1H), 3.65 (dd, $J$ = 8.0, 5.9 Hz, 1H), 2.09 (dd, $J$ = 13.0, 3.8 Hz, 1H), 2.00 (dd, $J$ = 13.0, 9.7 Hz, 1H), 1.54 (s, 3H), 1.37 (s, 3H), 0.91 (s, 9H), 0.90 (s, 9H), 0.18 (s, 9H), 0.13 (s, 3H), 0.12 (s, 3H), 0.09 (s, 3H), 0.08 (s, 3H).

$^{13}$C NMR (126 MHz, $CDCl_3$) $\delta$ 110.0, 90.8, 81.1, 79.6, 77.8, 77.4, 71.2, 67.7, 27.9, 26.5, 26.4, 26.3, 18.3, 18.2, –0.1, –3.7, –3.7, –4.1, –4.4.

HRMS (ESI-TOF) *m/z*: $[M + H]^+$ Calcd for $C_{26}H_{53}O_5Si_3$ 529.3195; Found 529.3196.

**Preparation of alkyne 430**

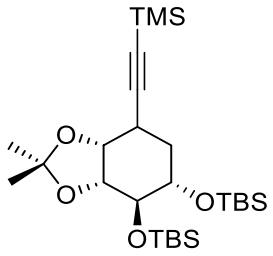


**430**

To a stirred solution of alkyne **420** (203 mg, 0.384 mmol) in $CH_2Cl_2$ (3 mL) at 0 °C was added *N*,*N*-dimethylaminopyridine (280 mg, 2.29 mmol) followed by methyl 2-chloro-2-oxoacetate (220 µL, 2.39 mmol) in a dropwise manner. Ice bath was removed, and the reaction mixture was warmed to room temperature and stirred for 12 h. The reaction mixture was treated with cold saturated aq $NaHCO_3$ solution (5 mL) and extracted with EtOAc (20 mL). The aqueous layer was separated and further extracted with EtOAc (2 × 20 mL). The combined organic phases were dried over anhydrous $Na_2SO_4$, filtered, concentrated and the resulting crude product was quickly purified by column chromatography (15% $Et_2O$ in hexane) to afford the corresponding ester. This ester was dissolved in toluene (1 mL) in a microwavable glass tube. To this reaction mixture was added 2,2′-Azobis(2-methylpropionitrile) (75 mg, 0.46 mmol) and the $N_2$ gas was bubbled through the solution for 30 min. In another microwavable glass tube, neat *n*-tributyltin hydride (1.20 mL, 4.46 mmol) was added and the $N_2$ gas was bubbled through the solution for 30 min, after which time the reaction mixture was heated at 120 °C for 10 min. The above crude reaction mixture was added dropwise over 2 min and stirred at 120 °C for 2 h, after which time the solution was cooled to room temperature over 20 min. The reaction mixture was treated with saturated aq $NH_4Cl$ solution (10 mL) and extracted with EtOAc (20 mL). The aqueous layer was separated and further extracted with EtOAc (2 × 20 mL). The combined organic phases were washed with brine (20 mL), dried over anhydrous $Na_2SO_4$, filtered, concentrated and the resulting crude product was purified by column chromatography (5% $Et_2O$ in hexane) to afford **430** (117 mg, 59% over the two steps) as a colorless viscous liquid which exhibits ~3:1

(**417**:**438**) diastereomeric ratio, as determined by $^1$H NMR spectroscopy in $CDCl_3$ at 27 °C.

**Preparation of alkynes 439 and 440**

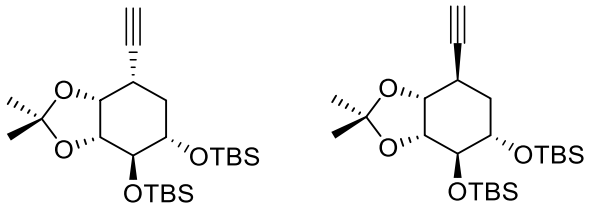


**439** **440**

Potassium carbonate (18 mg, 0.13 mmol) was individually added to a stirred solution of alkynes **417** and **438** (44.9 mg, 87.5 µmol) in $CH_3OH$ (1 mL) and $CH_2Cl_2$ (0.2 mL) and stirred for 23 h. The reaction mixture was concentrated under reduced pressure. The solid mass thus obtained was treated with saturated aq $NH_4Cl$ solution (5 mL) and extracted with ethyl acetate (10 mL). The aqueous layer was separated and further extracted with EtOAc (2 × 10 mL). The combined organic phases were washed with brine (10 mL), dried over anhydrous $Na_2SO_4$, filtered, concentrated and the resulting crude product was purified by column chromatography (5% $Et_2O$ in hexane) to afford pseudo D-altro isomer **440** (25.3 mg, 66%) as a colorless viscous liquid and pseudo L-fuco isomer **439** (9 mg, 23%) as a colorless viscous liquid.

**Data for 439:**

$^1$H NMR (500 MHz, $CDCl_3$) $\delta$ 4.30 (m, 1H), 3.98 (m, 1H), 3.61 (m, 1H), 3.51 (m, 1H), 2.82 (m, 1H), 2.17 (d, $J$ = 2.5 Hz, 1H), 1.97–1.85 (m, 2H), 1.54 (s, 3H), 1.38 (s, 3H), 0.89 (s, 9H), 0.88 (s, 9H), 0.11 (s, 3H), 0.08 (s, 6H), 0.07 (s, 3H).

$^{13}$C NMR (126 MHz, $CDCl_3$) $\delta$ 109.5, 83.9, 80.4, 77.2, 74.9, 72.7, 69.8, 33.2, 27.6, 27.5, 26.2, 26.1, 25.8, 18.2, –3.8, –3.9, –4.2, –4.3.

HRMS (ESI-TOF) *m/z*: $[M + H]^+$ Calcd for $C_{23}H_{45}O_4Si_2$ 441.2851; Found 441.2850.

**Data for 440:**

$^1$H NMR (500 MHz, $CDCl_3$) $\delta$ 4.10 (dd, $J$ = 8.5, 5.2 Hz, 1H), 4.00 (dd, $J$ = 5.1, 2.7 Hz, 1H), 3.88 (m, 1H), 3.75 (m, 1H), 3.00 (m, 1H), 2.10 (d, $J$ = 2.5 Hz, 1H), 1.88 (m, 1H),

1.72 (m, 1H), 1.49 (s, 3H), 1.34 (s, 3H), 0.90 (s, 9H), 0.89 (s, 9H), 0.10 (s, 3H), 0.08 (s, 6H), 0.07 (s, 3H).

$^{13}$C NMR (126 MHz, $CDCl_3$) $\delta$ 108.9, 86.6, 78.5, 77.5, 72.1, 69.7, 69.1, 32.2, 28.5, 27.1, 26.2, 25.9, 18.1, –4.5, –4.6, –4.7, –4.8.

HRMS (ESI-TOF) *m/z*: $[M + H]^+$ Calcd for $C_{23}H_{45}O_4Si_2$ 441.2851; Found 441.2847.

**Preparation of 5-alkynylcarbafucose 395**

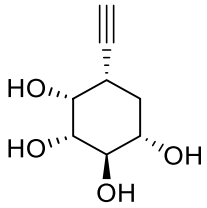


**395**

To a stirred solution of alkyne **439** (15 mg, 34 µmol) in $CH_3OH$ (1 mL) was added 1 M HCl (0.4 mL, 0.4 mmol) and stirred for 14 h. The reaction mixture was concentrated under reduced pressure and co-evaporated with toluene (3 × 2 mL) and the resulting crude product was purified by column chromatography (5% $CH_3OH$ in EtOAc) to afford **395** (4.7 mg, 80%) as a colorless viscous liquid.

$^1$H NMR (500 MHz, $CD_3OD$) $\delta$ 3.93 (m, 1H), 3.49 (m, 1H), 3.35 (m, 1H), 3.25 (dd, $J$ = 9.6, 3.0 Hz, 1H), 2.55 (m, 1H), 2.37 (d, $J$ = 2.5 Hz, 1H), 1.93–1.83 (m, 2H).

$^{13}$C NMR (126 MHz, $CD_3OD$) $\delta$ 85.2, 76.0, 75.5, 73.0, 72.9, 70.7, 34.1, 31.8.

HRMS (ESI-TOF) *m/z*: $[M + H]^+$ Calcd for $C_8H_{12}O_4$ 190.1074; Found 190.1074.

$[\alpha]_D^{20}$ = + 4.8 (c = 0.17) in $CH_3OH$

**Preparation alcohol 421**

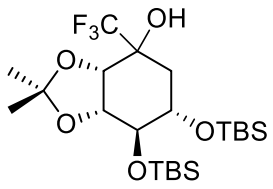


**421**

To a stirred solution of ketone **423** (141 mg, 0.327 mmol) in THF (2 mL) at 0 °C was added trimethyl(trifluoromethyl)silane (2.00 M in THF, 180 µL, 360 µmol) followed by tetra-*n*-butylammonium fluoride (1.0 M in THF, 10 µL, 10 µmol). Ice bath was removed and the reaction mixture was warmed to room temperature and stirred for 30 min. The reaction mixture was treated with saturated aq $NH_4Cl$ solution (5 mL) and extracted with EtOAc (20 mL). The organic layer was dried over anhydrous $Na_2SO_4$, filtered, concentrated and the resulting crude material was dissolved in $CH_3OH$ (2 mL). Potassium carbonate (50 mg, 0.36 mmol) was added to the above solution and stirred for 1 h. The reaction mixture was concentrated under reduced pressure. The solid mass thus obtained was treated with saturated aq $NH_4Cl$ solution (5 mL) and extracted with ethyl acetate (20 mL). The aqueous layer was separated and further extracted with EtOAc (2 × 20 mL). The combined organic phases were washed with brine (10 mL), dried over anhydrous $Na_2SO_4$, filtered, concentrated and the resulting crude product was purified by column chromatography (10% $Et_2O$ in hexane) to afford **421** (110 mg, 67%) as a colorless viscous liquid:

$^1$H NMR (500 MHz, $CDCl_3$) $\delta$ 4.3 (d, $J$ = 6.4 Hz, 1H), 4.17–4.11 (m, 2H), 3.92 (m, 1H), 2.00 (m, 2H), 1.56 (s, 3H), 1.38 (s, 1H), 0.91 (s, 9H), 0.88 (s, 9H), 0.12 (s, 12H).

HRMS (ESI-TOF) *m/z*: $[M + H]^+$ Calcd for $C_{22}H_{44}F_3O_5Si_2$ 501.2674; Found 501.2679.

**Preparation of protected 6,6,6-trifluorocarbafucose 418 and 447**

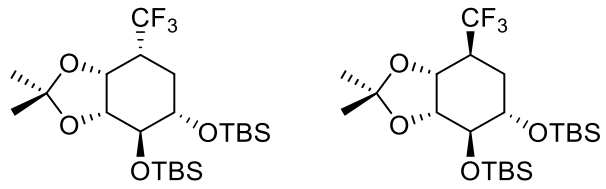


**418** **447**

To a stirred solution of alcohol **421** (352 mg, 0.703 mmol) in $CH_2Cl_2$ (3 mL) at 0 °C was added *N*,*N*-dimethylaminopyridine (515 mg, 4.22 mmol) followed by methyl 2-chloro-2-oxoacetate (0.40 mL, 4.4 mmol) in a dropwise manner. Ice bath was removed, and the reaction mixture was warmed to room temperature and stirred for 14 h. The reaction mixture was treated with cold saturated aq $NaHCO_3$ solution (5 mL) and extracted with EtOAc (30 mL). The aqueous layer was separated and the organic phase was dried over anhydrous $Na_2SO_4$, filtered, concentrated and the resulting crude product was quickly purified by column chromatography (10% $Et_2O$ in hexane) to afford the corresponding ester along with the hydrolysed ester (starting material). This crude material was dissolved in toluene (1 mL) in a microwable glass tube. To this reaction mixture was added 2,2′-Azobis(2-methylpropionitrile) (60 mg, 0.37 mmol) and the $N_2$ gas was bubbled through the solution for 30 min. In an another microwable glass tube, neat *n*-tributyltin hydride (900 µL, 3.35 mmol) was added and the $N_2$ gas was bubbled through the solution for 30 min, after which time the reaction mixture was heated at 120 °C for 10 min. The above crude reaction mixture was added dropwise over 2 min and stirred at 120 °C for 2 h, after which time the solution was cooled to room temperature over 20 min. The reaction mixture was treated with saturated aq $NH_4Cl$ solution (10 mL) and extracted with EtOAc (30 mL). The aqueous layer was separated and further extracted with EtOAc (2 × 20 mL). The combined organic phases were washed with brine (20 mL), dried over anhydrous $Na_2SO_4$, filtered, concentrated and the resulting crude product was purified by column chromatography (2.5% $Et_2O$ in hexane) to afford **447** (119 mg, 35% over the two steps) as a colorless viscous liquid which exhibits ~1.2:1 diastereomeric ratio, as determined by $^1H$ NMR spectroscopy in $CDCl_3$ at 27 °C along with **418** (65 mg, 18%).

**Preparation of protected 6,6,6-trifluorocarbafucose 448 and 449**

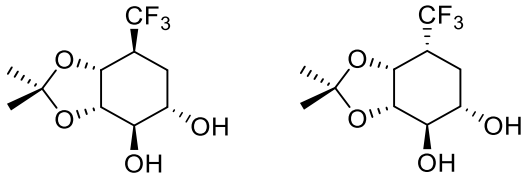

**448** **449**

To a stirred solution of **418** and **447** (100 mg, 0.206 mmol) in THF (2 mL) was added tetra-*n*-butylammonium fluoride (1.0 M in THF, 1.0 mL, 1.0 mmol) and stirred for 10 h. The reaction mixture was then treated with $H_2O$ and extracted with ethyl acetate (20 mL). The aqueous layer was separated and further extracted with EtOAc (2 × 20 mL). The combined organic phases were washed with brine (10 mL), dried over anhydrous $Na_2SO_4$, filtered, concentrated and the resulting crude product was purified by column chromatography (65% EtOAc in hexane) to afford pseudo D-altro isomer **448** (24 mg, 46%) as a colorless viscous liquid and pseudo L-fuco isomer **449** (80% EtOAc in hexane, 20 mg, 38%) as a white solid.

**Data for 448:**

$^1$H NMR (500 MHz, $CDCl_3$) $\delta$ 4.35 (t, $J$ = 5.3 Hz, 1H), 4.03 (t, $J$ = 6.8 Hz, 1H), 3.78 (m, 1H), 3.67 (t, $J$ = 7.7 Hz, 1H), 2.81 (m, 1H), 2.04 (m, 1H), 1.88 (m, 1H), 1.53 (s, 3H), 1.38 (s, 3H).

$^{13}$C NMR (126 MHz, $CDCl_3$): $\delta$ 126.9, 109.8, 78.6, 75.6, 72.2, 68.0, 40.2, 28.1, 26.2, 25.9.

HRMS (ESI-TOF) *m/z*: $[M + H]^+$ Calcd for $C_{10}H_{16}F_3O_4$ 257.0995; Found 257.0991.

$[\alpha]_D^{20}$ = –15.9 (c = 0.07) in $CHCl_3$

**Data for 449:**

$^1$H NMR (500 MHz, $CDCl_3$) $\delta$ 4.37 (m, 1H), 3.95 (m, 1H), 3.56 (m, 1H), 3.48 (m, 1H), 2.54 (m, 1H), 2.06 (m, 1H), 1.85 (m, 1H), 1.55 (s, 3H), 1.38 (s, 3H).

$^{13}$C NMR (126 MHz, $CDCl_3$) $\delta$ 127.0, 110.9, 80.5, 77.8, 71.5, 70.4, 40.1, 28.4, 26.4, 25.9.

HRMS (ESI-TOF) *m/z*: $[M + H]^+$ Calcd for $C_{10}H_{16}F_3O_4$ 257.0995; Found 257.0997.

**Preparationof 6,6,6-trifluorocarbafucose-5a-β-L-fucopyranose C-5 epimer 450**

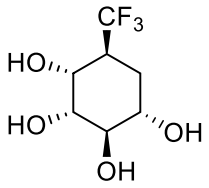

**450**

To a stirred solution of diol **448** (10.1 mg, 39.4 μmol) in $CH_3OH$ (0.9 mL) was added 1 M HCl (0.2 mL, 0.2 mmol) and stirred for 12 h. The reaction mixture was concentrated under reduced pressure and co-evaporated with toluene (3 × 2 mL) and the resulting crude product was purified by column chromatography (3% $CH_3OH$ in EtOAc) to afford **450** (6.1 mg, 72%) as a colorless viscous liquid:

$^1H$ NMR (500 MHz, $CD_3OD$) $\delta$ 4.02 (dd, $J$ = 7.1, 3.1 Hz, 1H), 3.80–3.72 (m, 2H), 3.70 (m, 1H), 2.72 (m, 1H), 1.99–1.88 (m, 2H).

$^{13}C$ NMR (126 MHz, $CD_3OD$) $\delta$ 129.0, 74.7, 73.4, 70.6, 68.2, 41.8, 27.7.

$^{19}F$ NMR (377 MHz, $CD_3OD$) $\delta$ –68.7.

HRMS (ESI-TOF) *m/z*: $[M + NH_4]^+$ Calcd for $C_7H_{15}F_3NO_4$ 234.0948; Found 234.0951.

$[\alpha]_D^{20}$ = +31.4 (c = 0.23) $CH_3OH$.

**Preparation of 6,6,6-trifluorocarbafucose-5a-β-L-fucopyranose 394**

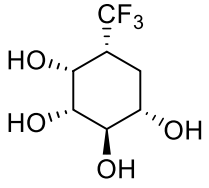

**394**

To a stirred solution of diol **449** (7.40 mg, 28.9 μmol) in $CH_3OH$ (0.9 mL) was added 1N HCl (0.2 mL, 0.2 mmol) and stirred for 12 h. The reaction mixture was concentrated under reduced pressure and co-evaporated with toluene (3 × 2 mL) and the resulting

crude product was purified by column chromatography (3% $CH_3OH$ in EtOAc) to afford **394** (5.1 mg, 82%) as a colorless viscous liquid:

$^1$H NMR (500 MHz, $CD_3OD$) $\delta$ 4.13 (m, 1H), 3.53 (m, 1H), 3.43 (m, 1H), 3.28 (dd, $J$ = 9.6, 3.0 Hz, 1H), 2.35 (m, 1H), 1.93–1.82 (m, 2H).

$^{13}$C NMR (126 MHz, $CD_3OD$) $\delta$ 128.2, 76.1, 75.4, 72.5, 68.8, 42.7, 27.2.

HRMS (ESI-TOF) *m/z*: $[M + NH_4]^+$ Calcd for $C_7H_{15}F_3NO_4$ 234.0948; Found 234.0952.

$[\alpha]_D^{20}$ = –3.8 (c = 0.21) in $CH_3OH$.

**Preparation of alcohol 422**

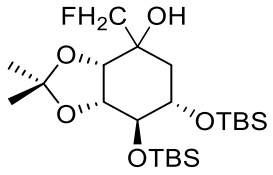


**422**

To a stirred solution of ketone **423** (464 mg, 1.077 mmol) in THF/$Et_2O$ (1:1) (17 mL) at -78 °C was added iodofluoromethane (0.086 M in pentane, 8.37 mL, 0.72 mmol) followed by MeLi.LiBr (1:1) (1.6 M in $Et_2O$, 1.34 mL, 2.15 mmol). The reaction mixture is stirred 5 min at -78 °C. Next, the reaction mixture was treated with saturated aq $NH_4Cl$ solution and extracted with $Et_2O$. The organic layer was dried over anhydrous $MgSO_4$, filtered, concentrated, and the resulting crude product was purified by column chromatography (5% $Et_2O$ in hexane) to afford **422** (207 mg, 62%) as a colorless viscous liquid.

$^1$H NMR (400 MHz, $CDCl_3$) $\delta$ 4.23 (dd, $J$ = 8.9, 59.9 Hz, 1H), 4.13–4.11 (m, 2H), 4.10 (dd, $J$ = 8.9, 60.2 Hz, 1H), 4.08 (d, $J$ = 2.6 Hz, 1H), 3.90–3.85 (m, 1H), 2.04 (ddd, $J$ = 2.1, 4.1, 14.6 Hz, 1H), 1.78 (dd, $J$ = 4.9, 14.6 Hz, 1H), 1.55 (s, 3H), 1.37 (s, 1H), 0.91 (s, 9H), 0.89 (s, 9H), 0.12 (s, 9H), 0.10 (s, 3H).

$^{13}$C NMR (101 MHz, $CDCl_3$): $\delta$ 109.4, 84.7 (d, $J$ = 174.9 Hz), 78.5, 73.5 (d, $J$ = 3.0 Hz), 72.4, 71.5, 70.8 (d, $J$ = 18.1 Hz), 33.3 (d, $J$ = 2.5 Hz), 26.3, 26.0, 25.9, 25.5, 18.1 (d, $J$ = 13.3 Hz), -4.3, -4.4, -4.5, -4.8.

$^{19}$F NMR (377 MHz, $CDCl_3$): $\delta$ -228.3 (t, $J$ = 12.7, 47.4 Hz).

HRMS (ESI-TOF) *m/z*: $[M + H]^+$ Calcd for $C_{22}H_{45}FO_5Si_2$ 465.2862; Found 465.2858.

IR (neat): v 3468, 2930, 2370, 1255, 1082, 837 $cm^{-1}$

$[\alpha]_D^{20}$ = +7.5 (c = 0.96) in $CHCl_3$

**Preparation of 6-fluorocarbafucose 419 and 451**

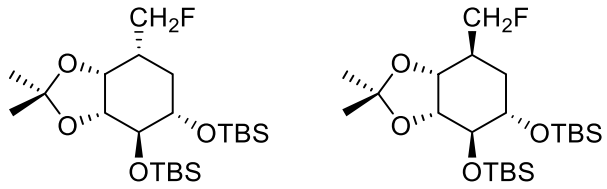


**419** **451**

To a stirred solution of alcohol **422** (40 mg, 0.086 mmol) in $CH_2Cl_2$ (1.2 mL) at -17 °C was added *N*,*N*-dimethylaminopyridine (63.2 mg, 0.516 mmol) followed by methyl 2-chloro-2-oxoacetate (47.5 µL, 0.516 mmol) in a dropwise manner. After 2 h, ice bath was removed, and the reaction mixture was warmed to room temperature and stirred 1 h. The reaction mixture was treated with cold saturated aq $NaHCO_3$ solution and extracted with EtOAc. The aqueous layer was separated, and the organic phase was dried over anhydrous $MgSO_4$, filtered, concentrated and the resulting crude product was quickly purified by column chromatography (33% $Et_2O$ in hexane) to afford the corresponding ester.

$^1H$ NMR (400 MHz, $CDCl_3$) $\delta$ 5.04 (dd, *J* = 10.3, 48.1 Hz, 1H), 4.58 (dd, *J* = 10.3, 45.7 Hz, 1H), 4.50 (d, *J* = 6.7 Hz, 1H), 3.99 (t, *J* = 6.5 Hz, 1H), 3.89 (s, 3H), 3.81 (dd, *J* = 6.7, 7.9 Hz, 1H), 3.65 (m, 1H), 2.25 (m, 2H), 1.51 (s, 3H), 1.32 (s, 3H), 0.90 (s, 9H), 0.89 (s, 9H), 0.13 (s, 3H), 0.10 (s, 3H), 0.09 (s, 3H), 0.08 (s, 3H).

This crude material was dissolved in toluene (1 mL) in a microwable glass tube. To this reaction mixture was added 2,2′-Azobis(2-methylpropionitrile) (28.2 mg, 0.172 mmol) and the $N_2$ gas was bubbled through the solution for 30 min. In an another microwable glass tube, neat *n*-tributyltin hydride (463 µL, 1.72 mmol) was added and the $N_2$ gas was bubbled through the solution for 30 min, after which time the reaction mixture was heated at 120 °C. The former crude reaction mixture was added quickly into the latter and stirred at 120 °C for 2 h, after which time the solution was cooled to room temperature. The reaction mixture was treated with saturated aq $NH_4Cl$ solution and

extracted with EtOAc. The aqueous layer was separated and further extracted with EtOAc. The combined organic phases were washed with brine (20 mL), dried over anhydrous $MgSO_4$, filtered, concentrated and the resulting crude product was purified by column chromatography (5% $Et_2O$ in hexane) to afford **419** and **451** (34 mg, 88% over the two steps) as a colorless viscous liquid which exhibits ~2:1 diastereomeric ratio in favor of **419**, as determined by $^1H$ NMR spectroscopy in $CDCl_3$ at 25 °C.

$^1H$ NMR (400 MHz, $CDCl_3$) $\delta$ 4.67–4.26 (m, 2H), 4.24 (m, 0.6H), 4.07–3.94 (m, 1.7H), 3.81 (m, 0.4H), 3.61–3.48 (m, 1.3H), 2.38–2.13 (m, 1H), 1.81–1.68 (m, 1H), 1.64–1.43 (m, 1H), 1.50 (s, 2H), 1.47 (s, 1H), 1.36 (s, 1H), 1.35 (s, 2H), 0.93–0.90 (s, 18H), 0.15–0.07 (s, 12H).

$^{13}C$ NMR (101 MHz, $CDCl_3$): $\delta$ 109.2, 108.5, 85.4 (d, $J$ = 167.5 Hz), 84.6 (d, $J$ = 167.9 Hz), 81.7, 79.0, 78.4, 77.4, 73.3, 73.2, 71.8, 70.2, 35.9 (d, $J$ = 18.9 Hz), 35.2 (d, $J$ = 18.6 Hz), 29.6 (d, 4.9 Hz), 29.6 (d, $J$ = 3.1 Hz), 28.6, 28.0, 26.3, 26.2, 25.9, 25.8, 18.4, 18.3, 18.1, -3.5, -3.7, -4.0, -4.3, -4.6, -4.7, -4.8, -4.8.

$^{19}F$ NMR (377 MHz, $CDCl_3$): $\delta$ -222.7 (dt, $J$ = 12.7, 46.9 Hz), -231.1 (dt, $J$ = 29.9, 48.0 Hz).

HRMS (ESI-TOF) *m/z*: $[M + H]^+$ Calcd for $C_{22}H_{45}FO_4Si_2$ 449.2913; Found 449.2912.

IR (neat): v 3698, 3621, 2929, 2369, 1470, 1245, 829 $cm^{-1}$

**Preparation of protected 6-fluorocarbafucose 452 and 453**

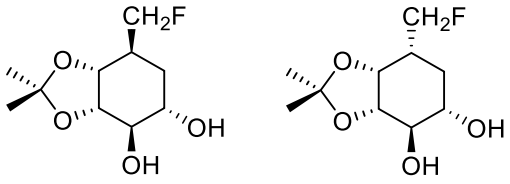


**453** **452**

To a stirred solution of acetonide **419** and **451** (129 mg, 0.288 mmol) in THF (3 mL) was added tetra-*n*-butylammonium fluoride (1.0 M in THF, 1.15 mL, 1.15 mmol) and stirred for 12 h. The reaction mixture was then treated with saturated aq $NH_4Cl$ solution and extracted with ethyl acetate. The aqueous layer was separated and further extracted with EtOAc. The combined organic phases were washed with brine, dried

over anhydrous $MgSO_4$, filtered, concentrated and the resulting crude product was purified by column chromatography (20% Acetone in DCM) to afford isomer **452** (21.8 mg, 38%) as a white solid and isomer **453** (37.0 mg, 46%) as a white solid.

**Data for 453:**

$^1$H NMR (400 MHz, $CDCl_3$) $\delta$ 4.59 (ddd, *J* = 7.6, 8.9, 46.7 Hz, 1H), 4.42 (ddd, *J* = 6.9, 8.9, 47.1 Hz, 1H), 4.26 (t, *J* = 4.3 Hz, 1H), 3.93 (m, 1H), 3.57–3.44 (m, 2H), 2.50 (d, *J* = 2.7 Hz, 1H), 2.34 (d, *J* = 2.4 Hz, 1H), 2.29 (m, 1H), 1.88 (m, 1H), 1.51 (s, 3H), 1.48 (m, 1H), 1.36 (s, 3H).

$^{13}$C NMR (101 MHz, $CDCl_3$) $\delta$ 109.9, 85.0, 83.4, 80.7, 78.7, 73.7 (d, *J* = 6.1 Hz), 71.0 (d, *J* = 1.5 Hz), 36.3 (d, *J* = 19.1 Hz), 28.6 (d, *J* = 5.7 Hz), 28.5, 26.5.

$^{19}$F NMR (377 MHz, $CDCl_3$): $\delta$ -222.6 (dt, *J* = 12.8, 46.7 Hz).

HRMS (ESI-TOF) *m/z*: $[M + H]^+$ Calcd for $C_{10}H_{17}FO_4$ 221.1184; Found 221.1183.

IR (neat): v 3721, 3694, 3624, 3597, 3214, 2369, 1366, 1218 1024 $cm^{-1}$

$[\alpha]_D^{20}$ = + 30.7 (c = 1.4) in acetone

**Data for 452:**

$^1$H NMR (500 MHz, $CDCl_3$) $\delta$ 4.56 (ddd, *J* = 4.5, 9.3, 36.7 Hz, 1H), 4.46 (ddd, *J* = 4.0, 9.3, 36.0 Hz, 1H), 4.20 (t, *J* = 5.7 Hz, 1H), 4.00 (t, *J* = 6.6 Hz, 1H), 3.77–3.55 (m, 2H), 2.52 (s, 1H), 2.47 (s, 1H), 2.34 (m, 1H), 1.87 (m, 2H), 1.52 (s, 3H), 1.37 (s, 3H).

$^{13}$C NMR (101 MHz, $CDCl_3$): $\delta$ 109.3, 85.6 (d, *J* = 170.0 Hz), 79.0 (d, *J* = 1.1 Hz), 76.5, 74.8 (d, *J* = 4.8 Hz), 68.8 (d, *J* = 1.9 Hz), 36.3 (d, *J* = 18.8 Hz), 29.8 (d, *J* = 3.1 Hz), 28.2, 25.9.

$^{19}$F NMR (377 MHz, $CDCl_3$): $\delta$ -225.0 (dt, *J* = 31.3, 47.5 Hz).

HRMS (ESI-TOF) *m/z*: $[M + H]^+$ Calcd for $C_{10}H_{17}FO_4$ 221.1184; Found 221.1182.

IR (neat): v 3712, 3695, 3677, 3665, 2919, 2852, 1446, 1369, 1004 $cm^{-1}$

$[\alpha]_D^{20}$ = + 17.4 (c = 1.1) in acetone

**Preparation of 6-fluorocarbafucose C5-epimer 454**

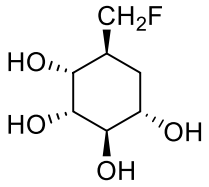

**454**

To a stirred solution of diol **453** (24 mg, 93.7 μmol) in $CH_3OH$ (4.8 mL) was added 1 M HCl (1.2 mL) and stirred for 2 h. The reaction mixture was concentrated under reduced pressure and the resulting crude product was purified by column chromatography (20% $CH_3OH$ in EtOAc) to afford **454** (15.4 mg, 91%) as a colorless viscous liquid:

$^1$H NMR (400 MHz, $CD_3OD$) $\delta$ 4.50 (dt, $J$ = 8.5, 47.5 Hz, 1H), 4.32 (ddd, $J$ = 6.5, 8.7, 47.3 Hz, 1H), 3.94 (m, 1H), 3.53 (t, 9.3 Hz, 1H), 3.50–3.39 (m, 1H), 3.29 (dd, $J$ = 3.0, 9.5 Hz, 1H), 1.92 (m, 1H), 1.64 (dt, $J$ = 4.2, 12.5 Hz, 1H), 1.47 (q, $J$ = 12.4 Hz, 1H), 1.02 (d, $J$ = 6.7 Hz, 1H).

$^{13}$C NMR (151 MHz, $CD_3OD$) $\delta$ 83.7 (d, $J$ = 166.7 Hz), 75.2, 74.7, 72.0, 68.5 (d, $J$ = 5.3 Hz), 37.9 (d, $J$ = 18.6 Hz), 28.0 (d, $J$ = 6.5 Hz).

$^{19}$F NMR (377 MHz, $CD_3OD$): $\delta$ -225.0 (dt, $J$ = 12.4, 47.4 Hz).

HRMS (ESI-TOF) *m/z*: $[M + NH_4]^+$ Calcd for $C_7H_{17}FNO_4$ 198.1136; Found 198.1139.

IR (neat): v 3728, 3694, 2345, 1598, 1044 cm$^{-1}$

$[\alpha]_D^{20}$ = + 2.8 (c = 1.4) in $CH_3OH$

**Preparation of 6-fluorocarbafucose 396**

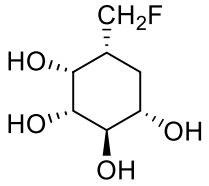

**396**

To a stirred solution of diol **452** (18 mg, 70.3 μmol) in $CH_3OH$ (4.8 mL) was added 1 M HCl (1.2 mL) and stirred for 2 h. The reaction mixture was concentrated under reduced

pressure and the resulting crude product was purified by column chromatography (20% $CH_3OH$ in EtOAc) to afford **396** (12.2 mg, 96%) as a colorless viscous liquid:

$^1$H NMR (500 MHz, $CD_3OD$) $\delta$ 4.59 (ddd, $J$ = 5.2, 9.2, 47.8 Hz, 1H), 4.47 (ddd, $J$ = 4.4, 9.2, 47.7 Hz, 1H), 3.85–3.78 (m, 2H), 3.75–3.68 (m, 2H), 2.21 (m, 1H), 1.87–1.83 (m, 2H).

$^{13}$C NMR (151 MHz, $CD_3OD$) $\delta$ 85.9 (d, $J$ = 167 Hz), 74.8, 73.9, 71.4, 69.7 (d, $J$ = 3.8 Hz), 37.8 (d, $J$ = 17.9 Hz), 30.5 (d, $J$ = 3.5 Hz).

$^{19}$F NMR (377 MHz, $CD_3OD$): $\delta$ -229.0 (br s).

HRMS (ESI-TOF) *m/z*: $[M + NH_4]^+$ Calcd for $C_7H_{17}FNO_4$ 198.1136; Found 198.1141.

IR (neat): v 3731, 3691, 2346, 1645, 1064 $cm^{-1}$

$[\alpha]_D^{20}$ = + 5.8 (c = 0.3) in $CH_3OH$

**Preparation of peracetylated 6-fluorocarbafucose 455**

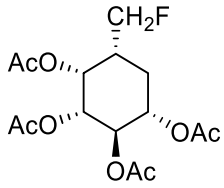


**455**

To a stirred solution of tetrol **396** (3 mg, 16.7 µmol) in pyridine (0.6 mL) was added $Ac_2O$ (0.02 mL, 0.2 mmol) and stirred for 12 h at 50 °C. The reaction mixture was concentrated under reduced pressure and co-evaporated with toluene and the resulting crude product was purified by column chromatography (30% EtOAc in hexanes) to afford **455** (5.2 mg, 89%) as a colorless viscous liquid:

$^1$H NMR (400 MHz, $CDCl_3$) $\delta$ 5.32–5.25 (m, 2H), 5.18 (d, $J$ = 3.3, 7.5 Hz, 1H), 5.08–5.02 (m, 1H), 4.56 (ddd, $J$ = 4.4, 9.7, 47.5 Hz, 1H), 4.49 (ddd, $J$ = 4.4, 9.7, 47.1 Hz, 1H), 2.37 (m, 1H), 2.09 (s, 3H), 2.06 (s, 3H), 2.05 (s, 3H), 2.04 (s, 3H), 2.05–2.01 (m, 2H).

$^{13}$C NMR (151 MHz, $CDCl_3$) $\delta$ 170.0, 170.0, 169.9, 169.7, 84.0 (d, $J$ = 171.2 Hz), 70.2, 69.6 (d, $J$ = 3.1 Hz), 69.5 (d, $J$ = 2.5 Hz), 69.4 (d, $J$ = 1.8 Hz), 35.9 (d, $J$ = 19.5 Hz), 27.6 (d, $J$ = 3.1 Hz, 21.1, 21.0, 20.9, 20.8.

$^{19}F$ NMR (377 MHz, $CDCl_3$): $\delta$ -223.9 (br s).

HRMS (ESI-TOF) *m/z*: $[M + NH_4]^+$ Calcd for $C_{15}H_{25}FNO_8$ 366.1559; Found 366.1557.

IR (neat): v 2919, 2849, 1748, 1369, 1218, 1040 $cm^{-1}$

$[\alpha]_D^{20}$ = + 12.6 (c = 0.6) in $CHCl_3$

**Preparation of alkene 456**

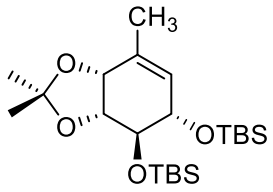


**456**

A flame-dried 50-mL flask equipped with a magnetic stirring bar, an argon inlet, and a septum was charged with vinyl bromide **424** (199 mg, 0.403 mmol) and THF (3 mL). The mixture was cooled to –55 °C using dry-ice and acetone bath, then *tert*-butyllithium (1.55 M in pentane, 410 µL, 0.636 mmol) was added dropwise. The reaction mixture was stirred at –55 °C for 30 min, then methyl iodide (0.10 mL, 1.6 mmol) was added dropwise. The dry-ice and acetone bath was removed and the reaction mixture was slowly warmed up to room temperature and stirred for 2 h. The reaction mixture was treated with saturated aq $NH_4Cl$ solution (10 mL) and extracted with $Et_2O$ (30 mL). The aqueous layer was separated and further extracted with $Et_2O$ (2 × 20 mL). The combined organic phases were washed with brine (20 mL), dried over anhydrous $Na_2SO_4$, filtered, concentrated and the resulting crude product was purified by column chromatography (2% $Et_2O$ in hexane) to afford **456** (104 mg, 60% over the two steps) as a colorless viscuous liquid:

$^1H$ NMR (500 MHz, $CDCl_3$) $\delta$ 5.36 (m, 1H), 4.42 (d, *J* = 7.0 Hz, 1H), 4.02 (m, 1H), 3.99 (m, 1H), 3.56 (m, 1H), 1.80 (s, 3 H), 1.45 (s, 3 H), 1.35 (s, 3H), 0.91 (s, 9H), 0.90 (s, 9H), 0.13 (s, 3H), 0.09 (s, 6H), 0.08 (s, 3H).

$^{13}C$ NMR (126 MHz, $CDCl_3$) $\delta$ 131.6, 129.0, 109.5, 78.8, 76.1, 75.8, 71.7, 28.0, 26.3, 26.2, 25.8, 19.9, 18.4, 18.3, –3.5, –3.7, –3.9, –4.4.

HRMS (ESI-TOF) *m/z*: $[M + H]^+$ Calcd for $C_{22}H_{45}O_4Si_2$ 429.2851; Found 429.2850.

**Preparation of alkene 458**

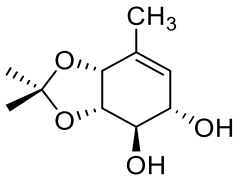


**458**

To a stirred solution of acetonide **456** (119.5 mg, 0.2787 mmol) in THF (2 mL) was added tetra-*n*-butylammonium fluoride (1.0 M in THF, 1.4 mL, 1.4 mmol) and stirred for 10 h. The reaction mixture was then treated with $H_2O$ and extracted with ethyl acetate (20 mL). The aqueous layer was separated and further extracted with EtOAc (2 × 20 mL). The combined organic phases were washed with brine (10 mL), dried over anhydrous $Na_2SO_4$, filtered, concentrated and the resulting crude product was purified by column chromatography (95% EtOAc in hexane) to afford **458** (50 mg, 90%) as a colorless viscous liquid:

$^1$H NMR (500 MHz, $CDCl_3$) $\delta$ 5.50 (s, 1H), 4.42 (d, $J$ = 6.5 Hz, 1H), 4.07 (dd, $J$ = 8.9, 6.6 Hz, 1H), 4.03 (m, 1H), 3.52 (t, $J$ = 8.5 Hz, 1H), 1.82 (s, 3H), 1.48 (s, 3H), 1.37 (s, 3H).

$^{13}$C NMR (126 MHz, $CDCl_3$) $\delta$ 131.9, 128.0, 110.3, 77.7, 76.1, 75.4, 70.5, 28.3, 25.9, 20.1.

HRMS (ESI-TOF) *m/z*: $[M + H]^+$ Calcd for $C_{10}H_{17}O_4$ 201.1121; Found 201.1121.

**Preparation of protected carbafucose 459 and 460**

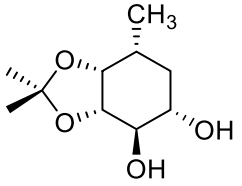


**459**

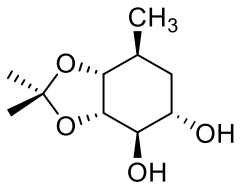


**460**

A solution of diol **458** (216 mg, 1.08 mmol) in $CH_3OH$ (6 mL) was stirred under an argon balloon. To this solution was added potassium carbonate (15 mg, 0.11 mmol) followed by $PtO_2$ (26 wt%, 56 mg, 0.25 mmol) under an argon atmosphere. The argon balloon was replaced with a $H_2$ balloon (1 atm) and the solution was flushed with $H_2$ for 10 sec.

The reaction mixture was stirred under $H_2$ balloon for 24 h and then the $H_2$ balloon was replaced with argon balloon and flushed with argon for 1 min. The reaction mixture was diluted with $CH_3OH$ (30 mL) and filtered over a pad of Celite-545. The filtrate was concentrated, and the resulting crude product was purified by column chromatography (95% EtOAc in hexane) to afford **459** (126 mg, 58%) as a colorless viscuous liquid along with D-altro isomer **460** (26 mg, 12%).

**Data for 459:**

$^1$H NMR (500 MHz, $CDCl_3$) $\delta$ 4.07 (m, 1H), 3.86 (m, 1H), 3.48 (m, 1H), 3.44 (m, 1H), 1.92 (m, 1H), 1.80–1.69 (m, 2H), 1.51 (s, 3H), 1.35 (s, 3H), 1.12 (d, $J$ = 6.9 Hz, 3H).

$^{13}$C NMR (126 MHz, $CDCl_3$) $\delta$ 109.2, 81.0, 78.6, 78.3, 71.4, 34.5, 30.0, 28.6, 26.5, 17.4.

HRMS (ESI-TOF) *m/z*: $[M + NH_4]^+$ Calcd for $C_{10}H_{22}NO_4$ 203.1278; Found 203.1275.

$[\alpha]_D^{20}$ = –64.0 (c = 0.60) in $CHCl_3$

**Preparation of carbafucose 377**

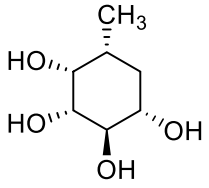


**377**

To a stirred solution of diol **459** (62.0 mg, 0.307 mmol) in $CH_3OH$ (8.3 mL) was added 1 M HCl (1.7 mL, 1.7 mmol) and stirred for 12 h. The reaction mixture was concentrated under reduced pressure and co-evaporated with toluene (3 × 3 mL) and the resulting crude product was purified by column chromatography (5% $CH_3OH$ in EtOAc) to afford **377** (42 mg, 85%) as a white solid.

$^1$H NMR (600 MHz, $CD_3OD$) $\delta$ 3.68 (brs, 1H), 3.48–3.45 (m, 1H), 3.39–3.35 (m, 1H), 3.27 (dd, $J$ = 9.6, 3.0 Hz, 1H), 1.65–1.60 (m, 1H), 1.57–1.48 (m, 2H), 1.02 (d, $J$ = 6.8 Hz, 3H).

$^{13}$C NMR (151 MHz, $CD_3OD$): $\delta$ 76.5, 76.4, 74.9, 73.8, 35.8, 33.1, 17.8.

IR (neat): v 3368, 2958, 2928, 2857, 1731, 1668, 1462, 1261, 1067, 1022, 799 cm$^{-1}$

HRMS (ESI-TOF) *m/z*: $[M + Na]^+$ Calcd for $C_7H_{14}NaO_4$ 185.0784; Found 185.0784.

$[\alpha]_D^{20}$ = +22.3 (c = 0.05) in $CH_3OH$

**Preparation of peracetylated carbafucose 461**

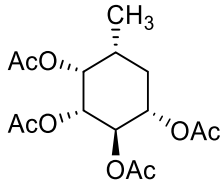


**461**

To a stirred solution of diol **377** (6 mg, 29 µmol) in $CH_3OH$ (1 mL) was added 1 M HCl (0.2 mL, 0.4 mmol) and stirred for 12 h. The reaction mixture was concentrated under reduced pressure and co-evaporated with toluene (3 × 2 mL) and the resulting crude product was dissolved in pyridine (1 mL). $Ac_2O$ (0.10 mL, 1.1 µmol) was added and heated at 50 °C for 12 h. The reaction mixture was concentrated under reduced pressure and co-evaporated with toluene (3 × 2 mL) and the resulting crude product was purified by column chromatography (20% EtOAc in hexane) to afford **461** (7.8 mg, 80% over the two steps) as a white solid:

$^1H$ NMR (500 MHz, $CDCl_3$) $\delta$ 5.36 (t, *J* = 10.1 Hz, 1H), 5.31 (m, 1H), 4.92–4.86 (m, 2H), 2.14 (s, 3H), 2.03 (s, 3H), 2.02 (s, 3H), 1.97 (s, 3H), 1.92 (m, 1H), 1.89 (m, 1H), 1.64 (m, 1H).

HRMS (ESI-TOF) *m/z*: $[M + NH_4]^+$ Calcd for $C_{15}H_{26}NO_8$ 348.1653; Found 348.1650.

$[\alpha]_D^{20}$ = –10.4 (c = 0.26) in $CHCl_3$

# References


(1) Siegel, R. L.; Miller, K. D.; Jemal, A. Cancer Statistics, 2015. *Ca-Cancer J. Clin* **2015**, *65* (1), 5–29.

(2) Why are cancer rates increasing? - Cancer Research UK - Cancer news https://news.cancerresearchuk.org/2015/02/04/why-are-cancer-rates-increasing/ (accessed 2021 -08 -23).

(3) White, M. C.; Holman, D. M.; Boehm, J. E.; Peipins, L. A.; Grossman, M.; Jane Henley, S. Age and Cancer Risk. *Am. J. Prev. Med.* **2014**, *46* (3), 7–15.

(4) Silvester, K. R.; Cummings, J. H. Does Digestibility of Meat Protein Help Explain Large Bowel Cancer Risk? *Nutr. Cancer* **1995**, *24* (3), 279–288.

(5) Manne, S. L.; Coups, E. J.; Jacobsen, P. B.; Ming, M.; Heckman, C. J.; Lessin, S. Sun Protection and Sunbathing Practices Among At-Risk Family Members of Patients with Melanoma. *BMC Public Health* **2011**, *11* (1), 122–132.

(6) GBD Results Tool | GHDx http://ghdx.healthdata.org/gbd-results-tool (accessed 2021 -09 -11).

(7) Sung, H.; Ferlay, J.; Siegel, R. L.; Laversanne, M.; Soerjomataram, I.; Jemal, A.; Bray, F. Global Cancer Statistics 2020: Globocan Estimates of Incidence and Mortality Worldwide for 36 Cancers in 185 Countries. *Ca-Cancer J. Clin* **2021**, *71* (3), 209–249.

(8) Cancer - Our World in Data https://ourworldindata.org/cancer (accessed 2021 -09 -09).

(9) Brenner, D. R.; Weir, H. K.; Demers, A. A.; Ellison, L. F.; Louzado, C.; Shaw, A.; Turner, D.; Woods, R. R.; Smith, L. M. Projected Estimates of Cancer in Canada in 2020. *Can. Med. Assoc. J.* **2020**, *192* (9), 199–205.

(10) Jemal, A.; Ward, E. M.; Johnson, C. J.; Cronin, K. A.; Ma, J.; Ryerson, A. B.; Mariotto, A.; Lake, A. J.; Wilson, R.; Sherman, R. L.; Anderson, R. N.; Henley, S. J.; Kohler, B. A.; Penberthy, L.; Feuer, E. J.; Weir, H. K. Annual Report to the Nation on the Status of Cancer, 1975–2014, Featuring Survival. *J. Natl. Cancer Inst.* **2017**, *109* (9), 1–22.

(11) Miller, K. D.; Nogueira, L.; Mariotto, A. B.; Rowland, J. H.; Yabroff, K. R.; Alfano, C. M.; Jemal, A.; Kramer, J. L.; Siegel, R. L. Cancer Treatment and Survivorship Statistics, 2019. *Ca-Cancer J. Clin* **2019**, *69* (5), 363–385.

(12) Hollingsworth, R. E.; Jansen, K. Turning the Corner on Therapeutic Cancer Vaccines. *NPJ Vaccines* **2019**, *4* (1), 7–16.

(13) Kaufmann, S. H. E. Paul Ehrlich: Founder of Chemotherapy. *Nat. Rev. Drug Discov.* **2008**, *7* (5), 373.

(14) Androutsos, G. Paul Ehrlich (1854-1915): Founder of Chemotherapy and Pioneer of Haematology, Immunology and Oncology. *J BUON* **2004**, *9*, 485–491.

(15) DeVita, V. T.; Chu, E. A History of Cancer Chemotherapy. *Cancer Res.* **2008**, *68* (21), 8643–8653.

(16) Spurr, Charles. L.; Smith, Taylor. R.; Block, M.; Jacobson, Leon. O. The Role of Nitrogen Mustard Therapy in the Treatment of Lymphomas and Leukemias. *Am. J. Med.* **1950**, *8* (6), 710–723.

(17) Al-Anazi, K. A.; Eltayeb, K. I.; Bakr, M.; Al-Mohareb, F. I. Methotrexate-Induced Acute Leukemia: Report of Three Cases and Review of the Literature. *Clin.* **2009**, *2*, 43–49.

(18) Munshi, P. N.; Lubin, M.; Bertino, J. R. 6-Thioguanine: A Drug with Unrealized Potential for Cancer Therapy. *Oncologist* **2014**, *19* (7), 760–765.

(19) Longley, D. B.; Harkin, D. P.; Johnston, P. G. 5-Fluorouracil: Mechanisms of Action and Clinical Strategies. *Nat. Rev. Cancer* **2003**, *3* (5), 330–338.

(20) Noble, R. L.; Beer, C. T.; Cutts, J. H. Role of Chance Observations in Chemotherapy: Vinca Rosea. *Ann. N. Y. Acad. Sci.* **1958**, *76* (3), 882–894.

(21) Vanchieri, C. National Cancer Act: A Look Back and Forward. *J. Natl. Cancer Inst.* **2007**, *99* (5), 342–345.

(22) Martin, V. Overview of Paclitaxel (Taxol®). *Semin* **1993**, *9* (4), 2–5.

(23) Research Areas: Treatment - National Cancer Institute https://www.cancer.gov/research/areas/treatment (accessed 2021 -08 -23).

(24) Wei, N.; Liang, J.; Peng, S.; Sun, Q.; Dai, Q.; Dong, M. Design, Synthesis, and Biological Evaluation of Axitinib Derivatives. *Molecules* **2018**, *23* (4), 747–757.

(25) Xiao, G.; Kue, P.; Bhosle, R.; Bargonetti, J. Decarbamoyl Mitomycin C (DMC) Activates P53-Independent Ataxia Telangiectasia and Rad3 Related Protein (ATR) Chromatin Eviction. *Cell Cycle* **2015**, *14* (5), 744–754.

(26) De Lathouder, S.; Gerards, A. H.; Dijkmans, B. A. C.; Aarden, L. A. Two Inhibitors of DNA-Synthesis Lead to Inhibition of Cytokine Production via a Different Mechanism. *Nucleosides Nucleotides Nucleic Acids* **2004**, *23* (8), 1089–1100.

(27) Uchida, Y.; Itoh, M.; Taguchi, Y.; Yamaoka, S.; Umehara, H.; Ichikawa, S.; Hirabayashi, Y.; Holleran, W. M.; Okazaki, T. Ceramide Reduction and Transcriptional Up-Regulation of Glucosylceramide Synthase through Doxorubicin-Activated Sp1 in Drug-Resistant HL-60/ADR Cells. *Cancer Res.* **2004**, *64* (17), 6271–6279.

(28) Villicaña, C.; Cruz, G.; Zurita, M. The Basal Transcription Machinery as a Target for Cancer Therapy. *Cancer Cell Int* **2014**, *14* (1), 18–32.

(29) Sainsbury, R. Aromatase Inhibition in the Treatment of Advanced Breast Cancer: Is There a Relationship between Potency and Clinical Efficacy? *Br. J. Cancer.* **2004**, *90* (9), 1733–1739.

(30) Fujita, Y.; Morinobu, S.; Takei, S.; Fuchikami, M.; Matsumoto, T.; Yamamoto, S.; Yamawaki, S. Vorinostat, a Histone Deacetylase Inhibitor, Facilitates Fear Extinction and Enhances Expression of the Hippocampal NR2B-Containing NMDA Receptor Gene. *J Psychiatr Res.* **2012**, *46* (5), 635–643.

(31) Hüsemann, L. C.; Reese, A.; Radine, C.; Piekorz, R. P.; Budach, W.; Sohn, D.; Jänicke, R. U. The Microtubule Targeting Agents Eribulin and Paclitaxel Activate Similar Signaling Pathways and Induce Cell Death Predominantly in a Caspase-Independent Manner. *Cell Cycle* **2020**, *19* (4), 464–478.

(32) Dobosz, P.; Dzieciątkowski, T. The Intriguing History of Cancer Immunotherapy. *Front. Immunol.* **2019**, *10*, 2965–2974.

(33) Wiemann, B.; Starnes, C. O. Coley's Toxins, Tumor Necrosis Factor and Cancer Research: A Historical Perspective. *Pharmacol. Ther.* **1994**, *64* (3), 529–564.

(34) Decker, W. K.; Safdar, A. Bioimmunoadjuvants for the Treatment of Neoplastic and Infectious Disease: Coley's Legacy Revisited. *Cytokine Growth Factor Rev.* **2009**, *20* (4), 271–281.

(35) Morales, A.; Eidinger, D.; Bruce, A. W. Intracavitary Bacillus Calmette-Guerin in the Treatment of Superficial Bladder Tumors. *J. Urol.* **2017**, *197*, 142–145.

(36) Ribatti, D. The Concept of Immune Surveillance Against Tumors: The First Theories. *Oncotarget* **2017**, *8* (4), 7175–7180.

(37) Dunn, G. P.; Bruce, A. T.; Ikeda, H.; Old, L. J.; Schreiber, R. D. Cancer Immunoediting: From Immunosurveillance to Tumor Escape. *Nat. Immunol.* **2002**, *3* (11), 991–998.

(38) Rosenberg, S. A.; Lotze, M. T.; Muul, L. M.; Leitman, S.; Chang, A. E.; Ettinghausen, S. E.; Matory, Y. L.; Skibber, J. M.; Shiloni, E.; Vetto, J. T.; Seipp, C. A.; Simpson, C.; Reichert, C. M. Observations on the Systemic Administration of Autologous Lymphokine-Activated Killer Cells and Recombinant Interleukin-2 to Patients with Metastatic Cancer. *N. Engl. J. Med.* **1985**, *313* (23), 1485–1492.

(39) Milstein, C. The Hybridoma Revolution: An Offshoot of Basic Research. *Bioessays* **1999**, *21*, 966–973.

(40) Cheever, M. A.; Higano, C. S. Provenge (Sipuleucel-T) in Prostate Cancer: The First Fda-Approved Therapeutic Cancer Vaccine. *Clin. Cancer Res.* **2011**, *17* (11), 3520–3526.

(41) Bagchi, S.; Yuan, R.; Engleman, E. G. Immune Checkpoint Inhibitors for the Treatment of Cancer: Clinical Impact and Mechanisms of Response and Resistance. *Annu. Rev. Pathol.* **2021**, *16* (1), 223–249.

(42) Tran, E.; Robbins, P. F.; Lu, Y.-C.; Prickett, T. D.; Gartner, J. J.; Jia, L.; Pasetto, A.; Zheng, Z.; Ray, S.; Groh, E. M.; Kriley, I. R.; Rosenberg, S. A. T-Cell Transfer Therapy Targeting Mutant Kras in Cancer. *N. Engl. J. Med.* **2016**, *375* (23), 2255–2262.

(43) Peng, M.; Mo, Y.; Wang, Y.; Wu, P.; Zhang, Y.; Xiong, F.; Guo, C.; Wu, X.; Li, Y.; Li, X.; Li, G.; Xiong, W.; Zeng, Z. Neoantigen Vaccine: An Emerging Tumor Immunotherapy. *Mol. Cancer* **2019**, *18* (1), 128–141.

(44) Badiu, D. C.; Zgura, A.; Gales, L.; Iliescu, L.; Anghel, R.; Haineala, B. Modulation of Immune System – Strategy in the Treatment of Breast Cancer. *In Vivo* **2021**, *35* (5), 2889–2894.

(45) Akdis, M.; Aab, A.; Altunbulakli, C.; Azkur, K.; Costa, R. A.; Crameri, R.; Duan, S.; Eiwegger, T.; Eljaszewicz, A.; Ferstl, R.; Frei, R.; Garbani, M.; Hess, L.; Huitema, C.; Kubo, T.; Komlosi, Z.; Konieczna, P.; Kovacs, N.; Kucuksezer, U. C.; Meyer, N. Interleukins (from Il-1 to Il-38), Interferons, Transforming Growth Factor B, and Tnf-A: Receptors, Functions, and Roles in Diseases. *J. Allergy Clin. Immunol.* **2016**, *138* (4), 984–1010.

(46) Moore, M. A. S. Hematopoietic Growth Factors in Cancer. *Cancer* **1990**, *65* (3), 836–844.

(47) Erythropoietin | Hormone Health Network https://www.hormone.org/your-health-and-hormones/glands-and-hormones-a-to-z/hormones/erythropoietin (accessed 2021 -08 -24).

(48) Cardier, J. E.; Balogh, V.; Perez-Silva, C.; Romano, E.; Rivas, B.; Bosch, N.; Rothman, A. L. Relationship of Thrombopoietin and Interleukin-11 Levels to Thrombocytopenia Associated with Dengue Disease. *Cytokine* **2006**, *34* (3), 155–160.

(49) Lee, J.-H.; Kim, N.-S.; Kwon, T.-H.; Jang, Y.-S.; Yang, M.-S. Increased Production of Human Granulocyte-Macrophage Colony Stimulating Factor (Hgm-Csf) by the Addition of Stabilizing Polymer in Plant Suspension Cultures. *J. Biotechnol* **2002**, *96* (3), 205–211.

(50) Xue, D.; Hsu, E.; Fu, Y.-X.; Peng, H. Next-Generation Cytokines for Cancer Immunotherapy. *Antib. Ther.* **2021**, *4* (2), 123–133.

(51) Borchardt, John. K. The Beginnings of Drug Therapy: Ancient Mesopotamian Medicine. *Drug News Perspect.* **2002**, *15* (3), 187–192.

(52) Chan, K. The Pharmacology of Chinese Herbs. *J. Pharm. Pharmacol* **2011**, *46* (2), 159–160.

(53) Ekor, M. The Growing Use of Herbal Medicines: Issues Relating to Adverse Reactions and Challenges in Monitoring Safety. *Front. Pharmacol.* **2014**, *4*, 1–10.

(54) Malakoff, D. Extinction on the High Seas. *Science* **1997**, *277* (5325), 486–488.

(55) Khalifa, S. A. M.; Elias, N.; Farag, M. A.; Chen, L.; Saeed, A.; Hegazy, M.-E. F.; Moustafa, M. S.; Abd El-Wahed, A.; Al-Mousawi, S. M.; Musharraf, S. G.; Chang, F.-R.; Iwasaki, A.; Suenaga, K.; Alajlani, M.; Göransson, U.; El-Seedi, H. R. Marine Natural Products: A Source of Novel Anticancer Drugs. *Mar. Drugs* **2019**, *17* (9), 491–521.

(56) Scriabine, A.; Landau, R.; Achilladelis, B. Discovery and Development of Major Drugs Currently in Use. *J. Pharm. Innov* **1999**, 148–270.

(57) Buss, A. D.; Waigh, R. D. Natural Products as Leads for New Pharmaceuticals. *Burger's medicinal chemistry and drug discovery. Principles and practice, vol. 1, John Wiley & Sons, Inc., New York, NY* **1995**, 983–1033.

(58) Newman, D. J.; Cragg, G. M. Natural Products as Sources of New Drugs Over the 30 Years from 1981 to 2010. *J. Nat. Prod.* **2012**, *75* (3), 311–335.

(59) Koehn, F. E.; Carter, G. T. The Evolving Role of Natural Products in Drug Discovery. *Nat. Rev. Drug Discov.* **2005**, *4* (3), 206–220.

(60) Corbett, P. T.; Leclaire, J.; Vial, L.; West, K. R.; Wietor, J.-L.; Sanders, J. K. M.; Otto, S. Dynamic Combinatorial Chemistry. *Chem. Rev.* **2006**, *106* (9), 3652–3711.

(61) Von Nussbaum, F.; Brands, M.; Hinzen, B.; Weigand, S.; Häbich, D. Antibacterial Natural Products in Medicinal Chemistry—Exodus or Revival? *Angew. Chem. Int. Ed.* **2006**, *45* (31), 5072–5129.

(62) Pye, C. R.; Bertin, M. J.; Lokey, R. S.; Gerwick, W. H.; Linington, R. G. Retrospective Analysis of Natural Products Provides Insights for Future Discovery Trends. *Proc. Natl. Acad. Sci. U.S.A.* **2017**, *114* (22), 5601–5606.

(63) Borman, S. Organic Lab Sparks Drug Discovery. *Chem. Eng. News* **2002**, *80* (2), 23–36.

(64) Thomas, A.; Teicher, B. A.; Hassan, R. Antibody–Drug Conjugates for Cancer Therapy. *Lancet Oncol.* **2016**, *17* (6), 254–262.

(65) Carter, P. J.; Lazar, G. A. Next Generation Antibody Drugs: Pursuit of the "High-Hanging Fruit." *Nat. Rev. Drug Discov.* **2018**, *17* (3), 197–223.

(66) Diamantis, N.; Banerji, U. Antibody-Drug Conjugates—an Emerging Class of Cancer Treatment. *Br. J. Cancer* **2016**, *114* (4), 362–367.

(67) Chau, C. H.; Steeg, P. S.; Figg, W. D. Antibody–Drug Conjugates for Cancer. *Lancet Oncol.* **2019**, *394* (10200), 793–804.

(68) Lindel, T.; Jensen, P. R.; Fenical, W.; Long, B. H.; Casazza, A. M.; Carboni, J.; Fairchild, C. R. Eleutherobin, a New Cytotoxin That Mimics Paclitaxel (Taxol) by Stabilizing Microtubules. *J. Am. Chem. Soc.* **1997**, *119* (37), 8744–8745.

(69) Fenical, W. H.; Mar, D.; Diego, S.; Lindel, T. *The Regents of the University of California*, Eleutherobin and Analogs Thereof. 5,473,057, 1995.

(70) Nicolaou, K. C.; van Delft, F.; Ohshima, T.; Vourloumis, D.; Xu, J.; Hosokawa, S.; Pfefferkorn, J.; Kim, S.; Li, T. Total Synthesis of Eleutherobin. *Angew. Chem. Int. Ed. Engl.* **1997**, *36* (22), 2520–2524.

(71) Chen, X.-T.; Bhattacharya, S. K.; Zhou, B.; Gutteridge, C. E.; Pettus, T. R. R.; Danishefsky, S. J. The Total Synthesis of Eleutherobin. *J. Am. Chem. Soc.* **1999**, *121* (28), 6563–6579.

(72) Castoldi, D.; Caggiano, L.; Panigada, L.; Sharon, O.; Costa, A. M.; Gennari, C. A Formal Total Synthesis of Eleutherobin Through an Unprecedented Kinetically Controlled Ring-Closing-Metathesis Reaction of a Densely Functionalized Diene. *Angew. Chem. Int. Ed.* **2005**, *44* (4), 588–591.

(73) Chang, S.; Holmes, M.; Mowat, J.; Meanwell, M.; Britton, R. A-Arylation and Ring Expansion of Annulated Cyclobutanones: Stereoselective Synthesis of Functionalized Tetralones. *Angew. Chem. Int. Ed.* **2017**, *56* (3), 748–752.

(74) Wade, R. H. On and Around Microtubules: An Overview. *Mol. Biotechnol.* **2009**, *43* (2), 177–191.

(75) Xiao, H.; Verdier-Pinard, P.; Fernandez-Fuentes, N.; Burd, B.; Angeletti, R.; Fiser, A.; Horwitz, S. B.; Orr, G. A. Insights into the Mechanism of Microtubule Stabilization by Taxol. *Proc. Natl. Acad. Sci. U.S.A.* **2006**, *103* (27), 10166–10173.

(76) Sirajuddin, M.; Rice, L. M.; Vale, R. D. Regulation of Microtubule Motors by Tubulin Isotypes and Post-Translational Modifications. *Nat. Cell Biol.* **2014**, *16* (4), 335–344.

(77) Bodakuntla, S.; Jijumon, A. S.; Villablanca, C.; Gonzalez-Billault, C.; Janke, C. Microtubule-Associated Proteins: Structuring the Cytoskeleton. *Trends Cell Biol.* **2019**, *29* (10), 804–819.

(78) Waterman-Storer, C. M.; Salmon, E. D. Microtubule Dynamics: Treadmilling Comes Around Again. *Curr. Biol.* **1997**, *7* (6), 369–372.

(79) Mitchison, T.; Kirschner, M. Dynamic Instability of Microtubule Growth. *Nature* **1984**, *312* (5991), 237–242.

(80) Wilson, L.; Jordan, M. A. Microtubule Dynamics: Taking Aim at a Moving Target. *Chem. Biol.* **1995**, *2* (9), 569–573.

(81) Panda, D.; Miller, H. P.; Wilson, L. Rapid Treadmilling of Brain Microtubules Free of Microtubule-Associated Proteins in Vitro and Its Suppression by Tau. *Proc. Natl. Acad. Sci. U.S.A.* **1999**, *96* (22), 12459–12464.

(82) Margolis, R. L.; Wilson, L. Microtubule Treadmilling: What Goes Around Comes Around. *Bioessays* **1998**, *20*, 830–836.

(83) Rusan, N. M.; Fagerstrom, C. J.; Yvon, A.-M. C.; Wadsworth, P. Cell Cycle-Dependent Changes in Microtubule Dynamics in Living Cells Expressing Green Fluorescent Protein-α Tubulin. *Mol. Biol. Cell* **2001**, *12*, 971–980.

(84) Sacristan, C.; Ahmad, M. U. D.; Keller, J.; Fermie, J.; Groenewold, V.; Tromer, E.; Fish, A.; Melero, R.; Carazo, J. M.; Klumperman, J.; Musacchio, A.; Perrakis, A.; Kops, G. J. Dynamic Kinetochore Size Regulation Promotes Microtubule Capture and Chromosome Biorientation in Mitosis. *Nat. Cell Biol.* **2018**, *20* (7), 800–810.

(85) Saxton, W. M.; Stemple, D. L.; Leslie, R. J.; Salmon, E. D.; Zavortink, M.; McIntosh, J. R. Tubulin Dynamics in Cultured Mammalian Cells. *J. Cell Biol.* **1984**, *99* (6), 2175–2186.

(86) The Development and Causes of Cancer - The Cell - NCBI Bookshelf https://www.ncbi.nlm.nih.gov/books/NBK9963/ (accessed 2021 -09 -28).

(87) Jordan, M. A.; Wilson, L. Microtubules as a Target for Anticancer Drugs. *Nat. Rev. Cancer* **2004**, *4* (4), 253–265.

(88) *Tubulin-Binding Agents*; Carlomagno, T., Ed.; Topics in Current Chemistry; Springer: Berlin, Heidelberg, **2009,** Vol. 286.

(89) Cormier, A.; Knossow, M.; Wang, C.; Gigant, B. The Binding of Vinca Domain Agents to Tubulin. In *Methods in Cell Biology*; Elsevier, **2010**, 373–390.

(90) Nogales, E.; Grayer Wolf, S.; Khan, I. A.; Ludueña, R. F.; Downing, K. H. Structure of Tubulin at 6.5Å and Location of the Taxol-Binding Site. *Nature* **1995**, *375* (6530), 424–427.

(91) Dorleans, A.; Gigant, B.; Ravelli, R. B. G.; Mailliet, P.; Mikol, V.; Knossow, M. Variations in the Colchicine-Binding Domain Provide Insight into the Structural Switch of Tubulin. *Proc. Natl. Acad. Sci. U.S.A.* **2009**, *106* (33), 13775–13779.

(92) Lee, J. J.; Swain, S. M. The Epothilones: Translating from the Laboratory to the Clinic. *Clin. Cancer Res.* **2008**, *14* (6), 1618–1624.

(93) Ambudkar, S. V.; Kimchi-Sarfaty, C.; Sauna, Z. E.; Gottesman, M. M. P-Glycoprotein: From Genomics to Mechanism. *Oncogene* **2003**, *22* (47), 7468–7485.

(94) Mukhtar, E.; Adhami, V. M.; Mukhtar, H. Targeting Microtubules by Natural Agents for Cancer Therapy. *Mol. Cancer Ther.* **2014**, *13* (2), 275–284.

(95) Nanayakkara, A. K.; Follit, C. A.; Chen, G.; Williams, N. S.; Vogel, P. D.; Wise, J. G. Targeted Inhibitors of P-Glycoprotein Increase Chemotherapeutic-Induced Mortality of Multidrug Resistant Tumor Cells. *Sci. Rep.* **2018**, *8* (1), 967–984.

(96) Thomas, H.; Coley, H. M. Overcoming Multidrug Resistance in Cancer: An Update on the Clinical Strategy of Inhibiting P-Glycoprotein. *Cancer Control* **2003**, *10* (2), 159–165.

(97) Safa, A. Identification and Characterization of the Binding Sites of P-Glycoprotein for Multidrug Resistance-Related Drugs and Modulators. *Curr. Med. Chem. Anticancer Agents* **2004**, *4* (1), 1–17.

(98) Kavallaris, M.; Tait, A. S.; Walsh, B. J.; He, L.; Horwitz, S. B.; Norris, M. D.; Haber, M. Multiple Microtubule Alterations Are Associated with Vinca Alkaloid Resistance in Human Leukemia Cells. *Cancer Res. 61*, 5803–5810.

(99) Giannakakou, P.; Gussio, R.; Nogales, E.; Downing, K. H.; Zaharevitz, D.; Bollbuck, B.; Poy, G.; Sackett, D.; Nicolaou, K. C.; Fojo, T. A Common Pharmacophore for Epothilone and Taxanes: Molecular Basis for Drug Resistance Conferred by Tubulin Mutations in Human Cancer Cells. *Proc. Natl. Acad. Sci. U.S.A.* **2000**, *97* (6), 2904–2909.

(100) Čermák, V.; Dostál, V.; Jelínek, M.; Libusová, L.; Kovář, J.; Rösel, D.; Brábek, J. Microtubule-Targeting Agents and Their Impact on Cancer Treatment. *Eur. J. Cell Biol.* **2020**, *99* (4), 151075–151088.

(101) Benbow, S. J.; Wozniak, K. M.; Kulesh, B.; Savage, A.; Slusher, B. S.; Littlefield, B. A.; Jordan, M. A.; Wilson, L.; Feinstein, S. C. Microtubule-Targeting Agents Eribulin and Paclitaxel Differentially Affect Neuronal Cell Bodies in Chemotherapy-Induced Peripheral Neuropathy. *Neurotox. Res.* **2017**, *32* (1), 151–162.

(102) Stierle, D. B.; Carte, B.; Faulkner, D. J.; Tagle, B.; Clardy, J. The Asbestinins, a Novel Class of Diterpenes from the Gorgonian Briareum Asbestinum. *J. Am. Chem. Soc.* **1980**, *102* (15), 5088–5092.

(103) Ellis, J. M.; Crimmins, M. T. Strategies for the Total Synthesis of C2−C11 Cyclized Cembranoids. *Chem. Rev.* **2008**, *108* (12), 5278–5298.

(104) Lin', Y.; Bewley, C. A.; Faulkner, D. J. The Valdivones, Anti-Inflammatory Diterpene Esters from the South African Soft Coral Akyonium Vaklivae. *Tetrahedron* **1993**, *49* (36), 7977–7984.

(105) D'Ambrosio, M.; Guerriero, A.; Pietra, F. Sarcodictyin a and Sarcodictyin B, Novel Diterpenoidic Alcohols Esterified by (e)-N(1)-Methylurocanic Acid. Isolation from the Mediterranean Stolonifersarcodictyon Roseum. *Helv. Chim. Acta* **1987**, *70* (8), 2019–2027.

(106) Ketzinel, S.; Rudi, A.; Schleyer, M.; Benayahu, Y.; Kashman, Y. Sarcodictyin A and Two Novel Diterpenoid Glycosides, Eleuthosides a and B, from the Soft Coral Eleutherobia Aurea. *J. Nat. Prod.* **1996**, *59* (9), 873–875.

(107) Long, B. H.; Carboni, J. M.; Wasserman, A. J.; Cornell, L. A.; Casazza, A. M.; Jensen, P. R.; Lindel, T.; Fenica, W.; Fairchild, C. R. Eleutherobin, a Novel Cytotoxic Agent That Induces Tubulin Polymerization, Is Similar to Paclitaxel (Taxol®). *Cancer Res.* **1998**, *58*, 1111–1115.

(108) Cinel, B.; Roberge, M.; Behrisch, H.; van Ofwegen, L.; Castro, C. B.; Andersen, R. J. Antimitotic Diterpenes from Erythropodium Aribaeorum Test Pharmacophore Models for Microtubule Stabilization. *Org. Lett.* **2000**, *2* (3), 257–260.

(109) Britton, R.; de Silva, E. D.; Bigg, C. M.; McHardy, L. M.; Roberge, M.; Andersen, R. J. Synthetic Transformations of Eleutherobin Reveal New Features of Its Microtubule-Stabilizing Pharmacophore. *J. Am. Chem. Soc.* **2001**, *123* (35), 8632–8633.

(110) Nicolaou, K. C.; Xu, J. Y.; Kim, S.; Pfefferkorn, J.; Ohshima, T.; Vourloumis, D.; Hosokawa, S. Total Synthesis of Sarcodictyins A and B. *J. Am. Chem. Soc.* **1998**, *120* (34), 8661–8673.

(111) Chen, X.-T.; Gutteridge, C. E.; Zhou, B.; Pettus, T. R. R.; Hascall, T.; Danishefsky, S. J. A Convergent Route for the Total Synthesis of the Eleuthesides. *Angew. Chem. Int. Ed.* **1998**, *37* (1), 185–186.

(112) Chen, X.-T.; Zhou, B.; Bhattacharya, S. K.; Gutteridge, C. E.; Pettus, T. R. R.; Danishefsky, S. J. The Total Synthesis of Eleutherobin: A Surprise Ending. *Angew. Chem. Int. Ed.* **1998**, *110*, 831–834.

(113) Hafner, A.; Duthaler, R. O.; Marti, R.; Rihs, G.; Rothe-Streit, P.; Schwarzenbach, F. Enantioselective Syntheses with Titanium Carbohydrate Complexes. *J. Am. Chem. Soc.* **1992**, *114* (7), 2321–2336.

(114) McDaid, H. M.; Chen, X.-T.; Gutteridge, C. E.; Danishefsky, S. J. Structure-Activity Profiles of Eleutherobin Analogs and Their Cross-Resistance in Taxol-Resistant Cell Lines. *Cancer Chemother. Pharmacol.* **1999**, *44*, 131–137.

(115) Nicolaou, K. C.; Winssinger, N.; Vourloumis, D.; Ohshima, T.; Kim, S.; Pfefferkorn, J.; Xu, J.-Y.; Li, T. Solid and Solution Phase Synthesis and Biological Evaluation of Combinatorial Sarcodictyin Libraries. *J. Am. Chem. Soc.* **1998**, *120* (42), 10814–10826.

(116) Hamel, E.; Sackett, D. L.; Vourloumis, D.; Nicolaou, K. C. The Coral-Derived Natural Products Eleutherobin and Sarcodictyins a and B: Effects on the Assembly of Purified Tubulin with and Without Microtubule-Associated Proteins and Binding at the Polymer Taxoid Site. *Biochemistry* **1999**, *38* (17), 5490–5498.

(117) Britton, R.; Roberge, M.; Berisch, H.; Andersen, R. J. Antimitotic Diterpenoids from Erythropodium Caribaeorum: Isolation Artifacts and Putative Biosynthetic Intermediates. *Tetrahedron Lett.* **2001**, *42* (16), 2953–2956.

(118) Cinel, B.; Patrick, B. O.; Roberge, M.; Andersen, R. J. Solid-State and Solution Conformations of Eleutherobin Obtained from X-Ray Diffraction Analysis and Solution Noe Data. *Tetrahedron Lett.* **2000**, *41* (16), 2811–2815.

(119) Grasa, G. A.; Colacot, T. J. α-Arylation of Ketones Using Highly Active, Air-Stable (DtBPF)$PdX_2$ (X = Cl, Br) Catalysts. *Org. Lett.* **2007**, *9* (26), 5489–5492.

(120) Mehta, G.; Venkateswaran, R. V. Haller–Bauer Reaction Revisited: Synthetic Applications of a Versatile C–C Bond Scission Reaction. *Tetrahedron* **2000**, *56* (11), 1399–1422.

(121) Hirasawa, S.; Cho, M.; Brust, T. F.; Roach, J. J.; Bohn, L. M.; Shenvi, R. A. O6c-20-nor-Salvinorin a Is a Stable and Potent Kor Agonist. *Bioorg. Med. Chem. Lett.* **2018**, *28* (16), 2770–2772.

(122) Prantz, K.; Mulzer, J. Synthetic Applications of the Carbonyl Generating Grob Fragmentation. *Chem. Rev.* **2010**, *110* (6), 3741–3766.

(123) Hook, J. M.; Mander, L. N. Recent Developments in the Birch Reduction of Aromatic Compounds: Applications to the Synthesis of Natural Products. *Nat. Prod. Rep.* **1986**, *3*, 35.

(124) Carvalho, J. F. S.; Silva, M. M. C.; Sá e Melo, M. L. Highly Efficient Epoxidation of Unsaturated Steroids Using Magnesium Bis(Monoperoxyphthalate) Hexahydrate. *Tetrahedron* **2009**, *65* (14), 2773–2781.

(125) Grainger, W. S.; Parish, E. J. Allylic Oxidation of Steroidal Olefins by Vanadyl Acetylacetonate and Tert-Butyl Hydroperoxide. *Steroids* **2015**, *101*, 103–109.

(126) Shabashov, D.; Doyle, M. P. Rhodium Acetate-Catalyzed Aerobic Mukaiyama Epoxidation of Alkenes. *Tetrahedron* **2013**, *69* (47), 10009–10013.

(127) Kamata, K.; Nakagawa, Y.; Yamaguchi, K.; Mizuno, N. Efficient, Regioselective Epoxidation of Dienes with Hydrogen Peroxide. *J. Catal.* **2004**, *224* (1), 224–228.

(128) Morton, D.; Dick, A. R.; Ghosh, D.; Davies, H. M. L. Convenient Method for the Functionalization of the 4- and 6-Positions of the Androgen Skeleton. *Chem. Commun.* **2012**, *48* (47), 5838–5840.

(129) Garcia-Cabeza, A. L.; Marin-Barrios, R.; Azarken, R.; Moreno-Dorado, F. J.; Ortega, Maria. J.; Vidal, H.; Gatica, J. M.; Massanet, G. M.; Guerra, F. M. DoE (Design of Experiments) Assisted Allylic Hydroxylation of Enones Catalyzed by a Copper–Aluminium Mixed Oxide. *Eur. J. Org. Chem* **2013**, *2013* (36), 8307–8314.

(130) Jensen, F. R.; Bushweller, C. H.; Beck, B. H. Conformational Preferences in Monosubstituted Cyclohexanes Determined by Nuclear Magnetic Resonance Spectroscopy. *J. Am. Chem. Soc.* **1969**, *91* (2), 344–351.

(131) Blanchette, M. A.; Choy, W.; Davis, J. T.; Essenfeld, A. P.; Masamune, S.; Roush, W. R.; Sakai, T. Horner-Wadsworth-Emmons Reaction: Use of Lithium Chloride and an Amine for Base-Sensitive Compounds. *Tetrahedron Lett.* **1984**, *25* (21), 2183–2186.

(132) Still, I. W. J.; Drewery, M. J. Synthesis of 2-Butenolide and Tetronic Acid Analogs of Thiolactomycin. *J. Org. Chem.* **1989**, *54* (2), 290–295.

(133) Chen, J.; Ni, S.; Ma, S. Tuning of Regioselectivity in Inorganic Iodide-Catalyzed Alkylation of 2-Methoxyfurans Via Electronic and Steric Effects. *Adv. Synth. Catal.* **2012**, *354* (6), 1114–1128.

(134) Martin, M. R.; Mateo, A. I. Synthesis of Diastereoisomerically Pure 5-Substituted 5-(l-Menthyloxy)-4-(Pyrrolidin-l-Yl)Furan-(5H)-Ones. *Tetrahedron: Asymmetry* **1995**, *6* (7), 1621–1632.

(135) Bruyère, H.; Ballereau, S.; Selkti, M.; Royer, J. Asymmetric Synthesis of 5-(1-Hydroxyalkyl)-5-Methyl-5H-Furan-2-Ones. *Tetrahedron* **2003**, *59* (31), 5879–5886.

(136) Sato, M.; Sakaki, J.; Sugita, Y.; Yasuda, S.; Sakoda, H.; Kaneko, C. Two Lactone Formation Reactions from 1,3-Dioxin-4-Ones Having Hydroxyalkyl Group at the 6-Position: Difference in Ring Opening and Closure. *Tetrahedron* **1991**, *47* (30), 5689–5708.

(137) Still, W. C.; Gennari, C. Direct Synthesis of Z-Unsaturated Esters. a Useful Modification of the Horner-Emmons Olefination. *Tetrahedron Lett.* **1983**, *24* (41), 4405–4408.

(138) Huckin, S. N.; Weiler, L. Aldol Reactions of the Dianion of β-Keto Esters. *Tetrahedron Lett.* **1971**, *12* (50), 4835–4838.

(139) Placzek, A. T.; Donelson, J. L.; Trivedi, R.; Gibbs, R. A.; De, S. K. Scandium Triflate as an Efficient and Useful Catalyst for the Synthesis of β-Amino Alcohols by Regioselective Ring Opening of Epoxides with Amines Under Solvent-Free Conditions. *Tetrahedron Lett.* **2005**, *46* (52), 9029–9034.

(140) Nicolaou, K. C.; Trujillo, I.; Chibale, K. Design, Synthesis and Biological Evaluation of Carbohydrate-Based Mimetics of CRGDFV. *Tetrahedron* **1997**, *53* (26), 8751–8778.

(141) Sutton, B.; Davies, A.; Bax, H.; Karagiannis, S. IgE Antibodies: From Structure to Function and Clinical Translation. *Antibodies* **2019**, *8* (1), 19–59.

(142) Voskoboinik, I.; Whisstock, J. C.; Trapani, J. A. Perforin and Granzymes: Function, Dysfunction and Human Pathology. *Nat. Rev. Immunol.* **2015**, *15* (6), 388–400.

(143) Cobb, B. A. The History of IgG Glycosylation and Where We Are Now. *Glycobiology* **2020**, *30* (4), 202–213.

(144) Shields, R. L.; Lai, J.; Keck, R.; O'Connell, L. Y.; Hong, K.; Meng, Y. G.; Weikert, S. H. A.; Presta, L. G. Lack of Fucose on Human IgG1 N-Linked Oligosaccharide Improves Binding to Human FcγRIII and Antibody-Dependent Cellular Toxicity. *JBC* **2002**, *277* (30), 26733–26740.

(145) Nguyen Dang, A.; Mun, M.; Rose, C. M.; Ahyow, P.; Meier, A.; Sandoval, W.; Yuk, I. H. Interaction of Cell Culture Process Parameters for Modulating MAb Afucosylation. *Biotechnol. Bioeng.* **2019**, *116*, 831–845.

(146) Yamane-Ohnuki, N.; Kinoshita, S.; Inoue-Urakubo, M.; Kusunoki, M.; Iida, S.; Nakano, R.; Wakitani, M.; Niwa, R.; Sakurada, M.; Uchida, K.; Shitara, K.; Satoh, M. Establishment Of FUT8 Knockout Chinese Hamster Ovary Cells: An Ideal Host Cell Line for Producing Completely Defucosylated Antibodies with Enhanced Antibody-Dependent Cellular Cytotoxicity. *Biotechnol. Bioeng.* **2004**, *87* (5), 614–622.

(147) Giddens, J. P.; Lomino, J. V.; DiLillo, D. J.; Ravetch, J. V.; Wang, L.-X. Site-Selective Chemoenzymatic Glycoengineering of Fab and Fc Glycans of a Therapeutic Antibody. *Proc. Natl. Acad. Sci. U.S.A.* **2018**, *115* (47), 12023–12027.

(148) von Horsten, H. H.; Ogorek, C.; Blanchard, V.; Demmler, C.; Giese, C.; Winkler, K.; Kaup, M.; Berger, M.; Jordan, I.; Sandig, V. Production of Non-Fucosylated Antibodies by Co-Expression of Heterologous Gdp-6-Deoxy-D-Lyxo-4-Hexulose Reductase. *Glycobiology* **2010**, *20* (12), 1607–1618.

(149) Shalel Levanon, S.; Aharonovitz, O.; Maor-Shoshani, A.; Abraham, G.; Kenett, D.; Aloni, Y. An Efficient Method to Control High Mannose and Core Fucose Levels in Glycosylated Antibody Production Using Deoxymannojirimycin. *J. Biotechnol.* **2018**, *276–277*, 54–62.

(150) Allen, J. G.; Mujacic, M.; Frohn, M. J.; Pickrell, A. J.; Kodama, P.; Bagal, D.; San Miguel, T.; Sickmier, E. A.; Osgood, S.; Swietlow, A.; Li, V.; Jordan, J. B.; Kim, K.-W.; Rousseau, A.-M. C.; Kim, Y.-J.; Caille, S.; Achmatowicz, M.; Thiel, O.; Fotsch, C. H.; Reddy, P.; McCarter, J. D. Facile Modulation of Antibody Fucosylation with Small Molecule Fucostatin Inhibitors and Cocrystal Structure with Gdp-Mannose 4,6-Dehydratase. *ACS Chem. Biol.* **2016**, *11* (10), 2734–2743.

(151) Okeley, N. M.; Toki, B. E.; Zhang, X.; Jeffrey, S. C.; Burke, P. J.; Alley, S. C.; Senter, P. D. Metabolic Engineering of Monoclonal Antibody Carbohydrates for Antibody–Drug Conjugation. *Bioconjug. Chem.* **2013**, *24* (10), 1650–1655.

(152) Zhou, Q.; Shankara, S.; Roy, A.; Qiu, H.; Estes, S.; McVie-Wylie, A.; Culm-Merdek, K.; Park, A.; Pan, C.; Edmunds, T. Development of a Simple and Rapid Method for Producing Non-Fucosylated Oligomannose Containing Antibodies with Increased Effector Function. *Biotechnol. Bioeng.* **2008**, *99* (3), 652–665.

(153) Yu, M.; Brown, D.; Reed, C.; Chung, S.; Lutman, J.; Stefanich, E.; Wong, A.; Stephan, J.-P.; Bayer, R. Production, Characterization and Pharmacokinetic Properties of Antibodies with N-Linked Mannose-5 Glycans. *MAbs* **2012**, *4* (4), 475–487.

(154) Zimmermann, M.; Ehret, J.; Kolmar, H.; Zimmer, A. Impact of Acetylated and Non-Acetylated Fucose Analogues on IgG Glycosylation. *Antibodies* **2019**, *8* (1), 9–21.

(155) Senter, P.; Alley, S.; Benjamin, D. *Seattle Genetics Inc*, Methods of Inhibition of Protein Fucosylation in Vivo Using Fucose Analogs. WO 2012/019165 A3, 2012.

(156) Norris, A. J.; Whitelegge, J. P.; Strouse, M. J.; Faull, K. F.; Toyokuni, T. Inhibition Kinetics of Carba- and C-Fucosyl Analogues of GDP-Fucose Against Fucosyltransferase V: Implication for the Reaction Mechanism. *Bioorg. Med. Chem. Lett.* **2004**, *14* (3), 571–573.

(157) Zandberg, W. F.; Kumarasamy, J.; Pinto, B. M.; Vocadlo, D. J. Metabolic Inhibition of Sialyl-Lewis X Biosynthesis by 5-Thiofucose Remodels the Cell Surface and Impairs Selectin-Mediated Cell Adhesion. *JBC* **2012**, *287* (47), 40021–40030.

(158) Lairson, L. L.; Henrissat, B.; Davies, G. J.; Withers, S. G. Glycosyltransferases: Structures, Functions, and Mechanisms. *Annu. Rev. Biochem.* **2008**, *77* (1), 521–555.

(159) Järvå, M. A.; Dramicanin, M.; Lingford, J. P.; Mao, R.; John, A.; Jarman, K. E.; Grinter, R.; Goddard-Borger, E. D. Structural Basis of Substrate Recognition and Catalysis by Fucosyltransferase 8. *JBC* **2020**, *295* (19), 6677–6688.

(160) Bergeron-Briek, M.; Teoh, T.; Britton, R. A Tandem Organocatalytic A-Chlorination-Aldol Reaction That Proceeds with Dynamic Kinetic Resolution: A Powerful Tool for Carbohydrate Synthesis. *Org. Lett.* **2013**, *15* (14), 3554–3557.

(161) Meanwell, M.; Silverman, S. M.; Lehmann, J.; Adluri, B.; Wang, Y.; Cohen, R.; Campeau, L.-C.; Britton, R. A Short De Novo Synthesis of Nucleoside Analogs. *Science* **2020**, *369* (6504), 725–730.

(162) Banwell, M. G.; Ma, X.; Karunaratne, O. P.; Willis, A. C. A First Generation Chemoenzymatic Synthesis of (+)-Galanthamine. *Aust. J. Chem.* **2010**, *63* (10), 1437–1447.

(163) Blanco, B.; Prado, V.; Lence, E.; Otero, J. M.; Garcia-Doval, C.; van Raaij, M. J.; Llamas-Saiz, A. L.; Lamb, H.; Hawkins, A. R.; González-Bello, C. Mycobacterium Tuberculosis Shikimate Kinase Inhibitors: Design and Simulation Studies of the Catalytic Turnover. *J. Am. Chem. Soc.* **2013**, *135* (33), 12366–12376.

(164) Barrero, A. F.; Alvarez-Manzaneda, E. J.; Chahboun, R. Synthesis of Wiedendiol A and Wiedendiol B from Labdane Diterpenes. *Tetrahedron* **1998**, *54* (21), 5635–5650.

(165) Adlington, M. G.; Orfanopoulos, M.; Fry, J. L. A Convenient One-Step Synthesis of Hydrocarbons from Alcohols Through Use of the Organosilane-Boron Trifluoride Reducing System. *Tetrahedron Lett.* **1976**, *17* (34), 2955–2958.

(166) Egi, M.; Kawai, T.; Umemura, M.; Akai, S. Heteropolyacid-Catalyzed Direct Deoxygenation of Propargyl and Allyl Alcohols. *J. Org. Chem.* **2012**, *77* (16), 7092–7097.

(167) Prakash, G. K. S.; Krishnamurti, R.; Olah, G. A. Fluoride-Induced Trifluoromethylation of Carbonyl Compounds with Trifluoromethyltrimethylsilane (TMS-CF3). a Trifluoromethide Equivalent. *J. Am. Chem. Soc.* **1989**, *111* (1), 393–395.

(168) Parisi, G.; Colella, M.; Monticelli, S.; Romanazzi, G.; Holzer, W.; Langer, T.; Degennaro, L.; Pace, V.; Luisi, R. Exploiting a “Beast” in Carbenoid Chemistry: Development of a Straightforward Direct Nucleophilic Fluoromethylation Strategy. *J. Am. Chem. Soc.* **2017**, *139* (39), 13648–13651.

# Appendix.

# Former Member's Contributions

**Chapter 2:**

Regarding eleutherobin's total synthesis, I first worked in collaboration with Dr. Weiwu Ren in several early synthetic strategies. More specifically, Dr. Ren and I have been working on the ring expansion strategy (oxidative dearomatization and Birch alkylation strategies). He also worked on the early stage of the step-by-step approach for macrocyclization (Scheme 2.38). His contributions were numerous such as several scale-up of key intermediates (**65**, **121**, **139**, and **189**), as well as attempts in performing some reactions (Scheme 2.40, Scheme 2.45, Table 2.8).

**Chapter 3:**

Regarding the synthesis of fucosyltransferase inhibitors, I worked in collaboration with Dr. Narasimha Thota. More specifically, Dr. Thota improved the synthesis of ketone **423** from 10% to 78% yield. Furthermore, Dr. Thota also helped in scaling up some of the desired targets such as carbafucose **377**, and carbafucose analogs **394** and **395**. Dr. Thota also worked on the synthesis of several carbafucose phosphate analogs that were not described within this thesis.